Radiometalle in der nuklearmedizinischen Anwendung

Prozessentwicklung und Translation in die klinische Routineanwendung

Dissertation

zur Erlangung des Doktorgrades

der Mathematisch-Naturwissenschaftlichen Fakultät

der Rheinischen Friedrich-Wilhelms-Universität

Bonn

Michael Meisenheimer

aus Bergisch-Gladbach

2022

Angefertigt mit Genehmigung der Mathematisch-Naturwissenschaftlichen Fakultät der Rheinischen Friedrich-Wilhelms-Universität

1. Gutachter: Prof. Dr. med. Markus Essler
2. Gutachter: Univ.-Prof. Dr. rer. nat. Jeroen S. Dickschat

Tag der Mündlichen Prüfung: 08.03.2022

Erscheinungsjahr: 2022

Aus der Klinik und Poliklinik für Nuklearmedizin

Direktor: Prof. Dr. med. Markus Essler

Kurzfassung

In der vorliegenden Arbeit wurden mehrere Aspekte der täglichen radiopharmazeutischen Arbeit in der Nuklearmedizin bearbeitet. Der Fokus lag dabei auf der Translation von neuen Tracern aus der Forschung in die klinische Routine, insbesondere hinsichtlich der Automatisierung von Synthesen.

Lange Zeit war der Bedarf an ^{68}Ga-markierten Radiotracern und die Zahl der damit verbundenen Synthesen überschaubar. Häufig reichten wenige Synthesen pro Woche aus. Diese konnten in manuellen Verfahren durchgeführt werden, wenn der Strahlenschutz gegeben war. Neue Tracer, insbesondere [^{68}Ga]Ga-PSMA-11, haben zu einem erhöhten Patientenaufkommen, und damit verbunden, zu mehr Synthesen geführt. Hinzu kommt, dass die Anforderungen, durch Strahlenschutz und GMP, über die Jahre zugenommen haben. Eine der großen Herausforderungen der klinischen Routine ist es aktuell dieser Nachfrage gerecht zu werden, ökonomisch zu arbeiten und dabei der Gesundheit des Personals und dem Schutz der Patienten Rechnung zu tragen.

Module ermöglichen es, dass verschiedene Radiopharmaka mit robusten Synthesen und vor allem GMP-konformen Materialien bei geringer Dosisbelastung für das Personal hergestellt werden können. Für die Entwicklung einer automatischen Synthese, ist das vorherige systematische Untersuchen der jeweiligen Radiometalltracer die Voraussetzung. Darauf aufbauend konnte eine Standardsynthese etabliert werden, welche mit geringfügigen Anpassungen geeignet ist, um neue Tracer zügig für die Routine verfügbar zu machen. Dennoch ist das Implementieren, trotz dieser Vorarbeiten, nicht ohne Herausforderung. Für jeden Tracer und jedes Radionuklid müssen seine chemischen, aber auch physikalischen Eigenschaften bedacht und berücksichtigt werden, um die Qualität des Produktes gewährleisten zu können. Zusätzlich können nicht immer alle auftretenden Probleme zufriedenstellend gelöst werden.

Schlussendlich konnten mehrerere neue Tracer automatisiert werden. Die Automatisierung, aber auch die dazugehörige Qualitätskontrolle, wurde hinsichtlich ihrer optimalen Parameter evaluiert und für die Routine validiert. Die Tracer konnten dann erfolgreich in der klinischen Anwendung weiter evaluiert werden.

Schlagwörter: Automatisierung; Radiopharmaka; klinische Routine, Radiometalle, Theranostik

Abstract

In the present work, several aspects of daily radiopharmaceutical work in nuclear medicine were dealt with. The main focus was on the translation of new tracers from research into clinical routine, especially with regard to the automation of syntheses.

For a long time, the demand for ^{68}Ga-labelled radiotracers and the number of associated syntheses was manageable. Often, a few syntheses per week were sufficient. These could be carried out in manual procedures if radiation protection was given. New tracers, especially [^{68}Ga]Ga-PSMA-11, have led to an increased number of patients and thus to more syntheses. In addition, the demands of radiation protection and GMP have increased over the years. One of the great challenges of clinical routine is currently to meet this demand, to work economically and at the same time to take into account the health of the staff and the protection of the patients.

Modules make it possible to produce various radiopharmaceuticals with robust syntheses and, above all, GMP-compliant materials with low dose exposure for the personnel. A prerequisite for the development of an automatic synthesis is the prior systematic investigation of the respective tracers. Based on this, a standard synthesis could be established which, with minor adjustments, is suitable for making new tracers quickly available for routine use. Nevertheless, despite this preliminary work, implementation is not without its challenges. For each tracer and each radionuclide, its chemical and physical properties must be considered and taken into account in order to guarantee the quality of the product. In addition, not all problems can always be solved satisfactorily.

Finally, several new tracers could be automated. The automation, but also the associated quality control, was evaluated with regard to its optimal parameters and validated for routine use. The tracers were then successfully further evaluated in clinical application.

Keywords: automated syntheses, radiopharmaceuticals, clinical routine, radiometals, theranostics

Inhaltsverzeichnis

1. **Einleitung**

Aufgrund des demographischen Wandels in der Gesellschaft gibt es immer mehr Krebserkrankungen. Laut Statistischem Bundesamt wächst die Gruppe der über 65-Jährigen in Deutschland kontinuierlich an. Lag ihr Anteil an der Gesamtbevölkerung 1990 mit 11,9 Mio. noch bei 15 % so stieg er bis 2018 auf 22 % (17,9 Mio.). Bei der Gruppe der über 85-Jährigen ist der Zuwachs nochmals stärker, hier hat sich der Anteil sogar von 1 % (1,2 Mio.) 1990 auf 3 % (2,3 Mio.) in 2018 gut verdreifacht (Abbildung 1) [1].

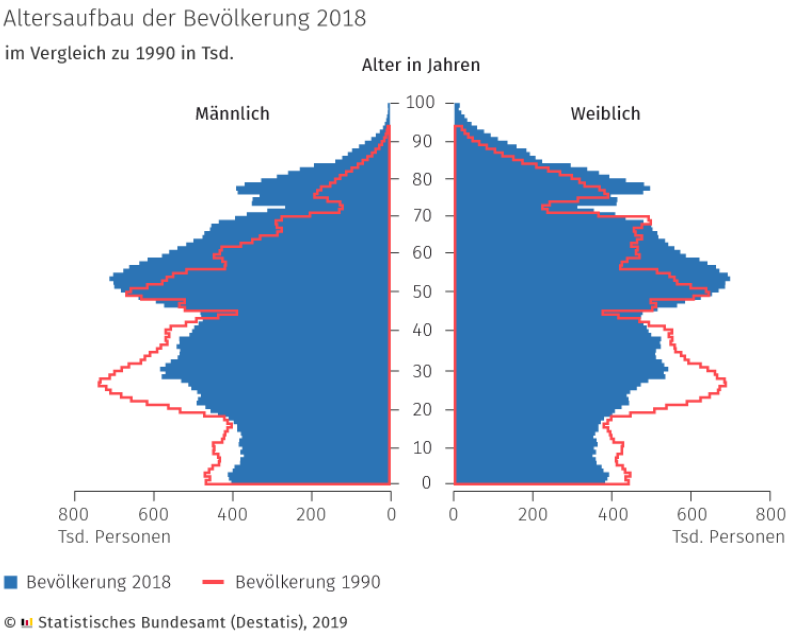

Abbildung 1: Demografischer Wandel in Deutschland seit 1990 [1].

Als Folge des allgemeinen Anstiegs der Lebenserwartung treten altersbedingte Krankheiten wie Krebs statistisch signifikant häufiger auf. Bei Menschen über 60 Jahren beträgt das Risiko über 20 %, innerhalb von fünf Jahren an einer der zehn häufigsten Krebsarten zu erkranken. Das bedeutet, dass in Deutschland etwa 500.000 Menschen jährlich neu an Krebs erkranken. Davon sind ca. 50 % zum Zeitpunkt der Diagnose über 65 Jahre alt (Durchschnittsalter: Frauen 68 Jahre; Männer 69 Jahre) [2].

In der modernen Medizin gibt es viele verschiedene Behandlungsmöglichkeiten, um einen Patienten durch seine Krebserkrankung zu begleiten. Ein wichtiger Aspekt hierbei ist, dass es nicht DEN Krebs als Krankheit gibt. Vielmehr ist es ein Oberbegriff für eine Vielzahl von Erkrankungen, bei denen sich Körperzellen unkontrolliert vermehren und

gesundes Gewebe zerstören oder verdrängen. Je nach befallenem Organ können heute über 100 Krebsarten voneinander unterschieden werden [3]. Diese unterscheiden sich zum Teil deutlich in Überlebenschance, Verlauf und Behandlungsoptionen. Selbst bei Patienten mit „gleicher“ Diagnose können die Krankheitsverläufe starke Differenzen aufweisen. Daher ist für jeden Patienten eine personalisierte Therapie notwendig, die auf seine individuelle Situation eingeht. Viele verfügbare Therapien greifen auch nur zu einem bestimmten Zeitpunkt. Für einen optimalen Therapieerfolg ist es also wichtig, das richtige Medikament dem richtigen Patienten zum richtigen Zeitpunkt zu verabreichen, das personalisierte Patientenmanagment.

Viele Krebserkrankungen in frühen Stadien oder deren Vorstufen bleiben oft unbemerkt, da sie keine Beschwerden verursachen. In fortgeschrittenen Stadien gehen sie jedoch in der Regel mit einem Verlust an Lebensqualität einher. Eine frühzeitige und exakte Diagnose und eine darauf aufbauende Therapie könnten die Prognose einer Krebserkrankung verbessern und im günstigsten Fall zu einer Heilung führen. Dementsprechend stehen neue Wege und Möglichkeiten der Prävention und frühzeitigen Diagnostik sowie neue Therapieansätze seit Jahren im Fokus der Krebsforschung.

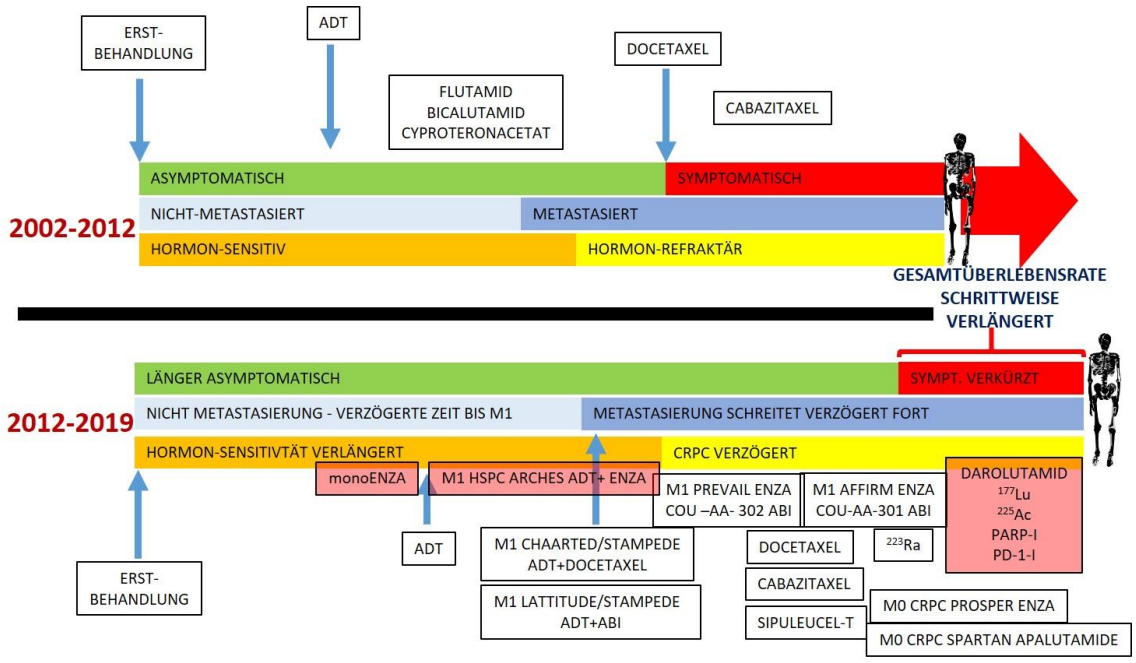

Abbildung 2: Veränderung der Therapiemöglichkeiten durch die Mithilfe der Nuklearmedizin schematisch dargestellt während des Verlaufs einer Prostatakrebserkrankung. 2002-2012 PSA-Ära; 2012-2019 PSMA-Ära (Dankenswerter Weise zur Verfügung gestellt von: Dr. Masha Mahara).

1.1 Strahlung

Strahlung bezeichnet zunächst nur die Form einer Energieausbreitung. Der Bereich der hier betrachteten Energien liegt im atomaren Maßstab und wird in Elektronenvolt (eV; 1 eV = 1,6022*10^{-19} J) anstatt der makroskopischen Einheit Joule (J) angegeben. Strahlung lässt sich in zwei Kategorien einteilen in Korpuskularstrahlung (Teilchenstrahlung) und elektromagnetische Strahlung (Wellenstrahlung; EM-Strahlung).

Die ausgesandten Teilchen der Teilchenstrahlung besitzen eine bestimmte Ruhemasse (m_0), eine Ausdehnung (r) und eventuell eine Ladung (q). Zur Teilchenstrahlung zählen unter anderem α- und β-Strahlung.

Elektromagnetische Strahlung besteht aus räumlich und zeitlich begrenzten Wellenpaketen. Sie haben keine Ruhemasse, bewegen sich im Vakuum mit Lichtgeschwindigkeit und werden je nach Anwendung durch ihre Energie (20), ihre Frequenz (2) oder die Wellenlänge (3) beschrieben. Zur EM-Strahlung zählen unter anderem γ-Strahlen und Röntgenstrahlen.

$$E = h * \nu;\ Einheit: 1\ eV \qquad (1)$$

E: Energie; h: Planck'sche Wirkungsquantum; ν: Frequenz des Photons; eV: Elektronenvolt

$$\nu = \frac{1}{T};\ Einheit: 1\ s^{-1} = 1\ Hz \qquad (2)$$

ν: Frequenz des Photons; t: Zeit; s: Sekunde; Hz: Hertz

$$\lambda = \frac{c}{\nu}\ ;\ Einheit: 1\ m \qquad (3)$$

λ: Wellenlänge des Photons; c: Lichtgeschwindigkeit 2,99792458*10^8 m/s; ν: Frequenz des Photons

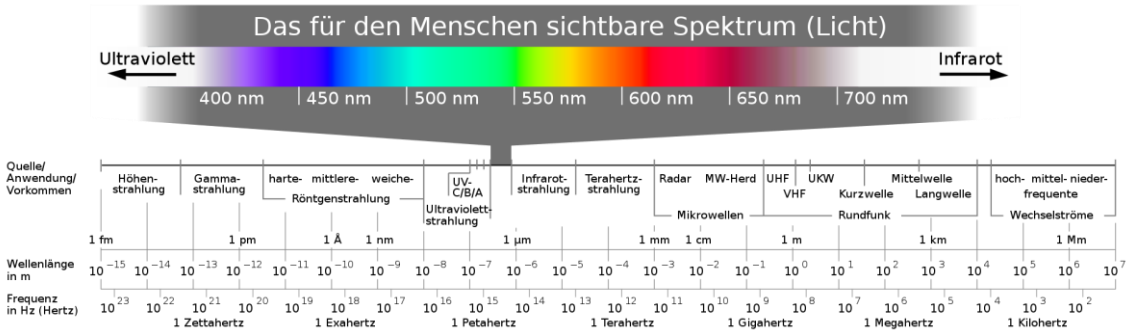

Abbildung 3 EM-Wellenbereich. (Elektromagnetisches Spektrum)

Im Alltag sind wir ständig ionisierender Strahlung ausgesetzt. Diese Strahlung kommt aus natürlichen Quellen, sowohl von der Erde (terrestrisch) als auch aus dem Weltraum (kosmisch). Die daraus resultierende Strahlenbelastung setzt sich aus ≈ 19 % terrestrischer, ≈ 14 % kosmischer und ≈ 67 % interner Strahlung (aufgenommene Nahrung; Inhalation von Radon aus der Luft) zusammen [4]. In Deutschland kommt man damit im Schnitt auf eine natürliche Strahlenexposition von ca. 2 mSv/a, die geographisch und geologisch bedingt jedoch deutlich variieren kann (Abbildung 4).

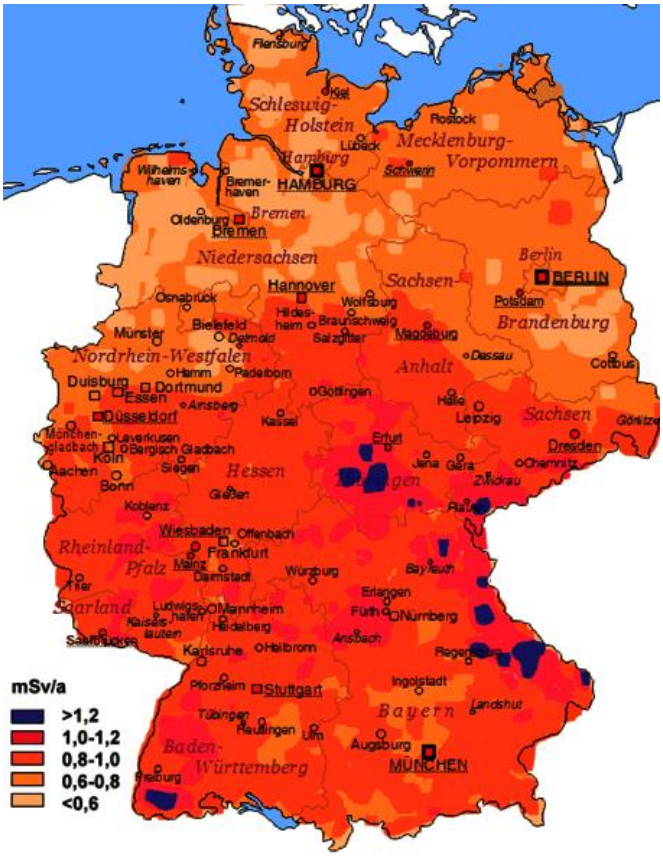

Abbildung 4: Mittlere natürliche Dosisleistung pro Jahr in Deutschland [5].

Zusätzlich zu den natürlichen Strahlenquellen tragen noch künstliche zur Strahlenbelastung bei. Dazu zählen vor allem medizinische Untersuchungen (z. B. Computertomographie (CT); Röntgenuntersuchungen), der Fallout von Kernwaffenversuchen oder Reaktorunfällen (z. B. Tschernobyl, Fukushima), aber auch die Förderung und Verbrennung von Kohle.

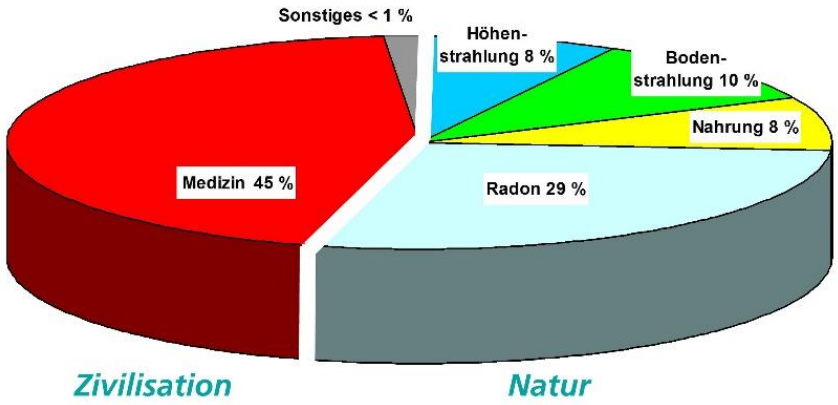

Abbildung 5 Zusammensetzung der Jährlich durchschnittlichen Strahlendosis in Deutschland [4].

1.1.1 Biologische Strahlenwirkung

Für die medizinische Anwendung relevant ist die biologische Wirksamkeit von Strahlung, das heißt welchen Effekt eine Energieübertragung von Strahlung auf exponierte Körperzellen hat. Die Reaktion eines Gewebes auf eine Strahlenexposition ist abhängig von der Energie und Art der Strahlung, aber auch vom bestrahlten Gewebe. Diese individuelle Gewebereaktion nach ionisierender Strahlung kann sehr unterschiedlich ausfallen. Die Strahlen- bzw. Radioempfindlichkeit ist meist direkt proportional zur Zellteilungsrate, jedoch umgekehrt proportional zur Differenzierung des Zelltyps eines Gewebes [6–8].

Beschrieben wird die biologische Wirkung von Strahlung mit Hilfe der Äquivalentdosis und der effektiven Dosis. Die Äquivalentdosis beschreibt dabei die Größe des Schadens ausschließlich aufgrund der Art der Strahlenexposition. Die effektive Dosis zieht zusätzlich die Art des bestrahlten Gewebes in Betracht.

Die Aktivität beschreibt die Stärke einer Strahlenquelle. Diese ist abhängig von der Masse, das heißt der Anzahl der noch nicht zerfallenen Kerne, und der Halbwertszeit des Nuklides (4).

$$A(t) = -\frac{dN}{dt}(t) = \lambda \cdot N(t) \qquad (4)$$

A: Aktivität; N: Anzahl der Kerne, t: Zeit; λ: Zerfallskonstante

Die Energiedosis dagegen beschreibt, wie Strahlung auf einen Körper wirkt. Je mehr Dosis übertragen wird, desto größer ist auch die Wirkung.

$$D = \frac{dE}{dm} = \frac{1}{\rho} \cdot \frac{dE}{dV} \qquad (5)$$

D: Dosis; E: Energie; m: Masse; ρ: Dichte; V: Volumen

Die Äquivalentdosis berücksichtigt zusätzlich die Wirkung der verschiedenen Strahlenarten auf Gewebe und enthält hierfür den Bewertungsfaktor q. Die Werte von q sind einheitenlos und bewegen sich von 1 für Photonen bis hin zu 20 für α-Teilchen.

$$H_R = Q_R \cdot D_R \qquad (6)$$

H_R: Äquivalentdosis; Q_R: Qualitätsfaktor; D_R: Energiedosis

Hinsichtlich ihrer Wirkung unterscheidet man zwischen ionisierender Strahlung und nichtionisierender Strahlung. Erstere unterteilt sich weiter in direkt ionisierende (α- und β-Strahlung) und indirekt ionisierende Strahlung (γ- und n-Strahlung).

Die Energie der nichtionisierenden Strahlung ist zu gering, um Atome zu ionisieren, da sie unterhalb der meisten Bindungsenergien liegt. Das heißt, die minimale stabile Bindungsenergie zwischen Molekülen von 3 eV wird nicht überschritten. Zur nichtionisierenden Strahlung werden Wellen im Frequenzbereich unterhalb von 750 THz oder einer Wellenlänge oberhalb von 400 nm gezählt.

Ionisierende Strahlung bezeichnet Teilchen- bzw. jede EM-Strahlung, die durch ihre Energie Elektronen aus Atomen oder Molekülen lösen kann. Hierfür ist es auch nicht entscheidend, ob bei der Wechselwirkung mit der Materie auch tatsächlich Ionisierungen stattfinden, sondern nur das genug Energie vorhanden ist, damit sie stattfinden können. Die dafür notwendige Energie ist typischerweise größer als 5 eV. Die einzelnen Strahlenarten unterscheiden sich darin wie viele elektrisch neutrale Moleküle pro Wegstrecke ionisiert werden können und ihrer daraus resultierenden biologischen Wirkung. Die Ionisation durch EM-Strahlung findet hierbei über einen der folgenden drei Prozesse statt: Compton-Effekt, Photoeffekt oder Paarbildung.

Der Compton-Effekt beschreibt einen der wichtigsten Ionisationsprozesse und stellt den größten Teil der Wechselwirkungen von Photonen mit Elektronen dar. Hierbei wird ein Teil der Energie auf das Elektron übertragen. Dabei ändert sich die Wellenlänge und Richtung des Photons. Der Effekt kommt zu tragen bei Photonen mit mittlerer Energie, welche mit äußeren Valenzelektronen interagieren. Das dabei gestreute Elektron wird als Compton-Elektron bezeichnet.

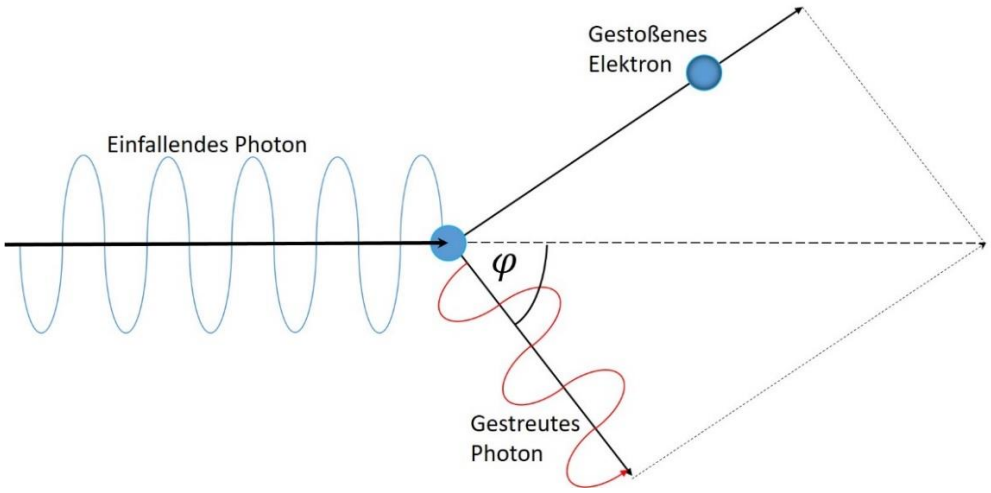

Abbildung 6: Schematische Darstellung der Compton Streuung.

Beim Photoeffekt wird die Energie eines Photons vollständig auf ein Valenzelektron übertragen. Die übertragene Energie muss jedoch größer als 5 eV sein, um das Elektron aus der Bindung zu lösen (7). Sie ist die Hauptenergieumwandlung bei Photonen mit niedrigen Energien. Die Wechselwirkung findet zumeist mit Elektronen aus der inneren Schale statt.

$$E = h * \nu - W_0 \qquad (7)$$

E: Energie; h: Planck'sches Wirkungsquantum; v: Frequenz des Photons; W_0: Austrittsarbeit des Elektrons.

Unter Paarbildung versteht man die Umwandlung eines Photons in ein Elektron-Positron-Paar (Teilchen-Antiteilchen-Paar). Sobald die Energie eines einzelnen Photons die doppelte Ruheenergie des Elektrons ($2*m_ec^2$ = 1,022 MeV) überschreitet, wird Paarbildung im Feld eines Kernes möglich (8).

$$\gamma K \rightarrow e^{-}e^{+}K \qquad (8)$$

K: Kern; e^{-}: Elektron; e^{+}: Positron; γ: einfallendes Photon

$$E_{\gamma} \geq 2m_e c^2 + 2\frac{m_e^2}{m_{Kern}}c^2 \qquad (9)$$

Eγ: Energie des Photons; m_e: Masse des Elektrons; c: Lichtgeschwindigkeit

Oberhalb von etwa 3 MeV dominiert Paarbildung die anderen beiden Prozesse der Energieübertragung. Der gegenteilige Effekt, die Vernichtung eines Teilchen-Antiteilchen-Paares unter Aussendung von Photonen, ist die Annihilation (Paarvernichtung).

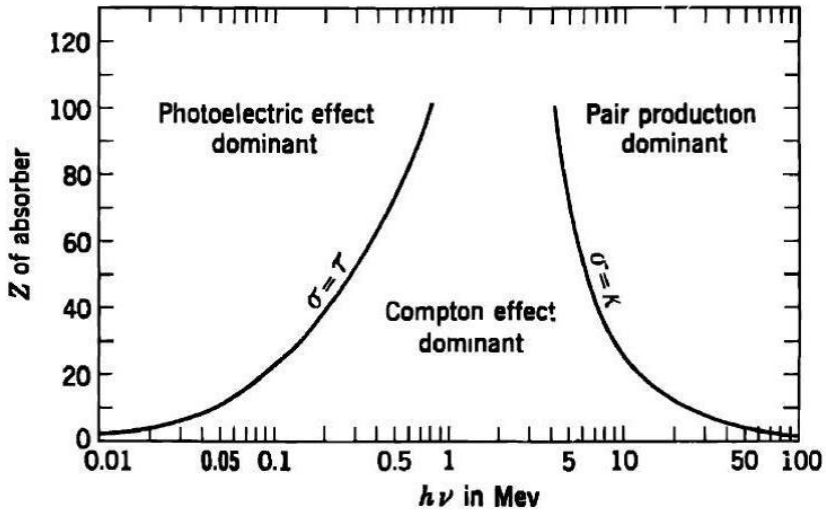

Abbildung 7: Übersicht der Abgrenzungen des Photo-, Compton-Effekts und der Paarbildung [9].

1.1.2 Strahlenschäden

Ionisierende Strahlung ist ein Träger von Energie, welche bei Wechselwirkung mit Materie abgegeben werden kann. Handelt es sich bei dem bestrahlten Stoff um biologisches Gewebe so kann die absorbierte Energie vielfältige Effekte haben. Ob und wieviel Schaden die Strahlenexposition anrichtet, hängt von der Art der Strahlung, der absorbierten Dosis und der betroffenen Körperregion (Organ, Gewebe) ab.

Ionisierende Strahlung kann entweder deterministische oder stochastische Strahlenschäden im Organismus hervorrufen. Deterministische Strahlenschäden treten ab einem

Schwellenwert von 500 mSv auf. Sie sind die Folge einer massiven Abtötung von Zellen durch Apoptose oder Nekrose. Diese tritt auf, wenn die körpereigenen Reparaturmechanismen nicht mehr in der Lage sind, die entstandenen Schäden zu reparieren. Sterben zu viele Zellen in einem Gewebe oder Organ ab, kommt es zu Funktionseinbußen des betroffenen Organs. Folgende Körperregionen sind besonders betroffen: Haut; Haare; Schleimhaut des Magen-Darm-Traktes, Lunge und Fortpflanzungsorgane. Als erstes sichtbar werden Veränderungen an der Haut, es entstehen Rötungen ähnlich wie bei einem Sonnenbrand. Nach 2-3 Tagen kann es dann zu Haarausfall kommen. Ist der Magen-Darmtrakt betroffen, sind Übelkeit und Durchfall möglich. Bei Strahlendosen über 6 Sv tritt der Tod meist innerhalb von 14 Tagen ein.

Oberhalb des Schwellenwertes ist die Schwere des Schadens proportional zur Dosis der ausgesetzten Strahlenexposition. Liegt die Dosis unterhalb des Schwellenwerts, treten keine deterministischen Schäden auf. Eine Schädigung kann dennoch nicht ausgeschlossen werden. Diese zufällig auftretenden Schäden werden stochastische Strahlenschäden genannt.

Stochastischen Strahlenschäden treten mit einer bestimmten Wahrscheinlichkeit auf, welche proportional zur Dosis der Strahlenexposition ist. Sie können immer, sowohl bei niedrigen als auch bei hohen Dosen, eintreten. Dabei ist die Schwere des Schadens von der Dosis unabhängig. Stochastische Strahlenschäden führen aufgrund einer unzureichenden oder fehlerhaften Reparatur der DNA zu Veränderungen im Erbmaterial von Zellen. Die dadurch veränderte genetische Information der Zelle wird beim natürlichen Prozess der Zellteilung an die Tochterzellen weitergegeben. Dieser Vorgang kann noch Jahre nach der Strahlenexposition zur Entstehung von Krebs führen. Die Zeit die zwischen der Einwirkung der Strahlung und der Erkrankung vergeht, nennt man Latenzzeit. Stochastische Schäden sind beispielsweise Krebserkrankungen, Unfruchtbarkeit oder Leukämie.

1.1.3 α-Strahlung

Radioaktive Nuklide, die unter Aussendung von α-Strahlung zerfallen, nennt man α-Strahler. Bei dieser Art der radioaktiven Kernumwandlung sendet der zerfallende Atomkern einen Helium-Atomkern (α-Teilchen) aus. Dieses ist ein zweiwertiges Kation und besteht aus zwei Protonen und zwei Neutronen. Für den Zerfall gilt die allgemeine Gleichung:

$$^{A}_{Z}X \rightarrow ^{A-4}_{Z-2}Y + ^{4}_{2}He + \Delta E \qquad (10)$$

X: Mutternuklid; Y: Tochternuklid; A: Massenzahl; Z: Protonenzahl; E: Energie

Die Austrittsenergie der α-Teilchen liegt in einem Bereich von 2 bis 5 MeV. Künstlich erzeugte α-Teilchen können aber auch Energien von 10 MeV erreichen. Das Energiespektrum des α-Zerfalls, kann nur diskrete Werte annehmen. Dieses Linienspektrum ist charakteristisch für jedes Nuklid und kann zu seiner Identifikation genutzt werden (Abbildung 8).

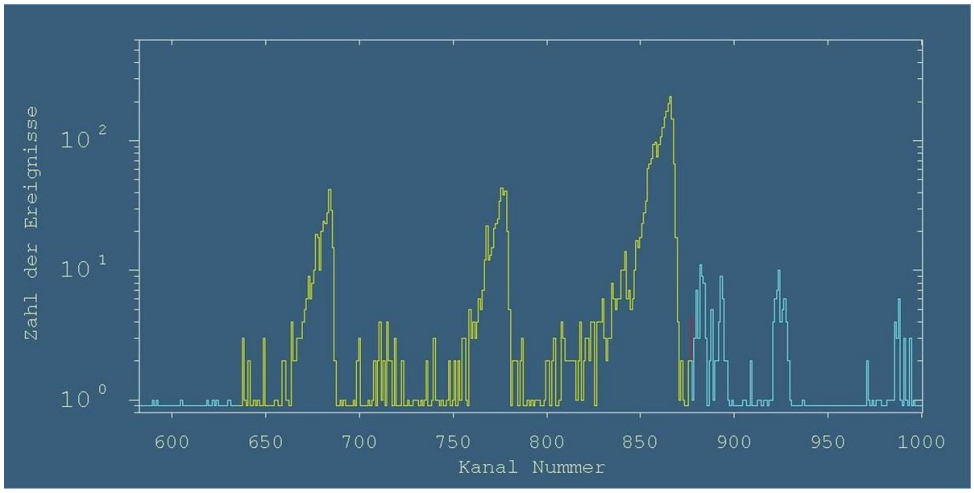

Abbildung 8: Alpha-Spektrum von natürlichen Uran [10].

Aufgrund ihrer Masse und ihrer Kernladung haben α-Teilchen nur eine geringe Eindringtiefe in Materie. Dabei geben sie jedoch nahezu kontinuierlich Energie an die Moleküle in ihrer Umgebung ab. Sie ionisieren also sehr viele Moleküle, das aber nur auf einer relativ kurzen Strecke. Diese Eigenschaften machen α-Strahler für die Nuklearmedizin äußerst interessant. Da sich ihre Energie nur lokal sehr begrenzt auswirkt, durchdringt sie nur wenige Zellschichten. Gekoppelt an einen geeigneten Tracer können α-Strahler im Tumorgewebe angereichert und dort therapeutisch wirksam werden, während das umgebende gesunde Gewebe nur minimal von der Strahlenexposition geschädigt wird.

1.1.4 β-Strahlung

β-Strahlung wird in zwei Kategorien unterteilt, in β^-- und in β^+-Strahlung. β^--Strahlung entsteht durch den Zerfall eines Neutrons in ein Proton, ein Elektron und ein Antineutrino (12).

Die allgemeine Zerfallsgleichung lautet:

$$^{A}_{Z}X \rightarrow {}_{Z+1}{}^{A}Y + e^{-} + \bar{\nu}_e \qquad (11)$$

X: Mutternuklid; Y: Tochternuklid; A: Massenzahl; Z: Protonenzahl; e^-: Elektron; $\bar{\nu}_e$: Antineutrino

$$^{1}_{0}n \rightarrow {}^{1}_{1}p + e^{-} + \bar{\nu}_e \qquad (12)$$

n: Neutron; p: Proton; e^-: Elektron; $\bar{\nu}_e$: Antineutrino

Diese Art der Kernumwandlung geschieht vorzugweise in neutronenreichen Nukliden wie z. B. Molybdän-99 und Lutetium-177.

β^+-Strahlung entsteht durch den Zerfall eines Protons in ein Neutron, ein Positron und ein Neutrino (14). Die allgemeine Zerfallsgleichung lautet:

$$^{A}_{Z}X \rightarrow {}_{Z-1}{}^{A}Y + e^{+} + \nu_e \qquad (13)$$

X: Mutternuklid; Y: Tochternuklid; A: Massenzahl; Z: Protonenzahl; e^+: Positron; ν_e: Neutrino

$$^{1}_{1}p \rightarrow {}^{1}_{0}n + e^{+} + \nu_e \qquad (14)$$

n: Neutron; p: Proton; e^+: Positron; ν_e: Neutrino

Diese Art der Kernumwandlung wird von protonenreichen Nukliden wie z. B. Gallium-68 oder Fluor-18 bevorzugt.

Eine weitere Möglichkeit für protonenreiche Nuklide an Stabilität zu gewinnen, ist der Elektroneneinfang (eng. **e**lectron **c**apture; EC). Hierbei wird ein kernnahes Elektron eingefangen und verbindet sich mit einem Proton zu einem Neutron. Die Massezahl bleibt dabei konstant, während sich die Protonenzahl verringert (16). Der EC stellt eine direkte

Konkurrenzreaktion zur β⁺-Emission dar. Die minimal notwendige Energie von 1022 MeV welche für die Erzeugung von zwei Photonen notwendig ist, stellt hierbei die Abgrenzung dar. Unterhalb dieser Energie wird EC bevorzugt, oberhalb die β⁺-Emission.

$$ {}^{A}_{Z}X \rightarrow {}^{A}_{Z-1}Y + \nu_e \qquad (15) $$

X: Mutternuklid; Y: Tochternuklid; A: Massenzahl; Z: Protonenzahl; ν_e: Neutrino

$$ {}^{1}_{1}p + e^{-} \rightarrow {}^{1}_{0}n + \nu_e \qquad (16) $$

n: Neutron; p: Proton; e^+: Positron; ν_e: Neutrino

Auf die beim Betazerfall erzeugten Neutrinos bzw. Antineutrinos geht ein unbestimmter Anteil der Zerfallsenergie über. Aufgrund dieses Drei-Teilchen-Problems ist das resultierende β-Energiespektrum nicht konkret, sondern kontinuierlich bis zu einer Maximalenergie. Dabei liegt das Maximum der Energieverteilung bei etwa einem Drittel der maximalen Energie. Tabellarische Betaenergien, welche beispielsweise zur Dosisberechnung herangezogen werden, beziehen sich hingegen stets auf den maximalen Wert und vernachlässigen das restliche Spektrum.

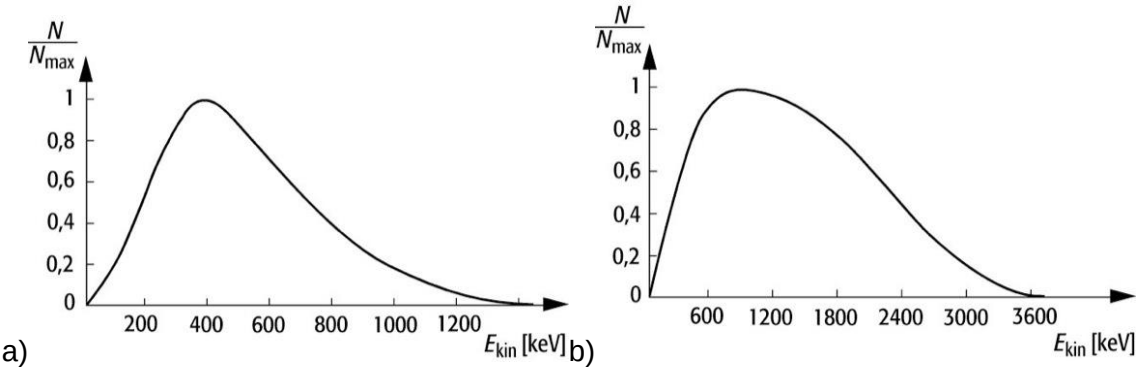

Abbildung 9: in a) ist das β^--Spektrum von Kalium-40 dargestellt. In b) ist das β^+-Spektrum von Phosphor-30 dargestellt [11].

β⁺- und β⁻-Strahler unterscheiden sich zudem in ihrer Wechselwirkung mit Materie. β⁻-Teilchen wechselwirken über ihre gesamte Wegstrecke mit Kernen. Solange sie noch energiereich sind, verringern sie ihre Energie durch elastische Stöße und erzeugen dabei Photonen (Bremsstrahlung). Sobald sie genug Energie abgegeben haben werden

sie in ein leeres Valenzband eines Kerns aufgenommen, wodurch dieser negativ ionisiert wird.

Auch β^+-Teilchen wechselwirken über ihre gesamte Wegstrecke mit Kernen durch Erzeugung von Bremsstrahlung, solange sie noch energiereich sind. Sobald das β^+-Teilchen seine Ruheenergie erreicht hat, interagiert es mit einem Elektron in Form einer Annihilation und der Bildung von zwei γ-Quanten (einzelne γ-Quanten werden auch Photonen genannt), die sich in einem Winkel von 180° voneinander entfernen. Die zur Erlangung der Ruheenergie zurückgelegte Wegstrecke ist abhängig vom Medium und dessen Dichte [12]. Für die Einstellung und Kalibrierung der SPECT bzw. PET werden, aufgrund der dichteabhängigen Wegstrecke der β-Teilchen, verschiedene Arten von Phantomen benutzt.

1.1.5 γ-Strahlung

γ-Strahlung ist eine elektromagnetische Strahlung. Sie wechselwirkt nur wenig mit Materie und hat dementsprechend eine hohe Eindringtiefe in diese. Zur γ-Strahlung zählen EM-Strahlen bis zu einer Energie <200 keV oder Wellenlängen von 5 pm. γ-Strahlung entsteht in der Regel als Folge eines α- oder β-Zerfalls, bei denen der Tochterkern meist noch einen Energieüberschuss aufweist. Dieser angeregte Tochterkern wandelt sich nach einer bestimmten Zeit in einen niederenergetischen Zustand um. Die überschüssige Energie wird bei der Umwandlung in Form von γ-Strahlung abgegeben.

$$ {}^{A}_{Z}X^{*} \rightarrow {}^{A}_{Z}X + \gamma \qquad (17) $$

X^{*}: Nuklid im angeregten Zustand; X: Nuklid im Grundzustand; A: Massenzahl;
Z: Protonenzahl; γ: ausgesandtes Photon

$$ {}^{Am}_{Z}X \rightarrow {}^{A}_{Z}X + \gamma \qquad (18) $$

^{m}X: metastabile Form des Nuklids; X: Nuklid im Grundzustand; A: Massenzahl;
Z: Protonenzahl; γ: ausgesandtes Photon

Diese Art der Umwandlung wird auch γ-Übergang oder γ-Zerfall genannt. Die Energie von γ-Strahlung ist immer diskret und charakteristisch für jedes Nuklid. Die scharfe Energie der γ-Strahlung erklärt sich daraus, dass die Lebensdauern von γ-Übergängen kernphysikalisch gesehen vergleichsweise lang sind. Da die Lebensdauer eines angeregten

Kernzustandes stets höher als 10^{-15} s ist führt dies nur zu diskreten Photonenenergien mit einer Halbwertsbreite von unter 0,3 eV [13]. γ-Strahlung kommt auch zur Sterilisation zum Einsatz, z. B. bei medizinischen Produkten. γ-Strahlung kann für die Diagnostik verwendet werden.

1.2 Radionuklide in der Medizin

Radionuklide dienen in der Nuklearmedizin als Strahlenquelle für diagnostische (z. B. Positronen-Emissions-Tomographie (PET)) oder therapeutische Zwecke. Die radioaktiv markierten Medikamente, auch Radiopharmaka genannt, werden den Patienten zumeist intravenös verabreicht. Sie bestehen in der Regel entweder nur aus der radioaktiven Substanz, welche z. B. in Form eines Salzes (z. B. $[^{226}Ra]Cl_2$, $Na[^{18}F]F$) vorliegt, oder aus dem Radionuklid gebunden an einen Carrier (z. B. ^{18}F-Fluro-Desoxy-glucose ($[^{18}F]$-FDG)). Mit diesen Tracern können, basierend auf dem Tracer-Prinzip von George de Hevesy [14], einerseits Stoffwechselprozesse abgebildet und andererseits Krankheiten behandelt werden.

1.2.1 Nuklearmedizinische tomographische Verfahren

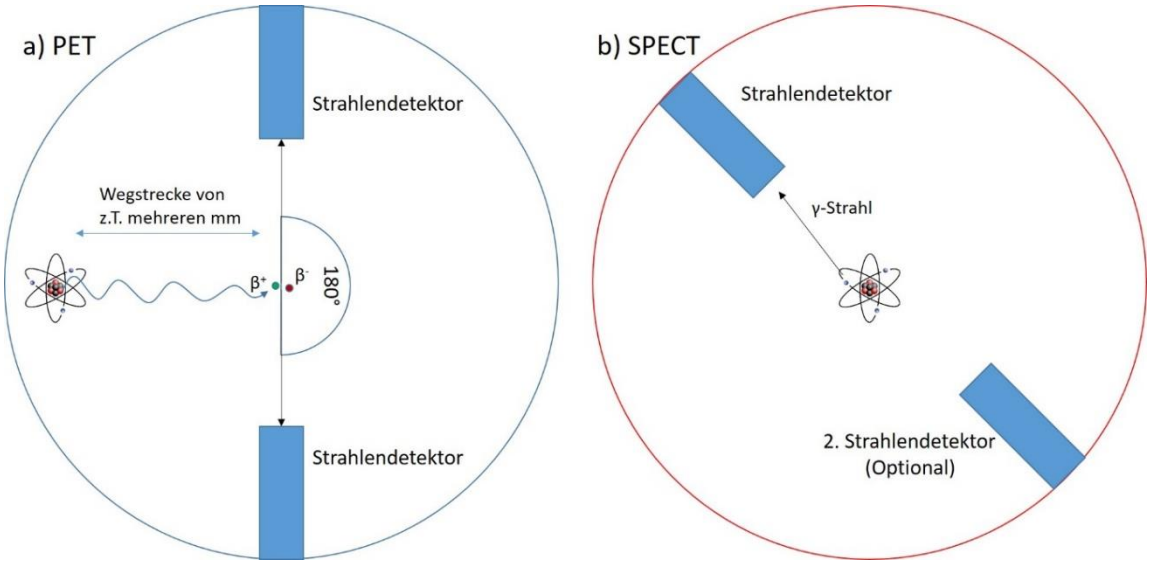

Abbildung 10: Schematische Darstellung der Detektion in einem PET und einem SPECT.

Der Nuklearmedizin stehen verschiedene Radionuklide (z. B. Technetium-99m) für die *In-vivo*-Diagnostik zur Verfügung deren ausgesandte Strahlung außerhalb des Patienten detektiert wird. Durch die Verteilung des Radiopharmakons im Patienten können Rückschlüsse auf die Funktion verschiedener Organe oder Gewebe gezogen werden.

Für die diagnostische Bildgebung kommen entweder Positronen- oder γ-emittierende Radionuklide zum Einsatz. Beide Strahlungsarten werden von den Detektoren in den Tomographen in Form von Photonen registriert. Jedes detektierte Photon wird dabei als "Punkt" dargestellt, wobei während eines Scans typischerweise hunderttausende dieser Punkte gesammelt werden, um ein endgültiges Bild zu erstellen. In der Art und Weise ähnelt das der Malerei von Paul Signac oder Georges-Pierre Seurat, welche ihre Bilder Punkt für Punkt zusammensetzten [15] (Abbildung 11). Die Bildgebung kann in Form von statischen, bewegten, Querschnitts- und dreidimensionalen Bildern erfolgen.

Querschnittsbilder werden überwiegend mit Hilfe der sogenannten Single-Photon-Emissions-Computertomographie (SPECT) aufgenommen. Die meisten SPECT-Geräte verfügen über zwei Gamma-Detektorköpfe auf einer Drehachse (Abbildung 10) welche um den Patienten rotieren und werden häufig mit einer CT-Einheit kombiniert. Das ermöglicht es funktionale und anatomische Bildsätze miteinander zu kombinieren. Die Detektoren der Kamera bestehen im Einzelnen aus einer Kollimatorblende, Szintillationskristall, Lichtleiter und Photomultiplier. Beim Auftreffen eines γ-Quants auf den Kristall wird

ein Lichtblitz erzeugt, welcher verstärkt und dann in ein elektronisches Signal umgewandelt wird. Entsprechend ihrer Häufigkeit werden die Einzelsignale als Bildpunkt in unterschiedlich dunklen Farben eines Gesamtbildes dargestellt (Abbildung 11). Die zu untersuchenden Organe können einfach planar dargestellt werden. Aus diesen planaren Bildern kann die Verteilung des Radiopharmazeutikums im Körper bestimmt werden und dann z. B. als Schnittbild durch den Körper dargestellt werden. Dabei werden mehrere Bilder derselben Körperregion zu einem dreidimensionalen Modell errechnet.

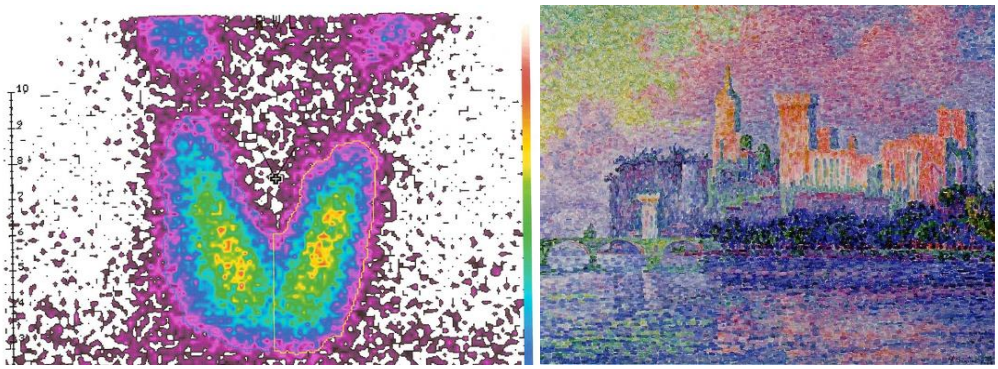

Abbildung 11: Links: Szintigramm einer gesunden Schilddrüse mitTechnetium-99m-pertechnetat als Radiotracer in einem SPECT [16]. Rechts: Der Papstpalast zu Avignon von Paul Signac derzeit ausgestellt in Musée d'Orsay, Paris, Frankreich.

Bei der Positronen-Emissions-Tomographie werden Positronenemitter eingesetzt. Das Positron annihiliert mit einem Elektron, nachdem es seine Ruheenergie erlangt hat, zu zwei Photonen. Idealerweise strahlen diese im 180° Winkel ab (1.1.4). Diese beiden Photonen werden anschließend mit Hilfe einer Koinzidenzmessung detektiert. Koinzidenzmessung ist die Aufnahme vom Zusammentreffen bestimmter Ereignisse (hier: die Detektion der zwei γ-Quanten der Annihilation) innerhalb eines bestimmten, vorgegebenen Zeitfensters (Abbildung 10). Mit einer geeigneten Software kann dann der ursprüngliche Ort des Kernzerfalls errechnet und eventuelle Fehlkoinzidenzen kompensiert werden (Abbildung 12).

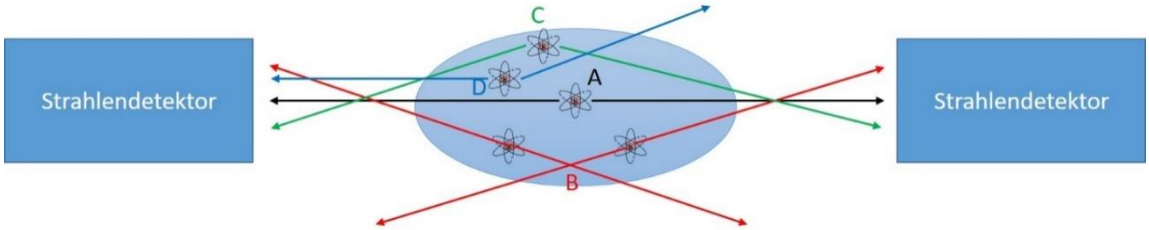

Abbildung 12: Schematische Darstellung der verschiedenen Koinzidenzdetektionen. A: echte Koinzidenz; B: Zufällige Koinzidenz; C: gestreute Koinzidenz; D: Streuung.

Dadurch ist es möglich im PET eine quantifizierte Untersuchung durchzuführen. Die Quantifizierung ist gleichbedeutend mit der Bestimmung lokaler Aktivitätskonzentrationen im Gewebe und, gegebenenfalls durch zusätzliche Schritte, quantitativer physiologischer Parameter [17]. Voraussetzung dafür ist, dass das PET unter ordnungsgemäßen Arbeitsbedingungen betrieben wird (Qualitätskontrolle, Normalisierung, Kalibrierung). Die Quantifizierung erfordert Korrekturen für die Totzeit, Dämpfung, Streuung und ggf. gegen zufällige Koinzidenzen (Abbildung 12). Die Überlegenheit von PET gegenüber SPECT basiert auf den Vorteilen der Koinzidenzdetektion (elektronische Kollimation, PET) gegenüber der mechanischen Kollimation (SPECT). Bei entsprechend ausgelegten Ringsystemen führen diese Vorteile zu einer besseren Bildqualität [18]. Weitere Vorteile sind ein deutlich reduzierter Streuanteil und die Verbesserung der Zählratenleistung, mittels einer erhöhten Anzahl unabhängiger Zählkanäle bei Verwendung von Blockdetektoren. Die Kombination dieser Vorteile führt zu kontrastreichen und detailreichen Bildern. Die höhere Zählratenleistung bietet zudem eine verbesserte statistische Bildqualität, bei gleichbleibender applizierter Aktivität [19]. Die Abschwächung und Streukorrektur führt dazu, dass eine Quantifizierung im SPECT nicht durchführbar ist. In den letzten Jahren gemachte Fortschritte bei Rekonstruktionsalgorithmen und Korrekturmethoden ermöglichen eine Verbesserung der Bildqualität und verringern die derzeitigen Einschränkungen der SPECT-Technik [20]. Dennoch kann die SPECT die Leistungsfähigkeit der PET rein physikalisch nicht erreichen.

Fluor-18 ist das am häufigsten genutzten PET-Isotop und wird bis heute zumeist in Form von radioaktiv markiertem Zucker ([^{18}F]-FDG) verwendet, welches immer noch der Goldstandard in der onkologischen Bildgebung ist.

Tabelle 1: Gegenüberstellung der Details zu PET und SPECT

	PET	SPECT
Bsp. Verwendete Radionuklide	^{11}C; ^{18}F; ^{68}Ga	^{99m}Tc; ^{123}I; ^{111}In
Produktion der Nuklide	Zyklotron, Generator	Generator
emittierte Photonen	2*511 keV	1 ca. 140 keV
$T_{1/2}$	Minuten bis wenige Stunden	Stunden bis Tage
Mögliche räumliche Auflösung	3-7 mm	7-10 mm
Mögliche zeitliche Auflösung	5 s – 1 min	>1 min
Notwendige Rechenleistung	sehr hoch	relativ gering
Durchschnittliche Kosten (D)	350-440 €	70-120 €

1.2.2 Radionuklide Produktion

Für die Routineproduktion von Radionukliden, gibt es verschiedene Möglichkeiten. So kann ein stabiles Nuklid beispielsweise durch Bestrahlung mit Kernteilchen (z. B. Neutronen, Protonen oder Gammastrahlen) in einen instabilen Zustand gebracht werden. Dies geschieht entweder an Teilchenbeschleunigern (z. B. Zyklotron) oder in Kernreaktoren. Die enorme Vielfalt der auf diese Weise entdeckten Radionuklide und vor allem die Möglichkeit diese dann auch in einem entsprechend notwendigen Maßstab herzustellen, hat zu zahlreichen Anwendungen in der Industrie und Technik als auch natürlich in der Medizin geführt. Eine Alternative Route der Radionuklidproduktion sind Radionuklid-Generatoren, welche kontinuierlich das Radionuklid produzieren.

1.2.3 Zyklotron

Ein Zyklotron besteht zumeist aus zwei hohlen, halbkreisförmigen Metallelektroden (Duanten). An die Duanten ist eine hochfrequente Wechselspannung angeschlossen, welche sie abwechselnd positiv und negativ lädt. Durch die gegensätzliche Ladung der beiden Duanten entsteht im Spalt zwischen ihnen ein starkes elektrisches Feld (E-Feld).

Oberhalb und unterhalb der Duanten befinden sich Elektromagnete, welche ein konstantes, homogenes Magnetfeld (B-Feld) innerhalb der Duanten erzeugen. Im Inneren der Duanten befindet sich eine Teilchenquelle, die freie Ionen abgibt (*Abbildung* 13) [21].

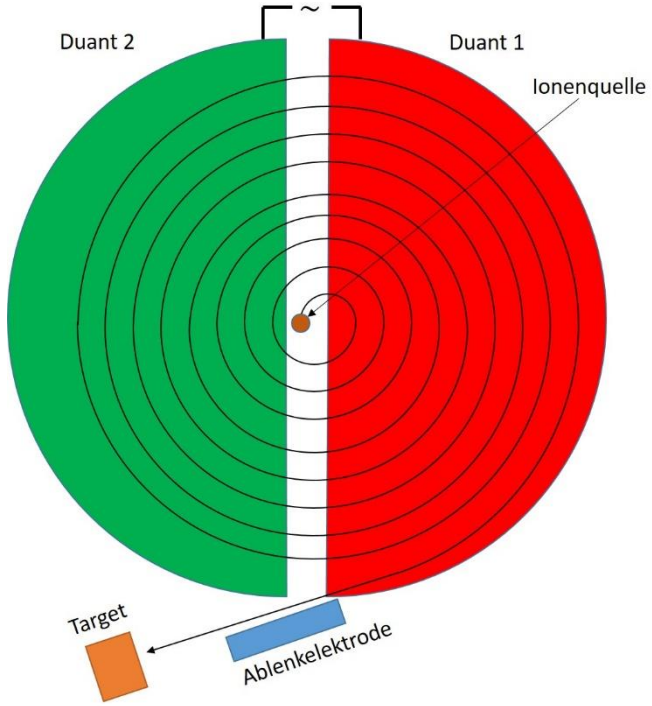

Abbildung 13: Schematische Darstellung der Funktionsweise eines Zyklotrons.

Die Teilchenquelle gibt geladene Ionen (zumeist positiv geladene Protonen) in den Spalt zwischen den Duanten ab. Bei negativer Ladung von Duant 1 werden die Protonen durch das E-Feld im Spalt in Richtung Duant 1 beschleunigt. Tritt das Proton in den Duanten ein, so verlässt es das E-Feld. Beide Duanten wirken hier als Faraday'sche Käfige, in denen kein E-Feld herrscht. Durch das B-Feld des Elektromagneten wird das Proton innerhalb des Duanten durch die Lorentzkraft beeinflusst. Dadurch wird es auf eine Kreisbahn gezwungen. Während sich das Proton noch innerhalb des Duanten befindet, wird die Polung des E-Feldes umgekehrt. Nach Durchlaufen eines Halbkreises verlässt das Proton den Duanten und tritt wieder in das E-Feld ein. Hier wird es, bis zu seinem Eintritt, in Richtung Duant 2 beschleunigt. Mit jeder Runde erhöht sich so die Geschwindigkeit des Teilchens und damit auch der Radius seiner Kreisbahn. Dadurch kann die Durchlaufzeit durch einen Duanten konstant gehalten werden. Durch Wiederholung dieses Prozesses wird das Teilchen immer weiter beschleunigt, bis es durch eine Ablenkelektrode aus dem Duanten in Richtung des Targets gelenkt wird. Durch das Beschießen von definierten Targets mit den beschleunigten Teilchen können gezielt radioaktive Isotope, unter anderem für die medizinische Anwendung, erzeugt werden [22].

1.2.4 Reaktor

Die Herstellung von Radionukliden an einem Kernreaktor stellt eine der frühsten Möglichkeiten dar, diese für die Medizin nutzbar zu machen [23]. Früher kamen viele medizinisch verwendete Radionuklide aus den Abfallprodukten der Atomkraftwerke. Heutzutage werden, ähnlich der Herstellung am Zyklotron, Targets verwendet, welche mit Neutronen in einem Kernreaktor beschossen werden. So können die gewünschten Radionuklide selektiv hergestellt werden. Die Bestrahlung kann Stunden bzw. auch Tage dauern, bevor das Target entnommen und das gefragte Radionuklid chemisch abgetrennt wird. Die unterschiedlichen Bestrahlungszeiten hängen vom Wirkungsquerschnitt *(19)*, und damit von der Wahrscheinlichkeit mit der ein Teilchen mit einem Targetteilchen wechselwirkt, ab.

$$\sigma = \omega \frac{F}{N_T} \qquad (19)$$

σ: Wirkungsquerschnitt; ω: Wechselwirkungswahrscheinlichkeit; F: Bestrahlte Targetfläche; N_T: Anzahl der im Target enthaltenen Teilchen

Das so erhaltene reine Radionuklid wird dann entsprechend weiterverarbeitet (*Abbildung* 14). Das in Abbildung 13 gezeigte Verfahren zur Herstellung von Molybdän-99 steht dabei beispielhaft für viele Verfahren dieser Art. Ein weiteres Beispiel ist Lutetium-177. Es werden derzeit zwei Wege kommerziell genutzt Lutetium-177 am Reaktor herzustellen. Indirekt über die Bestrahlung von einem ^{176}Yb-Target mit Neutronen (Kurzschreibweise: ^{176}Yb(n,γ)^{177}Yb $\rightarrow$ ^{177}Lu), dabei entsteht zunächst das kurzlebige Ytterbium-177 ($t_{1/2}$ = 1,9 h), welches dann zu dem gewünschten Lutetium-177 ($t_{1/2}$ = 6,71 d) zerfällt [24]. Die zweite Möglichkeit ist das direkte Verfahren. Hierbei wird ein ^{176}Lu-Target mit Neutronen bestrahlt (Kurzschreibweise: ^{176}Lu(n,γ)^{177}Lu) wobei direkt das gewünschte Lutetium-177 entsteht. Der Nachteil des Verfahrens ist, dass zusätzlich bis zu 0,1 % Lutetium-177m ($t_{1/2}$ = 160,1 d) entstehen. Die lange Halbwertszeit von Lutetium-177m kann, insbesondere im Abfall- bzw. Abwasser-Management, zu Problemen führen.

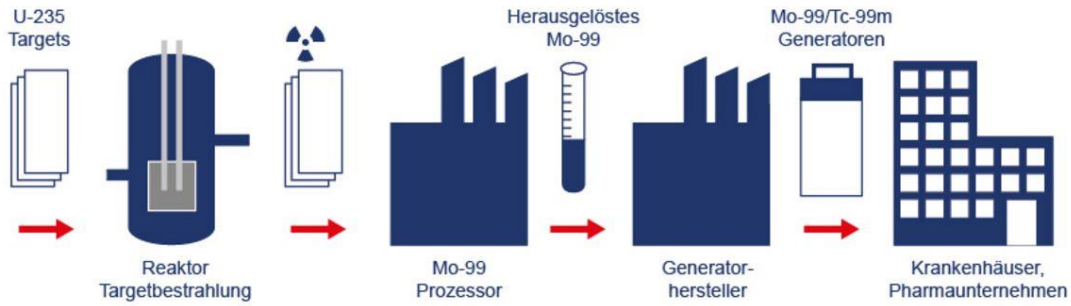

Abbildung 14: Versorgungskette von Technetium-99m für die Anwendung im Krankenhaus [25].

1.2.5 Radionuklid-Generatoren

Radionuklid-Generatoren sind traditionell wichtige Lieferanten für medizinisch verwendete Radionuklide. Die andauernde Entwicklung und ihr anhaltender Erfolg in der diagnostischen Nuklearmedizin sind zum großen Teil auf den ^{99}Mo/^{99m}Tc-Generator zurückzuführen. Dieser wurde 1957 im Brookhaven National Laboratory [26] entwickelt und 1961 erstmalig klinisch erprobt [27]. Die Nuklearmedizin hätte, ohne die kommerzielle Verfügbarkeit dieses Generators und damit von Technetium-99m, nicht zu einem integralen Spezialgebiet der diagnostischen Bildgebung werden können. Mit geschätzten 35 Millionen jährlichen Studien weltweit zählen ^{99m}Tc- zusammen mit ^{68}Ga-Radiodiagnostika zu den am häufigsten genutzten Generator-produzierten Nukliden [28].

Die Nutzung von Radionuklid-Generatoren ist insofern attraktiv da im Vergleich zu den Zyklotron-produzierten Nukliden weniger Equipment und Personal benötigt wird. Es ist daher möglich auf minimalem Raum mit entsprechender Abschirmung relativ kostengünstig eine In-House Produktion zu betreiben.

Tabelle 2: Typen von Radionuklidgeneratoren und Zerfallsarten.

Generator	Mutternuklid $T_{1/2}$	Zerfall	Tochternuklid $T_{1/2}$	Zerfall	Anwendung
^{99}Mo/^{99m}Tc	66 h	β^-	6,01 h	γ	Diagnostik
^{44}Ti/^{44}Sc	60 a	EC	3,93 h	β^+	Diagnostik
^{68}Ge/^{68}Ga	270,8 d	EC	67,71 min	β^+	Diagnostik
^{90}Sr/^{90}Y	28,78 a	β^-	64,10 h	β^-	Therapie

$^{188}W/^{188}Re$	69,4 d	β^-	17,00 h	β^-	Therapie
$^{225}Ac/^{213}Bi$	10 d	α	45,59 min	α	Therapie

Die ersten $^{68}Ge/^{68}Ga$-Generatoren wurden 1964 beschrieben [29]. Prinzipiell ist der Aufbau der unterschiedlichen Generatoren identisch. Ihr Kernstück ist eine Säule, die ein Adsorbermaterial (Matrix) mit aufgetragenem Mutternuklid enthält. Diese befindet sich in einer Abschirmung aus Blei und ist nach außen mit Verschlauchungen verbunden (Abbildung 15). $^{68}Ge/^{68}Ga$-Generatoren können entweder manuell eluiert oder mit einer automatisierten Syntheseanlage verwendet werden.

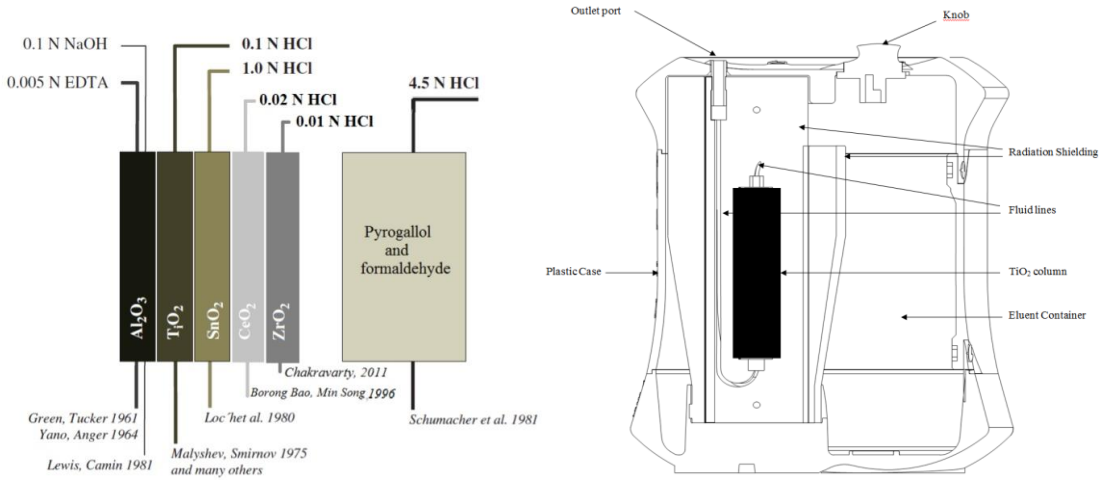

Abbildung 15: Links: Schematische Darstellung der verschiedenen $^{68}Ge/^{68}Ga$-Generatorsysteme [30]. Rechts: Querschnitt durch einen $^{68}Ge/^{68}Ga$-Generator [31].

Das Mutternuklid (Mutter; hier: Germanium-68) ist auf der Matrix fest eingebettet wo es permanent in sein Tochternuklid (Tochter; hier: Gallium-68) zerfällt, welche wiederum in stabiles Zink umwandelt. Der Zerfall und die Bildung von Gallium-68 stehen dabei in einem Gleichgewicht (säkulares Gleichgewicht) mit seiner Mutter. Ist die Halbwertszeit der Mutter ($t_{1/2}$=270,8 d) deutlich größer als die der Tochter ($t_{1/2}$=67,71 min) nähert sich ihre Aktivität mit der Zeit an die der Mutter an (Abbildung 16). Befinden sich beide Radionuklide im Gleichgewicht zerfällt das Gemisch mit der Halbwertszeit der Mutter, bis es durch einen äußeren Einfluss (z. B. Elution) gestört wird. Wird durch Elution die Tochter entfernt, stellt sich das Gleichgewicht nach ca. zehn Halbwertszeiten der Tochter wieder vollständig ein. In der klinischen Routine werden $^{68}Ge/^{68}Ga$-Generatoren in der Regel nach ca. zwei bis fünf ^{68}Ga-Halbwertszeiten erneut eluiert.

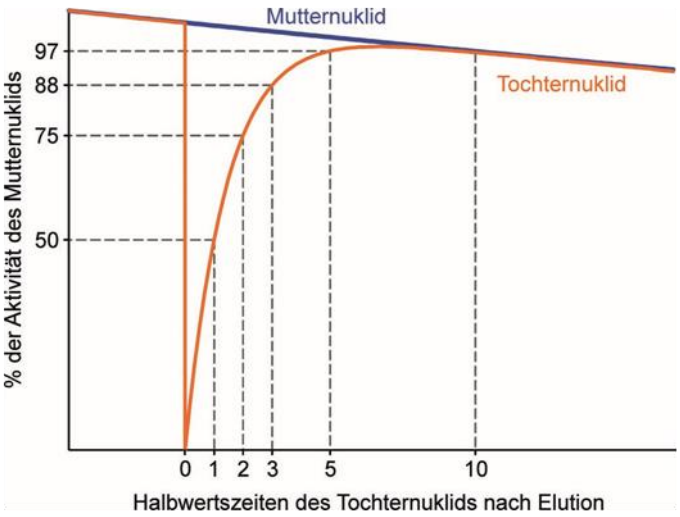

Abbildung 16: Theoretischer Aktivitätsverlauf nach einer Elution des Radionuklidgenerators mit anschließender Regeneration [32].

Derzeit (2020) sind verschiedene ^{68}Ge/^{68}Ga-Generatoren, mit unterschiedlichen Matrizen, kommerziell erhältlich. Bevorzugt werden TiO_2, SnO_2 oder organische Harze als Matrix verwendet. Die Ausbeuten an Gallium-68 im Eluat eines neuen Generators reichen von etwa 60 % (z. B. GalliaPharm; Eckert & Ziegler) bis 80 % (z. B. iThemba LABS) bezogen auf das Kalibrierdatum. Die Ausbeute kann im Laufe der Zeit abnehmen.

Eines der ersten verfügbaren ^{68}Ga-Diagnostika war [^{68}Ga]Ga-EDTA und konnte direkt von den Generatoren eluiert werden. Die salzsauren Eluate der heutigen, kommerziell erhältlichen Generatoren liefern dagegen positiv geladene $^{68}Ga^{3+}$-Ionen anstelle der ^{68}Ga-Komplexe früherer Entwicklungen.

Die einfache Verfügbarkeit der $^{68}Ga^{3+}$-Ionen förderte die Entwicklung weiterer Tracer für die Anwendung [33, 34]. Gleichzeitig erforderte die Radiomarkierung der Vorläufer Reaktionsbedingungen die nicht direkt vom Eluat geliefert werden konnten. Vor allem der niedrige pH, Metallverunreinigungen und das große Volumen des Eluats waren problematisch. Durch die Entwicklung verschiedener Post-Prozessings konnten diese und weitere Probleme adressiert werden [35–37].

Typische Metallverunreinigungen, die reduziert werden können, sind unter anderem Germanium-68, Eisen und Zink. Die Europäische Pharmacopoeia gibt für den Anteil eines Mutternuklids der im Eluat eines medizinisch genutzten Generators vorliegen darf, den sogenannten Durchbruch, Limits vor, die eingehalten werden müssen. Im Fall eines ^{68}Ge/^{68}Ga-Generatoren liegt das Limit für Germanium-68 bei 0,001 % bezogen auf die Gesamtaktivität an Gallium-68 zum Zeitpunkt der Elution [38]. Der Durchbruch ist über

die Lebensdauer des intakten Generators, abgesehen von statistischen Schwankungen, relativ konstant. Entscheidend ist das relative Aktivitätsverhältnis von Mutter zu Tochter. Da sich die durch Elution verfügbare Aktivität an Gallium-68 des Generators mit der Zeit verringert, wird das Verhältnis von Mutter- zu Tochteraktivität kontinuierlich größer, auch wenn der Durchbruch (Ausbluten) der Mutter konstant ist.

Durch die wachsende Palette an Tracern und ihrer zunehmenden Anwendung/Bedeutung in der Nuklearmedizin wuchs nicht nur der Bedarf, sondern auch die Anforderungen an die Herstellung von ^{68}Ge/^{68}Ga-Generatoren (GMP; Zulassung als Medizinprodukt). Als Folge wurden die Generatoren hinsichtlich ihrer Matrix weiterentwickelt [30] und ihre Herstellung den Anforderungen angepasst. Durch ein geeignetes Voraufreinigung des Eluats, aber auch die Verbesserung der Matrix, kann die Nutzungsdauer auf ca. ein Jahr ausgedehnt werden. Durch die Einhaltung der verschiedenen Regularien und die notwendige Zertifizierung für GMP ist der Preis in den letzten Jahren deutlich gestiegen und für zugelassene Generatoren deutlich höher als für nicht zugelassene.

1.2.6 Chelatoren

Radiometall markierte Radiopharmaka bestehen im Allgemeinen aus einem Radionuklid, einem Chelator/Linker und einer biologisch aktiven Komponente, dem Pharmakophor (Abbildung 17). Die verfügbaren Radioisotope die Anwendung in der Nuklearmedizin finden sind Metalle bzw. Metalloide und Nichtmetalle. Sie können entweder direkt als Salz oder zur Markierung der biologisch aktiven Komponente, ohne deren Funktionalität einzuschränken, eingesetzt werden. Salze von Radiometallen wie [^{82}Rb]$RbCl_2$ [39], [^{67}Ga]Ga-Citrat [40], [^{89}Sr]$SrCl_2$ [41] oder Alpharadien ([^{223}Ra]$RaCl_2$) [42] werden so zur Diagnostik und Therapie eingesetzt.

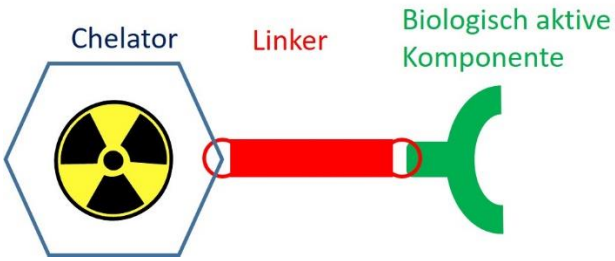

Abbildung 17: Vereinfachte Darstellung des Prinzipiellen Aufbaus eines Tracers.

Damit Target-Vektoren mit einem Radiometall markiert werden können, sind in der Regel Chelatoren und Linker erforderlich. Chelatoren sind mehrzähnige Liganden die, durch

ihre 3D-Struktur, bestimmte Ionen bevorzugt koordinativ binden. Dieses Koordinationsvermögen wird in der Natur von Chlorophyll (Zentralion Mg^{2+}) oder Hämoglobin (Zentralion Fe^{2+}) genutzt. Der Chelator sollte stehts zur Aufgabe passen, die an ihn gestellt wird. Diese entscheidet darüber, welches Ion komplexiert werden soll und vor allem in welcher Umgebung der Komplex stabil sein muss.

Der Linker wird verwendet, um den Chelator mit dem Pharmakophor zu koppeln. Die Interaktion zwischen dem Chelator und der biologisch aktiven Komponente sollte dabei minimal sein und, was am wichtigsten ist, die Pharmakokinetik des Verbandes nicht modifizieren. Es ist dokumentiert, dass der Linker einen tiefgreifenden Einfluss auf die Biodistribution des Pharmakophors hat [43, 44]. Verschiedene Arten von Linkern können verwendet werden, um die Pharmakokinetik zu modulieren. Die Länge, Flexibilität, Hydrophilie und Ladungen (kationisch, anionisch und neutral) sind hierbei Schlüsselfaktoren, die bei der Auswahl eines geeigneten Linkers berücksichtigt werden müssen [45].

Einer der vielseitigsten verfügbaren Chelatoren ist der Makrozyklus DOTA (1,4,7,10-Tetraazacyclododecan 1,4,7,10-Tetraessigsäure, Abbildung 1, Abbildung 18). Er ist seit 1976 bekannt und wurde ursprünglich für die Komplexierung von Lanthanoiden verwendet, da er mit den meisten zwei- und dreiwertigen Metallen stabile Komplexe bildet [46]. Darüber hinaus ist die Synthese von DOTA sehr einfach und schnell, was die Entwicklung vieler Derivate mit verschiedenen funktionellen Gruppen erleichterte, die seine medizinische Anwendung ermöglichten [47]. Die erste und bis heute noch in der Medizin angewandte Form von DOTA ist die Gadotersäure, unfunktionalisiertes DOTA, welches Gadolinium (Gd^{3+}) komplexiert und bis heute weite Anwendung als Kontrastmittel in der Magnetresonanztomographie findet [48].

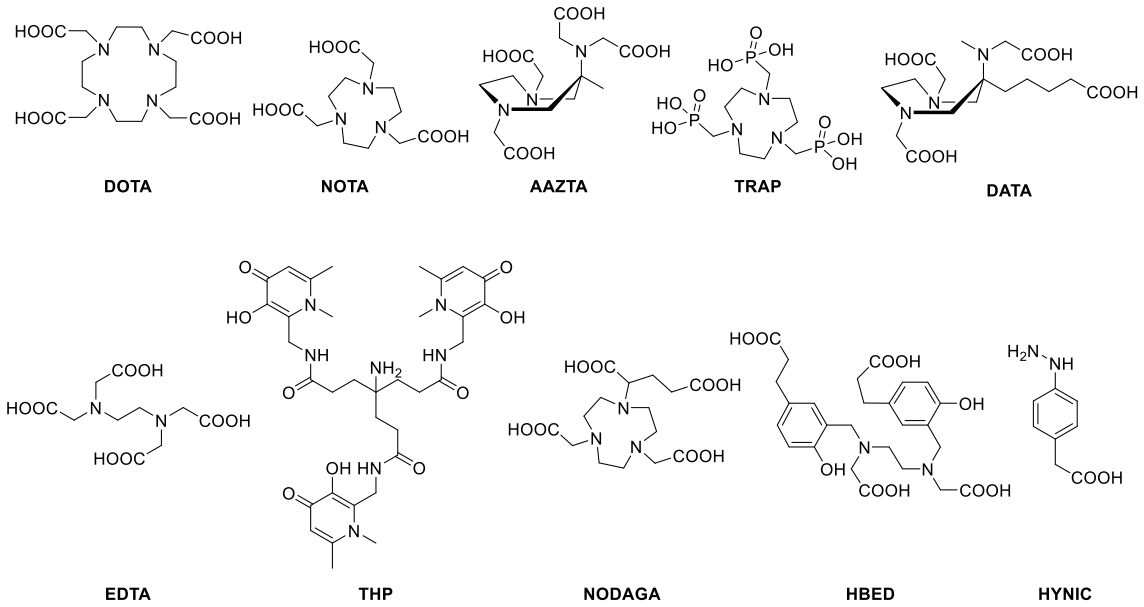

Abbildung 18: Darstellung verschiedener Chelatoren die aktuell in der Nuklearmedizin im Einsatz sind.

Eines der ersten DOTA-Derivate das in der Nuklearmedizin angewandt wurde, ist DOTA-TOC (DOTA-(0)-Phe(1)-Tyr(3))octreotid; INN: Edotreotid, Abbildung 18

Abbildung 18: Darstellung verschiedener Chelatoren die aktuell in der Nuklearmedizin im Einsatz sind.

). In der Diagnostik wird DOTA-TOC mit Positronenemittern (z. B. Gallium-68) und in der Therapie mit alpha-, beta-, oder Auger-Emittern (z. B. Actinium-225, Lutetium-177 [49] oder Iod-125 [50]) markiert [51].

Die Reaktionsbedingungen der Komplexierung mit einem spezifischen Radiometall hängen vor allem von der Halbwertszeit des Radiometalls, seinen chemischen Eigenschaften und dem jeweiligen Chelator ab. So sind, wegen seiner relativ kurzen Halbwertszeit, erhöhte Temperauren (80-100 °C) für die Markierung von DOTA-Derivaten mit Gallium-68 nötig damit die Reaktion ausreichend schnell mit guten Ausbeuten abläuft. Zudem ist ein pH-Wert im Bereich von 3-4 bevorzugt [35]. Diese Bedingungen sind immer auch ein Kompromiss. So steigt einerseits das Komplexierungsvermögen von DOTA mit dem pH-Wert [52], andererseits bildet Gallium bei steigendem pH-Wert zunehmend schwerlösliche Hydroxide (kolloidales Gallium; Kolloide), welche nicht mehr zur Komplexierung zur Verfügung stehen [53]. Diese Bedingungen sind für viele mögliche Tracer (z. B. Antikörper) nicht geeignet und führen zu ihrer Inaktivierung [54].

Anders dagegen sieht es z. B. bei Lutetium-177 aus. Aufgrund seiner deutlich längeren Halbwertszeit ($T_{1/2}$= 6,65 d) kann die Markierungsdauer bei Bedarf auf mehrere Stunden ohne nennenswerte Verluste in der Aktivität des Endproduktes ausgedehnt werden. Zusätzlich bilden sich die in der Markierung störenden Kolloide erst ab einen pH > 6. Dadurch kann der pH-Wert der Reaktion auf 4,5-5 angehoben werden [55]. Der höhere pH-Wert ist von Vorteil, da sich das Markierungspotential des DOTA-Chelators ab einen pH-Wert > 4 deutlich erhöht [52].

Die Forschung arbeitet immer weiter daran, neue, für die medizinische Anwendung mit Radiometallen geeignete, Chelatoren zu entwickeln [56]. Unter anderem in Hinsicht auf die Radiomarkierung von sensiblen Vektoren oder Kit-Synthesen. Letztere sind vor allem bei Technetium-99m im Einsatz. In einer solchen Kit-Synthese sind alle benötigten Chemikalien und der Vorläufer schon soweit vorbereitet, dass nur noch das Radionuklid hinzugefügt werden muss und nach Inkubation und bestandener Qualitätskontrolle das Radiopharmakon direkt appliziert werden kann. Der Vorteil dieser Methode besteht in ihrer Einfachheit und der damit verbundenen sehr guten Verfügbarkeit von Untersuchungsmethoden.

Einer der limitierenden Faktoren für Dauer und Komplexität einer Synthese ist die Halbwertszeit des Radionuklides. Daher sollte ein idealer Chelator selektiv kinetisch aber auch thermodynamisch stabile Komplexe mit dem jeweiligen Radiometall bilden. Eine quantitative Ausbeute ist zu bevorzugen, wenn eine Aufreinigung schwierig oder nicht möglich bzw. gewünscht (z. B. Kit-Synthese) ist.

Jeder Targetvektor hat unterschiedlichen Bedingungen, unter denen er stabil ist bzw. seine Funktionalität erhalten bleibt. Während für PSMA-11 hohe Temperaturen (> 100 °C) für die Funktionalität des Pharmakophors kein Problem darstellen [57] sind Antikörper nicht nur Temperatur-sensibel (> 45 °C), sondern auch empfindlich gegenüber verschiedene organische Lösemittel.

Einer der Chelatoren der diese Probleme adressiert ist NOTA (1,4,7-Triazacyclononanetriessigsäure, Abbildung 18). Studien haben gezeigt das die Komplexierung von NOTA mit Gallium-68 schon bei deutlich milderen Bedingungen (25 °C, 10 min, Ausbeute ≥ 90 %) möglich ist [58–60]. Trotz seines Potentials hat auch NOTA noch Defizite, vorrangig im Komplexierungsvermögen von divalenten Radiometallen, die einen breiten Einsatz verhindern [61].

Ein weiterer geeigneter Chelator für Gallium-68 ist TRAP (Methyl-(hydroxymethyl)phosphinsäure; Abbildung 18). Die Komplexierung erfolgt schneller als mit NOTA bei pH 0 und Raumtemperatur [62]. Daraus resultierend kann das Eluat vom ^{68}Ge/^{68}Ga-Generator

ohne weitere Aufreinigung für eine Markierung mit TRAP verwendet werden. Doch obwohl [^{68}Ga]Ga-TRAP gute Stabilitäten aufweist, ist es aufgrund seiner Trimerisierung nicht immer die beste Wahl [63].

Die Chelatoren TRAP, NOTA und DOTA sind alle Stickstoffbasierte Makrozyklen. Durch die Größe der Ringe wird die Stabilität der Ga-Komplexe beeinflusst, wobei Ga-DOTA ($\log K_{(GaL)} = 21,3$) als größter der drei Ringe die geringste und Ga-NOTA ($\log K_{(GaL)} = 31,0$) bzw. Ga-TRAP ($\log K_{(GaL)} = 26,2$) höhere Stabilitäten aufweisen [64]. Auch für die Stabilität der Komplexe entscheidend sind die Carboxyl-Gruppen. Werden diese zur Bindung an den Targetvektor genutzt verringert sich die Stabilität weiter. Dieser Verlust ist für Ga-Komplexe weniger stark als für größere Metalle wie den Lanthaniden. Während Gallium in einer Oktaeder-ähnlichen Struktur (Koordinationszahl 6; KZ 6) koordiniert, wofür 6 Liganden benötigt werden, bevorzugt die Gruppe der Lanthanide die Struktur der dreifach überkappten trigonalen Prismen (KZ 9), wofür 9 Liganden benötigt werden [65]. Die Ringstruktur von DOTA liefert über seine vier Stickstoffatome vier Koordinationstellen, vier weitere werden über die äußeren Carboxylgruppen bereitgestellt. Entfällt durch die Kopplung des Targetvektors eine der Carboxylgruppen, kann diese die Komplexbildung nun nicht mehr unterstützen. Dieser Verlust an Koordinationsvermögen, wirkt sich weniger auf Metalle mit niedrigen Koordinationszahlen aus.

Ein anderer Ansatz wurde mit THP (Tris(hydroxypyridinon); Abbildung 18) verfolgt. THP ist wie TRAP ein trivalenter Chelator und wurde zunächst zur Markierung von Proteinen und Peptiden unter milden Bedingungen (pH = 7; 5-7 min; RT) genutzt [66]. Ein Vorteil von [^{68}Ga]Ga-THP für die Anwendung ist die Stabilität gegenüber Humanserum [67]. Erste Studien zu ^{68}Ga-Kit-Synthesen mit THP-PSMA konnten realisiert werden [68].

Ein weiterer Chelator der, ähnlich wie DOTA, zunächst als MRT-Kontrastmittel eingesetzt wurde ist AAZTA (1,4-Bis(carboxymethyl)-6-[bis(carboxymethyl)]amino-6-methylperhydro-1,4-diazepin; Abbildung 18) [69]. AAZTA bildet nicht nur mit Gadolinium sondern auch mit Gallium, Scandium oder Lutetium stabile Komplexe, weshalb dessen Anwendungsbereiche weiter erforscht werden [70, 71].

Ein vielversprechendes Derivat von AAZTA ist DATA ((6-pentansäure)-6-(amino)methy-1,4-diazepinetriacetat; Abbildung 18), welches sein Potential auch in klinischen Studien zeigen konnte [72, 73].

AAZTA und DATA sind chimäre Chelatoren. Sie kombinieren einen makrozyklischen 1,4-Diazapamring mit einem freien azyklischen Arm. Diese Verknüpfung von Ring und freien Arm erlaubt es die Markierung unter milden Bedingungen durchzuführen (10 Minuten; pH =4–5,5; RT) [71]. Ein Nachteil von AAZTA ist seine Instabilität in humanem Serum und gegenüber anderen Chelatoren wie z. B. EDTA oder DTPA [70]. DATA dagegen zeigte gegenüber beiden eine höhere Stabilität [70].

Beispiele wie TRAP, DATA und THP (Abbildung 18) ermöglichen eine effiziente Radiomarkierung bei Raumtemperatur, niedrigen pH-Werten oder Substrat-Konzentrationen. Diese Eigenschaften könnten in Zukunft ^{68}Ga-Kit-Präparationen auch mit sensibleren Targetvektoren ermöglichen.

1.2.7 Targetvektoren

Radiopharmaka sind Pharmakophore, die mit einem Radionuklid markiert sind. Das Konzept der Pharmakophore wurde schon 1909 von Paul Ehrlich erstmals beschrieben[74]. Es wird laut IUPAC (International Union of Pure and Applied Chemistry) definiert wie folgt:

„*A pharmacophore is the ensemble of steric and electronic features that is necessary to ensure the optimal supramolecular interactions with a specific biological target structure and to trigger (or to block) its biological response.*

A pharmacophore does not represent a real molecule or a real association of functional groups, but a purely abstract concept that accounts for the common molecular interaction capacities of a group of compounds towards their target structure. The pharmacophore can be considered as the largest common denominator shared by a set of active molecules. This definition discards a misuse often found in the medicinal chemistry literature which consists of naming as pharmacophores simple chemical functionalities such as guanidines, sulfonamides or dihydroimidazoles (formerly imidazolines), or typical structural skeletons such as flavones, phenothiazines, prostaglandins or steroids." [75]

Das Pharmakophor ist definiert über die wesentlichen sterischen und elektronischen, funktionsbestimmenden Punkte, die für eine optimale Interaktion mit dem jeweiligen pharmakologischen Ziel notwendig sind.

Zu den Pharmakophoren gehören unter anderem Salze, Aminosäuren, Peptide, Antikörper oder Nanopartikel. Diese Moleküle können bestimmte Biomarker (z. B. Enzyme, Rezeptoren und Transporter), Zellpopulationen (z. B. krebsassoziierte Fibroblasten, Immunzellen) oder biologische Prozesse (z. B. Energiestoffwechsel, Hypoxie, Azidose und oxidativer Stress) selektiv ansteuern [76].

Konventionelle Pharmazeutika sind so konzipiert und entwickelt, dass sie in die biologischen Prozesse von Krankheiten eingreifen und diese verändern und zu einem positiven Behandlungsergebnis führen, und gleichzeitig eine minimale Toxizität im normalen Gewebe aufweisen. Daher sind die Wirksamkeit und Sicherheit in der Regel zwei der wichtigsten Überlegungen für ein Medikament [77]. Im Vergleich dazu sind Radiopharmaka

so konzipiert, dass sie die Krankheiten nicht-invasiv beeinflussen. Insgesamt wird erwartet, dass ein zielgerichtetes Radiopharmakon mit klinischem Translationspotenzial die folgenden Eigenschaften aufweist [78]:

Hohe Spezifität: Zielspezifische Radiopharmaka interagieren selektiv mit bestimmten Biomarkern (z. B. Enzymen, Rezeptoren oder Transportern) die an verschiedenen biologischen Prozessen in Verbindung mit bestimmten Zellpopulationen und subzellulären Kompartimenten beteiligt sind [79, 80]. Sie stellen biologische Prozesse auf molekularer Ebene dar wobei die hohe Spezifität die unspezifische Aufnahme in andere Gewebe reduziert. Dadurch sind sie sehr nützlich für das Verständnis von einer Krankheit zugrunde liegenden Stoffwechselprozessen aber auch für die Therapie mit radioaktiver Strahlung.

Hohe Bindungsaffinität: Eine hohe Bindungsaffinität zum biologischen Target ist eine Voraussetzung, um eine ideale Anreicherung des Radiopharmakons im Zielgewebe zu erreichen. Um eine hohe Aufnahme innerhalb einer begrenzten Zirkulationszeit zu erreichen, muss das Radiopharmakon eine schnelle Assoziation und eine langsame Dissoziation aufweisen.

Rasches Auswaschen aus Nicht-Zielgeweben: Radiopharmaka sollten renal, hepatobiliär oder über beide Wege ausgeschieden werden. Der Eliminationsweg hängt von mehreren Faktoren ab: der Größe, Lipophilie, Ladung und Plasma-Protein-Bindung. Bei anhaltender Tumoraufnahme verbessert sich der Bildgebungskontrast mit raschem Auswaschen aus Blut und Nicht-Zielgewebe. Darüber hinaus reduziert sich die Strahlenbelastung entschieden für den Patienten.

***in-vivo* Stabilität:** Da Radiopharmaka zumeist injiziert werden und die Geschwindigkeit der Aufnahme im Zielgewebe schwankt (Minuten bei [^{18}F]FDG; Tage bei Antikörpern), müssen sie gegenüber verschiedenen Enzymen, Proteasen, andere Chelatoren oder Ionen, welche im Serum oder im Zielgewebe vorhanden sind, stabil bleiben. Informationen, die durch Metaboliten des Radiopharmakons erhalten werden, machen die Bildauswertung komplexer und verfälschen das Ergebnis. Die Qualität der quantitativen Analyse und, darauf basierend, die Diagnostik hängt stark von der *in-vivo*-Stabilität ab.

Geringe Immunogenität oder Toxizität: Es ist unwahrscheinlich, dass die applizierte Mikrodosis des Pharmakons zu einer allergischen Reaktion führt oder pharmakologische Wirkung hat. Trotzdem müssen die biologischen Wirkungen, die ein Radiopharmakon verursacht genau überwacht werden, da einige zum Teil mehrfach eingesetzt werden [81].

Zugänglich und kosteneffektiv: Radiopharmazeutika, einschließlich der Vorläufer für die Radiomarkierung, sollten leicht und günstig verfügbar sein, um eine klinische Routineanwendung zu ermöglichen.

In einigen Fällen hat das Radionuklid auch die biologische Funktion inne und kann direkt, z.B. in Form seines Salzes, als Radiopharmakon verwendet werden. So wird z.B. die Durchblutung des Herzmuskels im PET mit [^{82}Rb]$RbCl_2$, alternativ H_2[^{15}O]O oder [^{13}N]NH_3, dargestellt [39, 82]. Auch Iod, dessen Isotope zur Diagnose und Therapie eingesetzt werden, kommt gegebenenfalls ohne zusätzlichen Targetvektor aus. In der Diagnostik wird unter anderem Iod-123 [83], in der Brachytherapie Iod-125 [50] und in der Schilddrüsentherapie Iod-131 [84], verwendet.

In anderen Fällen kann der Targetvektor ohne jeglichen Funktionalitätsverlust mit einem Radionuklid markiert werden. So ist [^{11}C]Cholin biochemisch nicht von natürlichem Cholin unterscheidbar. Die relativ kurze Halbwertszeit von Kohlenstoff-11 (20,364 min) erfordert jedoch eine komplexe Infrastruktur vor Ort, und die Bildaufnahme muss früh nach der Injektion erfolgen. Diese praktischen Probleme führten zur Entwicklung von fluorierten Derivaten wie [^{18}F]Fluorethyl-Cholin (FEC) oder [^{18}F]Fluormethyl-Cholin (FCH) [85]. Diese Tracer zeigen Unterschiede in ihrer Biodistribution zu Cholin, welche allerdings für die klinische Anwendung vernachlässigbar sind [85].

Ein anderer Ansatz in der Diagnostik ist die Darstellung von Stoffwechselvorgängen (z. B. Zuckermetabolismus). Viele Tumorarten haben eine erhöhte Stoffwechselrate und damit zumeist verbunden einen höheren Energiebedarf [86]. Die als Warburg-Effekt bezeichnete Umwandlung der Energiegewinnung durchlaufen ca. 70 % der Krebszellen, hierbei scheidet die Krebszelle Laktat aus anstatt diese dem Zitratzykluss zur verfügung zu stellen [87]. Der erhöhte Energieverbrauch kann dann mit Hilfe von [^{18}F]FDG , welches sich als Goldstandard in der PET-Diagnostik etabliert hat, dargestellt werden [88].

Das Prostata-spezifisches Membran-Antigen (PSMA) ist ein Transmembranmolekül im Prostatagewebe und wird bei den meisten Prostatakrebsarten stark überexprimiert [89, 90]. Sein extrazellulärer N-terminaler Teil, der die katalytische Domäne enthält, ist für ein selektives Tumortargeting geeignet [91]. Aufgrund der geringen Expression von PSMA in gesundem Gewebe, mit Ausnahme von Speichel- und Tränendrüsen, ist eine hochdosierte Radioligandentherapie (RLT) möglich. Der aktuell am häufigsten genutzten Tracer in der Diagnostik ist [^{68}Ga]Ga-PSMA-11 [92].

Somatostatin-Rezeptoren (SSTR) gehören zur Gruppe von G-Protein-gekoppelten Rezeptoren, die in Neuronen und endokrinen Zellen vorkommt und eine hohe Dichte im

Gehirn, in den peripheren Neuronen, in der endokrinen Pankreas und im Gastrointestinaltrakt aufweisen. Es sind fünf Subtypen bekannt (SSTR1-SSTR5), wobei durch alternative Spleißung der SSTR2-mRNA zwei Subtypen hinzukommen, nämlich SSTR2A und SSTR2B [93]. Die meisten neuroendokrinen Tumore (NET) überexprimieren SSTRs, die als Targets für die Theranostik verwendet werden können. [94]. NET sind eine heterogene Gruppe verschiedener Neoplasmen, die in den Zellen neuroendokrinen Ursprungs in vielen verschiedenen Organen entstehen, am häufigsten jedoch im Gastrointestinaltrakt und in der Lunge. Da die metabolische Stabilität von natürlichem Somatostatin sehr gering (1-3 min) ist, wurden synthetische Analoga mit wesentlich höherer Stabilität entwickelt. In der Diagnose bzw. Therapie von neuroendokrinen Tumoren wird z. B. [^{68}Ga]Ga-DOTA-TOC bzw. [^{177}Lu]Lu-DOTA-TATE verwendet, die SSTR als Target ansteuern [95, 96].

Bei vielen Tumorarten treten Metastasen des Knochens als Nebenerkrankung auf, welche die Lebensqualität und -erwartung der Patienten signifikant beeinflussen. Hier werden Knochen-affine Targetvektoren eingesetzt, welche z. B. an das im Knochen enthaltene Mineral Hydroxylapatit binden [97]. Zu diesen zählen unter anderen [^{68}Ga]Ga-DOTA-ZOL [98], [^{177}Lu]Lu-EDTMP (Ethylendiamintetramethylen Phosphorsäure [99]), [^{99m}Tc]Tc-MDP (Methylendiphosphonat; [100]), oder [^{99m}Tc]Tc-HDP (Hydroxymethylenbisphosphonat; [101]).

1.3 Theranostik

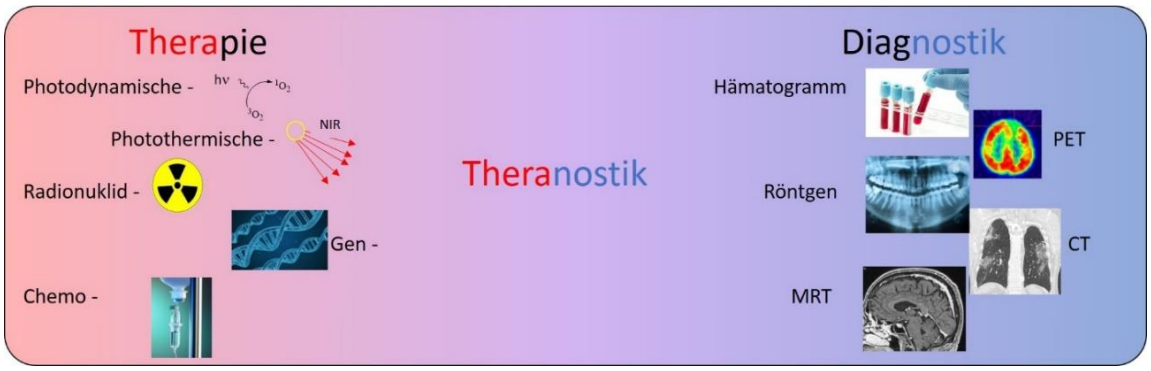

Abbildung 19: Darstellung einige der wichtigsten Verfahren zu Diagnose und Therapiemöglichkeiten von Tumorerkrankungen.

2005 wurde erstmals der Begriff Theragnostik (Theranostik) für die Beschreibung des Einsatzes bildgebender Diagnostik zur Therapieplanung in der Radioonkologie verwendet [102]. Theranostik ist definiert als Verwendung von Informationen aus medizinischen

Diagnoseverfahren zur Bestimmung der optimalen Therapie für einen einzelnen Patienten [102].

Das erste Radiotheranostikum der Nuklearmedizin war Radiojod (Iod-131) [103]. Zur Behandlung gutartiger Schilddrüsenerkrankungen mit Radiojod sind Empfehlungen für eine prätherapeutische Dosimetrie in der europäischen Leitlinie enthalten [104].

Anhand der Pharmakokinetik eines diagnostischen Radiopharmakons kann die Expression spezifischer Tumormarker bei einem Patienten nachgewiesen und quantifiziert werden. Darauf basierend kann eine Vorhersage über den Therapieverlauf getroffen werden. Die Therapie wird mit Hilfe einer darauffolgenden Dosimetrie geplant und mit Kontrollmessungen überwacht. Diese Kontrollmessung ermöglicht gegebenenfalls notwendige Anpassungen zu planen (Abbildung 20). Zudem liefert die Dosimetrie notwendige Daten in Hinsicht auf Effizienz und Toxizität neuer Tracer in der Behandlung [105].

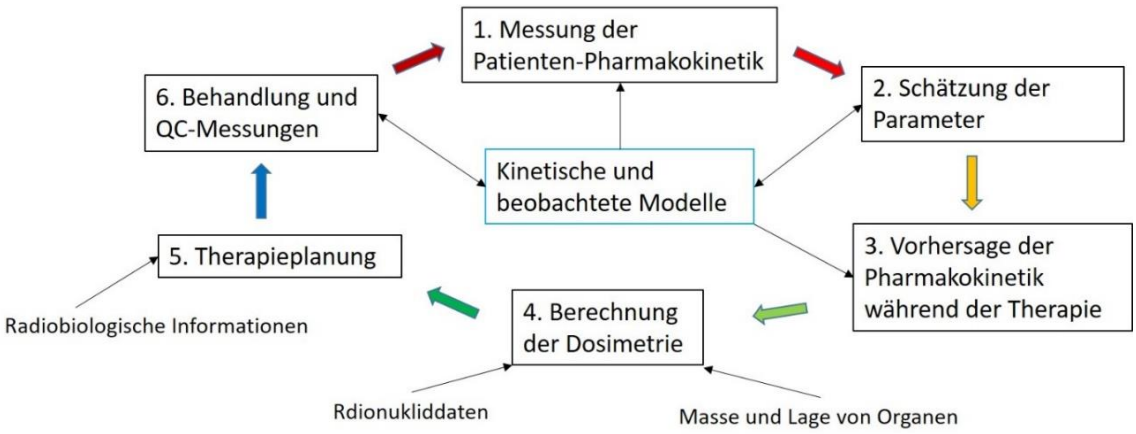

Abbildung 20: Vorgehensweise bei der individualisierten nuklearmedizinischen Therapie [106].

Für die Dosimetrie sind mehrere Schritte notwendig. Zuerst muss eine quantitative Bildgebung zu verschiedenen Zeitpunkten durchgeführt werden, um die Aktivität in den im Fokus stehenden Organen über die Zeit zu beurteilen. Die etablierte Methode beruht auf der Messung der Pharmakokinetik durch serielle γ-Kamera-Scans. Die Verwendung von SPECT-CT (oder, falls möglich, PET/CT) erhöht die quantitative Genauigkeit deutlich [107]. Diese hängt auch von einer zuverlässigen Kalibrierung und sorgfältigen Anpassung der Kamera- und Rekonstruktionseinstellungen ab. Für die Organ- oder Läsionsdosimetrie müssen individuelle Organ- oder Läsionsvolumina bestimmt werden. So kann beispielsweise bei der CT die Verwendung von Standardorganvolumina falsch sein und zu einer ernsthaften Unter- oder Überschätzung der absorbierten Dosen führen. Dies

kann zu einer Über- bzw. Unterdosierung führen, wodurch der Tumor nicht wirksam bekämpft oder gesundes Gewebe in Mitleidenschaft gezogen werden kann [108].

Der zweite Schritt besteht darin Zeit-Aktivitätskurven für die Akkumulation der Radioaktivität in den Organen und Läsionen zu erstellen. Diese wird dann über die Zeit zu integriert, um die Gesamtzahl der in den sogenannten Quellorganen auftretenden Zerfälle zu erhalten. Zu diesem Zweck ist es wichtig, sowohl die optimalen Zeitpunkte als auch die optimale Anpassungsfunktion zu wählen [108].

Der letzte Schritt ist die Wahl des S-Wertes. Der S-Wert, ist die radionuklidspezifische absorbierte Dosisleistung pro Aktivitätseinheit, die in die Zielregion von der Quellregion abgegeben wird. Der S-Wert berücksichtigt die bei jedem radioaktiven Zerfall freigesetzte Energie sowie die relative Geometrie des Quellorgans und des Zielorgans, für das die Energiedosis berechnet werden soll. So ist die kumulierte Aktivität von biologischen Parametern abhängig, während der S-Faktor die physikalischen Komponenten der Energiedosis berücksichtigt [108]. Es wird keine Annahme bezüglich der Quell- oder Zielorgane getroffen, außer dass die Verteilung der Aktivität im Quellorgan homogen ist. Die Quell- und Zielorgane können von beliebiger Größe oder Zusammensetzung sein. Wenn die Aktivität im Quellorgan heterogen verteilt ist, ist es theoretisch möglich, das Quellorgan in kleinere Volumina zu unterteilen, in denen die Aktivität als homogen betrachtet werden kann. S-Wert-Berechnungen hängen stark von der Wahl des Modells ab. Wenn tabellierte S-Werte verwendet werden, die aus mathematischen anthropomorphen Phantomen berechnet werden, dann sollten die Massen der Organe an die Gewichte der Organe der Patienten angepasst werden. Gegenwärtig werden häufig voxelbasierte (in der 3D-Computergrafik stellt ein Voxel einen Wert auf einem regelmäßigen Gitter im dreidimensionalen Raum dar) S-Wert Berechnungen für die patientenspezifische Dosis verwendet, wie z. B. in der Software NUKDOSE [109]. Die so berechnete Dosisverteilung ist einer der Hauptindikatoren für die Bewertung des festgelegten Therapieplans. Aufgrund der Dosisverteilung im Patienten kann der behandelnde Arzt entsprechende Anpassungen vornehmen um einen optimalen Therapieverlauf zu gewährleisten [110].

2. **Problemstellung und Zielsetzung**

In der vorliegenden Dissertation wurden mehrere Aspekte der täglichen radiopharmazeutischen Routine in der Nuklearmedizin bearbeitet. Der Fokus lag dabei auf der Translation von neuen Tracern aus der Forschung in die klinische Anwendung.

Entscheidende Regularien und Konzepte, welche bei der Herstellung von Radiopharmaka zu beachten sind, sind zum einen GMP (**G**ood **M**anufacturing **P**ractice [111]), das Arzneimittelbuch [112] und der Strahlenschutz [113]. Sie beeinflussen jeden Gesichtspunkt der Herstellung und Anwendung eines Radiopharmakons und inwieweit sie für den klinischen Alltag Anwendung finden. Oftmals ist ein Spagat zwischen Strahlenschutz und GMP notwendig, da hier, unter Umständen, konträre Anforderungen vorliegen können.

In den jungen Jahren der ^{68}Ga-markierten Radiotracer waren der Bedarf und die Zahl der damit verbundenen Synthesen überschaubar. Häufig wurden wenige Synthesen pro Woche benötigt. Diese konnten in manuellen Verfahren durchgeführt werden, wenn der Strahlenschutz gegeben war. Hinsichtlich GMP waren die Behörden, zumindest in Deutschland, bei dem sehr kleinen Patientenkollektiv lange Zeit sehr tolerant. Erst mit dem Erfolg von PSMA-11 [114] in der Prostatadiagnostik steigerten sich die Patientenzahlen und der damit verbunde Bedarf an Synthesen. Gleichzeitig stiegen die Anforderungen des Strahlenschutzes (mehr Synthesen = höhere Dosisbelastung des herstellenden Personals) aber auch an die Herstellung (Ausgangsmaterialien, Umgebung, Abfüllung etc.). Infolgedessen wurden automatisierte Module immer attraktiver. Die Hersteller, welche bis dato hauptsächlich Module für Fluor-18 anboten, passten ihr Angebot dem Bedarf an Gallium-68 an. Die Module bieten die Möglichkeit verschiedene Radiopharmaka mit robusten Synthesen und GMP-konformen Materialien bei geringer Dosisbelastung für das Personal herzustellen. Gleichzeitig wurde die Entwicklung neuer Tracer für Diagnostik und Therapie vorangetrieben was wieder zu steigenden Patientenzahlen führte. Eine der großen Herausforderungen der klinischen Routine ist es deshalb aktuell der Nachfrage gerecht zu werden, ökonomisch zu arbeiten und dabei der Gesundheit des Personals und dem Schutz der Patienten Rechnung zu tragen.

Teilprojekt: DOTA-ZOL

Ein Tracer für die Translation in die klinische Routine war DOTA-ZOL. Ein neues Agens sowohl für die Diagnostik als auch Therapie von Knochenmetastasen und anderen Knochen-umwandelnden Prozessen (z. B. Entzündungen). Ziel der vorliegenden Arbeit war die Implementierung der Radiomarkierung und Qualitätskontrolle in die klinische Routine

unter Beachtung der Anforderungen von Strahlenschutz und Arzneimittelbuch an ^{68}Ga/^{177}Lu-markierte Radiopharmaka.

Ausgangsbasis für die Etablierung von DOTA-ZOL waren eine manuelle Markierungsmethode mit Gallium-68 bzw. Lutetium-177 und eine DC-Methode für die Qualitätskontrolle. Für Lutetium-177 soll eine automatisierte Synthese ebenso wie eine vollständige Qualitätskontrolle evaluiert, validiert und etabliert werden, welche als Grundlage für eine analoge ^{68}Ga-Methode dient. Ansätze aus der Literatur zur Qualitätskontrolle sollen verfolgt und im Anschluss auch die gegebene Radiomarkierung nachverfolgt, evaluiert sowie optimiert werden. Die knochenaffinen Tracer sollen anschließend für klinische Dosimetriestudien zur verfügung stehen. Hierfür soll deren Potential für Diagnostik und Therapie von osteoblatstischen Knochenmetastasen untersucht.

Im Rahmen dieses Teilprojekts sind folgende Publikationen veröffentlicht worden:

- Michael Meisenheimer, Stefan Kürpig, Markus Essler, Elisabeth Eppard; DOTA-ZOL: A Promising Tool in Diagnosis and Palliative Therapy of Bone Metastasis—Challenges and Critical Points in Implementation into Clinical Routine; *Molecules* 2020, 25(13), 2988
- Khawar, A., Eppard, E., Roesch, F., Ahmadzadehfar, H., Kürpig, S., Meisenheimer, M., Gaertner, F., Essler, M., Bundschuh, R., Preliminary results of biodistribution and dosimetric analysis of [^{68}Ga]Ga-DOTAZOL: a new zoledronate-based bisphosphonate for PET/CT diagnosis of bone diseases; *Ann Nucl Med* 2019, 33, 404
- Khawar, A., Eppard, E., Roesch, F., Ahmadzadehfar, H., Kürpig, S., Meisenheimer, M., Gaertner, F., Essler, M., Bundschuh R., Biodistribution and post-therapy dosimetric analysis of [^{177}Lu]Lu-DOTA^{ZOL} in patients with osteoblastic metastases: first results; *EJNMMI Res* 2019*,* **9,** 102

Teilprojekt: PSMA

Die Markierung von PSMA-11 mit Gallium-68 wurde in der Anfangszeit noch manuell durchgeführt. Es wurde jedoch sehr schnell deutlich, dass der Strahlenschutz des Personals bei dem Patientenaufkommen nicht mehr gewährleistet werden kann. Auf Grundlage schon bekannter automatisierten Methoden für DOTA-TOC bzw. DOTA-TATE soll je eine eigenständige Methode für PSMA-11 bzw. PSMA-617 für Gallium-68 und Lutetium-177 entwickelt und für den Routineeinsatz validiert werden. Die Methoden werden, unter Berücksichtigung von GMP und Strahlenschutz, in den klinischen Alltag implementiert und etabliert. Für eine Markierung mit dem nicht-standard Isotop Scandium-44 soll

zuerst eine manuelle Synthese und, darauf aufbauend, eine automatisierte entwickelt und validiert werden. Ebenso soll in Anlehnung an die Pharmakopoeia eine geeignete Qualitätskontrolle etabliert werden. Anschließend soll das neue PET-Isotop in klinischen Studien mit dem Standard Gallium-68 verglichen werden.

Im Rahmen dieses Teilprojekts sind folgende Publikationen veröffentlicht worden:

- Lara Schwarte, Lena Thomas, Elisabeth Eppard, Michael Meisen-heimer, Christof Weiss-Wichert, Rolf Fimmers, et al. Comparison of Tumor Heterogeneity Assessed with Textural Parameters in ^{68}Ga-PSMA PET/CT and ^{177}Lu-PSMA SPECT/CT in Patients with Meta-staticProstate Cancer; *Biomed J Sci & Tech Res*, 2018, 11(5)
- Ambreen Khawar; Elisabeth Eppard; Jean Sinnes; Frank Roesch; Hojjat Ahmadzadehfar; Stefan Kürpig; Michael Meisenheimer; Florian Gaertner; Markus Essler; Ralph Bundschuh; Prediction of Nor-mal Organ Absorbed Doses for [^{177}Lu]Lu-PSMA-617 Using [^{44}Sc]Sc-PSMA-617 Pharmacokinetics in Patients With Metastatic Castration Resistant Prostate Carcinoma; *Clinical Nuclear Medicine.* 2018, 43(7), 486
- Ambreen Khawar; Elisabeth Eppard; Jean Sinnes; Frank Roesch; Hojjat Ahmadzadehfar; Stefan Kürpig; Michael Meisenheimer; Florian Gaertner; Markus Essler; Ralph Bundschuh; [^{44}Sc]Sc-PSMA-617 Biodistribution and Dosimetry in Patients With Metastatic Cas-tration-Resistant Prostate Carcinoma; *Clinical Nuclear Medicine.* 2018, 43(5), 323
- Yordanova, A., Linden, P., Hauser, S. Meisenheimer, M., Kürpig, S., Feldmann, G., Gaertner, F., Essler, M., Ahmadzadehfar, H. Out-come and safety of rechallenge [^{177}Lu]Lu-PSMA-617 in patients with metastatic prostate cancer; *Eur J Nucl Med Mol Imaging* 2019, 46, 1073

Teilprojekt: Prozessoptimierung

Während der Radiomarkierung sind die Vorläufersubstanzen direkt der ionisierenden Strahlung ausgesetzt, wodurch sie beschädigt werden können. Hinsichtlich der Radiolyse, die während der Markierung entstehen kann, soll für bestehende und neue Synthesen Inhibitoren getestet werden. Bekannte Radiolyseinhibitoren sind unter anderem Ascorbat, Wasser und Ethanol. Da die Festphasenaufreinigung der Modulsynthese Ethanol als Elutionsmittel der aufgereinigten Radiopharmaka ([^{68}Ga]Ga-DOTA-TOC & [^{68}Ga]Ga-PSMA-11) verwendet, wäre dessen Einsatz als Inhibitor während der Synthese wünschenswert. Außerdem soll überprüft werden, ob die verwendeten Mengen Ethanol in der Lage sind die Markierungseffizienz zu steigern. Beides wird anhand von [^{68}Ga]Ga-

DOTA-TOC bzw. -TATE evaluiert. Auf Basis der erhaltenen Ergebnisse wird eine Methodik für die klinische Routineproduktion erarbeitet und implementiert.

In einer retrospektiven Analyse wird die Auswirkung der resultierenden Änderungen in der Routine hinsichtlich Zuverlässigkeit und Ausbeute überprüft. Zu diesem Zweck werden die verschiedenen Prozesse (optimierte Manuell, Modul) statistisch untersucht und miteinander verglichen.

Im Rahmen dieses Teilprojekts sind folgende Publikationen veröffentlicht worden:

- Meisenheimer, M., Kürpig, S., Essler, M., Eppard, E., Ethanol ef-fects on ^{68}Ga-radiolabelling efficacy and radiolysis in automated synthesis utilizing NaCl post-processing; *EJNMMI radiopharm. chem.* 2019, 4, 26
- Meisenheimer, M., Kürpig, S., Essler, M., Eppard, E. Maunual vs automated ^{68}Ga-radiolabelling – A comparison of optimized processes. *J Labelled Comp Radiopharm.* 2020; 63, 162

Teilprojekt: Kontrolle zellulärer Transportmechanismen

Immer noch strittig ist die Frage, ob NAPMT oder GLUT1 das hauptsächliche zelluläre Ziel des GLUT1-Inhibitors STF-31 ist. Daher soll die Spezifität des Medikaments erneut untersucht werden. Hierzu werden Kurzzeit-Aufnahmeexperimente mit [^{18}F]FDG durchgeführt.

Im Rahmen dieses Teilprojekts ist folgende Publikation veröffentlicht worden:

- Kraus, D., Reckenbeil, J., Veit, N. Kürpig, S., Meisenheimer, M., Beier, I., Stark, H., Winter, J., Probstmeier, R. Targeting glucose transport and the NAD pathway in tumor cells with STF-31: a re-evaluation; *Cell Oncol.* 2018, 41, 485

Teilprojekt: Implementierung neuer Tracer für klinische Studien

Für klinischen Studien müssen die betreffenden Tracer auch unter GMP Bedingungen hergestellt werden. Das bedeutet in der Regel, dass basierend auf einer publizierten Methode eine für die klinische Anwendung adäquate entwickelt werden muss. Dafür soll zuerst die gegebene manuelle-Methode nachvollzogen und notwendige Anpassungen vorgenommen werden, z. B. um eine eine Sterilfiltration zu ermöglichen. Des Weiteren soll untersucht werden, ob eine Aufreinigung des Produktes möglich und integrierbar ist. Diese bietet den Vorteil, dass auch bei eventuellen Abweichungen in der Synthese noch ausreichend Produkt zur Verfügung steht, welches geeignete Reinheit besitzt. Ist dies alles für die manuelle Methode erreicht worden, soll geprüft werden, ob es auf dem Modul adaptiert werden kann.

Für den direkten Vergleich von DOTA-TOC gegen DATA-TOC in einer klinischen Studie soll zuerst eine adäquate manuelle Methode entwickelt werden, die es ermöglicht, erste Patienten-geeignete Dosen herzustellen. Auf dieser Grundlage soll des Weiteren eine Automatisierung für das Kassettenmodul erarbeitet werden. Für die Qualitätskontrolle sollen die gegebenen Methoden validiert und auf Zuverlässigkeit hin überprüft werden. Die beiden Tracer sollen in einer klinischen Studie hinsichtlich ihres Potenzials bei der Erkennung von Lebermetastasen verglichen werden.

DATA5m.SA.FAPi kann hilfreich sein, um eine Vielzahl von malignen und benignen Tumoren zu charakterisieren. Es besteht darüber hinaus Hinweise darauf, dass aktivierte Fibroblasten sichtbar gemacht werden können, die eine wichtige Rolle im Wachstum bestimmter Tumorarten spielen. Der neue Tracer DATA5m.SA.FAPi soll in einer ersten Humananwendung genutzt werden. Hierzu soll eine manuelle Methode und direkt darauf aufbauend eine automatisierte Methode entwickelt werden. Die Literatur-bekannten Qualitätskontrollen sollen überprüft, validiert und gegebenenfalls angepasst werden.

Im Rahmen dieses Teilprojekts ist folgende Publikation veröffentlicht worden:

- Kreppel B, Gärtner FC, Marinova M, Atteberger U, Meisenheimer M, Toma M, et al. [^{68}Ga]Ga-DATA5m.SA.FAPi PET/CT: Specific Tracer-uptake in Focal Nodular Hyperplasia and potential Role in Liver Tumor Imaging. *Nuklearmedizin.* 2020, 59, 387
- F.C. Gärtner, T. Plum, B. Kreppel, E. Eppard, M. Meisenheimer, H. Strunk, R.A. Bundschuh, J.P. Sinnes, F. Rösch, M. Essler; Clinical evaluation of [68Ga]Ga-DATA-TOC in comparison to [68Ga]Ga-DOTA-TOC in patients with neuroendocrine tumours; *Nuclear Medi-cine and Biology* 2019, 76–77, 1-9

3. References

1. Demografischer Wandel in Deutschland: Ursachen und Folgen. 01.08.2019. https://www.destatis.de/DE/Themen/Querschnitt/Demografischer-Wandel/_inhalt.html#sprg371138. Accessed 15 Jul 2020.
2. Robert Koch-Institut. Krebs in Deutschland | 2015/2016.
3. Krebsinformationsdienst DK. Krebsinformationsdienst, Deutsches Krebsforschungszentrum. 29.07.2020. https://www.krebsinformationsdienst.de/. Accessed 29 Jul 2020.
4. Koelzer. Strahlenexposition des Menschen, 2019-01-01.
5. Radioaktivität, natürliche. 2020. https://www.geothermie.de/bibliothek/lexikon-der-geothermie/r/radioaktivitaet-natuerliche.html. Accessed 20 Jul 2020.
6. Russell NS, Begg AC. Editorial radiotherapy and oncology 2002: predictive assays for normal tissue damage. Radiotherapy and Oncology. 2002;64:125–9. doi:10.1016/S0167-8140(02)00189-5.
7. BENTZEN SM, OVERGAARD M. Clinical Radiobiology and Normal-Tissue Morbidity after Breast Cancer Treatment. In: Altman KI, Lett JT, editors. Relative Radiation Sensitivities of Human Organ Systems. Burlington: Elsevier Science; 1994. p. 25–51. doi:10.1016/B978-0-12-035418-4.50006-5.
8. Burnet NG, Johansen J, Turesson I, Nyman J, Peacock JH. Describing patients' normal tissue reactions: Concerning the possibility of individualising radiotherapy dose prescriptions based on potential predictive assays of normal tissue radiosensitivity. Int. J. Cancer. 1998;79:606–13. doi:10.1002/(SICI)1097-0215(19981218)79:6<606::AID-IJC9>3.0.CO;2-Y.
9. Wechselwirkung ionisierender Photonenstrahlung. In: Krieger H, editor. Grundlagen der Strahlungsphysik und des Strahlenschutzes. 2nd ed. Wiesbaden: Teubner; 2007. p. 158–206. doi:10.1007/978-3-8351-9128-0_4.
10. Mineralienatlas - Fossilienatlas. 31.07.2020. https://www.mineralienatlas.de/lexikon/index.php/alpha-Spektrometrie. Accessed 31 Jul 2020.
11. Griffiths DJ. Einführung in die Physik des 20. Jahrhunderts: Relativitätstheorie, Quantenmechanik, Elementarteilchenphysik und Kosmologie. Hallbergmoos: Pearson; 2015.

12. Mogensen OE. Positron Annihilation in Chemistry. Berlin, Heidelberg: Springer; 1995.

13. Mayer-Kuckuk T. Kernphysik: Eine Einführung. 6th ed. Stuttgart: Teubner; 1994.

14. Hevesy G von, Paneth F, Lawson RW. A Manual of Radioactivity: Oxford University Press, H. Milford; 1926.

15. Schröder KA, Pelsers L, Baumgartner M, Berger H, Bernadac M-L, Grammont C, et al. Wege des Pointillismus: Seurat, Signac, Van Gogh. München, Wien: Hirmer; Albertina; 2016.

16. der Physik W. PET und SPECT: Diagnose in der Nuklearmedizin. 24.08.2020. https://www.weltderphysik.de/gebiet/leben/radiopharmaka/pet-und-spect/. Accessed 24 Aug 2020.

17. Boellaard R, O'Doherty MJ, Weber WA, Mottaghy FM, Lonsdale MN, Stroobants SG, et al. FDG PET and PET/CT: EANM procedure guidelines for tumour PET imaging: version 1.0. European Journal of Nuclear Medicine and Molecular Imaging. 2010;37:181–200. doi:10.1007/s00259-009-1297-4.

18. Bengel FM, Ziegler SI, Avril N, Weber W, Laubenbacher C, Schwaiger M. Whole-body positron emission tomography in clinical oncology: comparison between attenuation-corrected and uncorrected images. Eur J Nucl Med. 1997;24:1091–8. doi:10.1007/BF01254239.

19. Bettinardi V, Pagani E, Gilardi MC, Landoni C, Riddell C, Rizzo G, et al. An automatic classification technique for attenuation correction in positron emission tomography. Eur J Nucl Med. 1999;26:447–58. doi:10.1007/s002590050410.

20. Hutton BF. The origins of SPECT and SPECT/CT. European Journal of Nuclear Medicine and Molecular Imaging. 2014;41 Suppl 1:S3-16. doi:10.1007/s00259-013-2606-5.

21. Wille K. Physik der Teilchenbeschleuniger und Synchrotronstrahlungsquellen: Eine Einführung. 2nd ed. Wiesbaden: Springer Fachmedien GmbH; 1996.

22. Guest G. Electron cyclotron heating of plasmas. Weinheim: VCH; 2009.

23. Vértes A, Nagy S, Klencsár Z, Lovas RG, Rösch F, editors. Handbook of Nuclear Chemistry. 2nd ed. Boston, MA: Springer Science+Business Media B.V; 2011.

24. Verfahren zur Herstellung trägerfreier hochreiner 177Lu-Verbindungen sowie trägerfreie 177Lu-Verbindungen - European Patent Office - EP 2546839 B1.

25. Molybdän-99 - TUM FRMII. 06.08.2020. https://www.frm2.tum.de/industrie-medizin/radioisotopen-produktion/molybdaen-99/. Accessed 6 Aug 2020.

26. Stang LG, Tucker WD, Doering RF, Weiss AJ, Greene MW, Banks HO. Development of methods for the production of certain short-lived radioisotopes. Radioisotopes in Scientific Research. 1958;1:50–70.

27. HARPER PV. Preliminary observations on the use of six-hour ^Tc as a tracer in biology and medicine. Semiannual Report, Argonne Cancer Research Hospital. 1962;18:76.

28. The Supply of Medical Radioisotopes: OECD; 2019.

29. Gleason GI. A positron cow. The International Journal of Applied Radiation and Isotopes. 1960;8:90–4. doi:10.1016/0020-708X(60)90052-1.

30. Rösch F. (68)Ge/ (68)Ga generators: past, present, and future. Recent Results Cancer Res. 2013;194:3–16. doi:10.1007/978-3-642-27994-2_1.

31. Krautwurst M-L. Zulassungsformulier IRE Generator.

32. Notni J. Mit Gallium-68 in ein neues Zeitalter? Nachr. Chem. 2012;60:645–9. doi:10.1002/nadc.201290233.

33. Reischl G, editor. Targets, tracers and translation - novel radiopharmaceuticals boost nuclear medicine.

34. Nanabala R, Anees MK, Sasikumar A, Joy A, Pillai MRA. Preparation of (68)GaPSMA-11 for PET-CT imaging using a manual synthesis module and organic matrix based (68)Ge/(68)Ga generator. Nuclear Medicine and Biology. 2016;43:463–9. doi:10.1016/j.nucmedbio.2016.05.006.

35. Breeman WAP, Jong M de, Blois E de, Bernard BF, Konijnenberg M, Krenning EP. Radiolabelling DOTA-peptides with 68Ga. European Journal of Nuclear Medicine and Molecular Imaging. 2005;32:478–85. doi:10.1007/s00259-004-1702-y.

36. Seemann J, Eppard E, Waldron BP, Ross TL, Roesch F. Cation exchange-based post-processing of (68)Ga-eluate: a comparison of three solvent systems for labelling of DOTATOC, NO2AP(BP) and DATA(m.). Appl Radiat Isot. 2015;98:54–9. doi:10.1016/j.apradiso.2015.01.023.

37. Zoller F, Riss PJ, Montforts F-P, Rösch F. Efficient post-processing of aqueous generator eluates facilitates 68Ga-labelling under anhydrous conditions. Radiochimica Acta 2010. doi:10.1524/ract.2010.1698.

38. European Directorate for the Quality of Medicines & Healthcare (EDQM). Gallium (68Ga) chloride solution for radiolabelling. European Pharmacopoeia 7.8. 07/2013:2464: 5643–44 2013.

39. Cardiac System. In: Ziessman HA, Fahey FH, O'Malley JP, Thrall JH, editors. Nuclear medicine: The requisites. 4th ed. Philadelphia: Elsevier/Mosby; 2014. p. 378–423. doi:10.1016/B978-0-323-08299-0.00016-X.

40. Becker G, Deckner K, Hornung C, Kuytz U. Szintigraphische Tumordiagnostik mit 67-Galliumcitrat. In: Schlegel B, editor; 1972; Munich. Munich, s.l.: J.F. Bergmann-Verlag; 1972. p. 142–145.

41. Robinson RG, Preston DF, Schiefelbein M, Baxter KG. Strontium 89 therapy for the palliation of pain due to osseous metastases. JAMA. 1995;274:420–4.

42. Croke J, Leung E, Segal R, Malone S. Clinical benefits of alpharadin in castrate-chemotherapy-resistant prostate cancer: case report and literature review. BMJ Case Rep 2012. doi:10.1136/bcr-2012-006540.

43. Massoud TF, Gambhir SS. Molecular imaging in living subjects: seeing fundamental biological processes in a new light. Genes & Development. 2003;17:545–80. doi:10.1101/GAD.1047403.

44. Weissleder R. Molecular imaging in cancer. Science. 2006;312:1168–71. doi:10.1126/science.1125949.

45. Liu S, Edwards DS. Bifunctional chelators for therapeutic lanthanide radiopharmaceuticals. Bioconjugate Chem. 2001;12:7–34. doi:10.1021/BC000070V.

46. Stetter H, Frank W. Complex Formation with Tetraazacycloalkane-N,N?: ,N?,N?-tetraacetic Acids as a Function of Ring Size. Angew. Chem. Int. Ed. Engl. 1976;15:686. doi:10.1002/anie.197606861.

47. Alexander V. Design and Synthesis of Macrocyclic Ligands and Their Complexes of Lanthanides and Actinides. Chem. Rev. 1995;95:273–342. doi:10.1021/cr00034a002.

48. Caravan P, Ellison JJ, McMurry TJ, Lauffer RB. Gadolinium(III) Chelates as MRI Contrast Agents: Structure, Dynamics, and Applications. Chem. Rev. 1999;99:2293–352. doi:10.1021/cr980440x.

49. Khreish F, Ebert N, Ries M, Maus S, Rosar F, Bohnenberger H, et al. 225Ac-PSMA-617/177Lu-PSMA-617 tandem therapy of metastatic castration-resistant prostate

cancer: pilot experience. European Journal of Nuclear Medicine. 2020;47:721–8. doi:10.1007/s00259-019-04612-0.

50. Bundesumweltministerium (BMU) w. Biologische Wirksamkeit von Auger-Elektronen emittierenden Radionukliden.

51. Lamberts S.W.J., Barker W.H., Reubi J.-C., Krenning E.P. Somatostatin-Receptor Imaging in the Localization of Endocrine Tumors.

52. Moerlein SM. The Chemistry of Gallium and Indium as Related to Radiopharmaceutical Production. International Journal of Nuclear Medicine and Biology. 1981:277–87.

53. Brahim Hacht. Gallium(III) Ion Hydrolysis under Physiological Conditions. Bulletin of the Korean Chemical Society. 2008;29:372–6. doi:10.5012/bkcs.2008.29.2.372.

54. Pharmazeutische Zeitung;2011.

55. Banerjee S, Pillai MRA, Knapp FFR. Lutetium-177 therapeutic radiopharmaceuticals: linking chemistry, radiochemistry, and practical applications. Chemical Reviews. 2015;115:2934–74. doi:10.1021/cr500171e.

56. Nagy G, Szikra D, Trencsényi G, Fekete A, Garai I, Giani AM, et al. AAZTA: An Ideal Chelating Agent for the Development of 44 Sc PET Imaging Agents. Angew Chem Int Ed Engl. 2017;56:2118–22. doi:10.1002/anie.201611207.

57. M Szydło, M Jadwiński, A Chmura, K Gorczewski, M Sokół. Synthesis, isolation and purification of [(11)C]-choline. Contemp Oncol (Pozn). 2016.

58. Tsionou MI, Knapp CE, Foley CA, Munteanu CR, Cakebread A, Imberti C, et al. Comparison of macrocyclic and acyclic chelators for gallium-68 radiolabelling. RSC advances. 2017;7:49586–99. doi:10.1039/c7ra09076e.

59. Gijs M, Dammicco S, Warnier C, an Aerts, Impens NREN, D'Huyvetter M, et al. Gallium-68-labelled NOTA-oligonucleotides: an optimized method for their preparation. J Labelled Comp Radiopharm. 2016;59:63–71. doi:10.1002/jlcr.3363.

60. Spang P, Herrmann C, Roesch F. Bifunctional Gallium-68 Chelators: Past, Present, and Future. Semin Nucl Med. 2016;46:373–94. doi:10.1053/j.semnuclmed.2016.04.003.

61. Vojta. NOTA Complexes with Copper(II) and Divalent Metal Ions: Kinetic and Thermodynamic Studies.

62. Notni J, Pohle K, Wester H-J. Comparative gallium-68 labeling of TRAP-, NOTA-, and DOTA-peptides: practical consequences for the future of gallium-68-PET. EJNMMI Res. 2012;2:28. doi:10.1186/2191-219X-2-28.

63. Notni J, Šimeček J, Hermann P, Wester H-J. TRAP, a powerful and versatile framework for gallium-68 radiopharmaceuticals. Chemistry. 2011;17:14718–22. doi:10.1002/chem.201103503.

64. Clarke ET, Martell AE. Stabilities of trivalent metal ion complexes of the tetraacetate derivatives of 12-, 13- and 14-membered tetraazamacrocycles. Inorganica Chimica Acta. 1991;190:37–46. doi:10.1016/S0020-1693(00)80229-7.

65. Becke-Goehring M, Hoffmann H. Komplexchemie: Vorlesungen über Anorganische Chemie Von Margot Becke-Goehring. Berlin, Heidelberg: Springer; 1970.

66. Berry DJ, Ma Y, Ballinger JR, Tavaré R, Koers A, Sunassee K, et al. Efficient bifunctional gallium-68 chelators for positron emission tomography: tris(hydroxypyridinone) ligands. Chem. Commun. (Camb.). 2011;47:7068–70. doi:10.1039/c1cc12123e.

67. Ma MT, Cullinane C, Imberti C, Baguña Torres J, Terry SYA, Roselt P, et al. New Tris(hydroxypyridinone) Bifunctional Chelators Containing Isothiocyanate Groups Provide a Versatile Platform for Rapid One-Step Labeling and PET Imaging with (68)Ga(3.). Bioconjugate Chemistry. 2016;27:309–18. doi:10.1021/acs.bioconjchem.5b00335.

68. Young JD, Abbate V, Imberti C, Meszaros LK, Ma MT, Terry SYA, et al. 68Ga-THP-PSMA: A PET Imaging Agent for Prostate Cancer Offering Rapid, Room-Temperature, 1-Step Kit-Based Radiolabeling. J. Nucl. Med. 2017;58:1270–7. doi:10.2967/jnumed.117.191882.

69. Aime S, Calabi L, Cavallotti C, Gianolio E, Giovenzana GB, Losi P, et al. Gd-AAZTA-: a new structural entry for an improved generation of MRI contrast agents. Inorg Chem. 2004;43:7588–90. doi:10.1021/ic0489692.

70. Pfister J, Summer D, Rangger C, Petrik M, Guggenberg E von, Minazzi P, et al. Influence of a novel, versatile bifunctional chelator on theranostic properties of a minigastrin analogue. EJNMMI Res. 2015;5:74. doi:10.1186/s13550-015-0154-7.

71. Sinnes J-P, Nagel J, Rösch F. AAZTA5/AAZTA5-TOC: synthesis and radiochemical evaluation with 68Ga, 44Sc and 177Lu. EJNMMI Radiopharmacy and Chemistry. 2019;4:18. doi:10.1186/s41181-019-0068-1.

72. Sinnes J-P, Nagel J, Waldron BP, Maina T, Nock BA, Bergmann RK, et al. Instant kit preparation of 68Ga-radiopharmaceuticals via the hybrid chelator DATA: clinical translation of 68GaGa-DATA-TOC. EJNMMI Res. 2019;9:48. doi:10.1186/s13550-019-0516-7.

73. Seemann J, Waldron BP, Roesch F, Parker D. Approaching 'Kit-Type' Labelling with (68)Ga: The DATA Chelators. ChemMedChem. 2015;10:1019–26. doi:10.1002/cmdc.201500092.

74. Ehrlich P. Über den jetzigen Stand der Chemotherapie. Ber. Dtsch. Chem. Ges. 1909;42:17–47. doi:10.1002/cber.19090420105.

75. IUPAC Online. 19.09.2017. https://www.qmul.ac.uk/sbcs/iupac/medchem/ix.html#p7. Accessed 28 Nov 2020.

76. Syed M, Flechsig P, Liermann J, Windisch P, Staudinger F, Akbaba S, et al. Fibroblast activation protein inhibitor (FAPI) PET for diagnostics and advanced targeted radiotherapy in head and neck cancers. Eur J Nucl Med Mol Imaging. 2020;47:2836–45. doi:10.1007/s00259-020-04859-y.

77. Lüllmann H, Mohr K, Hein L. Pharmakologie und Toxikologie: Arzneimittelwirkungen verstehen - Medikamente gezielt einsetzen ; ein Lehrbuch für Studierende der Medizin, der Pharmazie und der Biowissenschaften, eine Informationsquelle für Ärzte, Apotheker und Gesundheitspolitiker. 17th ed. Stuttgart: Thieme; 2010.

78. Lau J, Rousseau E, Kwon D, Lin K-S, Bénard F, Chen X. Insight into the Development of PET Radiopharmaceuticals for Oncology. Cancers (Basel) 2020. doi:10.3390/cancers12051312.

79. Bernard-Gauthier V, Bailey JJ, Berke S, Schirrmacher R. Recent Advances in the Development and Application of Radiolabeled Kinase Inhibitors for PET Imaging. Molecules. 2015;20:22000–27. doi:10.3390/molecules201219816.

80. Krebs S, Veach DR, Carter LM, Grkovski M, Fornier M, Mauro MJ, et al. First-in-Humans Trial of Dasatinib-Derivative Tracer for Tumor Kinase-Targeted PET. J. Nucl. Med. 2020;61:1580–7. doi:10.2967/jnumed.119.234864.

81. Silberstein EB, Ryan J. Prevalence of adverse reactions in nuclear medicine. Pharmacopeia Committee of the Society of Nuclear Medicine. J. Nucl. Med. 1996;37:185–92.

82. Yoshinaga K, Klein R, Tamaki N. Generator-produced rubidium-82 positron emission tomography myocardial perfusion imaging-From basic aspects to clinical applications. Journal of Cardiology. 2010;55:163–73. doi:10.1016/j.jjcc.2010.01.001.

83. Bourguignon MH, Pauwels EK, Loc'h C, Mazière B. Iodine-123 labelled radiopharmaceuticals and single-photon emission tomography: a natural liaison. Eur J Nucl Med. 1997;24:331–44. doi:10.1007/BF01728774.

84. Pacini F, Lippi F, Formica N, Elisei R, Anelli S, Ceccarelli C, Pinchera A. Therapeutic doses of iodine-131 reveal undiagnosed metastases in thyroid cancer patients with detectable serum thyroglobulin levels. J. Nucl. Med. 1987;28:1888–91.

85. T. DeGrado, S. Baldwin, S. Wang, Malcolm D. Orr, R. P. Liao, H. Friedman, et al. Synthesis and evaluation of (18)F-labeled choline analogs as oncologic PET tracers. J. Nucl. Med. 2001.

86. Stamatiadis-Smidt H, zur Hausen H. Energiestoffwechsel von Krebszellen. In: Stamatiadis-Smidt H, Hausen H, editors. Thema Krebs: Fragen und Antworten. Berlin, Heidelberg, s.l.: Springer Berlin Heidelberg; 1998. p. 97–100. doi:10.1007/978-3-662-10418-7_23.

87. Almuhaideb A, Papathanasiou N, Bomanji J. 18F-FDG PET/CT imaging in oncology. Ann Saudi Med. 2011;31:3–13. doi:10.4103/0256-4947.75771.

88. Israeli RS, Powell CT, Fair WG, Heston WD. Molecular cloning of a complementary DNA encoding a prostate-specific membrane antigen. Cancer Research. 1993;53:227–30.

89. Israeli RS, Powell CT, Corr JG, Fair WG, Heston WD. Expression of the prostate-specific membrane antigen. Cancer Research. 1994;54:1807–11.

90. Davis MI, Bennett MJ, Thomas LM, Bjorkman PJ. Crystal structure of prostate-specific membrane antigen, a tumor marker and peptidase. Proc Natl Acad Sci U S A. 2005;102:5981–6. doi:10.1073/pnas.0502101102.

91. Perera M, Papa N, Roberts M, Williams M, Udovicich C, Vela I, et al. Gallium-68 Prostate-specific Membrane Antigen Positron Emission Tomography in Advanced Prostate Cancer-Updated Diagnostic Utility, Sensitivity, Specificity, and Distribution of Prostate-specific Membrane Antigen-avid Lesions: A Systematic Review and Meta-analysis. European Urology. 2020;77:403–17. doi:10.1016/j.eururo.2019.01.049.

92. V Prasad. Prasad V, Fetscher S, Baum RP. Changing role of somatostatin receptor targeted drugs in NET: nuclear Medicine's view. J Pharm Pharm Sci. 2007;10:321s–37s. J Pharm Pharm Sci. 2007;10:321s.

93. S. Petersenn. Neuroendokrine Tumoren. 2005.

94. Bashir A, Vestergaard MB, Binderup T, Broholm H, Marner L, Ziebell M, et al. Pharmacokinetic analysis of 68GaGa-DOTA-TOC PET in meningiomas for assessment of in vivo somatostatin receptor subtype 2. Eur J Nucl Med Mol Imaging. 2020;47:2577–88. doi:10.1007/s00259-020-04759-1.

95. Wang L-F, Lin L, Wang M-J, Li Y. The therapeutic efficacy of 177Lu-DOTATATE/DOTATOC in advanced neuroendocrine tumors: A meta-analysis. Medicine (Baltimore). 2020;99:e19304. doi:10.1097/MD.0000000000019304.

96. Meckel M, Bergmann R, Miederer M, Roesch F. Bone targeting compounds for radiotherapy and imaging: *Me(III)-DOTA conjugates of bisphosphonic acid, pamidronic acid and zoledronic acid. EJNMMI radiopharm. chem. 2017;1:14. doi:10.1186/s41181-016-0017-1.

97. Pfannkuchen N, Meckel M, Kubicek V, Hermann P, Bergmann R, Steinbach J, et al. 68Ga- und 177Lu-markierte Bisphosphonate als Knochenmetastasen-Theranostika. Nuklearmediziner. 2015;38:138–44. doi:10.1055/s-0035-1549862.

98. Ando A, Ando I, Tonami N, Kinuya S, Kazuma K, Kataiwa A, et al. 177Lu-EDTMP: a potential therapeutic bone agent. Nucl Med Commun. 1998;19:587–91.

99. Chopra A. Molecular Imaging and Contrast Agent Database (MICAD): 99mTc-Labeled 1-hydroxy-2-(2-isopropyl-1H-imidazole-1-yl)ethylidene-1,1-bisphosphonic acid. Bethesda (MD); 2004.

100. Wondergem M, van der Zant FM, Knol RJJ, Burgers AMG, Bos SD, Jong IJ de, Pruim J. 99mTc-HDP bone scintigraphy and 18F-sodiumfluoride PET/CT in primary staging of patients with prostate cancer. World J Urol. 2018;36:27–34. doi:10.1007/s00345-017-2096-3.

101. BENTZEN SM. Theragnostic imaging for radiation oncology: dose-painting by numbers. The Lancet Oncology. 2005;6:112–7. doi:10.1016/S1470-2045(05)01737-7.

102. Hertz B. Dr. Saul Hertz (1905–1950) Discovers the Medical Uses of Radioactive Iodine: The First Targeted Cancer Therapy. In: Ahmadzadehfar H, editor. Thyroid Cancer - Advances in Diagnosis and Therapy: InTech; 2016. doi:10.5772/64609.

103. Dietlein M, Dressler J, Grünwald F, Leisner B, Moser E, Reiners C, et al. Leitlinie zur Radioiodtherapie (RIT) bei benignen Schilddrüsenerkrankungen (Version 4). Nuklearmedizin. 2007;46:220–3.

104. Emami B, Lyman J, Brown A, Cola L, Goitein M, Munzenrider JE, et al. Tolerance of normal tissue to therapeutic irradiation. International Journal of Radiation Oncology*Biology*Physics. 1991;21:109–22. doi:10.1016/0360-3016(91)90171-Y.

105. Glatting G, Bardiès M, Lassmann M. Treatment planning in molecular radiotherapy. Z Med Phys. 2013;23:262–9. doi:10.1016/j.zemedi.2013.03.005.

106. Zimmerman BE, Grošev D, Buvat I, Coca Pérez MA, Frey EC, Green A, et al. Multi-centre evaluation of accuracy and reproducibility of planar and SPECT image quantification: An IAEA phantom study. Z Med Phys. 2017;27:98–112. doi:10.1016/j.zemedi.2016.03.008.

107. Rothe A, Hosse RJ, Power BE. In vitro display technologies reveal novel biopharmaceutics. The FASEB Journal. 2006;20:1599–610. doi:10.1096/fj.05-5650rev.

108. Kletting P, Schimmel S, Hänscheid H, Luster M, Fernández M, Nosske D, et al. The NUKDOS software for treatment planning in molecular radiotherapy. Z Med Phys. 2015;25:264–74. doi:10.1016/j.zemedi.2015.01.001.

109. BENTZEN SM, Mehta MP, Harari PM, Tomé WA. Radiation oncology advances. New York, NY: Springer; 2008.

110. Turner JH. An introduction to the clinical practice of theranostics in oncology. Br J Radiol. 2018;91:20180440. doi:10.1259/bjr.20180440.

111. steinrue. Die Regelung der Arzneimittel.

112. European Pharmacopoeia, 10th edition 2019, French: Subscription to Main volume + Supplement 1 + Supplement 2. 1st ed. Stuttgart: Deutscher Apotheker Verlag; 2019.

113. StrlSchG - nichtamtliches Inhaltsverzeichnis. 09.12.2020. https://www.gesetze-im-internet.de/strlschg/index.html. Accessed 9 Dec 2020.

114. Afshar-Oromieh A, Haberkorn U, Eder M, Eisenhut M, Zechmann CM. 68GaGallium-labelled PSMA ligand as superior PET tracer for the diagnosis of prostate cancer: comparison with 18F-FECH. European Journal of Nuclear Medicine. 2012;39:1085–6. doi:10.1007/s00259-012-2069-0.

115. APPLICATIONS OF FDG PET IN ONCOLOGY: Best clinical practice. [S.l.]: SPRINGER VERLAG, SINGAPOR; 2020.

116. Ulaner GA. Fundamentals of oncologic PET/CT. Philadelphia, PA: Elsevier; 2019.

4. **DOTA-ZOL**

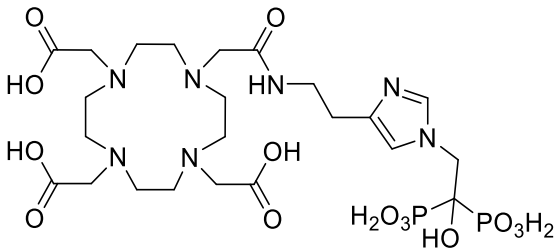

Abbildung 21 DOTA-ZOL

Bei vielen Tumorarten treten Metastasen des Knochens als Nebenerkrankung auf. Für die Langzeitüberlebensrate wirken sich diese Metastasen besonders negativ aus. Eine Heilung ist aktuell nicht möglich, jedoch können Symptome gelindert werden. DOTA-ZOL gehört zur Gruppe der Bisphosphonate. Diese sind Strukturanaloga des anorganischen Pyrophosphats und besitzen ebenso hohe Bindungsaffinität zu dem im Knochen vorhandenen Hydroxyapatit. Mit radioaktiv markiertem DOTA-ZOL können strukturelle Veränderungen am Knochen sichtbar gemacht bzw. behandelt werden. Zu den Bisphosphonaten die bisher Anwendung gefunden haben zählen unter anderem [^{68}Ga]Ga-DOTA-ZOL; [^{177}Lu]Lu-DOTA-ZOL, [^{177}Lu]Lu-EDTMP (Ethylendiamintetramethylen Phosphorsäure), [^{99m}Tc]Tc-MDP (Methylendiphosphonate;), oder [^{99m}Tc]Tc-HDP (hydroxymethylenbisphosphonat;).

4.1 DOTA-ZOL: A Promising Tool in Diagnosis and Palliative Therapy of Bone Metastasis—Challenges and Critical Points in Implementation into Clinical Routine

Michael Meisenheimer[1], Stefan Kürpig[1], Markus Essler[1], Elisabeth Eppard[*2]

[1]Department of Nuclear Medicine, University Hospital Bonn, D-53127 Bonn, Germany

[2]actual adress: PositronPharma S.A, Rancagua 878, 7500921 Providencia, Chile

*Corresponding author: eeppard@positronpharma.cl; PositronPharma S.A, Rancagua 878, 7500921 Providencia, Chile

https://doi.org/10.3390/molecules25132988

Abstract

The novel compound 1,4,7,10-tetraazacyclododecane-1,4,7,10-tetraacetic acid (DOTA)-ZOL (DOTA-conjugated zoledronic acid) is a promising candidate for the diagnosis and therapy of bone metastasis. The combination of the published methodology for this bisphosphonate with pharmaceutical and regulatory requirements turned out to be unexpectedly challenging. The scope of this work is the presentation and discussion of problems encountered during this process. Briefly, the radiolabelling process and purification, as well as the quality control published, did not meet the expectations. The constant effort setting up an automated radiolabelling procedure resulted in (a) an enhanced manual method using coated glass reactors, (b) a combination of three different reliable radio thin-layer chromatography (TLC) methods instead of the published and (c) a preliminary radio high-pressure liquid chromatography (HPLC) method for identification of the compound. Additionally, an automated radiolabelling process was developed, but it requires further improvement, e.g., in terms of a reactor vessel or purification of the crude product. The published purification method was found to be unsuitable for clinical routine, and an intense screening did not lead to a satisfactory result; here, more research is necessary. To sum up, implementation of DOTA-ZOL was possible but revealed a lot of critical points, of which not all could be resolved completely yet.

Keywords: gallium-68; bone metastasis; radiolabelling synthesis; quality control; module system

Introduction

The bone is, more than other tissues, affected by the metastasis of solid tumours [1, 2] and is a prevalent complication in cancers of breast (BCa), prostate (PCa) and lung (LCa) [3]. PCa metastasise preferentially into bone, which represents a matrix facilitating tumour growth and promoting a vicious cycle between metastasis and bone pathology [4, 5]. Of all new diagnosed patients with PCa, 3% already have, and about 11.5% will develop, bone metastases [6]. As shown by an autopsy study, approximately 90% of men dying from PCa suffer from bone metastases [7]. Apart from this, approximately 90% of patients diagnosed with stage IV PCa present bone metastases when diagnosed [8]. These bone lesions can induce skeletal-related events (SREs) as further complications of the disease, which are experienced by a further 5.9% of the patients [6]. These SREs, like pathological fractures, nerve compression syndromes or hypercalcemia, reduce the quality of life of the patients [9–11] and contribute to a major part to the significantly increased mortality and morbidity [12–14].

The first publications on the biological effects of diphosphonates, later renamed bisphosphonates, appeared in 1958 [15]. Since then, their importance and use in medicine has increased rapidly, and today, they are applied for treatments of a variety of bone diseases with excessive osteoclast activity (e.g., metastatic and osteolytic bone disease, osteoporosis and Paget's disease of bone) [16, 17].

Bisphosphonates are structural analogues of inorganic pyrophosphate (PPi). Although PPi contains two esterified phosphate groups (P-O-P bond) and bisphosphonates link two phosphonate groups covalently to a central carbon (P-C-P bond), they exhibit, to some extent, similar biological properties. In the human metabolism, PPi results from a multitude of reactions as a by-product but also plays a key role in biomineralization pathways [18, 19]. Already, in 1962, PPi was found to be responsible for calcification regulation under physiological conditions [20], which formed the basis for further investigations of its role in the calcification of soft tissue, bone mineralisation, metabolism and related clinical disorders [19]. Like PPi, bisphosphonates have a high affinity for hydroxyapatite (HAP) [21, 22], one of the main constituents of bone, but being chemically stable and enabling a number of variations in the structure based on the substitutions in the R_1 and R_2 positions on the carbon atom (Figure 1) [19].

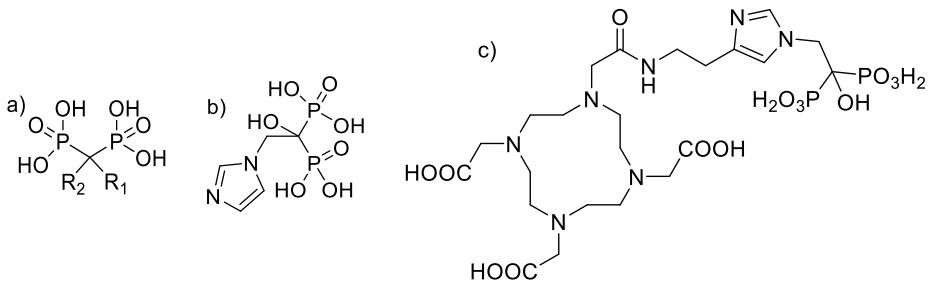

Figure 1: (**a**) Chemical backbone of bisphosphonates. (**b**) Chemical structure of zoledronate with R_1: OH and R_2: imidazol-1-ylethyliden. (**c**) Chemical structure of 1,4,7,10-tetraazacyclododecane-1,4,7,10-tetraacetic acid-conjugated zoledronic acid (DOTA-ZOL).

Since the first medicinal use of a bisphosphonate (etidronate in 1969; first-generation bisphosphonate) as an antiresorptive [17], the pharmacological properties of them have improved significantly. Bisphosphonates of the generation applied today, zoledronate or risedronate, provide a relative antiresorptive potency, which is between 1000- and 10,000-fold higher [23]. Pharmacokinetics are strongly influenced by the two moieties binding to the central carbon. While the two phosphate groups provide the strong affinity for HAP, a hydroxyl group in position R1 increases the ability of the bisphosphonate to bind calcium [23, 24]. Although this is essential for the affinity to the bone matrix, the antiresorptive potency is dependent on the moiety on R2, and a nitrogen or amino group in this position increases the antiresorptive potency relative to first-generation bisphosphonates like etidronate by 10 to 10,000 [23, 25]. As shown by some studies, bisphosphonates of the actual generation (nitrogen-containing R2) bind to farnesyl pyrophosphate synthase (FPPS) and inhibit its activity [25, 26]. The FFPS is a key enzyme in the mevalonic acid pathway (MVAP), and its inhibition correlates with a blockade of the MVAP [27, 28]. This intervention leads to a constrained isoprenylation of proteins, which is essential for the regulation of osteoclast activity [29], ultimately inducing osteoclast apoptosis [27, 30].

In the entire process, from diagnosis to the treatment of patients suffering from skeletal metastatic disease, the techniques of nuclear medicine play a key role. ^{99m}Tc-labelled bisphosphonates such as methylene diphosphate (MDP) or hydroxy methylene diphosphate (HMDP) have been used in the clinical diagnosis of metastatic bone cancer for many years [31], and therapeutic radionuclides have proven their value in bone pain palliation [32–34]. From the current generation of bisphosphonates, zoledronate's high affinity for hydroxyapatite and its high antiresorptive potency makes it particularly interesting as a targeting vector for theragnostic applications in nuclear medicine. One of the

first bisphosphonate derivates suitable for diagnostic imaging as well as therapeutic treatment was (4-{[(bis(phosphonomethyl))carbamoyl]methyl}-7,10-bis(carboxymethyl)-1,4,7,10-tetraazacyclododec-1-yl) acetic acid (BPAMD) [35, 36]. BPAMD combines the bisphosphonate with a chelator, namely 1,4,7,10-tetraazacyclododecane-1,4,7,10-tetraacetic acid (DOTA). DOTA forms stable complexes with a variety of medicinal applied radiometals, thus enabling the use of the entire spectrum of nuclear medicine techniques. The first patient studies with gallium-68 ^{68}Ga/^{177}Lu-labelled BPAMD proved the potential of this theragnostic approach of a DOTA-conjugated bisphosphonate [37–39]. This proof-of-principle paved the way for more sophisticated macrocyclic bisphosphonates, employing more potent bisphosphonate basic structures like pamidronate and zoledronate [40], the latter of which already proved its enhanced potential in diagnosis and therapy [41, 42].

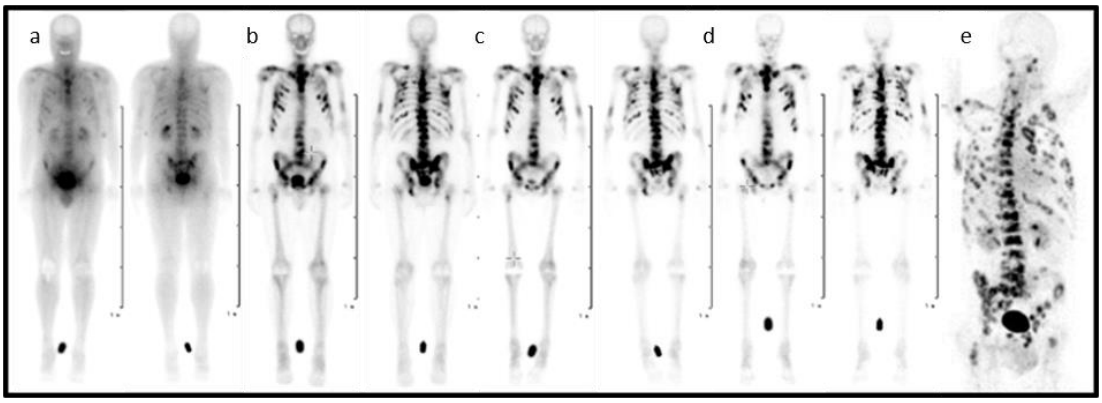

Figure 2: Planar scintigraphy (anterior and posterior) of [^{177}Lu]Lu-DOTA-ZOL at different time points (**a**–**d**) and PET/CT of [^{68}Ga]Ga-DOTA-ZOL (**e**) in a bronchial carcinoma patient with secondary bone metastases [41].

The presented work arises from the need to implement this novel compound DOTA-conjugated zoledronic acid (ZOL) into radiopharmaceutical routine production prior to patient studies. The transfer of the radiolabelling but particularly the proposed quality control methods exhibited a series of problems and flaws that need to be addressed. On the one hand, the setup of an automated radiolabelling method for gallium-68 using the available module system and its accessories presented some challenges. On the other hand, the quality control was not reliable. This combination of problems led to an extended effort on addressing all these issues. (1) The cassette and consumable kit, as well as the radiolabelling itself, needed to be adjusted accordingly. (2) The need for a purification method using solid-phase extraction (SPE). (3) The bisphosphonate presented issues with the glass reactor vial from the cassette. (4) The known radio thin-

layer chromatography (radio TLC) methods could not distinguish between the radiolabelled compound and gallium-68 in its colloidal form. (5) The known radio-TLC method presented a high percentage of false negative results. (6) The known radio-TLC method led to a decomposition of the final compound. (7) The proposed radio high-pressure liquid chromatography (radio HPLC) methods were not reproducible. Despite all efforts, a solution could only be found for a part of the observed challenges, which are described in the following.

Results & Discussion

The first attempts to implement the novel compound DOTA-ZOL into radiopharmaceutical routine production for intended patient studies exhibited a peck of trouble. An in-depth investigation of the reasons and possible solutions revealed a number of critical points. In the following, the results of the first attempts for the implementation are presented, as well as all findings that are based thereon. For a better explanation and understanding, the radiolabelling/synthesis and purification are divided in two paragraphs and discussed separately.

Radiolabelling I: The Manual Method

The initial starting point for the implementation was the published radiolabelling method by Meckel et al. [40]. To adapt the method for clinical use, the open vial concept was replaced by a closed vial setup, employing a sealed sterile reaction vessel. Consequently, the acetone present in the preparation due to the post-processing of the generator eluate was not evaporated any longer during the reaction. To avoid acetone in general, it was decided to modify the procedure according to Seemann et al. [43]. This radiolabelling method for bisphosphonate takes the advantage of ethanol-based post-processing, which was found to be more suitable in a clinical setting, with the aim to prepare patient doses. A schematic description of the radiolabelling is presented in Figure 3.

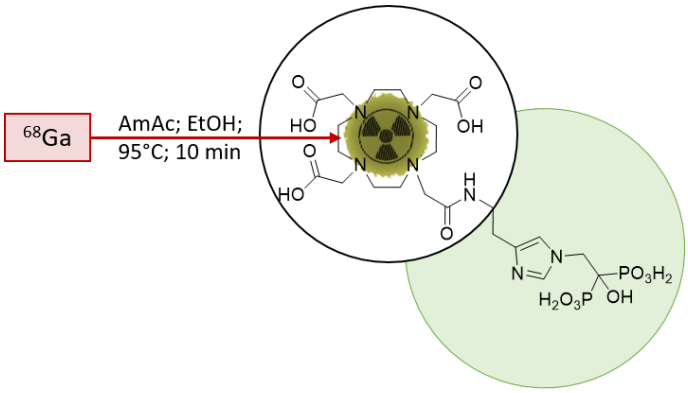

Figure 3: Scheme of the ^{68}Ga-radiolabelling of DOTA-ZOL. Highlighted in green, the bisphosphonate moiety and, encircled, the chelating moiety.

Taking this into account resulted in a modified method using 500-µL post-processed [44] gallium-68 with 25 µg (35.6 nmol) of DOTA-ZOL in an ammonium acetate buffer (1 M; pH 4.5) in a sealed, sterile reaction vessel that was agitated at 85 °C for 15 min. The result of the complexation reaction was monitored via radio TLC using the published radio TLC method [40]. For this, an aliquot of the crude product was taken, spotted on the TLC strip and developed in the described solvent system consisting of acetylacetone (acac), acetone (ac) and concentrated hydrochloric acid (HCl) in the ratio 10:10:1.

A series of five consecutive synthesis with starting activities of 441.3 ± 129.4 MBq proved the method to be more unstable than expected. The mean complexation yield (determined in the crude product) was found to be 75.82% ± 25.66%, with an range from 31.9% to 98.9%. Only one of the five synthesis yielded more than 95%. While lacking a suitable purification method, as described later on, the complexation yield of the crude product is equal to the radiochemical purity of the final product. As a result, 80% of the synthesis did not meet the quality control criteria for uncomplexed gallium-68 (<2%) and colloids (<3%) thereof present in the final product. These values were defined based on the pharmacopeial monograph for [^{68}Ga]Ga-DOTA-(0)-Phe(1)-Tyr(3))octreotid ([^{68}Ga]Ga-DOTA-TOC) [45].

Not only the standard deviation of the complexation yields, especially the wide range from 31.9% to 98.9%, was unforeseen and requested an in-depth investigation. The first revision of the synthesis and its parameters led to an improved method using 50-µg (71.3 nmol) DOTA-ZOL and 90 °C. The modifications resulted in higher complexation yields (mean 85.73% ± 12%), with an range from 68.9% to 96.05% in a series of three consecutive synthesis. Still, the rejection rate (66.6%) was high. Further experiments

with elevated temperatures (up to 120 °C) did not improve this result. Surprisingly, the increase of the precursor amount from 25 µg to 50 µg had a lower effect than expected.

With regards to these findings and the unavailability of a purification method, the high rejection rate led to the decision to start all over again, trying to adapt the institutional standard radiolabelling method from a clinical routine for DOTA-ZOL instead of a literature-based method development. Use of this method would have, additionally, the advantage of the availability and grade of the reagents. The second major revision of the synthesis led to the manual method described in the Materials and Methods section, applying 50-µg DOTA-ZOL and sodium chlorine post-processed gallium-68.

In a series of three consecutive synthesis (426.00 ± 87.78 MBq), this method was found to be significantly more reproducible, with a mean complexation yield of 99.56% ± 0.15% determined with the published radio TLC method. The range of the complexation yield was from 99.36% to 99.72%. The radioactivity yield was 73.27% ± 9.87% (n.c.) and the radiochemical yield 87.94% ± 7.99% (d.c.).

Due to this result, it was assumed that the problem was solved and the synthesis under control. Therefore, it was decided to proceed and translate the method on the synthesis module.

Radiolabelling II: First Attempt for Automation

First the available cassette and associated method were modified in terms of purification. As, at this particular time, none of the evaluated SPE methods were found to be suitable and the manual method expected to be reproducible, with complexation yields above 95%, it was decided to eliminate the purification step. The final cassette setup is depicted in Supplemental Figure 6. Using this cassette setup, the manual synthesis was transferred to the module system.

In principle, this was found to be successful. A first series of four consecutive synthesis (427.50 ± 77.87 MBq) revealed a mean complexation yield of 98.27% ± 0.89%, and a range from 97.51% to 99.71% seemed to prove this. Interestingly, with the increasing number of syntheses, it got worse and worse. In a set of 16 syntheses (532 ± 225.50 MBq) under equal reaction conditions, the mean complexation yield was 89.09% ± 11.15%, with a range from 71.07% to 99.71%. From these 16 syntheses, nine did not meet the criteria for quality control (56.3%). Further adjustments in terms of temperature, reaction time, buffer, and precursor amount did not show any effects. A subsequent eval-

uation with regards to the most common problems with gallium-68 (e.g., metal-contaminated solutions) and the implementation of citric buffer pH 4 as additional radio TLC method, switched the focus of the investigation in the direction of quality control.

Radio TLC Quality Control: Unexpected Outcomes

The radio TLC method applied for determination of the yield of the complexation reaction was taken from literature [40] making use of silica-coated TLC plates as a stationary, and a mixture of acac/ac/conc. HCl (10:10:1) as a mobile, phase. In this solvent system, free uncomplexed gallium-68 is complexed by acetylacetone to [^{68}Ga]Ga(acac)$_3$ travelling with the solvent front. Gallium-68 in its colloidal form is converted due to the very low pH into ionic [^{68}Ga]Ga^{3+}, which then also can be complexed and travel with the solvent front. The retention factors (R_f) for [^{68}Ga]Ga-DOTA-ZOL and free, uncomplexed gallium-68, respectively, and ^{68}Ga-colloids as an acetylacetone complex, are specified with 0.1 and 0.9, respectively [40].

Retention factors observed during the setup of the automated synthesis for [^{68}Ga]Ga(acac)$_3$ ranged from 0.5–0.9. Additionally, sometimes, an unusual smear or third peak occurred (Figure 7). To determine the amount of ionic [^{68}Ga]Ga^{3+} without ^{68}Ga-colloids, as well as to verify the results obtained by the published radio TLC method, the mobile phase was substituted with citric buffer pH 4. The retention factors for [^{68}Ga]Ga-DOTA-ZOL, free, uncomplexed gallium-68, respectively, and ^{68}Ga-colloids are with 0–0.1, 0.7–1 and 0.1–0.2. Discrimination of the radiopharmaceutical and low amounts of ^{68}Ga-colloids is not possible with this method.

In a comparison of the results for both radio TLC methods in terms of free, uncomplexed gallium-68, two observations were made. For the synthesis that would be rejected based on the result of the published method, the particular results always vary widely. Assuming that the amount of activity spotted is similar when applying an aliquot of the same volume from the same preparation, the amount of radiopharmaceuticals detected with the published method is significantly reduced.

Based on these findings, an inspection of the intermediate precision and robustness [46] of the previously published radio TLC method was performed. The survey is described in detail in the Supplementary Materials. The retention factor found for ^{68}Ga-colloids was 0.8–1, like published, but for free, uncomplexed gallium-68, an effective value of 0.6–0.9 was found. Additionally, the high concentration of HCl not only converted ^{68}Ga-colloids into ionic [^{68}Ga]Ga^{3+} travelling with the solvent front. Besides that, it seemed to facilitate the H^+-assisted dissociation of the DOTA complex [47–49].

Assuming that this dissociation in the mobile phase led to the significantly different results of ^{68}Ga-contents in both radio TLC methods and, thus, to the incorrect rejection rates, further experiments with [^{68}Ga]Ga-DOTA-ZOL were conducted. The incubation of [^{68}Ga]Ga-DOTA-ZOL in the mobile phase (acac/ac/conc. HCl (10:10:1)) at room temperature for 5 min resulted in the decomposition of the compound verified by radio TLC with a citric buffer pH 4. Less than 15% of the spotted activity was detected with R_f < 0.1, which is assigned to the compound as gallium-68 in its colloidal form, and was not present under these pH conditions. The majority of activity was found at R_f 0.5, which was assigned to [^{68}Ga]Ga(acac)$_3$.

To clarify whether the gallium-68 detected origins from an unintendedly produced outer-sphere complex or from the desired ^{68}Ga-DOTA complex, the experiment was repeated with a preparation of [^{68}Ga]Ga-DOTA-TOC. To the best of our knowledge, [^{68}Ga]Ga-DOTA-TOC did not form stable outer sphere complexes. Therefore, the only source for gallium-68 in a sample of known purity was the ^{68}Ga-DOTA complex. Additionally, quality control with radio TLC and radio HPLC of this compound was straightforward and reliable. The experiment confirmed the origin of gallium-68. The majority of activity (>90%) was found at R_f 0.5, which was assigned to [^{68}Ga]Ga(acac)$_3$. The retention factor of [^{68}Ga]Ga-DOTA-TOC, initial purity 98%, in citric buffer pH 4 was 0–0.2.

The subsequent prospection for a radio TLC method allowing the determination of free, uncomplexed gallium-68, ^{68}Ga-colloids and [^{68}Ga]Ga-DOTA-ZOL led to three radio TLC methods found to be suitable to determine the radiochemical purity (Table 1).

A detailed description, as well as images of the corresponding radio TLCs of the here-described experiments, can be found in the Supplementary Materials.

Table 1: List of the published (first row) and the finally used radio thin-layer chromatography (TLC) methods.

Mobile Phase	**R_f Compound**	**R_f [^{68}Ga]Ga^{3+}**	**R_f ^{68}Ga-colloids**
acac/ac/HCl (1:1:0.1) [40]	0–0.2	0.6–0.9	0.8–1
acac/ac (1:1)	0–0.1	0.7–0.8	0–0.1/0.5–0.9
Citric buffer pH 4	0–0.1	0.7–1	0.1–0.2
TBAP/MeOH (9:1)	0.7–0.8	0.1–0.3	0.1–0.2

By means of these three radio TLC methods, the high rate of falsely negative results was minimised, and a reliable quality control in terms of the complexation yield was possible. With this amendment, work on the implementation could continue.

Radiolabelling III: Revision of the Methods

Unfortunately, the decomposition of the radiolabelled compound during quality control questioned all previously achieved results for the radiolabelling. Therefore, a revision of the manual and automated method using the augmented radio TLC methods for quality control was executed. The previous results for the mean complexation yield were confirmed in both cases but with significantly reduced deviations. Nevertheless, especially the automated synthesis with a mean complexation yield of ~90% was, without a suitable SPE purification method, still a do-or-die procedure and required a solution.

Solid Phase Extraction: Close by

The simple and fast process of SPE purification is perfectly suitable for radiopharmaceutical needs where time matters. The separation of dissolved or suspended compounds from a mixture results from differences in the physical and chemical properties of the entire species. Based on the properties of the requested compound, it can be retained or pass through the stationary phase of the SPE cartridge during the purification process [50]. Purification of [^{68}Ga]Ga-DOTA-ZOL was published using a weak anion exchanger (25 mg, Merck LiChroprep NH_2), where the product was trapped on and eluted with 2-mL phosphate-buffered saline (PBS) [40].

Based on the published purification method, a SPE cartridge screening was conducted, as the Merck LiChroprep NH_2 SPE cartridge was not available anymore. In first place, the selection was based on recommendations and suggestions of the technical service of the manufacturers. In second place, after a couple of unexpected and or negative results, tests were extended to every resin type at our disposal. A total of 35 commercially available SPE cartridges were evaluated for their suitability to purify [^{68}Ga]Ga-DOTA-ZOL (Table 3). This was achieved using the automated method but with the original cassette setup where the C18 cartridge used for DOTA-peptide radiolabelling was replaced by the entire cartridge. The parameters of interest were trapping, recovery and final purity of the product.

Depending on the trapping behaviour, the cartridges were assigned to four groups: (1) no retention, (2) retention of both species, (3) retention of gallium-68 and (4) retention of the product.

Group 1 included 19 out of these 35 cartridges that did not retain either the product or free, uncomplexed gallium-68. This result was found for the pure reaction mixture containing up to 12 vol% ethanol, as well as for the diluted one containing only 5 vol%. The ethanol content did not affect this result at all. Due to this insufficient trapping performance, these 19 cartridges were dismissed.

Eleven cartridges were assigned to group 2, showing (partial) retention of both species, although not always equally strong. All were dismissed for nonselective trapping and final purity. In the relevant cases, the loss of the product was adjudged too high, with more than 10%, in conjunction with only partial purification.

Group 3 included three cartridges. They retained only gallium-68, while no retention for the product was observable. Two of these three cartridges retained gallium-68 unexpectedly, instead of [^{68}Ga]Ga-DOTA-ZOL. Nevertheless, the obtained retention gallium-68 was found to be incomplete in all cases. As a result, in the final product fraction, the amount of free, uncomplexed gallium-68 was reduced compared to the reaction mixture before purification but still present. To overcome this problem, an increased amount of resin should have been the solution. Admittedly, no bigger size was available for two (Chromafix SA and Chromafix HR-XAW) cartridges. For the third cartridge (Chromafix PS-H$^+$), the next larger size (L) showed a partial retention of both species and was assigned to group 2. The cartridges of group 3 may be used for purification. Nevertheless, their purifying effect was too low to achieve a product of sufficient quality in terms of free, uncomplexed gallium-68 when the initial amount of it was in a medium or high range. With regards to the mean complexation yield of the automated synthesis, ~90% of the cartridges of group 3 were excluded. The use of these would help in only the minority of syntheses to achieve a releasable product. The majority provided either perfect complexation yields (>95%) or yields with medium or high amounts of uncomplexed gallium-68 left.

The two cartridges in group 4 retained only [^{68}Ga]Ga-DOTA-ZOL. While the trapping of the product was nearly quantitative, the purifying effect could not be conclusively evaluated. In both cases, no recovery was achieved. For recovery, in the first place, solvent mixtures predefined as suitable for an injectable radiopharmaceutical were evaluated. Additionally, the supplier-recommended eluents were used. For one cartridge (Strata-X-C polymeric) also, the supplier recommendation did not lead to success; for the other (Chromafix PS-H$^+$ (s)), the product was decomposed due to the solvent composition. Both cartridges were found to be unsuitable.

The development of a purification strategy based on only one SPE cartridge was found to be more complicated than expected and hoped. A lack of the presented survey was its incompleteness. The number of commercially available resins or prepacked cartridges is appreciably higher and increases with ongoing research on dedicated materials every year. Besides this, only a single-step purification was evaluated, while a multilevel purification process may be the solution. Despite that, it is a first sight on the issue, indicating the problems due to the structural characteristics of bisphosphonates. It is a balancing act between radiopharmaceutical needs (purity and activity yield) and chemical demands. Nevertheless, if the demand for ^{68}Ga-labelled bisphosphonates increases in the future, SPE purifications shall be evaluated in more detail.

Radiolabelling IV: The Journey Goes on

Realising that the SPE purification problem will be a long-term project, the decision was made to figure out which parameters could be optimised to achieve reliable high complexation yields superseding a subsequent purification. From the previous radiolabelling experiments, two findings were scrutinised:

a) Why is the effect of elevated temperatures low?

b) Why is the effect of a doubled precursor mass low?

In comparison to other DOTA-conjugated compounds, the effects of these two parameters were too low. Being aware of this moved the chemical properties of zoledronic acid into the focus.

Reactor Screening: Minimal Change, Maximum Impact

Glass vessels are omnipresent in the pharmaceutical industry, as well as radiopharmacy, even though they cannot be considered quite inert; to the contrary, various interactions between glass surfaces and the products could appear [51, 52]. One class of pharmaceuticals known to interact with glass containers are bisphosphonates in solutions. These show an interaction with several polyvalent cations present in the glass, leading to an accelerated leaching of the cations and precipitation of the bisphosphonate and, finally, to a shortened drug potency [51]. This interaction is further driven by the pH and/or elevated temperatures. With regards to this, the nanomolar amount of the precursor, as well as a chelator requiring elevated temperatures in combination with a glass reactor, can be assumed to be problematic in a reaction known to be sensitive for metal contaminations and asking for precursor excesses. To avoid those glass-drug interactions in the pharmaceutical industry, special-coated containers are used. The silicon-based coating

aims to prevent direct contact of the pharmaceuticals with the glass surfaces and can sustain additional functionalities for further improvements of the surfaces of the container materials.

Based on this, the decision was made to evaluate the reaction vessels in stock for their suitability in radiolabelling DOTA-ZOL. To evaluate the effect of the container on the radiolabelling with gallium-68, two types of special-coated glass vials were compared with the vials in stock under equal radiolabelling conditions using the manual method as described. Reactors from the stock tested were Tc-Elu-15 vials (volume 15 mL; Cis-Bio, Berlin, Germany), as well as the reactors provided with the fluidic kit of the module (volume 10 mL; ABX, Radeberg, Germany). These were compared with SCHOTT Type I plus® with pure SiO_2 coating and SCHOTT TopLyo® with Si-O-C-H hydrophobic coating (both: volume 10 mL; Schott, Mainz, Germany).

The impressive effect of the silicone coating on the radiolabelling reaction is depicted in Figure 4. Compared to the two glass reactors (TC-ELU-15 75.43% ± 16.92% and ABX 70.9%7 ± 26.38%), the coated vials led to significantly increased and stable complexation yields (TopLyo® 96.99% ± 2.80% and Type I Plus® 97.68% ± 1.39%). While the difference between coated and noncoated vials was evident, no significant effect between the pure silicone coating and hydrophobic Si-O-C-H coating was observable. Both coatings were found to be effective in preventing glass-drug interactions and stabilising the synthesis outcome.

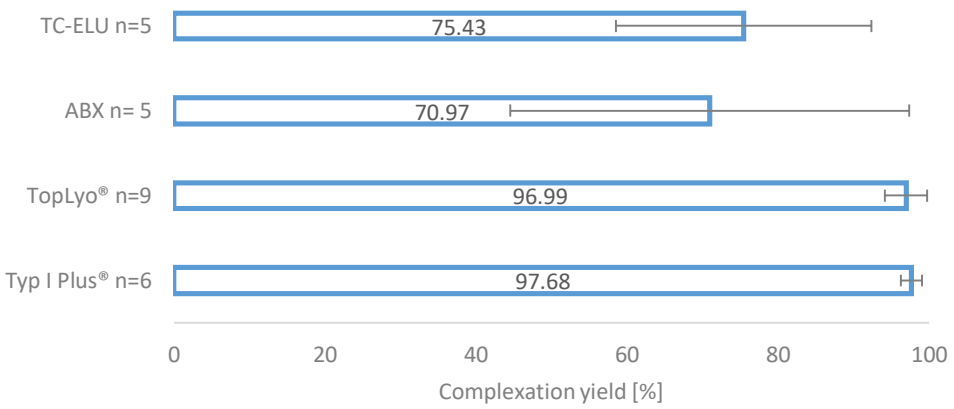

Figure 4: Comparison of the four different reactor vials for radiolabelling. Two normal glass reactors, as well as two silicone-coated glass reactors.

Radiolabelling V: Final Version

With regards to the results of the reactor screening, the manual synthesis was modified in terms of the reaction vial. The high repeatability in combination with complexation yields above 95% facilitated the use of DOTA-ZOL for diagnostic imaging, even without a purification method.

Unfortunately, the coated reactor vials did not fit into the heater of the module system. As the original reactor showed the poorest performance of the four tested reaction vials, the automated method was put on hold until a suitable replacement or a purification method was found. Although the manual method does not meet the demand for clinical routine production, the unfavourable reactor or SPE problem could not be satisfactory addressed; the manual method at least provided [^{68}Ga]Ga-DOTA-ZOL in good quality for the first clinical studies.

Radio-HPLC Quality Control

The previously described radio TLC methods provided a fast and reliable way to check the final product for the appearance of gallium-68, either free, uncomplexed or in its colloidal form. Albeit this is very important information in terms of quality control, the technique cannot assess every information needed or wanted, especially for a new investigational compound. This informational gap could be closed by radio HPLC. In a clinical routine, radio HPLC is used to determine not only the content of gallium-68 in ^{68}Ga-radiopharmaceuticals but, also, chemical and other radioactive impurities (e.g., radiolysis by-products). A critical requirement, not obtained by radio TLC but by radio HPLC, is the product identification.

The method published for radio HPLC [40] took a detour to take advantage of the standard available C18 columns and water/acetonitrile mixtures as the solvent system frequently used for metal-based radiopharmaceuticals. The aliquot for quality control was incubated with deferoxamine (DFO) to the complex-remaining free gallium-68. So complexed, it was possible to discriminate between [^{68}Ga]Ga-DOTA-ZOL and [^{68}Ga]Ga-DFO, which was, in contrast to the zoledronate, retained. With this method, the [^{68}Ga]Ga-DOTA-ZOL passed the column without retention. Therefore, it was not suitable for an identification of the ^{68}Ga-labelled species of interest or the determination of radiolysis products thereof or chemical purity. Additionally, for the theragnostic counterpart [^{177}Lu]Lu-DOTA-ZOL, it did not work. Based on this, it was decided to start from scratch again, searching for suitable radio HPLC conditions for [^{68}Ga]Ga-DOTA-ZOL.

A complete list of all evaluated radio HPLC conditions can be found in the Supplemental Materials (Table 4). Finally, a preliminary method was obtained that still has some weaknesses but can be used to identify the product compound. It is based on a method published by Reddy et al. [53] but adapted for [^{68}Ga]Ga-DOTA-ZOL (**Figure 5**).

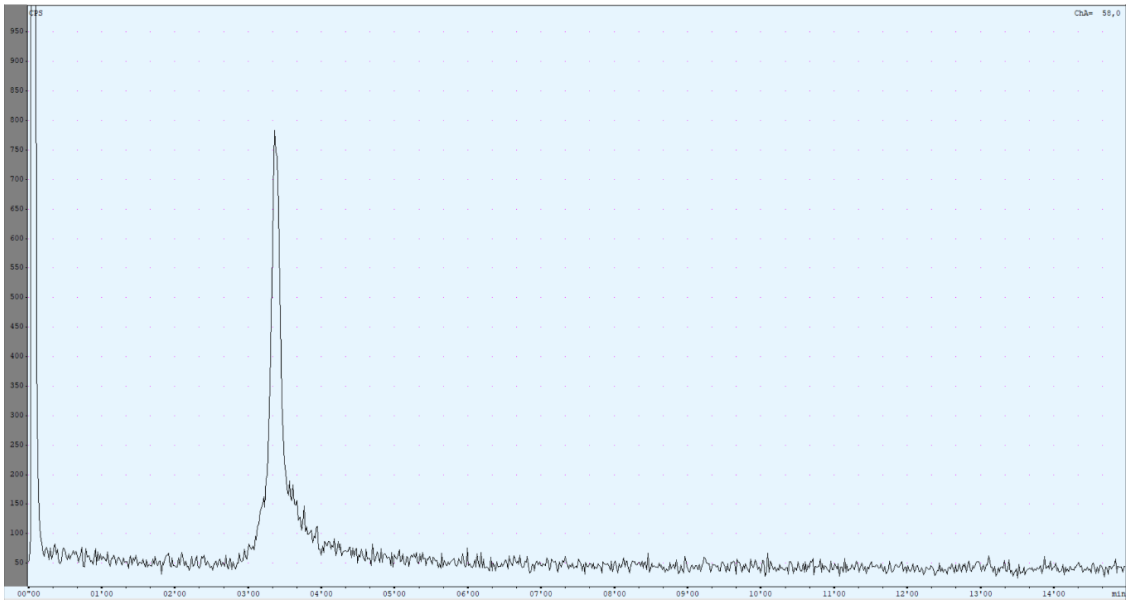

Figure 5: The currently used high-performance liquid chromatography (HPLC) method utilises an isocratic mixture of 90% 59-mM TBAP/10% MeOH (1.2 mL/min). The chromatogram shows the result of a [^{68}Ga]Ga-DOTA-ZOL synthesis (complexation yield determined with radio thin-layer chromatography (TLC) was 98%). The first peak refers to all injected activity measured before the column. The ratio between both peaks is nearly 50:50.

Due to the setup of the radio HPLC, recovery of the product could be determined immediately. The injected activity passed the radioactivity detector two times, before and after the column. Retention times were determined for free gallium-68 (R_t = 2.85 ± 0.03 min), [^{68}Ga]Ga-DOTA-ZOL (R_t = 3.35 ± 0.01 min), void volume (R_t = 2.35 ± 0.04 min) and [^{177}Lu]Lu-DOTA-ZOL (R_t = 6.30 ± 0.05 min).

The difference in retention times of the different species was very small. Up to now, this problem could not be solved either by changing the flow or the solvent ratio. Additionally, the product peak showed some tailing, which could be improved but not prevented yet. Reduced tailing can be achieved by dilution of the aliquot in an equal amount of the mobile phase before injection. Due to this, only occurring for the product peak, it was assumed that it was induced by the chemical properties of the compound. Further improvements may be achieved by adjusting the pH of the mobile phase.

Nevertheless, the method is not perfect and still requires improvements until a first step is achieved. As the compound shows retention, it is possible to determine it via its retention time directly and not only via the exclusion procedure. This represents an advantage, not only over the previously published method but, also, over the radio TLC. In total, the combination of radio TLC for the determination of the unlabelled ^{68}Ga-species and radio HPLC for product identification and chemical purity empowers a more reliable quality control.

Materials and Methods

Radiolabelling

Gallium-68 was obtained from a ^{68}Ge/^{68}Ga-generator (iThemba Labs, Cape town, South Africa). Synthesis was performed utilising an automated cassette module (GAIA; Elysia-Raytest, Straubenhardt, Germany). Standard fluidic and reagent kit for ^{68}Ga-radiolabelling of peptides (ABX advanced biochemical compounds; GmbH, Radeberg, Germany) were used. The standard strong cation exchanger (SCX) provided by the reagent kit was replaced by 200-mg STRATA SCX (Phenomenex, Torrance, CA, USA). All reagents used were from the reagent kit unless otherwise stated. TraceSelect water, as well as ethanol Ph. Eur., were purchased from Merck (Darmstadt, Germany). DOTA-ZOL, synthesised according to the literature [40], was obtained from CheMatech (CheMatech, Dijon, France) and diluted with TraceSelect water to a final concentration of 1 mg/mL.

Manual synthesis was performed by adding gallium-68 in 500-µL eluent to 60-µL DOTA-ZOL in 4.8-mL 0.08-M ammonium acetate buffer (pH 4.5) and 500-µL ethanol in a sealed reactor. After radiolabelling in a thermo-shaker (Hettich-Benelux, Geldermalsen, Netherlands) at 95 ± 4.5 °C for 600 s, an aliquot of the reaction mixture was analysed to investigate the chelate formation.

Reactors tested for radiolabelling were TYP I plus and TopLyo obtained from Schott (Mainz, Germany), the reactor provided with the fluidic kit of the module (ABX; Radeberg, Germany), as well as standard Tc-Elu-15 vials from Cis-Bio (Berlin, Germany). All reactors were tested under equal radiolabelling conditions using the manual method.

Automated synthesis was performed using the standard fluidic kit without C18 purification (Figure 6). Gallium-68 in 450-µL eluent were added to 3.28-mL 0.08-M ammonium acetate buffer (pH 4.5) and 500-µL ethanol. After radiolabelling at 95 ± 4.5 °C for 648 ± 112 s, the reaction mixture was diluted with isotonic saline solution and sterile-filtered

into the final product vial. Analysis of the complexation was performed on an aliquot of the final product solution.

SPE cartridges tested for purification of [^{68}Ga]Ga-DOTA-ZOL are listed in detail in the Supplementary Materials (Table 2). Preconditioning of the particular column was performed according to the manufacturer's instructions. To evaluate the different SPE columns for the automated method but with the original cassette setup trap, either [^{68}Ga]Ga-DOTA-ZOL or free, uncomplexed gallium-68 was used on the respective column. For all experiments, either the pure or diluted reaction mixture was passed over the entire cartridge. Recovery was evaluated using the data from the module providing 4 radioactivity detectors. Additional manual synthesis was performed in cases were only one species was retained. To obtain a product suitable for medical use, only ethanol, water, saline or mixtures thereof were considered as solvents for elution. Complexation yield and purity were quantified via radio TLC using the methods described in Table 1 utilising aliquots of each the pure reaction mixture, waste and eluate from the cartridge. Rejection criteria were: no selective trapping of one species, loss of product during purification steps >10% and purification effect not sufficient.

Quality Control

Solvents and chemicals for quality control are listed below. Optigrade acetonitrile (ACN) was obtained from PromoChem (LGC Standards; GmbH, Wesel, Germany); acetylacetone (acac) from Sigma-Aldrich (St. Louis, MO, USA); water for chromatography (LC-MS Grade) LiChrosolv, Certipur citric buffer pH 4, Certipur citric buffer pH 5, acetone (ac), methanol (MeOH), hydrochloric acid (HCl) suprapure 30% and trifluoroacetic acid (TFA) from Merck (KGaA, Darmstadt, Germany); ethylacetate (EtOAc) from ACROS Organics (Geel, Belgium) and saline solution from Fresenius Kabi (Bad Homburg, Germany). Triethylammonium phosphate (TEAP) solution for HPLC, buffer solution 1 M, pH 3.0 (Merck KGaA, Darmstadt, Germany). Tri-sodium citrate dihydrate for analysis EMSURE® 29.4 g (100 mMolar) (Merck KGaA, Darmstadt, Germany). Sodium phosphate 96% 16.3 g (100 mMolar) (Merck KGaA, Darmstadt, Germany). The 60-mM tetrabutylammonium phosphate buffer (TBAP) was prepared by dissolution of 40.0 g (0.294 mol) of dipotassium dihydrogen phosphate (Merck KGaA, Darmstadt, Germany) and 20.0 g (0.059 mol) of tetrabutylammonium hydrogensulfate (ACROS Organics, Geel, Belgium) in 1000 mL of water. Unless otherwise indicated, this solution was used for analyses.

For quality control, an aliquot of about 150 µL was taken from the reaction mixture (manual method) or from the final formulation (automated method). Radioactivity was measured with a dose calibrator (ISOMED 2010; MED Nuklear-Medizintechnik Dresden GmbH, Dresden, Germany).

Radio thin-layer chromatography (radio TLC) was analysed with a single trace radio TLC scanner (PET miniGITA; Elysia-Raytest, Straubenhardt, Germany) and an evaluation software (GinaStar TLC; Elysia-Raytest, Straubenhardt, Germany). A series of stationary phases were evaluated with a variety of different mobile phases, which are listed in detail in the Supplemental Materials (Table 2).

Radio-HPLC was performed using Agilent 1260 Infinity II reverse-phase HPLC system (Agilent Technologies, Santa Clara, CA, USA) equipped with GABI γ-HPLC flow detector (Elysia-raytest, Straubenhardt, Germany) and a PC interface running Gina Star software (Elysia-raytest, Straubenhardt, Germany). All columns evaluated, as well as the mobile phases and gradient systems, are listed in detail in the Supplemental Materials (Table 4).

Conclusions

The implementation of the novel radiopharmaceutical [^{68}Ga]Ga-DOTA-ZOL into clinical routine production exhibited more challenges than expected for a previously published compound. For all of these revealed issues, an intensive analysis for possible solutions was performed. Not every issue could be addressed to our entire satisfaction (e.g., still, the automated method is not suitable for routine production due to the lack of proper coated reactors) or even solved at all (e.g., SPE purification still not possible without a high loss of activity). Nevertheless, the previously published radio TLC method could be improved and provides reliable information about the complexation yield in combination with two other (one newly developed) methods. Additionally, as a first step forward, a radio HPLC identification was successfully made, even though there is still room and need for improvement. Further enhancements may be achieved by optimising the pH, as well as further adjustments in the solvent composition and/or flow rate, and are the focus of ongoing research.

In conclusion, the example of the DOTA-conjugated zoledronate showed that, sometimes, very little changes lead to a high impact on radiolabelling outcomes (e.g., normal glass reaction vessels vs. coated reaction vessels).

Author Contributions

Conceptualisation, E.E. and M.M.; methodology, M.M.; software, M.M.; validation, E.E., S.K. and M.M., formal analysis, E.E., S.K. and M.M.; investigation, M.M.; resources, S.K. and M.E.; data curation, E.E.; writing—original draft preparation, E.E. and M.M.; writing—review and editing, E.E., S.K. M.E. and M.M.; visualisation, E.E. and M.M.; supervision, E.E.; project administration, E.E. and funding acquisition, E.E. All authors have read and agreed to the published version of the manuscript.

Funding

This study was funded by BONFOR (grant number O-140.0008).

Acknowledgements

The authors would like to thank Isotope Technologies Garching (ITG GmbH) for the supply of DOTA-ZOL and technical support.

Conflicts of Interest

The authors declare that they have no conflict of interest.

References

1. Coleman RE, Lipton A, Roodman GD, Guise TA, Boyce BF, Brufsky AM, et al. Metastasis and bone loss: advancing treatment and prevention. Cancer Treatment Reviews. 2010;36:615–20. doi:10.1016/j.ctrv.2010.04.003.
2. Li S, Peng Y, Weinhandl ED, Blaes AH, Cetin K, Chia VM, et al. Estimated number of prevalent cases of metastatic bone disease in the US adult population. Clinical Epidemiology. 2012;4:87–93. doi:10.2147/CLEP.S28339.
3. Coleman RE. Bisphosphonates: clinical experience. The Oncologist. 2004;9 Suppl 4:14–27. doi:10.1634/theoncologist.9-90004-14.
4. van der Toom EE, Verdone JE, Pienta KJ. Disseminated tumor cells and dormancy in prostate cancer metastasis. Curr. Opin. Biotechnol. 2016;40:9–15. doi:10.1016/j.copbio.2016.02.002.
5. YIN JJ, POLLOCK CB, KELLY K. Mechanisms of cancer metastasis to the bone. Cell Research. 2005;15:57–62. doi:10.1038/sj.cr.7290266.
6. Nørgaard M, Jensen AØ, Jacobsen JB, Cetin K, Fryzek JP, Sørensen HT. Skeletal related events, bone metastasis and survival of prostate cancer: a population

based cohort study in Denmark (1999 to 2007). Journal of Urology. 2010;184:162–7. doi:10.1016/j.juro.2010.03.034.

7. Bubendorf L, Schöpfer A, Wagner U, Sauter G, Moch H, Willi N, et al. Metastatic patterns of prostate cancer: an autopsy study of 1,589 patients. Human Pathology. 2000;31:578–83. doi:10.1053/hp.2000.6698.
8. Gandaglia G, Karakiewicz PI, Briganti A, Passoni NM, Schiffmann J, Trudeau V, et al. Impact of the Site of Metastases on Survival in Patients with Metastatic Prostate Cancer. European Urology. 2015;68:325–34. doi:10.1016/j.eururo.2014.07.020.
9. Pfannkuchen N, Meckel M, Bergmann R, Bachmann M, Bal C, Sathekge M, et al. Novel Radiolabeled Bisphosphonates for PET Diagnosis and Endoradiotherapy of Bone Metastases. Pharmaceuticals (Basel). 2017;10:45. doi:10.3390/ph10020045.
10. Ye L, Kynaston H, Jiang W. Bone metastasis in prostate cancer: Molecular and cellular mechanisms (Review). Int J Mol Med 2007. doi:10.3892/ijmm.20.1.103.
11. Hensel J, Thalmann GN. Biology of Bone Metastases in Prostate Cancer. Urology. 2016;92:6–13. doi:10.1016/j.urology.2015.12.039.
12. Gonzalez-Sistal A, Baltasar A, Herranz M, Ruibal A. Advances in Medical Imaging Applied to Bone Metastases. In: Erondu OF, editor. Medical Imaging. [S.l.]: InTech; 2011. doi:10.5772/28519.
13. Agarwal MG, Nayak P. Management of skeletal metastases: An orthopaedic surgeon's guide. Indian Journal of Orthopaedics. 2015;49:83–100. doi:10.4103/0019-5413.143915.
14. Ulmert D, Solnes L, Thorek DL. Contemporary approaches for imaging skeletal metastasis. Bone Research. 2015;3:15024. doi:10.1038/boneres.2015.24.
15. Neuman WF, Neuman MW. The chemical dynamics of bone mineral; 1958.
16. Selby P, Davie M, Ralston S, Stone M. Guidelines on the management of Paget's disease of bone*. Bone. 2002;31:366–73. doi:10.1016/S8756-3282(02)00817-7.
17. Russell RGG. Bisphosphonates: the first 40 years. Bone. 2011;49:2–19. doi:10.1016/j.bone.2011.04.022.
18. Hughes EAB, Robinson TE, Bassett DB, Cox SC, Grover LM. Critical and diverse roles of phosphates in human bone formation. Journal of Materials Chemistry B. 2019;7:7460–70. doi:10.1039/C9TB02011J.
19. Orriss IR. Extracellular pyrophosphate: The body's "water softener". Bone. 2020;134:115243. doi:10.1016/j.bone.2020.115243.
20. FLEISCH H, BISAZ S. Isolation from urine of pyrophosphate, a calcification inhibitor. American Journal of Physiology-Legacy Content. 1962;203:671–5. doi:10.1152/ajplegacy.1962.203.4.671.

21. Jung A, BISAZ S, FLEISCH H. The binding of pyrophosphate and two diphosphonates by hydroxyapatite crystals. Calcified Tissue Research. 1973;11:269–80. doi:10.1007/BF02547227.

22. FLEISCH H, Russell RG, STRAUMANN F. Effect of pyrophosphate on hydroxyapatite and its implications in calcium homeostasis. Nature. 1966;212:901–3. doi:10.1038/212901a0.

23. Drake MT, Clarke BL, Khosla S. Bisphosphonates: mechanism of action and role in clinical practice. Mayo Clin Proc. 2008;83:1032–45. doi:10.4065/83.9.1032.

24. van Beek E, Löwik C, Que I, Papapoulos S. Dissociation of binding and antiresorptive properties of hydroxybisphosphonates by substitution of the hydroxyl with an amino group. J Bone Miner Res. 1996;11:1492–7. doi:10.1002/jbmr.5650111016.

25. Dunford JE, Thompson K, Coxon FP, Luckman SP, Hahn FM, Poulter CD, et al. Structure-activity relationships for inhibition of farnesyl diphosphate synthase in vitro and inhibition of bone resorption in vivo by nitrogen-containing bisphosphonates. J Pharmacol Exp Ther. 2001;296:235–42.

26. Kavanagh KL, Guo K, Dunford JE, Wu X, Knapp S, Ebetino FH, et al. The molecular mechanism of nitrogen-containing bisphosphonates as antiosteoporosis drugs. Proc Natl Acad Sci U S A. 2006;103:7829–34. doi:10.1073/pnas.0601643103.

27. Dhar MK, Koul A, Kaul S. Farnesyl pyrophosphate synthase: a key enzyme in isoprenoid biosynthetic pathway and potential molecular target for drug development. New Biotechnology. 2013;30:114–23. doi:10.1016/j.nbt.2012.07.001.

28. Räikkönen J, Taskinen M, Dunford JE, Mönkkönen H, Auriola S, Mönkkönen J. Correlation between time-dependent inhibition of human farnesyl pyrophosphate synthase and blockade of mevalonate pathway by nitrogen-containing bisphosphonates in cultured cells. Biochemical and Biophysical Research Communications. 2011;407:663–7. doi:10.1016/j.bbrc.2011.03.070.

29. Hall A. Rho GTPases and the actin cytoskeleton. Science. 1998;279:509–14. doi:10.1126/science.279.5350.509.

30. Luckman SP, Hughes DE, Coxon FP, Graham R, Russell G, Rogers MJ. Nitrogen-containing bisphosphonates inhibit the mevalonate pathway and prevent post-translational prenylation of GTP-binding proteins, including Ras. Journal of Bone and Mineral Research. 1998;13:581–9. doi:10.1359/jbmr.1998.13.4.581.

31. Ogawa K, Ishizaki A. Well-designed bone-seeking radiolabeled compounds for diagnosis and therapy of bone metastases. BioMed Research International. 2015;2015:676053. doi:10.1155/2015/676053.

32. Damerla V, Packianathan S, Boerner PS, Jani AB, Vijayakumar S, Vijayakumar V. Recent Developments in Nuclear Medicine in the Management of Bone Metastases. American Journal of Clinical Oncology. 2005;28:513–20. doi:10.1097/01.coc.0000162425.55457.10.

33. Den RB, George D, Pieczonka C, McNamara M. Ra-223 Treatment for Bone Metastases in Castrate-Resistant Prostate Cancer: Practical Management Issues for Patient Selection. American Journal of Clinical Oncology. 2019;42:399–406. doi:10.1097/COC.0000000000000528.

34. FRIEDELL HL, STORAASLI JP. The use of radioactive phosphorus in the treatment of carcinoma of the breast with widespread metastases to bone. Am J Roentgenol Radium Ther. 1950;64:559–75.

35. Kubícek V, Rudovský J, Kotek J, Hermann P, Vander Elst L, Muller RN, et al. A bisphosphonate monoamide analogue of DOTA: a potential agent for bone targeting. J. Am. Chem. Soc. 2005;127:16477–85. doi:10.1021/ja054905u.

36. Vitha T, Kubícek V, Hermann P, Elst LV, Muller RN, Kolar ZI, et al. Lanthanide(III) complexes of bis(phosphonate) monoamide analogues of DOTA: bone-seeking agents for imaging and therapy. J. Med. Chem. 2008;51:677–83. doi:10.1021/jm7012776.

37. Meckel M, Nauth A, Timpe J, Zhernosekov K, Puranik AD, Baum RP, Rösch F. Development of a 177LuBPAMD labeling kit and an automated synthesis module for routine bone targeted endoradiotherapy. Cancer Biotherapy and Radiopharmaceuticals. 2015;30:94–9. doi:10.1089/cbr.2014.1720.

38. Fellner M, Biesalski B, Bausbacher N, Kubícek V, Hermann P, Rösch F, Thews O. (68)Ga-BPAMD: PET-imaging of bone metastases with a generator based positron emitter. Nuclear Medicine and Biology. 2012;39:993–9. doi:10.1016/j.nucmedbio.2012.04.007.

39. Fellner M, Baum RP, Kubícek V, Hermann P, Lukes I, Prasad V, Rösch F. PET/CT imaging of osteoblastic bone metastases with (68)Ga-bisphosphonates: first human study. European Journal of Nuclear Medicine and Molecular Imaging. 2010;37:834. doi:10.1007/s00259-009-1355-y.

40. Meckel M, Bergmann R, Miederer M, Roesch F. Bone targeting compounds for radiotherapy and imaging: *Me(III)-DOTA conjugates of bisphosphonic acid, pamidronic acid and zoledronic acid. EJNMMI Radiopharmacy and Chemistry. 2017;1:14. doi:10.1186/s41181-016-0017-1.

41. Khawar A, Eppard E, Roesch F, Ahmadzadehfar H, Kürpig S, Meisenheimer M, et al. Preliminary results of biodistribution and dosimetric analysis of 68GaGa-DOTA-ZOL: a new zoledronate-based bisphosphonate for PET/CT diagnosis of bone diseases. Ann Nucl Med. 2019;33:404–13. doi:10.1007/s12149-019-01348-7.

42. Khawar A, Eppard E, Roesch F, Ahmadzadehfar H, Kürpig S, Meisenheimer M, et al. Biodistribution and post-therapy dosimetric analysis of 177LuLu-DOTAZOL in patients with osteoblastic metastases: first results. EJNMMI Res. 2019;9:102. doi:10.1186/s13550-019-0566-x.

43. Seemann J, Eppard E, Waldron BP, Ross TL, Rösch F. Cation exchange-based post-processing of 68Ga-eluate_ A comparison of three solvent systems for labelling of DOTATOC, NO2APBP and DATAm. Appl. Rad. Isot. 2015;98:54–9.

44. Eppard E, Wuttke M, Nicodemus PL, Rösch F. Ethanol-based post-processing of generator derived ^{68}Ga towards kit-type preparation of ^{68}Ga-radiopharmaceuticals. Journal of Nuclear Medicine. 2014;55:1023–8.

45. European Pharmacopoeia, 10th edition 2019: Subscription to Main volume + Supplement 1 + Supplement 2. 1st ed. Stuttgart: Deutscher Apotheker Verlag; 2019.

46. Gillings N, Todde S, Behe M, Decristoforo C, Elsinga P, Ferrari V, et al. EANM guideline on the validation of analytical methods for radiopharmaceuticals. EJNMMI Radiopharmacy and Chemistry. 2020;5:7. doi:10.1186/s41181-019-0086-z.

47. Baranyai Z, Tircsó G, Rösch F. The Use of the Macrocyclic Chelator DOTA in Radiochemical Separations. Eur. J. Inorg. Chem. 2020;2020:36–56. doi:10.1002/ejic.201900706.

48. Kumar K, Chang CA, Tweedle MF. Equilibrium and kinetic studies of lanthanide complexes of macrocyclic polyamino carboxylates. Inorganic Chemistry. 1993;32:587–93. doi:10.1021/ic00057a017.

49. Wang X, Jin T, Comblin V, Lopez-Mut A, Merciny E, Desreux JF. A kinetic investigation of the lanthanide DOTA chelates. Stability and rates of formation and of dissociation of a macrocyclic gadolinium(III) polyaza polycarboxylic MRI contrast agent. Inorganic Chemistry. 1992;31:1095–9. doi:10.1021/ic00032a034.

50. Molavipordanjani S, Tolmachev V, Hosseinimehr SJ. Basic and practical concepts of radiopharmaceutical purification methods. Drug Discovery Today. 2019;24:315–24. doi:10.1016/j.drudis.2018.09.018.

51. Pillai SA, Chobisa D, Urimi D, Ravindra N. Pharmaceutical glass interactions: A review of possibilities. 2016;8:103–11.

52. Borchert SJ, Ryan MM, Davison RL, Speed W. Accelerated extractable studies of borosilicate glass containers. J Parenter Sci Technol. 1989;43:67–79.

53. Maheswara Reddy L, Janardhan Reddy K, Raveendra Reddy P. A simple RP-HPLC method for related substances of zoledronic acid in pharmaceutical products. Arabian Journal of Chemistry. 2017;10:S196-S204. doi:10.1016/j.arabjc.2012.07.022.

4.2 DOTA-ZOL: A Promising Tool in Diagnosis and Palliative Therapy of Bone Metastasis—Challenges and Critical Points in Implementation into Clinical Routine Supplemental Material

Michael Meisenheimer[1], Stefan Kürpig[1], Markus Essler[1], Elisabeth Eppard[*2]

[1]Department of Nuclear Medicine, University Hospital Bonn, D-53127 Bonn, Germany

[2]actual adress: PositronPharma S.A, Rancagua 878, 7500921 Providencia, Chile

*Corresponding author: eeppard@positronpharma.cl; PositronPharma S.A, Rancagua 878, 7500921 Providencia, Chile

https://doi.org/10.3390/molecules25132988

Materials and Methods

Radiolabelling

Gallium-68 was obtained from a $^{68}Ge/^{68}Ga$-generator (iThemba Labs, South-Africa). Synthesis was performed utilizing an automated cassette module (GAIA, Elysia-Raytest, Straubenhardt, Germany). Standard fluidic and reagent kit for ^{68}Ga-radiolabelling of peptides (ABX advanced biochemical compounds GmbH, Radeberg, Germany) were used. The standard strong cation exchanger (SCX) provided by the reagent kit was replaced by 200 mg STRATA SCX (Phenomenex, USA). All reagents used are from the reagent kit unless otherwise stated. TraceSelect water as well as ethanol Ph. Eur. were purchased from Merck (Darmstadt, Germany). DOTA-ZOL was obtained from CheMatech (CheMatech, Dijon, France) and diluted with TraceSelect water to a final concentration of 1 mg/ml.

Manual synthesis was performed by adding gallium-68 in 500 µL eluent to 60 µL DOTA-ZOL in 4.8 mL 0.08 M ammonium acetate buffer (pH 4.5) and 500 µL ethanol in a sealed reactor. After radiolabelling in a thermo-shaker (Hettich-Benelux, Geldermalsen, Netherlands) at 95±4.5 °C for 600 s, an aliquot of the reaction mixture was analysed to investigate the chelate formation.

Reactors tested for radiolabelling were TYP I plus and TopLyo obtained from Schott (Mainz, Germany), the reactor provided with the fluidic kit of the module (ABX Radeberg, Germany) as well as standard Tc-Elu-15 vials from Cis-Bio (Berlin, Germany). All reactors were tested under equal radiolabelling conditions using the manual method.

Automated synthesis was performed using the standard fluidic kit without C18 purification (Figure 6). gallium-68 in 450 µL eluent were added to 60 µL DOTA-ZOL in 3.28 ml 0.08 M ammonium acetate buffer (pH 4.5) and 500 µL ethanol. After radiolabelling at 95±4.5 °C for 648±112 s the reaction mixture was diluted with isotonic saline solution and sterile filtered into the final product vial. Analysis of the complexation was performed on an aliquot of the final product solution.

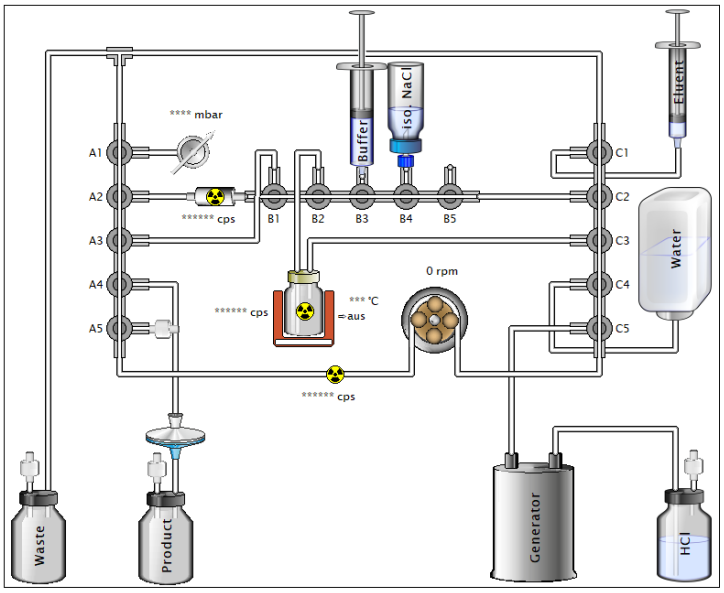

Figure 6: Schematic illustration of the fluidic kit setup of the automated synthesis of [^{68}Ga]Ga-DOTA-ZOL.

The solid phase extraction (SPE) cartridges tested for purification of [^{68}Ga]Ga-DOTA-ZOL are obtained from Agilent (Santa Clara, USA), Grace (Columbia, USA), Macherey-Nagel (Düren, Germany), Waters (Milford, USA), Phenomenex (Torrance, USA), Merck KGaA (Darmstadt, Germany). A detailed list is provided in Table 3. Preconditioning of the particular column was performed according to manufacturer's instructions. To obtain purified [^{68}Ga]Ga-DOTA-ZOL an attempt was made to trap either [^{68}Ga]Ga-DOTA-ZOL or free uncomplexed gallium-68 on the respective column. To obtain a product suitable for medical use only ethanol, water, saline or mixtures thereof were considered as solvents for elution.

Quality Control

Solvents and chemicals for quality control are listed below. Optigrade acetonitrile (ACN) was obtained from PromoChem (LGC Standards GmbH Wesel, Germany), acetylacetone (acac) from Sigma-Aldrich (St. Louis, USA), Water for chromatography (LC-MS Grade) LiChrosolv, Certipur citric buffer pH 4, Certipur citric buffer pH 5, acetone (ac), methanol (MeOH), hydrochloric acid (HCl) suprapure 30%, trifluoroacetic acid (TFA) from Merck (KGaA Darmstadt, Germany), ethyl acetate (EtOAc) from ACROS Organics (Geel, Belgium) and saline solution from Fresenius Kabi (Bad Homburg, Germany). Triethylammonium phosphate (TEAP) solution for HPLC, buffer solution 1 M pH 3.0 (Merck KGaA, Darmstadt, Germany). Tri-sodium citrate dihydrate for analysis EMSURE® 29.4

g (100mMolar) (Merck KGaA, Darmstadt, Germany). Sodium phosphate 96% 16.3 g (100 mMolar) (Merck KGaA, Darmstadt, Germany) in 1000 ml water.

The 60 mM tetrabutylammonium phosphate buffer (TBAP) was prepared by dissolution of 40.0 g (0.294 mol) of dipotassium dihydrogen phosphate (Merck KGaA, Darmstadt, Germany) and 20.0 g (0.059 mol) of tetrabutylammonium hydrogensulfate (ACROS Organics, Geel, Belgium) in 1000 mL water. Unless otherwise indicated, this solution was used for analysis.

For quality control an aliquot of about 150 µL was taken from the reaction mixture (manual method) or from the final formulation (automated method). Radioactivity was measured with a dose calibrator (ISOMED 2010, MED Nuklear-Medizintechnik Dresden GmbH, Dresden, Germany).

Radio thin-layer chromatography (radio-TLC) was analysed with a single trace radio-TLC-scanner (PET-miniGITA, Elysia-Raytest, Straubenhardt, Germany) and an evaluation software (GINA Star TLC, Elysia-Raytest, Straubenhardt, Germany). As stationary phase silica-gel coated aluminium TLC-plates (silica 60 F254, Merck, Darmstadt, Germany), silica-gel impregnated microfiber paper (iTLC-SG, Agilent Technologies, Santa Clara, California), silicic acid impregnated microfiber paper (iTLC-SA, Agilent Technologies, Santa Clara, California), silica-gel coated glass fibre paper (GF-DC Macherey-Nagel, Düren, Germany) as well as cellulose fibres (3MM CHR, Whatman International Ltd., Maidstone, England) were evaluated with a variety of different mobile phases (Table 2).

Radio-HPLC was performed using Agilent 1260 Infinity II reverse phase HPLC system (Agilent Technologies, Santa Clara, California) equipped with GABI γ-HPLC flow detector (Elysia-raytest, Straubenhardt, Germany) and a PC interface running Gina Star software (Elysia-raytest, Straubenhardt, Germany). Several columns where evaluated, namely Infinity Lab Poroshell 120 EC C18 4.6*50 mm 2.7 µm, ZORBAX Infinity Eclipse plus C18 4.6*100 mm 3.5 µm and ZORBAX SB-C18 9.4*250 mm 5 µm (Agilent Technologies Folson, CA), EC 125/4 Nucleodur 100-3 C18 ec; EC 150/3 Nucleodur C18 HTec 3 µm; 250/4 Nucleodur Hilic 5 µm; 250/4 Nucleodur 300-5 C18, VA 50/4.6 Nucleodur RP 4000-8 (Macherey-Nagel GmbH & Co, Kg, Düren Germany), as well as Kinetex 5 µm Biphenyl 100 Å 250*4.6 mm; Luna 5µm NH_2 100 Å 250*4.6 mm ; Jupiter 5 µm C5 300 Å 250*4.6 mm (Phenomenex Inc., Torrance CA), with several mobile phases and gradient systems (Table 2).

Results

Radio Thin-Layer Chromatography

[^{68}Ga]Ga-DOTA-ZOL was prepared using a manual method. Gallium-68 and ^{68}Ga-colloids were obtained from generator eluate in 0.6 M HCl which was adjusted with sodium hydroxide (NaOH) to pH 5.5 for the latter one. Order of appearance in the figures is always as followed: first row [^{68}Ga]Ga-DOTA-ZOL, second row ^{68}Ga-colloids, third row free uncomplexed gallium-68. Travel distance of the mobile phase was 7 cm in all cases. Count of replicates for every radio-TLC is three. All radio-TLCs shown in Figure 7 and Figure 8 are from the same batch of the respective substance.

Radio-TLCs of the different potentially present species using the published method (acac/ac/con. HCl (10:10:1) and silica 60 F254 TLC plates) (Figure 7) [1]. Retention factors of [^{68}Ga]Ga-DOTA-ZOL are 0-0.2 respectively 0.8-1 for ^{68}Ga-colloids, 0.6-0.9 for uncomplexed gallium-68.

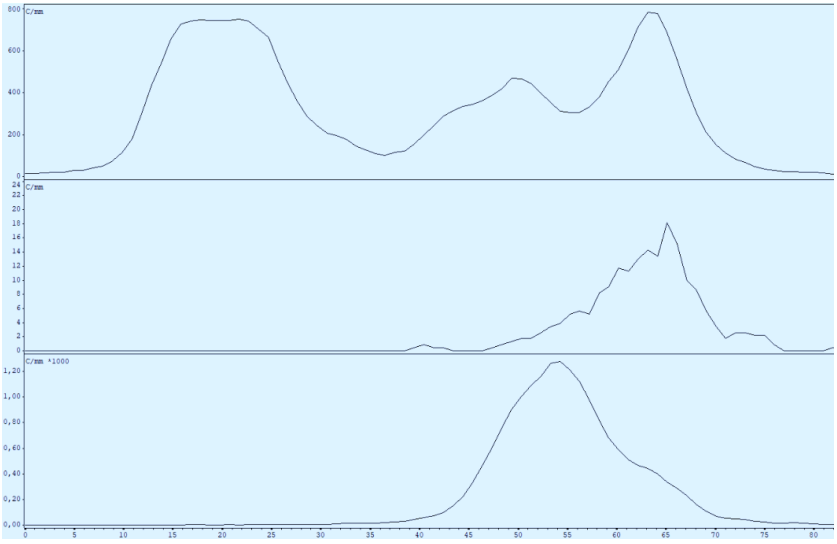

Figure 7: Radio-TLC chromatograms of the different species potentially present in a [^{68}Ga]Ga-DOTA-ZOL synthesis developed in acac/ac/conc. HCl (10:10:1) with silica 60 F254 TLC plates as stationary phase. Appearance in the following order: final product of a [^{68}Ga]Ga-DOTA-ZOL synthesis, ^{68}Ga-colloids, [^{68}Ga]Ga^{3+}.

Revised published method without concentrated HCl with silica 60 F254 TLC plates as stationary phase (Figure 8). Retention factors of [^{68}Ga]Ga-DOTA-ZOL are 0-0.1 respectively 0-0.1 and 0.5-0.9 for ^{68}Ga-colloids and 0.7-0.8 for uncomplexed gallium-68.

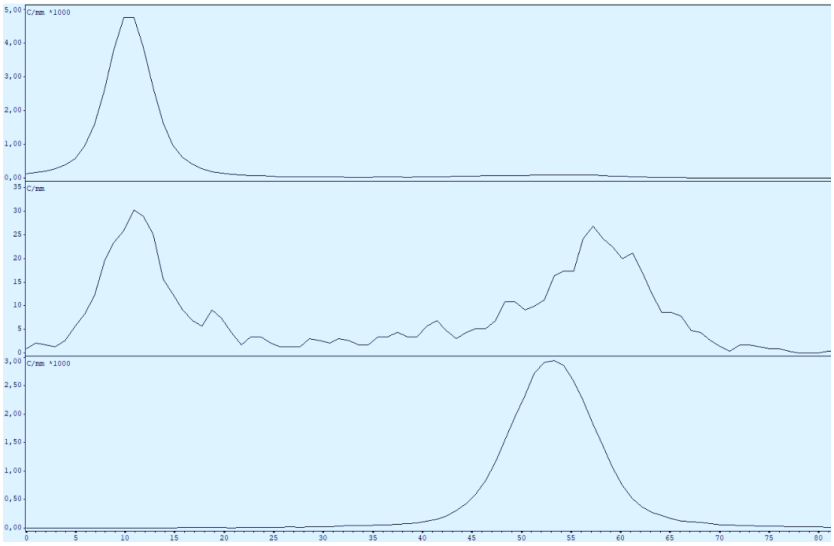

Figure 8: Radio-TLC chromatograms of the different species potentially present in a [^{68}Ga]Ga-DOTA-ZOL synthesis developed in acac/ac with silica 60 F254 TLC plates as stationary phase. Appearance in the following order: final product of a [^{68}Ga]Ga-DOTA-ZOL synthesis, ^{68}Ga-colloids, [^{68}Ga]Ga^{3+}.

Radioactive species developed in citric buffer pH 4 with silica 60 F254 TLC plates as stationary phase (Figure 9). Retention factors of [^{68}Ga]Ga-DOTA-ZOL are 0-0.1 respectively 0.1-0.2 for ^{68}Ga-colloids and 0.7-1 for uncomplexed gallium-68.

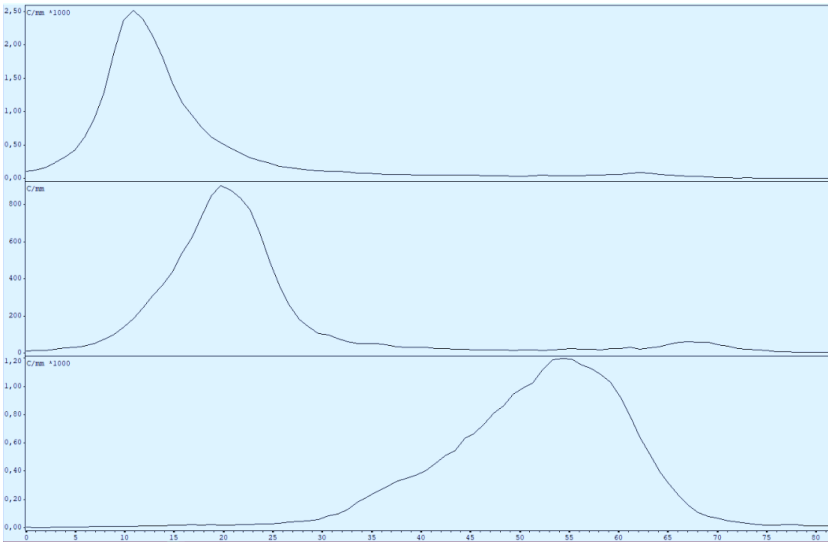

Figure 9: Radio-TLC chromatograms of the different species potentially present in a [^{68}Ga]Ga-DOTA-ZOL synthesis developed in citric buffer pH 4 with silica 60 F254 TLC plates as stationary phase. Appearance in the following order final product of a [^{68}Ga]Ga-DOTA-ZOL synthesis, ^{68}Ga-colloids, [^{68}Ga]Ga^{3+} present as citrate complex.

Radioactive species developed in TBAP/MeOH (9:1) with silica 60 F254 TLC plates as stationary phase (Figure 10). Retention factors of [^{68}Ga]Ga-DOTA-ZOL are 0.7-0.8 respectively 0.1-0.3 for ^{68}Ga-colloids and 0.1-0.2 for uncomplexed gallium-68.

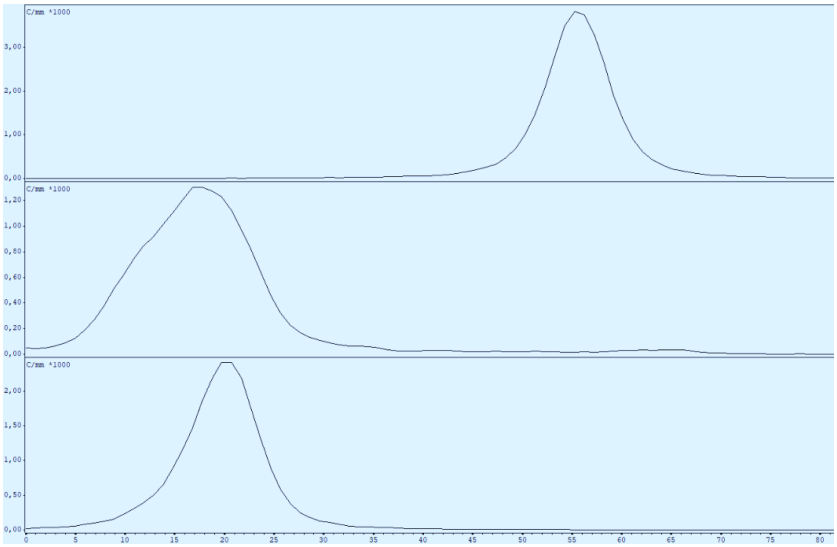

Figure 10: Radio-TLC chromatograms of the different species potentially present in a [^{68}Ga]Ga-DOTA-ZOL synthesis developed in TBAP/MeOH (9:1) with silica 60 F254 TLC plates as stationary phase. Appearance in the following order final product of a [^{68}Ga]Ga-DOTA-ZOL synthesis, ^{68}Ga-colloids, [^{68}Ga]Ga^{3+}.

A detailed tabulation of the tested mobile phases using TLC silica 60 F254 and iTLC SG plates as stationary phase is listed below (Table 2). All other stationary phases listed in the materials section were found to be unsuitable for quality control of radiolabelled [^{68}Ga]Ga-DOTA-ZOL.

Table 2: List of investigated radio-TLC conditions. Greyed cells represent no single peak or smear of the species.

	Stationary phase					
Mobile phase	**TLC silica 60 F254**			**iTLC SG**		
	R_f A	**R_f B**	**R_f C**	**R_f A**	**R_f B**	**R_f C**
0.9% saline						
ac						
acac	0-0.2	0.8-1				
acac/ac (1:1)	0-0.1	0.7-0.8				

acac/ac/HCl (1:1:0.1) [1]		0.6-0.9	0.8-1		
ACN				0-0.2	0.8-1
Citric buffer pH 4	0-0.1	0.7-1	0.1-0.2		
Citric buffer pH 5	0-0.1	0.7-1	0.1-0.2		
EtOAc					
H_2O					
MEK					
MeOH					
PrOH					
TBAP	0.7-1				
TBAP/ac (1:1)					
TBAP/acac (1:1)					
TBAP/acac (3:1)					
TBAP/MeOH (9:1)	0.7-0.8	0.1-0.3	0.1-0.2		

A: [^{68}Ga]Ga-DOTA-ZOL; B: [^{68}Ga]Ga^{3+}; C: ^{68}Ga-colloids

To verify the dissociation of the compound facilitated by the mobile phase of the published method, a further experiment was performed. An aliquot [^{68}Ga]Ga-DOTA-ZOL was incubated 5 min in a preparation of the mobile phase (acac/ac/conc. HCl (10:10:1) and subsequent control using citric buffer pH 4 as mobile phase. In both cases silica 60 F254 TLC plates was used as stationary phase. The obtained chromatograms are presented in Figure 11. Already after 5 min the majority of the radioactivity is observed in one peak at R_f 0.5. A control with an aliquot of pure ^{68}Ga eluate also incubated in acac/ac/conc. HCl (10:10:1) resulted in a similar chromatogram with the activity found at R_f 0.5. It can be assumed that gallium-68 is present as [^{68}Ga]$Ga(acac)_3$ instead of a weak gallium citrate complex. In a second experiment an aliquot of a preparation [^{68}Ga]Ga-DOTA-TOC (initial radiochemical purity > 98 % as determined by means of radio-HPLC and radio-TLC) was treated equally and exhibited the same behaviour as found for [^{68}Ga]Ga-DOTA-ZOL.

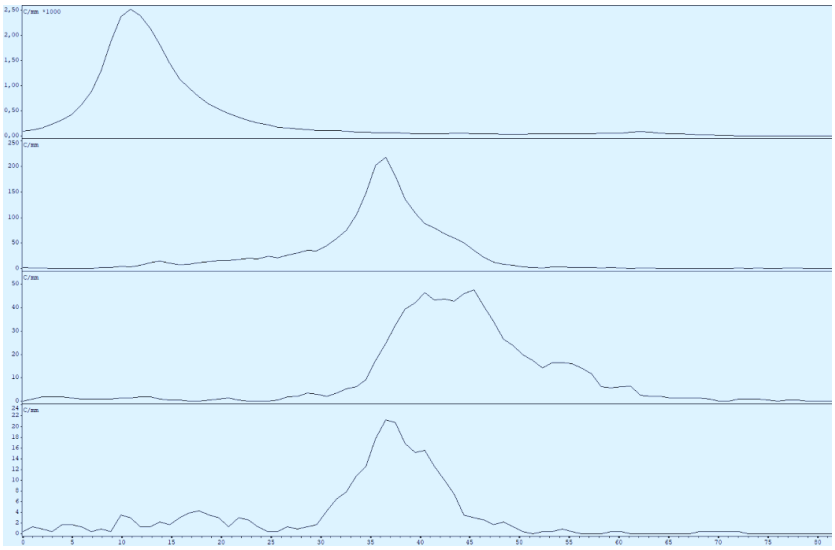

Figure 11: Change of composition during incubation in the solvent system of the published radio-TLC method developed in citric buffer pH 4 with silica 60 F254 TLC plates as stationary phase. First row: radioTLC chromatogram of [^{68}Ga]Ga-DOTA-ZOL after synthesis. Second row: [^{68}Ga]Ga-DOTA-ZOL incubated 5 min in a preparation of acac/ac/conc. HCl (10:10:1). Third row: ^{68}Ga eluate incubated 5 min in a preparation of acac/ac/conc. HCl (10:10:1). Fourth row: [^{68}Ga]Ga-DOTA-TOC (initial complexation rate 98 %) after 5 min incubation in a preparation of acac/ac/conc. HCl (10:10:1).

Solid phase extraction

To evaluate the different SPE columns for their suitability to purify [^{68}Ga]Ga-DOTA-ZOL the automated method was used but with original cassette setup. The cartridges listed in Table 3 were evaluated in terms of trapping, recovery and final achievable purity of the product. For all experiments either the pure or diluted reaction mixture was passed over the entire cartridge. Recovery was evaluated using the data from the module providing 4 radioactivity detectors. Additional manual synthesis was performed in cases were only one species was retained. Complexation yield and purity were quantified via radio-TLC using the methods described in Table 2 utilizing aliquots of each the pure reaction mixture, waste and eluate from the cartridge. Rejection criteria were:

- no selective trapping of one species
- loss of product during purification steps >10%
- purification effect not sufficient.

Table 3: List of all evaluated SPE cartridges.

	SPE cartridge	Size	Should retain	Retain	Comments
	Agilent				
1	Bond Elut SCX	500 mg	Ga	Ga; P	Dismissed
2	Bond Elut Certify	200 mg	Ga	-	Dismissed
	Grace				
3	Alltech Extract-Clean IC-Ag	1.5 ml	P	Ga; P	Dismissed
4	Alltech Extract-Clean IC-H	0.5 ml	P	-	Dismissed
5	Alltech Extract-Clean IC-OH	1.5 ml	P	Ga; P	Dismissed
	Macherey-Nagel				
6	Chromabond HILIC	500 mg	P	-	Dismissed
7	Chromabond HR-XC	60 mg	P	-	Dismissed
8	Chromafix HR-XC	S	P	Ga; P	Dismissed
9	Chromafix C18 ec	S	P	-	Dismissed
10	Chromafix C4	M	P	-	Dismissed
11	Chromafix HR-P	M	P	-	Dismissed
12	Chromafix HR-P	L	P	-	Dismissed
13	Chromafix HR-XA	S	P	Ga; P	Dismissed
14	Chromafix HR-XAW	S	P	-	Dismissed
15	Chromafix HR-XAW	M	P	Ga	Partial purification
16	Chromafix PS-Ag^+	L	P	Ga; P	Dismissed
17	Chromafix PS-BA	M	P	-	Dismissed
18	Chromafix PS-H^+	S	Ga	P	No recovery
19	Chromafix PS-H^+	M	Ga	Ga	Partial purification
20	Chromafix PS-H^+	L	Ga	Ga; P	Dismissed
21	Chromafix PS-OH-	M	P	Ga; P	Dismissed
22	Chromafix SA	M	P	Ga	Partial purification

23	Chromafix SB	M	P	Ga; P	Dismissed
	Waters				
24	Sep-Pak Alumina N Plus	280 mg	P	-	Dismissed
25	Sep-Pak C18 Plus	360 mg	P	Ga; P	Dismissed
26	Sep-Pak C18 Plus Light	130 mg	P	-	Dismissed
27	Sep-Pak Accell Plus QMA Plus	360 mg	P	-	Dismissed
28	Sep-Pak Accell Plus QMA Plus Light	130 mg	P	-	Dismissed
29	Sep-Pak Silica Plus	690 mg	P	-	Dismissed
30	Sep-Pak Silica Plus Light	120 mg	P	-	Dismissed
31	OASIS MCX 3 cc Vac	60 mg	P	-	Dismissed
32	OASIS MCX 6 cc Vac	150 mg	P	-	Dismissed
	Phenomenex				
33	Strata SCX	200 mg	Ga	Ga; P	Dismissed
34	Strata-X-C	200 mg	P	-	Dismissed
35	Strata-X-C polymeric	200 mg	P	P	No recovery

P: [^{68}Ga]Ga-DOTA-ZOL

19 cartridges did not show any retention, neither of product nor of free uncomplexed gallium-68. Consequently these 19 cartridges were dismissed.

11 cartridges retained both species, gallium-68 and the product, although not always equally strong. Each were dismissed because of product loss (> 10 %), insufficient purity of the final product or both.

3 cartridges retained gallium-68 while no retention for the product was observed. In 2 of these 3 cases gallium-68 was trapped instead of the product (expected). In all of these cases, the trapping was not completely meaning that the amount of gallium-68 left in the final product was reduced in comparison to the reaction mixture but still too high to achieve sufficient product quality. All were rejected.

2 cartridges retained only product while no retention for gallium-68 was observed. In both cases no recovery was achieved, neither with the solvents defined as suitable for the final product nor with supplier recommended eluents.

Radio High Pressure Liquid Chromatography

A detailed summary of the tested conditions is listed below (Table 4).

Table 4: List of investigated radio-HPLC conditions. Greyed cells represent no successful discrimination.

Mobile Phase	**Column**										
	A	**B**	**C**	**D**	**E**	**F**	**G**	**H**	**I**	**J**	**K**
TBAP[a]											
TBAP/MeOH 95:5 [a*]											
TBAP/MeOH 90:10[a*]							✓				
TBAP/MeOH 85:15[a*]											
TBAP/MeOH 75:25[b*]											
100 mM Na_3PO_4/100 mM $Na_3C_6H_5O_7$ pH 4.5[c]											
10 mM TBA-citrate pH 4.5/ACN[d]											
100 mM TEAP pH 2.24[a]											
0.1 % TFA in H_2O/0.1 % TFA in ACN[e]											
0.1 % TFA in H_2O/0.1 % TFA in ACN[f]											

[a]isocratic, flow 0.5; 0.7; 1; 1.2 (in 15 min) and 1.5 ml/min; in 25 min. [b]isocratic, flow 0.7; 1 and 1.2 ml/min; in 25 min. [c]gradient A:B (0:100) → A:B (0:100) in 30 min, flow 0.7; 1.2 ml/min, (provided by ITG, Germany). [d]gradient A:B (70:30) → A:B (20:80) in 30 min, flow 0.7; 1.2 ml/min, (provided by ITG, Germany). [e]gradient A:B (95:5) → A:B (20:80) in 25min, flow 0.7; 1.2 ml/min [1] [f]gradient A:B (100:0) → A:B (0:100) in 20min → A:B (50:50) from 20 to 25min, flow 0.7 ml/min

A: Agilent Infinity Lab Poroshell 120 EC C18 4.6*50 mm 2.7 µm; **B**: Agilent ZORBAX Infinity Eclipse plus C18 4.6*100 mm 3.5 µm; **C**: Agilent ZORBAX SB-C18 9.4*250 mm 5 µm; **D**: Macherey-Nagel EC 125/4 Nucleodur 100-3 C18 ec; **E**: Macherey-Nagel EC 150/3 Nucleodur C18 HTec 3 µm; **F**: Macherey-Nagel 250/4 Nucleodur Hilic 5 µm; **G**:

Macherey-Nagel 250/4 Nucleodur 300-5 C18; **H**: Macherey-Nagel VA 50/4.6 Nucleodur RP 4000-8; **I**: Phenomenex Kinetex 5 µm Biphenyl 100 Å 250*4.6 mm; **J**: Phenomenex Luna 5µm NH_2 100 Å 250*4.6 mm; **K**: Phenomenex Jupiter 5 µm C5 300 Å 250*4.6 mm
*on the basis of Maheswara Reddy et al. [2]

References

1. Meckel M, Bergmann R, Miederer M, Roesch F. Bone targeting compounds for radiotherapy and imaging: *Me(III)-DOTA conjugates of bisphosphonic acid, pamidronic acid and zoledronic acid. EJNMMI Radiopharmacy and Chemistry. 2017;1:14. doi:10.1186/s41181-016-0017-1.
2. Maheswara Reddy L, Janardhan Reddy K, Raveendra Reddy P. A simple RP-HPLC method for related substances of zoledronic acid in pharmaceutical products. Arabian Journal of Chemistry. 2017;10:S196-S204. doi:10.1016/j.arabjc.2012.07.022.

4.3 Preliminary results of biodistribution and dosimetric analysis of [^{68}Ga]Ga-DOTAZOL: A new zoledronate-based bisphosphonate for PET/CT diagnosis of bone diseases

Ambreen Khawar[1], E. Eppard[1], H. Ahmadzadehfar[1], S. Kürpig[1], M. Meisenheimer[1], F.C. Gaertner[1], F. Rösch[2], M. Essler[1], R.A. Bundschuh[1]

1. Department of nuclear medicine, University Medical Center, Bonn, Germany

2. Institute for nuclear chemistry, Johannes Gutenberg-University, Mainz, Germany

http://dx.doi.org/10.1007%2Fs12149-019-01348-7

Abstract

Objective: Pre-clinical studies with gallium-68 zoledronate ([^{68}Ga]Ga-DOTAZOL) have proposed it to be a potent bisphosphonate for PET/CT diagnosis of bone diseases and diagnostic counterpart to [^{177}Lu]Lu-DOTAZOL and [^{225}Ac]Ac-DOTAZOL. This study aims to be the first human biodistribution and dosimetric analysis of [^{68}Ga]Ga-DOTAZOL.

Methods: Five metastatic skeletal disease patients (mean age: 72 years, M: F; 4:1) were injected with 150–190 MBq (4.05–5.14 mCi) of [68Ga]Ga-DOTAZOL i.v. Biodistribution of [^{68}Ga]Ga-DOTAZOL was studied with PET/CT initial dynamic imaging for 30 min; list mode over abdomen (reconstructed as six images of 300 s) followed by static (skull to mid-thigh) imaging at 45 min and 2.5 h with Siemens Biograph 2 PET/CT camera. Also, blood samples (8 time points) and urine samples (2 time points) were collected over a period of 2.5 h. Total activity (MBq) in source organs was determined using interview fusion software (MEDISO Medical Imaging Systems, Budapest, Hungary). A blood-based method for bone marrow selfdose determination and a trapezoidal method for urinary bladder contents residence time calculation were used. OLINDA/EXM version 2.0 software (Hermes Medical Solutions, Stockholm, Sweden) was used to generate residence times for source organs, organ absorbed doses and effective doses.

Results: High uptake in skeleton as target organ, kidneys and urinary bladder as organs of excretion and faint uptake in liver, spleen and salivary glands were seen. Qualitative and quantitative analysis supported fast blood clearance, high bone to soft tissue and lesion to normal bone uptake with [^{68}Ga]Ga-DOTAZOL. Urinary bladder with the highest absorbed dose of 0.368 mSv/MBq presented the critical organ, followed by osteogenic cells, kidneys and red marrow receiving doses of 0.040, 0.031 and 0.027 mSv/MBq, respectively. The mean effective dose was found to be 0.0174 mSv/MBq which results in an effective dose of 2.61 mSv from 150 MBq.

Conclusions: Biodistribution of [^{68}Ga]Ga-DOTAZOL was comparable to [^{18}F]NaF, [^{99m}Tc]Tc-MDP and [^{68}Ga]Ga-PSMA-617. With proper hydration and diuresis to reduce urinary bladder and kidney absorbed doses, it has clear advantages over [^{18}F]NaF owing to its onsite, low-cost production and theranostic potential of personalized dosimetry for treatment with [^{177}Lu]Lu-DOTAZOL and [^{225}Ac]Ac-DOTAZOL.
Key words: [^{68}Ga]Ga-DOTAZOL; biodistribution; organ absorbed doses; effective dose.

INTRODUCTION

Metastatic skeletal disease is a long known complication in many solid tumors. It affects up to 70% of patients suffering from advanced breast or prostate cancer. It is a major contributor to increased morbidity and mortality in these patients [1–3]. The role of nuclear medicine in diagnosis, staging and assessment of treatment response in these patients is well established. Among available SPECT and PET tracers, [^{18}F]NaF PET/CT has shown sensitivity of 100% and specificity of 97% [4]. Using β− and α-emitting radionuclides for pain palliation in these patients has proved beneficial [5]. The theranostic role of nuclear medicine for management of skeletal metastatic disease has progressed from pain palliation to delivery of targeted cytotoxic radionuclide therapy as is seen with prostate-specific membrane antigen (PSMA) targeted therapies for prostate carcinoma [6]. However, targeted therapies for skeletal metastasis secondary to other tumor entities are still being investigated. Since many years, bisphosphonates have been used for pain palliation and prevention of complications from skeletal metastases. Their anti-resorptive effect has been proven in vivo and in vitro fact [7]. The high rate of adsorption by bisphosphonates encouraged its labeling with theranostic radionuclides [8]. Success in this regard has been found in successful development of ^{99m}Tc-labeleld bisphosphonates such as [^{99m}Tc]Tc-Alendronate [9] and various acyclic bisphosphonates such as, e.g., EDTMP [ethylenediamine tetra (methylene phosphonic acid] labeled with trivalent ^{68}Ga and ^{177}Lu such as [^{68}Ga]Ga-EDTMP [10], and [^{177}Lu]Lu-EDTMP [11–15]. In addition, there is a class of bisphosphonates conjugated to macrocyclic chelators, which allow for labeling with trivalent radiometals [16, 17]. Among this group, simple bisphosphonates have been investigated first such as BPAMD (4-{[(bis(phophonomethyl)carbamoyl]methyl}-7,10-bis(carboxymethyl)-1,4,7,10-tetraazacyclododec-1-yl) acetic acid, resulting in [^{68}Ga]Ga-BPAMD [18] and [^{177}Lu]Lu-BPAMD [18, 19]. Despite the great potential of BPAMD as a theranostic pair, further radiopharmaceutical research demonstrated, that the NOTA version [^{68}Ga]Ga-NO2APBP ([^{68}Ga]Ga-1,4,7-triazacyclonone-1,4-diacetic acid) of that bisphosphonate not only allowed for more effective labelling with gallium-68, but also demonstrated superior targeting quality [20]. It is superior with high thermodynamic stability and kinetic inertness as compared to DOTA-labeled ^{68}Ga bisphosphonates, labeling of which is less efficient and more vulnerable to experimental conditions. It was characterized by high skeletal uptake and less kidney uptake [20]. However, in pre-clinical animal biodistribution studies, ist therapeutic counterpart [^{177}Lu]Lu-NO2APBP was found inferior to [^{177}Lu]Lu-BPAMD with less affinity to skeleton [21]. To date, [^{68}Ga]Ga-NO2APBP and [^{177}Lu]Lu-BPAMD thus represent the theranostic combination of the simple bisphosphonate. Alpha-hydroxy bisphosphonates like pamidronate and, in particular,

alpha-hydroxy bisphosphonates containing a potent nitrogen-containing moiety like zoledronate represent the next generation of bisphosphonates [22–24]. In addition to binding with hydroxyapatite structure of the bone, their interaction with the HMG CoA reductase pathway results in inhibition of farnesyl diphosphate synthase (FPPS) culminating in apoptosis of osteoclasts, hence exhibiting a biochemical target [8]. Among them, zoledronic acid has shown the highest FPPS inhibition and best affinity to hydroxyl apatite making it the bisphosphonate of choice for labeling with diagnostic and therapeutic radionuclide [24]. The bifunctional chelate DOTA has facilitated labeling of these bisphosphonates with Me (III), Gallium-68 and Lutetium-177 [17] for diagnosis and treatment of skeletal metastatic disease, respectively, thus achieving a chemical goal of new theranostic development [17]. Pre-clinical in vitro and in vivo studies with [^{68}Ga]Ga-DOTAZOL have shown high hydroxyapatite binding, good target to background ratio with fast renal clearance and overall skeletal uptake comparable to other ^{68}Ga-labeled DOTA α-H and α-OH bisphosphonates as well as [^{18}F]Na-F [16, 17]. Moreover, in vivo biodistribution in a single patient with prostatic carcinoma showed intense uptake in skeletal metastatic lesions with lower activity in background and other normal organs in comparison with complimentary [^{68}Ga]Ga-PSMA image [16]. Recently, pre-clinical animal studies with alpha emitter [^{225}Ac]Ac-DOTAZOL [25] have shown biokinetics similar to [^{68}Ga]Ga-DOTAZOL and proposed its translational use with strategies to reduce nephrotoxicity, thus increasing the importance of theranostic use of [^{68}Ga]Ga-DOTAZOL. Literature-based comparison of [^{68}Ga]Ga-DOTAZOL [17] with [^{68}Ga]Ga-NO2APBP [20] revealed slightly less hydroxyapatite binding (92.7 ± 1.3% versus 93.8 ± 4.4%) and low bone uptake at 60 min p.i. (standard uptake value (SUV) of 5.27 ± 0.62 versus 6.19 ± 1.27). The in vivo biodistribution of [^{68}Ga]Ga-DOTAZOL in male Wistar rats showed faster kidney clearance with peak uptake in less than 5 min followed by clearance in comparison to [^{68}Ga]Ga-NO2APBP that showed continuous uptake till 50 min followed by clearance through urinary bladder [20]. However, SUV for kidneys at 60 min p.i was found to be higher for [^{68}Ga]Ga-DOTAZOL (0.53 ± 0.04) as compared to [^{68}Ga]Ga-NO2APBP (0.26 ± 0.09). Evaluation of [^{68}Ga]Ga-NO2APBP in female breast carcinoma patients already proved its excellent ability to detect lesions along with favorable radiation dosimetry with very low kidney absorbed dose [26]. However, [^{68}Ga]Ga-DOTAZOL has not been evaluated clinically so far. [^{68}Ga]Ga-DOTAZOL with benefit of low cost, onsite generator production of gallium-68 [27], having biodistribution and skeletal uptake comparable with [^{177}Lu]Lu-DOTAZOL [17, 25] and [^{225}Ac]Ac-DOTAZOL [25] suggests it to be better than [^{18}F]Na-F as potential theranostic tracer allowing for patient-individual

dosimetry. In this study, we evaluated human biodistribution and radiation dosimetry with [^{68}Ga]Ga-DOTAZOL.

MATERIALS AND METHODS

It is stated that [68Ga]Ga-DOTAZOL was applied to the patients within an individual treatment attempt according to German drug regulations. The data were evaluated afterwards retrospectively. All procedures were followed in accordance with ethical standards of our institutional review board and therefore been performed in accordance with the ethical standards laid down in the 1964 Declaration of Helsinki and all subsequent revisions. All patients gave their informed consent prior to their inclusion in the study.

Patient population:

Between April 2016 to March 2018, 5 patients (M: F; 4: 1) with metastatic skeletal disease not responding to other treatment modalities were included in this study [Table 1]. The patients were injected intravenously (i.v.) with mean ± SD dose of 168.25 ± 20.27 MBq (4.55 mCi) of [^{68}Ga]Ga-DOTAZOL. Skeletal metastatic disease in patients was secondary to breast, bronchial and metastatic castration resistant prostate carcinoma. All of these patients had shown painful progression while being treated with conventional treatment modalities.

Preparation of [^{68}Ga]Ga-DOTA^{ZOL}

Gallium-68 was obtained from a 1.85 GBq (50 mCi) 68Ge/68Ga generator (iThemba Labs; South Africa). Radiolabeling was performed according to the method described by Meckel et al. [17]. Development of silica TLC plates was conducted in acetylacetone/acetone (1:1) for iTLC plates. A radiochemical yield of ≥ 98% and radiochemical purity of ≥ 97% were obtained.

[^{68}Ga]Ga-DOTA^{ZOL} PET/CT imaging protocol:

For qualitative and dosimetric analysis, a Siemens Biograph 2 PET/CT scanner with a 58.5 cm axial field of view and a 16.2 cm longitudinal field of view was used for acquiring PET/CT images. The scanner has a spatial resolution of about 6 mm in axial and transversal direction (at a radius of 10 mm). All patients underwent a low dose CT scan (120kV, 40mAs) of abdomen for attenuation correction and patient positioning with kidneys in field of view, followed by dynamic imaging of abdomen for 30 minutes in list mode started simultaneously with i.v injection of [^{68}Ga]Ga-DOTAZOL. Later static skull to mid-thigh PET/CT images were acquired at 45 min and 2.5 h post injection (p.i), each preceded by low dose CT examination for patient positioning and attenuation correction.

Images were reconstructed using an iterative reconstruction algorithm (OSEM with 8 iterations, 16 subsets), application of Gaussian filter of 4mm and were corrected for scatter. The dynamic images were reconstructed into 6 images of 300s.

Qualitative analysis:

All dynamic and static images were visually analyzed to see physiological and pathological tracer distribution. Organs with increased tracer uptake were identified as source organs for further dosimetric analysis.

Quantitative dosimetric analysis:

Table 1: Characteristics of study population

	PT1	PT2	PT3	PT4	PT5	mean	SD
Age	83	83	66	64	64	72	10.07
Weight	76	76	85	82	82	80	4.02
Hematocrit	0.4	0.41	0.34	0.39	0.37	0.38	0.03
Dose	152	150	181	190	190	172.60	20.07
Tumor	CRPC	CRPC	Breast	Bronchial carcinoma	Bronchial carcinoma		
Previous therapies received	AH*/ CT#/ [^{177}Lu]Lu-PSMA-617	AH*/ CH#/ [^{177}Lu]Lu-PSMA-617	CH# + local Iradiation	CH# + carboplatin/ XGEVA, Nivolumab	CH# + carboplatin/ XGEVA, Nivolumab		

*Antihormonal; # Chemotherapy

For dosimetric analysis kidneys, liver, spleen, urinary bladder, lumbar (L1-L3) vertebrae, salivary glands and whole body were selected as source organs. MEDISO interview fusion software (MEDISO Medical Imaging Systems, Budapest, Hungary) was used to draw a volume of interest (VOI) encompassing the entire source organs on CT image for calculating organ volume and to determine mean counts/ml (kBq/ml) from a co-registered PET image. Total source organ activity (MBq) was calculated by multiplying source organ CT volume with corresponding mean counts/ml and dividing it with 1000. The percent of

injected activity in source organs was calculated to generate time activity curves and calculating residence time (MBq-h/MBq) using OLINDA/EXM version 2.0 (Hermes Medical Solutions, Stockholm, Sweden). Mono-exponential curve was fit on whole body and salivary glands. Biexponential curve was applied for the remaining source organs. Assuming homogenous distribution of tracer in the remainder of the body, the percentage of injected dose in the image was scaled proportional to percentage weight of body in the image by using Eq. (1) [28]. The percentage of body weight in image was calculated using Eq. (2) [28].

$$\%\, whole\ body\ activity(t) = \frac{Activity\ in\ static\ (skull-midthigh) image\ (t) \times 100}{Scaled\ injected\ activity\ in\ image}$$ --------Equation 1

$$\%\, Body\ weight(image) = \frac{CT\ volume\ of\ whole\ body image \times mean\ CT\ density \times 100}{Patient\ weight}$$ ---------Equation 2

For the remainder of body activity A × [1 − exp−ʎt] function was fit for cumulative urinary excretion using the method explained by Stabin [29]. For skeletal activity, the mean counts/ml in lumbar vertebrae were multiplied by 5000 (total weight of skeleton in an adult) [30].

To determine bone marrow dosimetry, 1–2 ml venous blood samples were collected at eight time points (5, 10, 15, 20, 25, 30, 45 min and 2.5 h) post-injection. Urine samples were also collected in pre-weighed containers after 45 min and 2.5 h p.i. Radioactivity in 1 ml blood and urine samples was measured along with known standard activity using 1480 WIZARD™ 3n Gamma counter. The indirect blood-based method using patient hematocritbased red marrow to blood ratio and bone marrow mass was used to determine bone marrow self-dose [31–34]. For urinary bladder contents residence time, a trapezoidal method was used while taking into account urinary bladder activity in images at 45 min, and 2.5 h along with activity in urinary samples. OLINDA/EXM version 2.0 (Hermes Medical Solutions, Stockholm, Sweden) software was used to calculate mean organ absorbed doses and effective doses after adjusting for the weight of patient organs by multiplying the reference adult male/female whole body weight with factor obtained by dividing patient weight with reference adult (male/female) weight, respectively. The mean of residence times, organ absorbed doses (mSv/MBq) and mean effective doses (mSv/MBq) were calculated. The total effective dose in mSv received after injection of 150 MBq of [^{68}Ga]Ga-DOTAZOL was calculated by multiplying the mean effective dose (mSv/MBq) with 150 MBq.

RESULTS

Qualitative [^{68}Ga]Ga-DOTA^{ZOL} distribution and kinetics analysis:

Visual analysis of PET/CT images revealed intense tracer uptake in kidneys, skeleton and urinary bladder. Faint uptake in liver, spleen and salivary glands was also seen. Rapid tracer kinetics was seen through kidneys as shown in Fig. 1 with early uptake in renal parenchyma as early as 2.5 min followed by clearance with minimal activity in the collecting system at 45 min p.i.. and minimal to no residual activity at 2.5 h p.i.. Uptake in bone increased over time. Good bone to soft tissue and metastatic lesion to normal bone uptake was visualized at 45 min p.i.. which increased at 2.5 p.i. as seen in Fig. 2. For dosimetric analysis, source organs identified on qualitative analysis included kidneys, urinary bladder, lumbar vertebrae (L1–L3) as representative of skeletal system, liver, spleen, salivary glands and whole body.

Comparison of mean SUV-based skeletal to soft tissue ratio was found to be 7.36 and 12.96 at 45 min p.i. that increased to 15.034 and 28.82 at 2.5 h p.i. for two representative lesions as shown in Fig. 2 in comparison to 4.81 and 3.30 on previous [^{68}Ga]Ga-PSMA-617 in a patient with mCRPC. Lesion to normal bone ratio for these lesions was found to be 7.53 and 12.95 at 45 min and 6.79 and 13.01 at 2.5 h p.i. on PET/CT images of [^{68}Ga]Ga-DOTAZOL in comparison to 7.5 and 5.14, respectively, on the [68Ga]Ga-PSMA-617 image. The number of lesions was also higher on [^{68}Ga]Ga-DOTAZOL as compared to [^{68}Ga]Ga-PSMA-617 in the mCRPC patient.

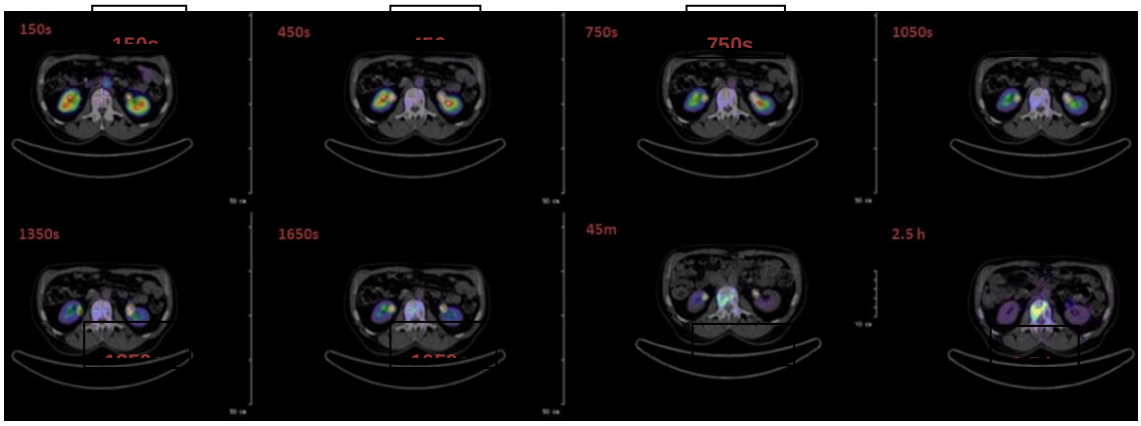

Figure 1: [^{68}Ga]Ga-DOTA^{ZOL} kinetics through kidneys in dynamic (150 s, 450 s, 750 s, 1050 s, 1350 s, 1650 s) and static images (45 min and 2.5 h).

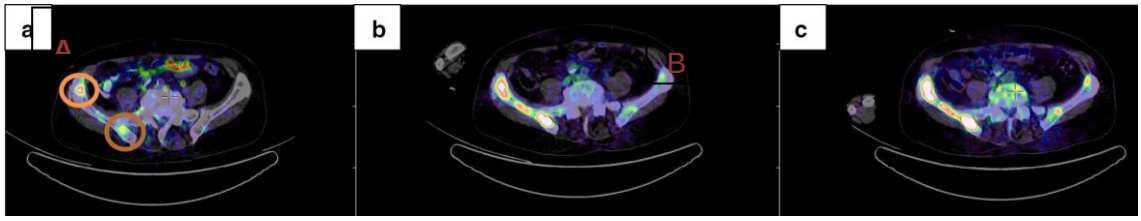

Figure 2 Uptake in two metastatic lesions on **a**. [^{68}Ga]Ga-PSMA-617, **b**. [^{68}Ga]Ga-DOTAZOL at 45 min p.i.. and **c**. [^{68}Ga]Ga-DOTAZOL at 2.5 h p.i.. showing higher and

progressive uptake with [^{68}Ga]Ga-DOTAZOL as a result of enhanced lesion to normal bone uptake.

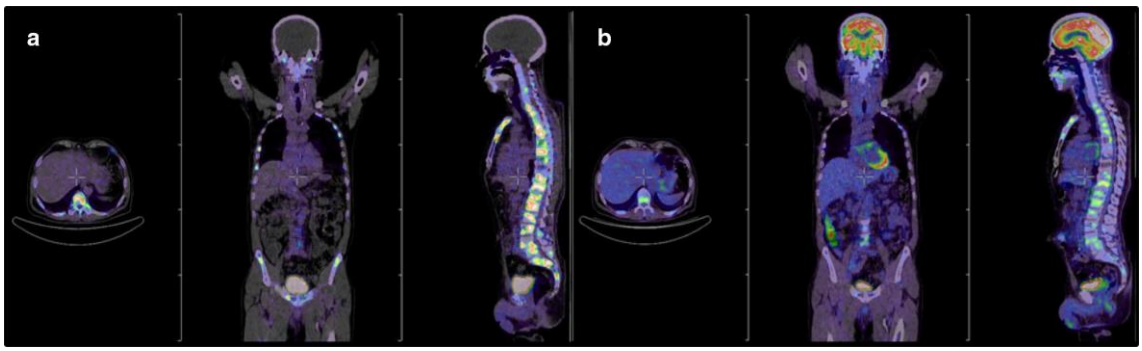

Figure 3: Comparison of PET/CT images of **a**. [^{68}Ga]Ga-DOTAZOL with **b**. [^{18}F]FDG in patient with skeletal metastases secondary to bronchial carcinoma.

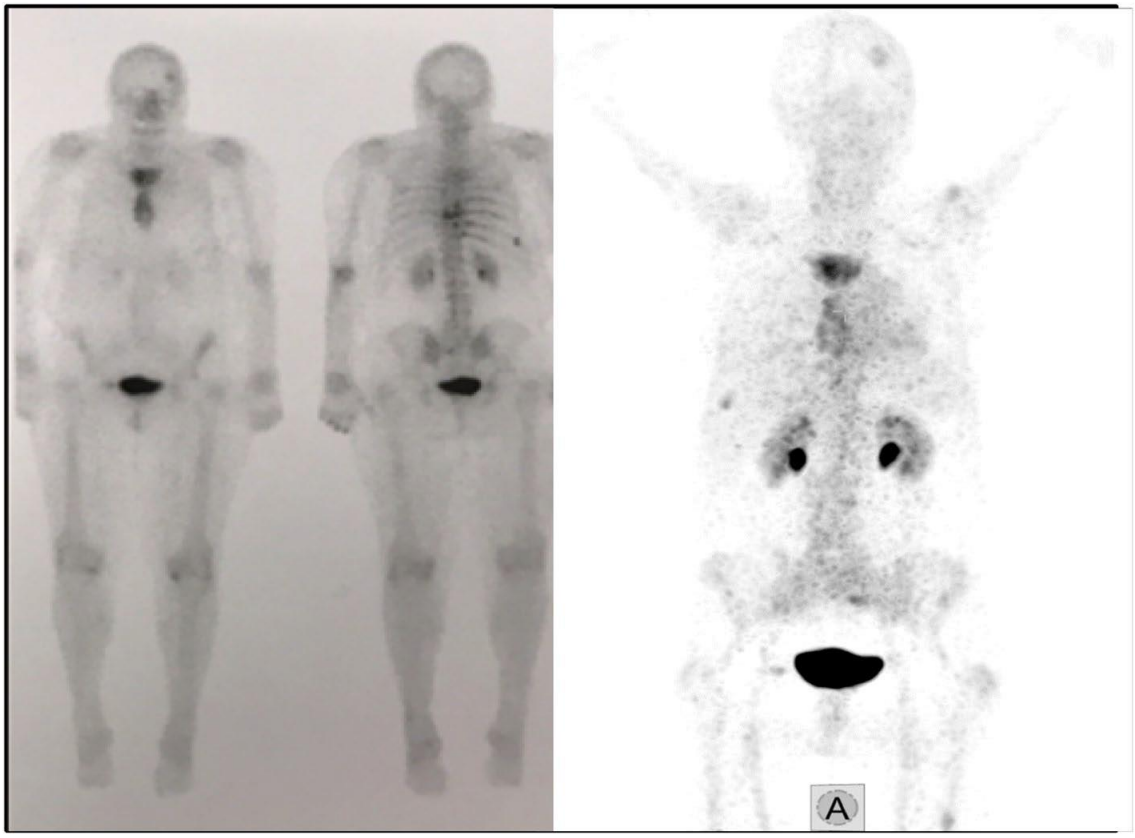

Figure 4: Comparison of [^{99m}Tc]Tc-MDP with [^{68}Ga]Ga-DOTA^{ZOL} in patient of skeletal metastases secondary to breast carcinoma.

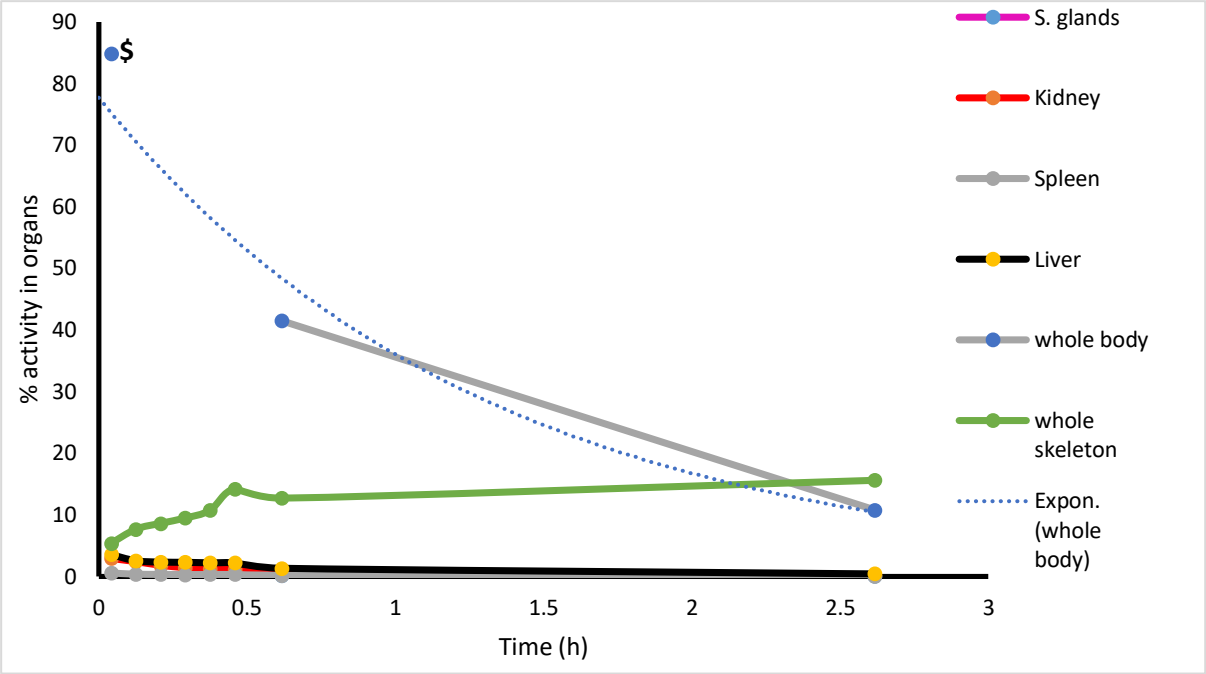

Figure 5: Tracer kinetics of [^{68}Ga]Ga-DOTA^{ZOL} in source organs with decay correction and $(estimated initial activity).

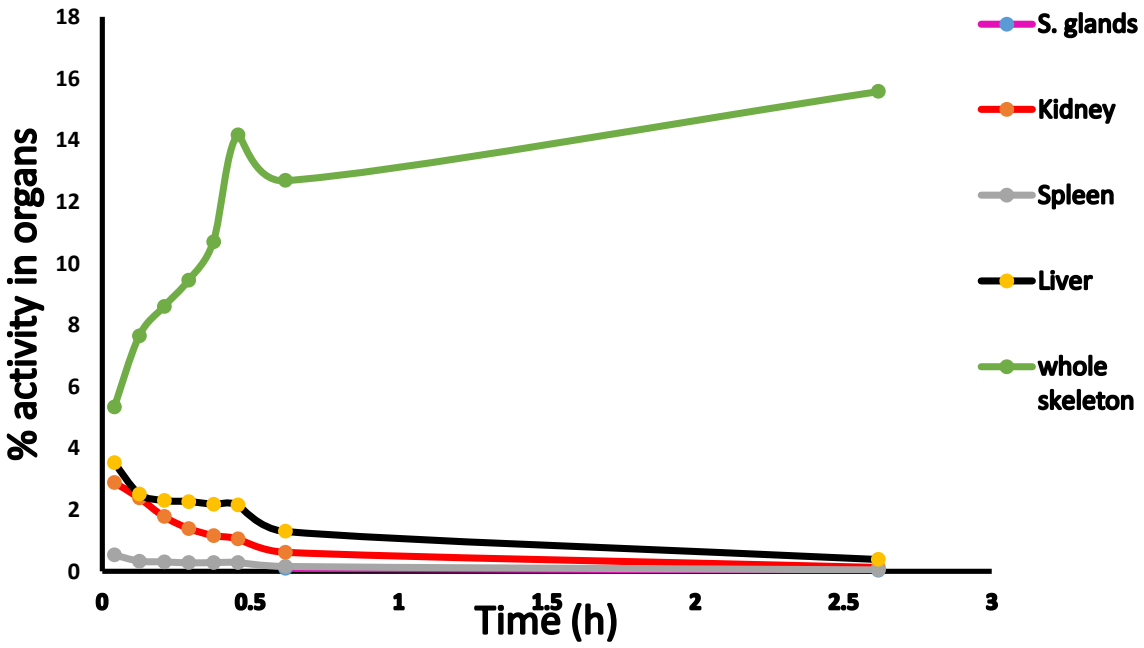

Figure 6: Change in % activity of [^{68}Ga]Ga-DOTA^{ZOL} in whole skeleton (with decay correction) and rest of source organs(without decay correction).

Visual comparison of [^{68}Ga]Ga-DOTAZOL with [^{18}F]FDG in bronchial carcinoma patients and [^{99m}Tc]Tc-MDP bone scan in the female patient as shown in Figs. 3 and 4, respectively, also revealed that uptake in lesions and the apparent number of lesions were also

higher. SUV max in lesion was also higher on [^{68}Ga]Ga-DOTAZOL (15.24 g/ml) as compared to [^{18}F]FDG PET/CT images (5.95 g/ml) in bronchial carcinoma patients.

Dosimetric analysis for normal organs:

Plotting of percentage injected activity in source organs with respect to time as shown in Figs. 5 and 6 further supported the results of visual analysis. The highest tracer localization was seen in the skeletal system followed by liver, kidneys, spleen and salivary glands. An initial rapid increase uptake was seen in the skeleton for almost half an hour p.i. followed by a slow rise. Simultaneous rapid tracer uptake and fast washout in the other source organs and blood pool was found. Rapid tracer kinetics with early peak physiological uptake as early as 2.5 min p.i. was seen in kidneys, followed by fast clearance with minimal to almost no activity at 2.5 h p.i.. Almost 11% of the injected activity remained in whole body at 2.5 h showing 89% renal excretion.

Table 2 shows the residence times (MBq-h/MBq) for source organs in individual patients as well as the mean ± SD of residence times. High residence time was seen in the remainder of the body followed by urinary bladder, cortical and trabecular bone, liver, red marrow, kidneys, spleen and salivary glands. Table 3 shows mean ± SD and ranges of organ absorbed doses as well as effective dose according to ICRP103. The results very clearly demonstrate that the urinary bladder receives the highest dose of 0.368 mSv/MBq (range 0.203–0.609 mSv/MBq) and is the organ at risk as kidneys were found to be the only route of its excretion. Osteogenic cells received dose of 0.040 mSv/MBq followed by kidneys (0.031 mSv/MBq), red marrow (0.027 mSv/MBq), spleen (0.018 mSv/MBq), liver (0.013 mSv/MBq) and salivary glands (0.011 mSv/MBq).

Table 2: Comparison of residence time (MBq-h/ MBq) in source organs with [^{68}Ga]Ga-DOTA^{ZOL} and [^{18}F]NaF

	[^{68}Ga]Ga-DOTA^{ZOL} this study							[^{18}F]NaF [32]	[^{18}F]NaF [33]
Organs	**PT 1**	**PT 2**	**PT 3**	**PT 4**	**PT 5**	**mean**	**± SD**	**mean**	
S. glands	0.004	0.002	0.001	0.001	0.001	0.002	0.001		
Kidney	0.024	0.024	0.020	0.018	0.016	0.021	0.003	0.010	
Spleen	0.005	0.004	0.008	0.004	0.006	0.005	0.001	0.002	
Liver	0.057	0.034	0.052	0.028	0.032	0.040	0.012	0.017	
Red marrow	0.034	0.038	0.053	0.039	0.058	0.042	0.009	0.130	

Trabecular Bone	0.148	0.117	0.116	0.225	0.150	0.127	0.041	0.207	0.830
Cortical bone	0.148	0.117	0.116	0.225	0.150	0.127	0.041	0.901	0.550
Urinary Bladder	0.172	0.191	0.160	0.534	0.496	0.174	0.177	0. 190	0.290
Remainder of body	0.392	0.468	0.213	0.251	0.377	0.358	0.095		0.330

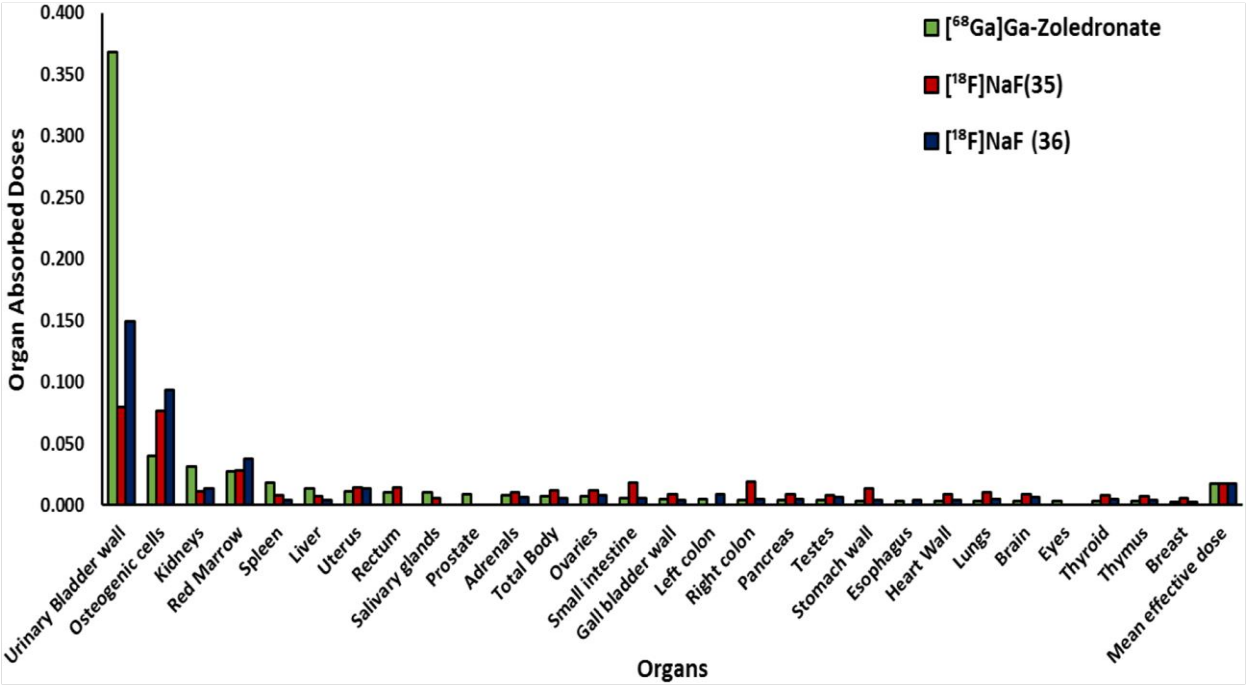

Figure 7: Comparison of Organ Absorbed Doses between [^{68}Ga]Ga-DOTA^{ZOL} and [^{18}F]NaF [30, 35].

DISCUSSION

In the current study, [^{68}Ga]Ga-DOTAZOL was evaluated in bronchial carcinoma patients in addition to mCRPC and breast carcinoma patients. [^{68}Ga]Ga-DOTAZOL showed fast kinetics with increased tracer elimination through kidneys resulting in whole body activity to decrease to almost 11% by 2.5 h p.i. In the skeletal target organ, there is an initial rapid uptake till 30 min followed by a further gradual rise. The maximum tracer accumulation was seen in the skeletal system with 18% of injected activity (IA) in one of the bronchial carcinoma patients with a high burden of skeletal metastases.

An initial uptake in liver, spleen and salivary glands was also seen followed by a sharp decline. Soft tissue and blood activity decreases with time and results in enhanced bone uptake and an increased metastatic lesion to bone ratio as can be seen in Fig. 2 which is consistent with the results of other ^{68}Ga–bisphosphonate agents and [^{18}F]NaF [17, 27].

PET/CT images of [^{68}Ga]Ga-DOTAZOL could be compared to previous [^{68}Ga]Ga-PSMA-617 and [^{18}F]FDG PET/CT images in the male patients and a [^{99m}Tc]Tc-MDP bone scan enrolled in this study. Here, the uptake of [^{68}Ga]Ga-DOTAZOL was 2.56 times higher than that of [^{18}F]FDG in a bronchial carcinoma patient. A greater number of apparent lesions was also found with [^{68}Ga]Ga-DOTAZOL as compared to [^{68}Ga]Ga-PSMA-617 (Fig. 2), [^{18}F]FDG in bronchial carcinoma (Fig. 3) and [^{99m}Tc]Tc-MDP in breast carcinoma patients (Fig. 4).

Compared with [^{68}Ga]Ga-PSMA-617, the qualitative analysis of [^{68}Ga]Ga-DOTAZOL showed better uptake in skeleton with higher skeleton to soft tissue and metastatic lesions to normal bone ratio as seen in Fig. 2. This finding is consistent with the in vivo biodistribution analysis of [^{68}Ga]Ga-DOTAZOL in one patient with prostate cancer [16].

Dosimetric analysis showed comparable residence times for the rest remainder of the body to that of [^{18}F]NaF which was 0.358 h in the current study and 0.33 reported in ICRP 106 report. Urinary bladder residence time (0.174 h) was found to be less than that of [^{18}F]NaF (0.19 and 0.29 h); however, the residence time for kidneys was found to be higher (0.022 h) as compared to [^{18}F]NaF (0.01 h). This could be explained by the fact that [^{68}Ga]Ga-DOTAZOL shows 89% renal excretion over a period of 2.5 h as compared to 15% and 50% in the case of [^{18}F]NaF [30, 35]. The residence time of [^{68}Ga]Ga-DOTAZOL in trabecular and cortical bone was found to be 0.127 with 50% weightage given to both. The residence time in bone components as well as bone marrow was lower as compared to [^{18}F]NaF. This might be a result of the lower half-life of 68Ga as compared to fluor-18 as well as the difference in osteogenic tumor load in patients evaluated by Kurdziel et al. [35] and the current study. Residence times for liver and spleen were higher than those of [^{18}F]NaF. The uptake of free/unbound ^{68}Ga can be responsible for prolonged residence times in these organs.

Table 4: Comparison of organ absorbed doses of [^{68}Ga]Ga-NO2AP^{BP} [27] with [^{68}Ga]Ga-DOTA^{ZOL}

Study	**[^{68}Ga]Ga-NO2AP^{BP}**	**[^{68}Ga]Ga-DOTA^{ZOL}**
Organs	**Organ Absorbed Doses(mSv/MBq)**	

Kidneys	0.00760	0.0314
Red marrow	0.02030	0.0272
Urinary bladder	0.00011	0.3680
Skeleton	0.05800	0.0400
Whole body	0.00583	0.0072
Mean effective dose	0.00860	0.0174

[^{68}Ga]Ga-DOTAZOL like other bone-seeking agents was found to be characterized by delivery of the highest radiation absorbed dose to urinary bladder, followed by osteogenic cells, red marrow and kidneys. This finding is comparable with dosimetric analysis of [^{18}F]NaF [30, 35]. Kidney being its physiological route of excretion results in the highest dose seen in urinary bladder. The doses delivered to urinary bladder and kidneys were higher and the radiation absorbed doses to osteogenic tissue and red marrow were lower as compared to [^{18}F]NaF as shown in Fig. 7 [30, 35]. Mean effective dose and total effective dose were found to be 0.017 mSv/MBq and 2.61 mSv with [^{68}Ga]Ga-DOTAZOL comparable to 0.017 mSv/MBq and 1.88–3.15 mSv with [^{18}F]NaF respectively [35].

Comparison of dosimetric analysis of [^{68}Ga]Ga-DOTAZOL with [^{68}Ga]Ga-NO2APBP [26] revealed high absorbed doses delivered to kidneys and urinary bladder, almost comparable absorbed doses to bone marrow and osteogenic cells, high total body absorbed dose and high effective dose equivalent as shown in Table 4 which illustrates the superiority of [^{68}Ga]Ga-NO2APBP [26]. The difference in kidney and urinary bladder absorbed doses could be due to differences in the collection of data points till 4 h for [^{68}Ga]Ga-NOTAPBP in comparison to 2.5 h in the current study. A further lack of detailed biodistribution analysis is also a limitation for comparing the results of the two studies. It was observed that the dosimetric results of [^{68}Ga]Ga-NO2APBP from breast carcinoma patients (M:F; 1:4) were not comparable to the results for the one female breast carcinoma patient (Pt 3) in the current study.

The resultant high urinary bladder and kidney absorbed doses from [^{68}Ga]Ga-DOTAZOL are consistent with those of other bone-seeking agents. These doses can very easily be reduced by proper hydration and rapid diuresis. As compared to various 68Ga-labeled octreotide [36] and PSMA agents [37, 38], [^{68}Ga]Ga-DOTAZOL delivered lower kidney and higher urinary bladder absorbed doses along with lower mean effective doses. Be-

sides having high radiation exposure to kidneys and urinary bladder, [^{68}Ga]Ga-DOTAZOL has advantages of its theranostic potential when labeled with lutetium-177 for therapy.

Conclusion

The results of this small patient study showed that [^{68}Ga]Ga-DOTAZOL is an excellent tracer with high and selective uptake in bone lesions. [^{68}Ga]Ga-DOTAZOL results in 2.4 times higher organ absorbed dose to urinary bladder and kidneys, while similar mean effective dose in comparison to that of [^{18}F]NaF which was found to be 0.017 mSv/MBq. Compared with [^{68}Ga]Ga-PSMA-617, the bisphosphonate [^{68}Ga]Ga-DOTAZOL showed a similar pharmacological pattern as well as higher metastatic to normal bone ratio and higher skeleton to soft tissue uptake in prostate carcinoma.

The possibility of treatment of bone metastases with [^{177}Lu]Lu-DOTAZOL gives it a clear advantage over other bone-seeking diagnostic agents such as [^{18}F]Na-F and [^{99m}Tc]Tc-MDP. These initial results are encouraging and support the use of [^{68}Ga]Ga-DOTAZOL as an imaging theranostic agent. However, prospective patient studies are required to explore its further potential for the treatment of bone metastases in different tumor entities.

Author contributions: The manuscript has been seen and approved by all authors. AK, MM, SK,EE: contributed equally in design and execution of study. AK, FR, HA, ME, RAB, FCG: contributed in drafting or revising of the manuscript critically for important intellectual content as well as final manuscript approval for submission and publication.

References

1. Gonzalez-Sistal. Advances in Medical Imaging Applied to Bone Metastases. 2011.
2. Agarwal MG, Nayak P. Management of skeletal metastases: An orthopaedic surgeon's guide. Indian Journal of Orthopaedics. 2015;49:83–100. doi:10.4103/0019-5413.143915.
3. Ulmert D, Solnes L, Thorek DL. Contemporary approaches for imaging skeletal metastasis. Bone Research. 2015;3:15024. doi:10.1038/boneres.2015.24.
4. O'Sullivan GJ, Carty FL, Cronin CG. Imaging of bone metastasis: An update. World J Radiol. 2015;7:202–11. doi:10.4329/wjr.v7.i8.202.
5. Damerla V, Packianathan S, Boerner PS, Jani AB, Vijayakumar S, Vijayakumar V. Recent developments in nuclear medicine in the management of bone metastases:

a review and perspective. American Journal of Clinical Oncology. 2005;28:513–20. doi:10.1097/01.coc.0000162425.55457.10.

6. Chatalic KLS, Heskamp S, Konijnenberg M, Molkenboer-Kuenen JDM, Franssen GM, Clahsen-van Groningen MC, et al. Towards Personalized Treatment of Prostate Cancer: PSMA I&T, a Promising Prostate-Specific Membrane Antigen-Targeted Theranostic Agent. Theranostics. 2016;6:849–61. doi:10.7150/thno.14744.
7. Luckman SP, Hughes DE, Coxon FP, Graham R, Russell G, Rogers MJ. Nitrogen-containing bisphosphonates inhibit the mevalonate pathway and prevent post-translational prenylation of GTP-binding proteins, including Ras. Journal of Bone and Mineral Research. 1998;13:581–9. doi:10.1359/jbmr.1998.13.4.581.
8. Fellner M, Biesalski B, Bausbacher N, Kubícek V, Hermann P, Rösch F, Thews O. (68)Ga-BPAMD: PET-imaging of bone metastases with a generator based positron emitter. Nuclear Medicine and Biology. 2012;39:993–9. doi:10.1016/j.nucmedbio.2012.04.007.
9. Ogawa K, Ishizaki A. Well-designed bone-seeking radiolabeled compounds for diagnosis and therapy of bone metastases. BioMed Research International. 2015;2015:676053. doi:10.1155/2015/676053.
10. Fellner M, Riss P, Loktionova NS, Zhernosekov KP, Thews O, Geraldes CFGC, et al. Comparison of different phosphorus-containing ligands complexing 68 Ga for PET-imaging of bone metabolism. Radiochim. Acta. 2011;99:43–51. doi:10.1524/ract.2011.1791.
11. Agarwal KK, Singla S, Arora G, Bal C. (177)Lu-EDTMP for palliation of pain from bone metastases in patients with prostate and breast cancer: a phase II study. European Journal of Nuclear Medicine. 2015;42:79–88. doi:10.1007/s00259-014-2862-z.
12. Alavi M, Omidvari S, Mehdizadeh A, Jalilian AR, Bahrami-Samani A. Metastatic Bone Pain Palliation using (177)Lu-Ethylenediaminetetramethylene Phosphonic Acid. World Journal of Nuclear Medicine. 2015;14:109–15. doi:10.4103/1450-1147.157124.
13. Mazzarri S, Guidoccio F, Mariani G. The emerging potential of 177Lu-EDTMP: an attractive novel option for radiometabolic therapy of skeletal metastases. Clin Transl Imaging. 2015;3:167–8. doi:10.1007/s40336-015-0099-x.
14. Shinto AS, Shibu D, Kamaleshwaran KK, Das T, Chakraborty S, Banerjee S, et al. ^{177}Lu-EDTMP for treatment of bone pain in patients with disseminated skeletal metastases. Journal of Nuclear Medicine Technology. 2014;42:55–61. doi:10.2967/jnmt.113.132266.

15. Yuan J, Liu C, Liu X, Wang Y, Kuai D, Zhang G, Zaknun JJ. Efficacy and safety of 177Lu-EDTMP in bone metastatic pain palliation in breast cancer and hormone refractory prostate cancer: a phase II study. Clin Nucl Med. 2013;38:88–92. doi:10.1097/RLU.0b013e318279bf4d.

16. Pfannkuchen N, Meckel M, Bergmann R, Bachmann M, Bal C, Sathekge M, et al. Novel Radiolabeled Bisphosphonates for PET Diagnosis and Endoradiotherapy of Bone Metastases. Pharmaceuticals (Basel). 2017;10:45. doi:10.3390/ph10020045.

17. Meckel M, Bergmann R, Miederer M, Roesch F. Bone targeting compounds for radiotherapy and imaging: *Me(III)-DOTA conjugates of bisphosphonic acid, pamidronic acid and zoledronic acid. EJNMMI radiopharm. chem. 2017;1:14. doi:10.1186/s41181-016-0017-1.

18. Fellner M, Baum RP, Kubícek V, Hermann P, Lukes I, Prasad V, Rösch F. PET/CT imaging of osteoblastic bone metastases with (68)Ga-bisphosphonates: first human study. European Journal of Nuclear Medicine and Molecular Imaging. 2010;37:834. doi:10.1007/s00259-009-1355-y.

19. Baum RP, Kulkarni HR. THERANOSTICS: From Molecular Imaging Using Ga-68 Labeled Tracers and PET/CT to Personalized Radionuclide Therapy - The Bad Berka Experience. Theranostics. 2012;2:437–47. doi:10.7150/thno.3645.

20. Holub J, Meckel M, Kubíček V, Rösch F, Hermann P. Gallium(III) complexes of NOTA-bis (phosphonate) conjugates as PET radiotracers for bone imaging. Contrast Media Mol Imaging. 2015;10:122–34. doi:10.1002/cmmi.1606.

21. Bergmann R, Meckel M, Kubíček V, Pietzsch J, Steinbach J, Hermann P, Rösch F. (177)Lu-labelled macrocyclic bisphosphonates for targeting bone metastasis in cancer treatment. EJNMMI Res. 2016;6:5. doi:10.1186/s13550-016-0161-3.

22. Ebetino FH, Hogan A-ML, Sun S, Tsoumpra MK, Duan X, Triffitt JT, et al. The relationship between the chemistry and biological activity of the bisphosphonates. Bone. 2011;49:20–33. doi:10.1016/j.bone.2011.03.774.

23. Russell RGG. Bisphosphonates: mode of action and pharmacology. Pediatrics. 2007;119 Suppl 2:S150-62. doi:10.1542/peds.2006-2023H.

24. Dalle Carbonare L, Zanatta M, Gasparetto A, Valenti MT. Safety and tolerability of zoledronic acid and other bisphosphonates in osteoporosis management. Drug, Healthcare and Patient Safety. 2010;2:121–37. doi:10.2147/DHPS.S6285.

25. Pfannkuchen N, Bausbacher N, Pektor S, Miederer M, Rosch F. In vivo Evaluation of 225AcAc-DOTAZOL for α-Therapy of Bone Metastases. Current Radiopharmaceuticals. 2018;11:223–30. doi:10.2174/1874471011666180604083911.

26. Passah A, Tripathi M, Ballal S, Yadav MP, Kumar R, Roesch F, et al. Evaluation of bone-seeking novel radiotracer 68Ga-NO2AP-Bisphosphonate for the detection of

skeletal metastases in carcinoma breast. European Journal of Nuclear Medicine. 2017;44:41–9. doi:10.1007/s00259-016-3469-3.

27. Chopra A. Molecular Imaging and Contrast Agent Database (MICAD): 68Ga-Labeled (4-{(bis(phosphonomethyl))carbamoylmethyl}-7,10-bis(carboxymethyl)-1,4,7,10-tetraazacyclododec-1-yl)acetic acid (BPAMD). Bethesda (MD); 2004.

28. Khawar A, Eppard E, Sinnes JP, Roesch F, Ahmadzadehfar H, Kürpig S, et al. 44ScSc-PSMA-617 Biodistribution and Dosimetry in Patients With Metastatic Castration-Resistant Prostate Carcinoma. Clin Nucl Med. 2018;43:323–30. doi:10.1097/RLU.0000000000002003.

29. Stabin MG. Fundamentals of Nuclear Medicine Dosimetry 2008. 1st ed. s.l.: Springer-Verlag. doi:10.1007/978-0-387-74579-4_5.

30. Basic anatomical and physiological data: The skeleton. Ann ICRP. 1995;25:1–80. doi:10.1016/S0146-6453(00)80004-4.

31. Hindorf C, Lindén O, Tennvall J, Wingårdh K, Strand S-E. Evaluation of methods for red marrow dosimetry based on patients undergoing radioimmunotherapy. Acta Oncol. 2005;44:579–88. doi:10.1080/02841860500244294.

32. S. Shen, G. Denardo, G. Sgouros, R. O'donnell, S. Denardo. Practical determination of patient-specific marrow dose using radioactivity concentration in blood and body. J. Nucl. Med. 1999.

33. Sgouros G, Stabin M, Erdi Y, Akabani G, Kwok C, Brill AB, Wessels B. Red marrow dosimetry for radiolabeled antibodies that bind to marrow, bone, or blood components. Medical Physics. 2000;27:2150–64. doi:10.1118/1.1288393.

34. Siegel JA. Establishing a clinically meaningful predictive model of hematologic toxicity in nonmyeloablative targeted radiotherapy: practical aspects and limitations of red marrow dosimetry. Cancer Biotherapy & Radiopharmaceuticals. 2005;20:126–40. doi:10.1089/CBR.2005.20.126.

35. Kurdziel KA, Shih JH, Apolo AB, Lindenberg L, Mena E, McKinney YY, et al. The kinetics and reproducibility of 18F-sodium fluoride for oncology using current PET camera technology. J. Nucl. Med. 2012;53:1175–84. doi:10.2967/jnumed.111.100883.

36. Walker RC, Smith GT, Liu E, Moore B, Clanton J, Stabin M. Measured human dosimetry of 68Ga-DOTATATE. J. Nucl. Med. 2013;54:855–60. doi:10.2967/jnumed.112.114165.

37. Afshar-Oromieh A, Hetzheim H, Kratochwil C, Benesova M, Eder M, Neels OC, et al. The Theranostic PSMA Ligand PSMA-617 in the Diagnosis of Prostate Cancer by PET/CT: Biodistribution in Humans, Radiation Dosimetry, and First Evaluation of Tumor Lesions. J. Nucl. Med. 2015;56:1697–705. doi:10.2967/jnumed.115.161299.

38. Herrmann K, Bluemel C, Weineisen M, Schottelius M, Wester H-J, Czernin J, et al. Biodistribution and radiation dosimetry for a probe targeting prostate-specific membrane antigen for imaging and therapy. J. Nucl. Med. 2015;56:855–61. doi:10.2967/jnumed.115.156133.

4.4 Biodistribution and post-therapy dosimetric analysis of [^{177}Lu]Lu-DOTAZOL in patients with osteoblastic metastases - first results

Ambreen Khawar[1], Elisabeth Eppard[1], Frank Roesch[2], Hojjat Ahmadzadehfar[1], Stefan Kürpig[1], Michael Meisenheimer[1], Florian. C. Gaertner[1], Markus Essler[1], Ralph. A. Bundschuh[1].

[1] Department of Nuclear Medicine, University Medical Center Bonn, Germany

[2] Institute of Nuclear Chemistry, Johannes Gutenberg-University Mainz, Germany

Corresponding author: Ambreen Khawar, MS Nuclear Medicine

E-mail address: ambreen_khawar@hotmail.com

Telephone number: +49 17623876558

Fax number: +49 (0)228-287 19096

https://doi.org/10.1186/s13550-019-0566-x

Abstract:

Background: Pre-clinical biodistribution and dosimetric analysis of [^{177}Lu]Lu-DOTAZOL suggests the bisphosphonate zoledronate as a promising new radiopharmaceutical for therapy of bone metastases. We evaluated biodistribution and normal organ absorbed doses resulting from therapeutic doses of [^{177}Lu]Lu-DOTAZOL in patients with metastatic skeletal disease.

Method: Four patients with metastatic skeletal disease (age range: 64 - 83 years) secondary to metastatic castration resistant prostate carcinoma or bronchial carcinoma were treated with a mean dose of 5968±64 MBq (161.3 mCi) of [^{177}Lu]Lu-DOTAZOL. Biodistribution was assessed with serial planar whole body scintigraphy at 20 min, 3, 24 and 167 h post injection (p.i.) and blood samples at 20 min, 3, 8, 24 and 167 h p.i.. Percent of injected activity in blood, kidneys, urinary bladder, skeleton and whole body were determined. Bone marrow self-dose was determined by an indirect blood based method. Urinary bladder wall residence time was calculated using Cloutier's dynamic urinary bladder model with a 4 h voiding interval. OLINDA/EXM version 2.0 (Hermes Medical Solutions, Stockholm, Sweden) software was used to determine residence times in source organs by applying biexponential curve fitting and to calculate organ absorbed dose.

Results: Qualitative biodistribution analysis revealed early and high uptake of [^{177}Lu]Lu-DOTAZOL in the kidneys with fast clearance showing minimal activity by 24 h p.i.. Activity in the skeleton increased gradually over time. Mean residence times were found to be highest in the skeleton followed by the kidneys. Highest mean organ absorbed dose was 3.33 mSv/MBq for osteogenic cells followed by kidneys (0.490 mSv/MBq), red marrow (0.461 mSv/MBq) and urinary bladder wall (0.322 mSv/MBq). The biodistribution and normal organ absorbed doses of [^{177}Lu]Lu-DOTAZOL are consistent with preclinical data.

Conclusion: [^{177}Lu]Lu-DOTA^{ZOL} shows maximum absorbed doses in bone and low kidney doses, making it a promising agent for radionuclide therapy of bone metastasis. Further studies are warranted to evaluate the efficacy and safety of radionuclide therapy with [^{177}Lu]Lu-DOTA^{ZOL} in the clinical setting.

Key words: [^{177}Lu]Lu-DOTA^{ZOL}; organ absorbed doses; bone seeking therapeutic radionuclides,; prostate carcinoma; bronchial carcinoma.

INTRODUCTION:

Occurrence of painful bone metastases is a frequent complication of solid tumors that reduces the quality of life in many patients [1]. Radionuclide therapy for bone pain palliation in patients with progressive skeletal metastatic disease has been established in the clinical routine already decades ago [2, 3]. Several radiopharmaceuticals are or have been in use such as [^{32}P]Na_2P, [^{89}Sr]$SrCl_2$, [^{153}Sm]Sm-EDTMP and [^{186}Re]Re-HEDP, [^{117m}Sn]$SnCl_2$ and [^{223}Ra]$RaCl_2$ [1, 2, 4]. The therapeutic effect requires accumulation of these radiopharmaceuticals at osteoblastic sites of metastases and deposition of energy by β^- or α particle. These radiopharmaceuticals are used either as monotherapy or in combination with systemic chemotherapy and bisphosphonates [4]. The choice of the radiopharmaceutical is dependent on its inherent properties such as physical half-life, energy and particle range, as well as ease of availability, efficacy and side effects [5].

Yet, the quest for a stable and effective bone seeking therapeutic radiopharmaceutical is still an ongoing process. Lutetium-177 with a half-life of 6.73 days, a low range of its β^- particles with maximum energy ($E_{\beta max}$ = 497 keV), gamma emissions at energies of 112 keV (6.4%) and 208 keV (11%), and the possibility of cost effective large scale production with high specific activity and radionuclide purity has gained high acceptance as a therapeutic radionuclide [6]. Owing to deposition of its β^- energy in the lesions and their close environment, it is best suited for small to medium sized tumor lesions when labeled with a suitable carrier [7]. [^{177}Lu]Lu-DOTA-TOC, [^{177}Lu]Lu-DOTA-TATE [8, 9] and [^{177}Lu]Lu-PSMA-617 [10, 11] have been proven effective for treatment of neuroendocrine tumors and metastatic castration resistant prostate carcinoma (mCRPC), respectively. Moreover, they allow for a good theranostic combination with their gallium-68 labeled imaging counter parts using positron emission tomography (PET) [12].

Bisphosphonates with antiresorptive properties [13] have also been labeled with lutetium-177. Among these are [^{177}Lu]Lu-DOTMP [14, 15], [^{177}Lu]Lu-EDTMP [16–21] and [^{177}Lu]Lu-BPAMD [22–25]. Phase I and II studies with [^{177}Lu]Lu-EDTMP for pain palliation in patients with bone metastases secondary to breast and prostate carcinoma have delivered encouraging results [16–21]. Radiation dosimetry analysis has also shown its safety with low dose delivery to the kidneys in patients with breast carcinoma and mCRPC in comparison to other bone pain palliating agents in use [5, 7, 26]. However, the lower kinetic stability of [^{177}Lu]Lu-EDTMP requires a high ligand concentration which is a drawback [2]. Also, [^{68}Ga]Ga-EDTMP showed lower skeletal accumulation compared

to its [^{177}Lu]Lu-EDTMP analogue and could not be paired as a theranostic agent. In contrast, DOTA-conjugated theranostic bisphosphonates, such as [^{177}Lu]Lu-BPAMD and [^{68}Ga]Ga-BPAMD, have shown excellent results and represent good theranostic pairs [23].

Zoledronate, a nitrogen containing hydroxy bisphosphonate, has recently been conjugated with DOTA (DOTA^{ZOL}), and labeled with gallium-68 for imaging and with lutetium-177 for therapy as new theranostic pair for targeting bone metastases [27]. Zoledronate is known to have improved antiresorptive effects owing to its higher hydroxyapatite binding and internalization by osteoclasts with subsequent increased apoptosis. The mode of action is accompanied by inhibition of farnesyl pyrophosphate enzyme of melavonate pathway that results in inhibition of osteoclastic activity [13]. Data from animal studies comparing the biodistribution and dosimetric analysis extrapolated for humans between [^{177}Lu]Lu-EDTMP and [^{177}Lu]Lu-DOTA^{ZOL} indicate a higher skeletal absorbed dose of 12.7 ± 1.018 for trabecular bone surface and 9.524 ± 0.803 for cortical bone surface with [^{177}Lu]Lu-DOTA^{ZOL} as compared to 10.019 ± 0.714 for cortical bone surface and 7.839 ± 0.655 for trabecular bone surface with [^{177}Lu]Lu-EDTMP. Hence, presented [^{177}Lu]Lu-DOTA^{ZOL} to be a better agent for radionuclide therapy of bone metastases [28]. Recently, [^{68}Ga]Ga-NODAGA^{ZOL} and [^{177}Lu]Lu-DOTA^{ZOL} have been reported as the most effective new bisphosphonate based theranostic radiopharmaceuticals [2, 3, 27–30]. Our current study aims at first in human biodistribution and dosimetric analysis of [^{177}Lu]Lu-DOTA^{ZOL} in mCRPC and metastazied bronchial carcinoma patients.

PATIENTS AND METHODS

Patient Selection:

In this retrospective study we analyzed four patients with metastatic skeletal disease secondary to mCRPC or bronchial carcinnoma, that were treated between July 2016 and September 2017 with [^{177}Lu]Lu-DOTA^{ZOL}. All treatments were performed in the context of an individual treatment attempt as no other treatment options were left for these patients. Written informed consent was obtained from all patients. The local ethical committee waived the ethical statement due to the retrospective character of the study. All procedures were followed in accordance with ethical standards of institutional review board and therefore been performed in accordance with the ethical standards laid down in the 1964 Declaration of Helsinki and all subsequent revisions.

After confirming sufficient uptake in the bone metastases with [^{68}Ga]Ga-DOTA^{ZOL} PET/CT shown in figure 1e, patients were hospitalized in our treatment unit. All patients

had normal kidney function confirmed by renal function tests and renal scintigraphy. Patients were administered a mean activity of 5968 MBq (161.3 mCi) (5873 – 6000 MBq) of [^{177}Lu]Lu-DOTA^{ZOL} intravenously. Table 1 shows patient details along with a history of previous treatments.

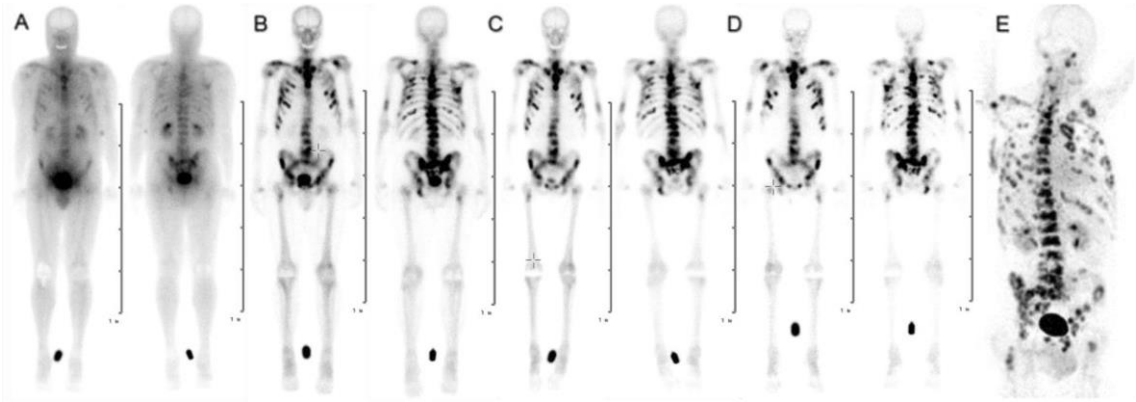

Fig. 1 Planar scintigraphy (anterior and posterior views) after therapeutic application of [^{177}Lu]Lu-DOTA^{ZOL} at **a** 20 min, **b** 3 h, **c** 24 h, **d** 168 h, and **e** PET/CT after application of [^{68}Ga]Ga-DOTA^{ZOL} in a patient with bone metastases secondary to bronchial carcinoma (patient no. 3)

Preparation of [^{177}Lu]Lu-DOTA^{ZOL}:

DOTAZOL was radiolabeled in 0.8 ml ascorbic buffer (210 mg Na-L-ascorbat + 42 mg gentisic acid in 1 ml 0.05 N HCl) with non-carrier-added lutetium-177, both obtained from ITG Isotope Technologies Garching GmbH, Garching, Germany. Manual synthesis was carried out on a thermoshaker at a temperature of 95°C for 30 min. For quality control, an aliquot was retained from the final formulation. Quality control was performed with silica-gel coated aluminium TLC-plates (silica 60 F254.5x4.5 cm, Merck, Darmstadt, Germany). Analysis was performed with a single trace radioTLC-scanner (PET-miniGITA, Elysia-Raytest, Straubenhardt, Germany) and an evaluation software (GinaStar TLC, Elysia-Raytest, Straubenhardt, Germany). Development of silica TLC-plates was conducted in 0.1 M citrate buffer (pH 4) mobile phase, wherer [^{177}Lu]Lu-DOTA-ZOL is found at R/F: 0-0.1 and DOTA at R/F: 0.5. Second, developted in 1 M Acetylaceton/Aceton mixture (1:1) as mobile phase, where [^{177}Lu]Lu-DOTA-ZOL is found at 0-0.1 and unlabelled lutetium-177 at 0.8-1. At last a phosphate-buffer with MeOH 19:1 as mobile phase, where lutetium-177 colloide is found at 0-0.2 and [^{177}Lu]Lu-DOTA-ZOL at 0.8-1. RadioHPLC was used to determine the radiochemical purity, especially the content of radiolysis products as well as unlabelled Gallium-68. RadioHPLC was performed using Agilent 1260 Infinity II reverse phase HPLC system (Agilent Technologies, Santa

Clara, California) equipped with GABI γ-HPLC flow detector (Elysia-raytest, Straubenhardt, Germany) and a PC interface running Gina Star software (Elysia-raytest, Straubenhardt, Germany). A Nucleodur 100-3 C18 ec 250/4 column (Macherey-Nagel GmbH & Co. KG, Düren, Germany) was used. The gradient elution system utilized mobile phase A (Puffer) and mobile phase B (MeOH) at a flow rate of 0.5 mL/min isocratic with 90% phase A and 10% phase B. Radioactivity was measured with a dose calibrator (ISOMED 2010, MED Nuklear-Medizintechnik Dresden GmbH, Dresden, Germany). A radiochemical yield of ≥95% and a radiochemical purity ≥98% was obtained. A comparison of the chemical structures of [^{177}Lu]Lu-DOTAZOL and [^{177}Lu]Lu-EDTMP can be found in figure 2.

Table 1 Subject details of patients receiving radionuclide therapy with [^{177}Lu]Lu-DOT-ZOL

	PT1	PT2	PT3	PT4	MEAN	± SD
Age	83	66	64	64	69.25	9.22
BSA	1.922	1.976	1.979	1.979	1.964	0.028
Hemoglobin (g/dl)	14.3	9.6	13.1	12.6	12.4	2
Thrombocytes (G/l)	187	394	226	189	249	98.32
Leucocytes (G/l)	5.47	9.77	5.37	3.35	5.99	2.7
Hematocrit	0.4	0.4	0.4	0.37	0.39	0.02
Dose (MBq)	6000	6000	5873	6000	5968.25	63.5
Tumor	mCRPC	mCRPC	Bronchial carcinoma	Bronchial carcinoma		
Previous therapies received	Degarelix/ denusumab [^{177}Lu]Lu-PSMA-617	Local Irradiation/docetaxel leuprorelin acetate, abiraterone/denosumab	Carboplatin/denosumab, nivolumab	Carboplatin/denosumab, nivolumab		
Extent of metastases	Extensive	Extensive	Extensive	Extensive		
ECOG status	0	0	0	0		

Imaging protocol:

Serial whole body planar scintigraphy (anterior and posterior views) was performed with dual head Symbia SPECT/CT system (Symbia T, Siemens Healthineers, Erlangen, Germany) at 20 min, 3, 24 and 167 h post injection (p.i). Acquisition was done in supine position at a speed of 10 cm/min using LEHR collimators with 20% energy window centered at a photopeak of 208 keV. Images were processed using an iterative ordered subset maximization algorithm provided by the manufacturer into a matrix of

256*1024. The first data set obtained at 20 min (prior to voiding of the bladder) was considered as reference with 100% of administered activity. A standard source of known activity was placed between the legs in all images at the time of acquisition. For conversion of counts/min to activity, the gamma camera was precalibrated using a known activity of [^{177}Lu]Lu-DOTA^{ZOL} and imaging it at the same speed and distance of 10 cm/min.

Blood sampling:

1-2 ml blood samples were drawn at 20 min, 3, 8, 24 and 167 h p.i.. Due to high counts that may lead to errors in measurement, 0.2 ml blood samples were prepared and measured along with 0.2 ml sample from known standard activity of [^{177}Lu]Lu-DOTA-^{ZOL} using a 1480 WIZARD^{TM} 3n Gamma counter. The calibration factor determined from the standard activity measurement was used to determine the activity in blood samples at the respective data points.

Data analysis:

The images were qualitatively analysed to assess biodistribution of [^{177}Lu]Lu-DOTA^{ZOL} in the whole body and organs. All organs with uptake equal to or more than that of the kidneys were considered as source organs that included kidneys and urinary bladder. Adductor muscle was measured as soft tissue reference. Whole body ROI's were drawn. A rectangular ROI was drawn near the head region above the shoulder for background measurement and an elliptical ROI was used for measurement of the standard source placed between the legs. Same sized ROI's were replicated on serial images (kidneys ROi's up to the 24-h data set and all remaining. ROI's in all subsequent image data sets).

Background corrected counts in right and left kidney, soft tissue, urinary bladder and whole body were determined on anterior and posterior images. The geometric mean counts/min in all source organs at all data time points was determined. Using EANM dosimetry committee guidelines [31], whole body activity at subsequent time points (T) was determined by multiplying the injected activity with the normalized geometric mean whole body counts at the respective time points as given in equation 1,

$$A_{WB,T} = A_0 . \frac{\sqrt{Anterior\ counts_T . Posterior\ counts_T}}{\sqrt{Anterior\ counts_t . Posterior\ counts_t}} \qquad (20)$$

where t = 20 min, T= subsequent time points and A_0 = initial injected activity. Likewise, activity in the urinary bladder was also determined by multiplying the injected activity with the normalized geometric mean counts in urinary bladder.

For calculation of activity in the right and left kidneys at all data points, a conjugate view method with a simple geometrically based subtraction technique given in eqation no 2 [32] was used,

$$A_j = \sqrt{\frac{I_A I_P}{e^{-\mu_e t}}} \frac{f_j}{C} \tag{21}$$

where I_A = anterior count rate , I_P = posterior count count rate, f_j represents source organ self-attenuation correction which was calculated from the source region linear attenuation coefficient μ_j and source thickness t_j using equation no 3 [32]. Factor $\mu_e t$ represents the transmission factor across the patient thickness t in the area of the ROI with a linear attenuation coefficient μ_e calculated using equation no 4 [32]. From [^{68}Ga]Ga-DOTA^{ZOL}-PET/CT of respective patient, CT based measurements of source organ thickness as well as whole body thickness and thickness anterior and posterior to source organs at same level were used. C is the calibration factor determined for gamma camera with a known standard source and was same in all the studies. For measurements of μ_j and μ_i (linear attenuation coefficients for whole thickness), we applied a CT based Hounsfield units method described by Kabasakal et al for [^{177}Lu]Lu-PSMA-617 dosimetric analysis [33].

$$f_j = \frac{\left(\frac{\mu_j t_j}{2}\right)}{\sinh\left(\frac{\mu_j t_j}{2}\right)} \tag{22}$$

$$\mu_e = \left(\frac{1}{t}\right)\sum_{i=1}^{n} \mu_i t_i = \mu_j + \left(\frac{1}{t}\right)\sum_{i=1}^{n} (\mu_i - \mu_j) t_i \; A_j = \sqrt{\frac{I_A I_P}{e^{-\mu_e t}}} \frac{f_j}{C} \tag{23}$$

A simple geometric based background subtraction technique using equation no 5 [32] was used,

$$F = \left\{\left[1 - \left(\frac{I_{ADJ}}{I_A}\right)\left(1 - \frac{t_j}{t}\right)\right]\left[1 - \left(\frac{I_{ADJ}}{I_P}\right)\left(1 - \frac{t_j}{t}\right)\right]\right\}^{\frac{1}{2}} \tag{24}$$

where I_{ADJ} is the count rate through the patient from a soft tissue area of same size as that of the organ ROI. I_A, I_P, t_j and t are the same a s previously defined.

Percent injected activity in the whole body, urinary bladder and kidneys at all time points was determined. To calculate percent injected activity in skeleton, from percent whole body activity, percent blood, urinary bladder and kidneys activities were subtracted.

Dosimetric analysis:

Percent injected activity in the whole body, kidneys and skeletal system at all data time points was used to determine residence times (MBq-h/MBq) by fitting bi exponential kinetic analysis using OLINDA/EXM version 2.0 (Hermes Medical Solutions, Stockholm, Sweden) software in these organs. The residence times for the skeletal system were assumed to be distributed equally between trabecular and cortical bone. An indirect blood-based method using patient based red marrow-to-blood ratio (RMBLR) and bone marrow mass was used to determine bone marrow self-dose [34, 35].

Urinary excretion fraction at all time points was determined by applying the function $A_0*(1-e^{-\lambda,T})$. With a logarithmic function fit on the urinary excretion curve, effective excretion half-life was obtained. Using the total urinary excretion fraction, effective excretion half-life and 4 h voiding interval as input in Cloutier's dynamic urinary bladder model, residence time for urinary bladder contents was obtained. By subtracting residence times for kidneys, bone marrow and skeletal system from whole body residence time, the remainder of body residence time was calculated.

Residence time for kidneys, cortical and trabecular bone, urinary bladder contents, red marrow self-dose and remainder of body were used as an input in OLINDA/EXM version 2.0 (Hermes Medical Solutions, Stockholm, Sweden) software for calculation of organ absorbed doses and effective doses after adjusting the weight of patient organs by multiplying the reference adult male weight with factor obtained by dividing patient weight with the reference adult male weight. The mean of residence times and organ absorbed doses (mSv/MBq) were calculated.

RESULTS

Qualitative analysis:

Figures 1 and 2 show the biodistribution of [^{177}Lu]Lu-DOTA^{ZOL} in one patient with bronchial carcinoma and one patient with mCRPC, respectively. In the initial 20 min p.i.. image data set, highest uptake was seen in the urinary bladder followed by kidneys and soft tissue with minimal uptake in skeletal system. The kidneys showed a rapid decrease in activity at 3 h with minimum to no uptake after 24 h p.i.. The Intense uptake was seen in the skeletal system from 3 h onwards. Blood and soft tissue clearance and lesion to normal bone contrast increased in later images up to 168 h. The mean ± SD 24 h whole body retention was found to be 31.25 ± 6.5.

In this small patient study, we observed fast uptake and clearance kinetics of kidneys in patients with bronchial carcinoma as compared to mCRPC patient, which resulted in better skeletal to soft tissue contrast as early as 3 h p.i.. in the bronchial carcinoma patient as compared to 24 h p.i.. in mCRPC patient.

Quantitative analysis:

Mean residence times (MBq-h/MBq) (Table 2) was found to be highest in trabecular and cortical bone (31.9 h) followed by remainder of the body (11.7 h), kidneys (1.84 h), urinary bladder (1.52 h) and bone marrow (0.03 h). In patient no 1, residence times for the skeletal system and the kidney were lower as compared to the other patients.

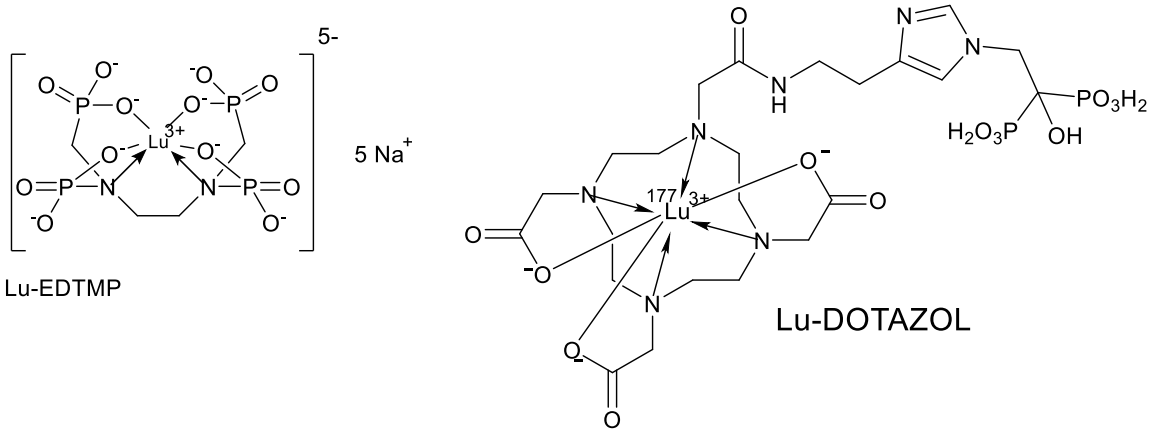

Fig. 2 Comparison of chemical structures of [^{177}Lu]Lu-DOTAZOL and [^{177}Lu]Lu-EDTMP.

Mean organ absorbed doses (Table 3) were found highest (3.33 ± 0.35 mSv/MBq) for osteogenic cells, followed by kidneys (0.49 ± 0.16 mSv/MBq), red marrow (0.461 ± 0.064 mSv/MBq) and urinary bladder wall (0.322 ± 0.022 mSv/MBq). Kidney and osteogenic cell absorbed doses were lowest in patient no 1. The mean total body dose was 0.092 ± 0.033 mSv/MBq.

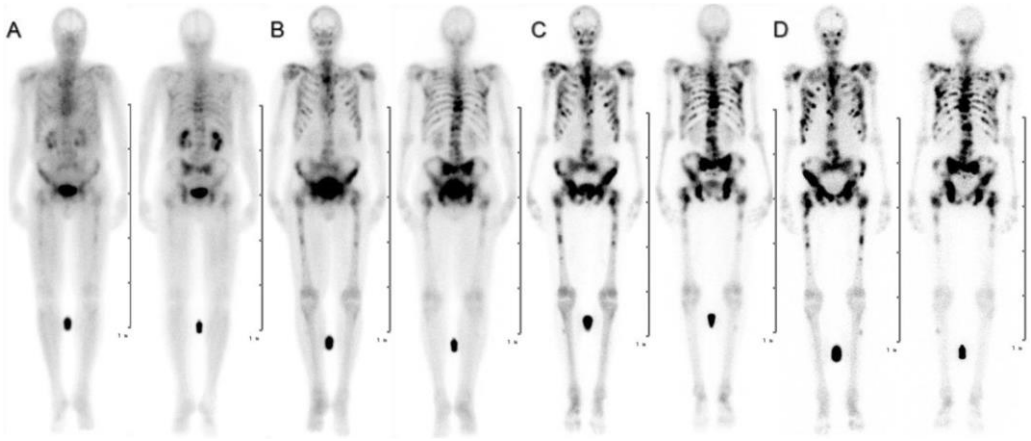

Fig. 3 Planar scintigraphy (anterior and posterior views) after therapeutic application of [^{177}Lu]Lu-DOTA^{ZOL} at **a** 20min, **b** 3h, **c** 24h, and **d** 168h in a patient with bone metastases secondary to prostate cancer (patient no. 1).

Table 2 Residence times (MBq-h/MBq) of [^{177}Lu]Lu-DOTAZOL in comparison with [^{177}Lu]Lu-EDTMP [5]

	[177Lu]Lu-DOTAZOL						[177Lu]Lu-
Organs	PT1	PT2	PT3	PT4	MEAN	± SD	EDTMP [5]
Kidneys	0.96	2.01	2.43	1.96	1.84	0.63	
Trabecular bone	27.45	34.95	33.45	31.85	31.93	3.24	48.62
Cortical bone	27.45	34.95	33.45	31.85	31.93	3.24	48.62
Red marrow	0.01	0.03	0.04	0.03	0.03	0.01	0.07
Urinary bladder contents	1.59	1.48	1.51	1.5	1.52	0.05	7.23
Remainder of body	0.23	44.06	0.93	1.4	11.65	21.61	27.37
Whole body	56.1	116	70.3	67.1	77.38	26.46	131.91
Blood	0.19	0.34	0.35	0.46	0.34	0.11	0.98

DISCUSSION

Zoledronate presents as an ideal candidate for labeling with the therapeutic radionuclide lutetium-177 for radionuclide therapy of bone metastases, as it shows high osteoclast and hydroxyl apatite binding [27] and no in vivo biotransformation [3]. Preclinical small animal studies using [^{177}Lu]Lu-DOTA^{ZOL} and [^{68}Ga]Ga-DOTA^{ZOL} showed comparable results, suggesting the two tracers as new theranostic pair for bone-targeted radionuclide therapy [27].

Extrapolation of dosimetric analysis of [^{177}Lu]Lu-DOTA^{ZOL} and [^{177}Lu]Lu-EDTMP from rats to humans revealed high kidney and trabecular bone absorbed doses as well as high trabecular bone to other organs absorbed dose ratios for [^{177}Lu]Lu-DOTA^{ZOL} [28]. The higher thermodynamic and kinetic stability, leading to high bone uptake with low soft tissue accumulation, suggests [^{177}Lu]Lu-DOTA^{ZOL} to be a better therapeutic bisphosphonate compared to [^{177}Lu]Lu-EDTMP [2].

The current study is the first ever human biodistribution and dosimetric anlaysis for [^{177}Lu]Lu-DOTA^{ZOL} in mCRPC and bronchial carcinoma patients. We noticed that biodistribution of [^{177}Lu]Lu-DOTA^{ZOL} in humans (figures 1 & 2) is consistent with preclinical biodistribution studies in male Wistar rats [27, 28]. We found highest accumulation in the skeleton with fast kidney uptake and clearance. As the kidneys are the sole route of its excretion, the urinary bladder showed high uptake as well. Blood and soft tissue showed rapid clearance which resulted in good skeleton to soft tissue contrast. A rapid and biphasic blood clearance curve was found (Figure 3) comparable to [^{177}Lu]Lu-EDTMP [5]. No uptake was seen in any other organ.

Table 3 Organ absorbed doses (mSv/MBq) of [^{177}Lu]Lu-DOTA^{ZOL}

Organs	PT1	PT2	PT3	PT4	Mean	± SD
Adrenals	0.010	0.069	0.016	0.015	0.027	0.028
Brain	0.007	0.061	0.009	0.009	0.021	0.027
Esophagus	0.004	0.060	0.006	0.006	0.019	0.027
Eyes	0.007	0.061	0.009	0.009	0.021	0.027
Gall bladder wall	0.003	0.060	0.005	0.005	0.018	0.028
Left colon	0.005	0.062	0.007	0.007	0.020	0.028
Small intestine	0.004	0.061	0.006	0.006	0.019	0.028
Stomach wall	0.003	0.058	0.004	0.004	0.017	0.027
Right colon	0.003	0.060	0.005	0.005	0.018	0.028
Rectum	0.006	0.062	0.007	0.007	0.021	0.028
Heart wall	0.003	0.059	0.005	0.005	0.018	0.027
Kidneys	0.263	0.555	0.632	0.511	0.490	0.160
Liver	0.003	0.059	0.005	0.005	0.018	0.027
Lungs	0.004	0.059	0.005	0.006	0.019	0.027
Pancreas	0.004	0.061	0.006	0.006	0.019	0.028
Prostate	0.005	0.060	0.006	0.006	0.019	0.027
Salivary glands	0.004	0.060	0.006	0.006	0.019	0.027

Red marrow	0.402	0.551	0.456	0.434	0.461	0.064
Osteogenic cells	2.940	3.770	3.330	3.170	3.300	0.350
Spleen	0.004	0.060	0.006	0.006	0.019	0.027
Testes	0.003	0.057	0.004	0.004	0.017	0.027
Thymus	0.003	0.058	0.004	0.005	0.017	0.027
Thyroid	0.004	0.060	0.006	0.006	0.019	0.027
Urinary bladder wall	0.333	0.364	0.316	0.316	0.332	0.023
Total body	0.069	0.142	0.081	0.077	0.092	0.034

Prominent uptake in the skeletal system in bronchial carcinoma patients was visualized at 3 h p.i. image in contrast to 24 h p.i. in mCRPC patients. The finding of best bone-to-soft tissue contrast at 24 h p.i. in mCRPC patients is consistent with similar observations with [^{177}Lu]Lu-EDTMP distribution in mCRPC patients [5, 7, 26]. To establish whether the early uptake in bronchial carcinoma patients is a patient dependent or tumor dependent finding and can be of any significance in relation to tumor lesion doses needs further large scale and tumor lesion dosimetry studies.

The source organs identified for dosimetric analysis included the kidneys, bone marrow, urinary bladder, skeletal system and the whole body. A biphasic kinetic behavior of [^{177}Lu]Lu-DOTA^{ZOL} was observed in all source organs and the whole body. Hence, biexponential curve fitting was used for residence time calculations. Residence time was highest in the skeleton similar to [^{177}Lu]Lu-EDTMP (table 2) [5]. Residence time for all source organs except the kidneys were lower in comparison to [^{177}Lu]Lu-EDTMP (Table 2) [5]. The low number of patients and the different methodology used for determination of residence time in our current study might be causes for this difference. However, the ratio of skeletal-to-whole body residence time was higher for [^{177}Lu]Lu-DOTA^{ZOL} compared to [^{177}Lu]Lu-EDTMP [5].

We found lower mean organ absorbed doses for osteogenic cells (3.33 ± 0.35 mSv/MBq) compared to 5.41 and 5.26 mSv/MBq reported for [^{177}Lu]Lu-EDTMP [5, 26], (figure 4) as well as 4.04 mSv/MBq for [^{153}Sm]Sm-EDTMP [26]. The difference might be due to humerus [5] or femoral [26] activity extrapolation for skeletal activity and residence time calculations for [^{177}Lu]Lu-EDTMP as compared to calculation of skeletal activity by deduction of percent kidney, blood and bladder activity from percent whole body activity in current study.

In our study we found a higher mean organ absorbed dose for the kidneys (0.49 mSv/MBq) as compared to [^{177}Lu]Lu-EDTMP (0.04 and 0.06 mSv/MBq) [5, 26]. In contrast to the use of the conjugate view method for kidney residence time calculation in our current study, Bal et al. [5] neglected kidney self-dose in absorbed dose determination and Sharma et al. [26] used a different methodology for calculation of percent injected doses in kidneys which resulted in lower kidney dose for [^{177}Lu]Lu-EDTMP. Hence, the kidney absorbed doses reported for [^{177}Lu]Lu-EDTMP cannot be compared with the results of [^{177}Lu]Lu-DOTA^{ZOL} in our current study. The mean organ absorbed dose to the urinary bladder wall (0.332 mSv/MBq) was found to be lower in our study as compared to [^{177}Lu]Lu-EDTMP (1.53 mSv/MBq) [5, 26]. This difference could be due to use of Cloutier´s method with cumulative urinary calculation from whole body retention and 4 h voiding intervals in our current study as compared to collection of urine samples for residence time calculation in the [^{177}Lu]Lu-EDTMP studies.

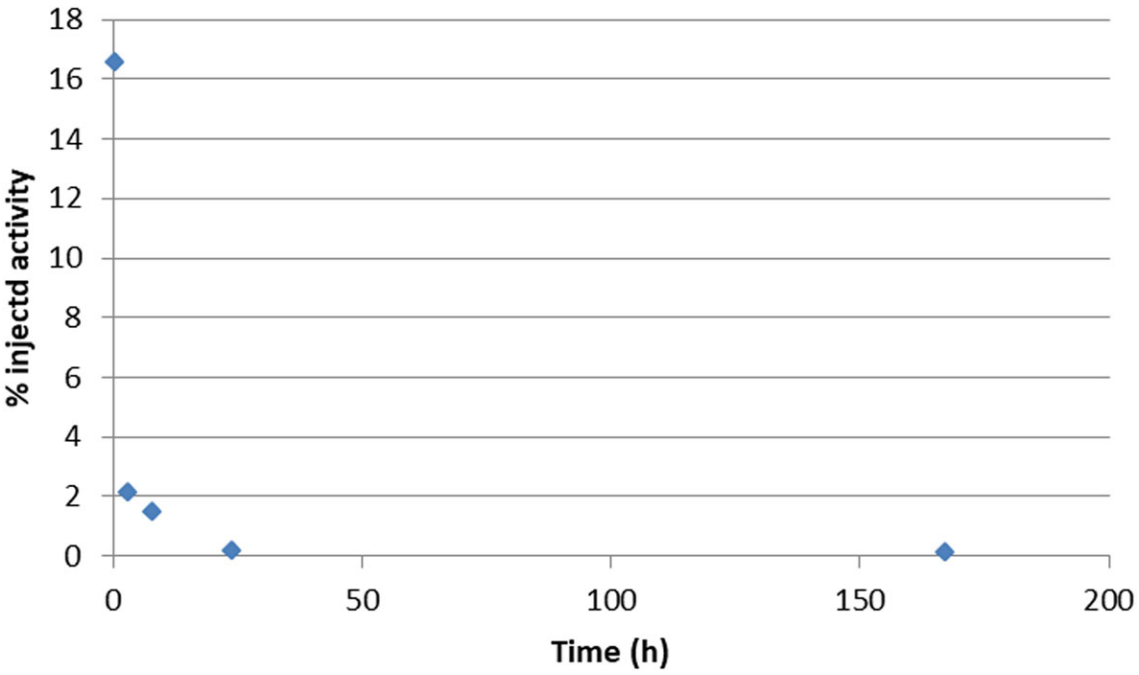

Fig. 4 Blood clearance curve in patient no. 4 with bronchial carcinoma

[^{177}Lu]Lu-DOTA^{ZOL} resulted in a lower bone marrow absorbed dose compared to [^{177}Lu]Lu-EDTMP [5, 7, 26], which in theory allows administration of higher therapeutic activities of [^{177}Lu]Lu-DOTA^{ZOL}. Based on a maximum permissible radiation absorbed dose to the bone marrow of 2Gy, the maximum tolerated dose for [^{177}Lu]Lu-DOTA^{ZOL} is estimated to be 3630-4980 MBq as compared to 2000–3250 MBq for [^{177}Lu]Lu-EDTMP [5]. As a result, radiation absorbed dose of 11 to 16 Gy will be delivered to osteogenic cells by [^{177}Lu]Lu-DOTA^{ZOL} which is comparable to 10.1 to 17.6 Gy for [^{177}Lu]Lu-EDTMP.

Using these thresholds, the kidney absorbed dose remains well below the maximum permissible dose limit of 23 Gy.

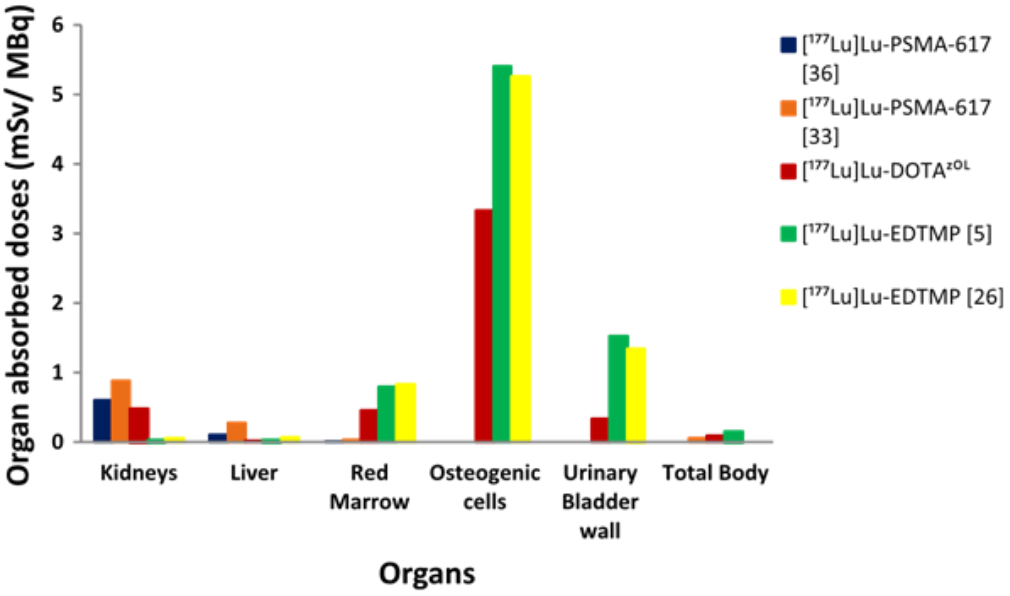

Fig. 5 Comparison of organ absorbed doses of [177Lu]Lu-DOTAZOL with [177Lu]Lu-EDTMP [5, 26], [177Lu]Lu-PSMA-617 [33, 36].

As absorbed dose to kidneys is one of the important factors in radionuclide therapy using Lutetium-177 labeled radiopharmaceuticals, we found that [^{177}Lu]Lu-DOTA^{ZOL} delivers a lower (by a factor of 1.2 to 1.88) kidney dose (Figure 3) in comparison to [^{177}Lu]Lu-PSMA-617 [33, 36].

CONCLUSION:

[^{177}Lu]Lu-DOTA^{ZOL} is a promising new therapeutic radiopharmaceutical for radionuclide therapy of bone metastases due to excellent skeletal uptake, a lower low bone marrow dose than [^{177}Lu]Lu-EDTMP and a very low kidney dose. Labeling with gallium-68 delivers [^{68}Ga]Ga-DOTA^{ZOL}, which represents an ideal theranostic counterpart for PET/CT imaging. Further studies are warranted to evaluate the efficacy and safety of radionuclide therapy with [^{177}Lu]Lu-DOTA^{ZOL} in the clinical setting.

Acknowledgements:

Not applicable

Consent for Publication:

Consent for publication is available on institutional forms, will be provided if asked

Ethics Approval and consent to participate:

All treatments were performed in the context of an individual treatment attempt as no other treatment options were left for these patients. Written informed consent was obtained from all patients. The local ethical committee waived the ethical statement due to the retrospective character of the study. All procedures were followed in accordance with ethical standards of institutional review board and therefore been performed in accordance with the ethical standards laid down in the 1964 Declaration of Helsinki and all subsequent revisions

Availability of data and materials:

The datasets used and/or analysed during the current study are available from the corresponding author on reasonable request.

Competing interests:

The authors declare that they have no competing interests

Funding:

It is declared that no funding has been secured for this research.

Authors Contribution:

The manuscript has been seen and approved by all authors. AK, MM, SK, EE: contributed equally in design and execution of study. AK, FR, HA, ME, RAB, FCG: contributed in drafting or revising of the manuscript critically for important intellectual content as well as final manuscript approval for submission and publication.

References

1. N Pandit-Taskar. Pandit-Taskar N, Batraki M, Divgi CR. Radiopharmaceutical therapy for palliation of bone pain from osseous metastases. J Nucl Med. 2004;45:1358–65. J Nucl Med. 2004;45:1358.
2. Bergmann R, Meckel M, Kubíček V, Pietzsch J, Steinbach J, Hermann P, Rösch F. (177)Lu-labelled macrocyclic bisphosphonates for targeting bone metastasis in cancer treatment. EJNMMI Res. 2016;6:5. doi:10.1186/s13550-016-0161-3.
3. Nikzad M, Jalilian AR, Shirvani-Arani S, Bahrami-Samani A, Golchoubian H. Production, quality control and pharmacokinetic studies of 177Lu–zoledronate for bone pain palliation therapy. J Radioanal Nucl Chem. 2013;298:1273–81. doi:10.1007/s10967-013-2490-2.
4. Ogawa K, Ishizaki A. Well-designed bone-seeking radiolabeled compounds for diagnosis and therapy of bone metastases. BioMed Research International. 2015;2015:676053. doi:10.1155/2015/676053.

5. Bal C, Arora G, Kumar P, Damle N, Das T, Chakraborty S, et al. Pharmacokinetic, Dosimetry and Toxicity Study of ^{177}Lu-EDTMP in Patients: Phase 0/I study. Current Radiopharmaceuticals. 2016;9:71–84. doi:10.2174/1874471008666150313105000.
6. A Fakhari. Fakhari A, Reza Jalilian A, Yousefnia H, Bahrami-Samani A, Johari-Daha F, Khalaj A. Radiolabeling and evaluation of two 177 Lu-labeled bis-phosphonates preparation of two 177Lu-labeled bis-phosphonates. Iran J Nucl Med. 2015;23:108–15. Iran J Nucl Med. 2015;23:108.
7. Balter H, Victoria T, Mariella T, Javier G, Rodolfo F, Andrea P, et al. ^{177}Lu-Labeled Agents for Neuroendocrine Tumor Therapy and Bone Pain Palliation in Uruguay. Current Radiopharmaceuticals. 2016;9:85–93. doi:10.2174/1874471008666150313112620.
8. Kam BLR, Teunissen JJM, Krenning EP, Herder WW de, Khan S, van Vliet EI, Kwekkeboom DJ. Lutetium-labelled peptides for therapy of neuroendocrine tumours. European Journal of Nuclear Medicine. 2012;39 Suppl 1:S103-12. doi:10.1007/s00259-011-2039-y.
9. Frilling A, Weber F, Saner F, Bockisch A, Hofmann M, Mueller-Brand J, Broelsch CE. Treatment with (90)Y- and (177)Lu-DOTATOC in patients with metastatic neuroendocrine tumors. Surgery. 2006;140:968-76; discussion 976-7. doi:10.1016/j.surg.2006.07.030.
10. Ahmadzadehfar H, Eppard E, Kürpig S, Fimmers R, Yordanova A, Schlenkhoff CD, et al. Therapeutic response and side effects of repeated radioligand therapy with 177Lu-PSMA-DKFZ-617 of castrate-resistant metastatic prostate cancer. Oncotarget. 2016;7:12477–88. doi:10.18632/oncotarget.7245.
11. Pfestroff A, Luster M, Jilg CA, Olbert PJ, Ohlmann CH, Lassmann M, et al. Current status and future perspectives of PSMA-targeted therapy in Europe: opportunity knocks. European Journal of Nuclear Medicine. 2015;42:1971–5. doi:10.1007/s00259-015-3186-3.
12. Yordanova A, Eppard E, Kürpig S, Bundschuh RA, Schönberger S, Gonzalez-Carmona M, et al. Theranostics in nuclear medicine practice. OncoTargets and Therapy. 2017;10:4821–8. doi:10.2147/OTT.S140671.
13. Russell RGG. Bisphosphonates: mode of action and pharmacology. Pediatrics. 2007;119 Suppl 2:S150-62. doi:10.1542/peds.2006-2023H.
14. Chakraborty S, Das T, Sarma HD, Venkatesh M, Banerjee S. Comparative studies of 177Lu-EDTMP and 177Lu-DOTMP as potential agents for palliative radiotherapy of bone metastasis. Applied Radiation and Isotopes. 2008;66:1196–205. doi:10.1016/j.apradiso.2008.02.061.

15. Das T, Shinto A, Karuppuswamy Kamaleshwaran K, Banerjee S. Theranostic Treatment of Metastatic Bone Pain With 177Lu-DOTMP. Clin Nucl Med. 2016;41:966–7. doi:10.1097/RLU.0000000000001409.

16. Mazzarri S, Guidoccio F, Mariani G. The emerging potential of 177Lu-EDTMP: an attractive novel option for radiometabolic therapy of skeletal metastases. Clin Transl Imaging. 2015;3:167–8. doi:10.1007/s40336-015-0099-x.

17. Shinto AS, Shibu D, Kamaleshwaran KK, Das T, Chakraborty S, Banerjee S, et al. ^{177}Lu-EDTMP for treatment of bone pain in patients with disseminated skeletal metastases. Journal of Nuclear Medicine Technology. 2014;42:55–61. doi:10.2967/jnmt.113.132266.

18. Agarwal KK, Singla S, Arora G, Bal C. (177)Lu-EDTMP for palliation of pain from bone metastases in patients with prostate and breast cancer: a phase II study. European Journal of Nuclear Medicine. 2015;42:79–88. doi:10.1007/s00259-014-2862-z.

19. Alavi M, Omidvari S, Mehdizadeh A, Jalilian AR, Bahrami-Samani A. Metastatic Bone Pain Palliation using (177)Lu-Ethylenediaminetetramethylene Phosphonic Acid. World Journal of Nuclear Medicine. 2015;14:109–15. doi:10.4103/1450-1147.157124.

20. Thapa P, Nikam D, Das T, Sonawane G, Agarwal JP, Basu S. Clinical Efficacy and Safety Comparison of 177Lu-EDTMP with 153Sm-EDTMP on an Equidose Basis in Patients with Painful Skeletal Metastases. J. Nucl. Med. 2015;56:1513–9. doi:10.2967/jnumed.115.155762.

21. Yuan J, Liu C, Liu X, Wang Y, Kuai D, Zhang G, Zaknun JJ. Efficacy and safety of 177Lu-EDTMP in bone metastatic pain palliation in breast cancer and hormone refractory prostate cancer: a phase II study. Clin Nucl Med. 2013;38:88–92. doi:10.1097/RLU.0b013e318279bf4d.

22. Baum RP, Kulkarni HR. THERANOSTICS: From Molecular Imaging Using Ga-68 Labeled Tracers and PET/CT to Personalized Radionuclide Therapy - The Bad Berka Experience. Theranostics. 2012;2:437–47. doi:10.7150/thno.3645.

23. Pfannkuchen N, Meckel M, Bergmann R, Bachmann M, Bal C, Sathekge M, et al. Novel Radiolabeled Bisphosphonates for PET Diagnosis and Endoradiotherapy of Bone Metastases. Pharmaceuticals (Basel). 2017;10:45. doi:10.3390/ph10020045.

24. Rösch F, Baum RP. Generator-based PET radiopharmaceuticals for molecular imaging of tumours: on the way to THERANOSTICS. Dalton Transactions. 2011;40:6104–11. doi:10.1039/c0dt01504k.

25. Passah A, Tripathi M, Ballal S, Yadav MP, Kumar R, Roesch F, et al. Evaluation of bone-seeking novel radiotracer 68Ga-NO2AP-Bisphosphonate for the detection of

skeletal metastases in carcinoma breast. European Journal of Nuclear Medicine. 2017;44:41–9. doi:10.1007/s00259-016-3469-3.

26. Sharma S, Singh B, Koul A, Mittal BR. Comparative Therapeutic Efficacy of 153Sm-EDTMP and 177Lu-EDTMP for Bone Pain Palliation in Patients with Skeletal Metastases: Patients' Pain Score Analysis and Personalized Dosimetry. Frontiers in Medicine. 2017;4:46. doi:10.3389/fmed.2017.00046.
27. Meckel M, Bergmann R, Miederer M, Roesch F. Bone targeting compounds for radiotherapy and imaging: *Me(III)-DOTA conjugates of bisphosphonic acid, pamidronic acid and zoledronic acid. EJNMMI radiopharm. chem. 2017;1:14. doi:10.1186/s41181-016-0017-1.
28. Yousefnia H, Zolghadri S, Jalilian AR. Absorbed dose assessment of (177)Lu-zoledronate and (177)Lu-EDTMP for human based on biodistribution data in rats. Journal of Medical Physics. 2015;40:102–8. doi:10.4103/0971-6203.158694.
29. Pfannkuchen N, Bausbacher N, Pektor S, Miederer M, Rosch F. In vivo Evaluation of 225AcAc-DOTAZOL for α-Therapy of Bone Metastases. Current Radiopharmaceuticals. 2018;11:223–30. doi:10.2174/1874471011666180604083911.
30. Holub J, Meckel M, Kubíček V, Rösch F, Hermann P. Gallium(III) complexes of NOTA-bis (phosphonate) conjugates as PET radiotracers for bone imaging. Contrast Media Mol Imaging. 2015;10:122–34. doi:10.1002/cmmi.1606.
31. Hindorf C, Glatting G, Chiesa C, Lindén O, Flux G. EANM Dosimetry Committee guidelines for bone marrow and whole-body dosimetry. European Journal of Nuclear Medicine. 2010;37:1238–50. doi:10.1007/s00259-010-1422-4.
32. J Siegel. Siegel J, Thomas SR. MIRD pamphlet no. 16: Techniques for quantitative radiopharmaceutical biodistribution data acquisition and analysis for use in human radiation dose estimates. J Nucl Med. 1999;40:37S–61S. J Nucl Med. 1999;40:37S.
33. Kabasakal L, AbuQbeitah M, Aygün A, Yeyin N, Ocak M, Demirci E, Toklu T. Pre-therapeutic dosimetry of normal organs and tissues of (177)Lu-PSMA-617 prostate-specific membrane antigen (PSMA) inhibitor in patients with castration-resistant prostate cancer. European Journal of Nuclear Medicine. 2015;42:1976–83. doi:10.1007/s00259-015-3125-3.
34. Siegel JA. Establishing a clinically meaningful predictive model of hematologic toxicity in nonmyeloablative targeted radiotherapy: practical aspects and limitations of red marrow dosimetry. Cancer Biotherapy & Radiopharmaceuticals. 2005;20:126–40. doi:10.1089/CBR.2005.20.126.

35. Hindorf C, Lindén O, Tennvall J, Wingårdh K, Strand S-E. Evaluation of methods for red marrow dosimetry based on patients undergoing radioimmunotherapy. Acta Oncol. 2005;44:579–88. doi:10.1080/02841860500244294.

36. Scarpa L, Buxbaum S, Kendler D, Fink K, Bektic J, Gruber L, et al. The 68Ga/177Lu theragnostic concept in PSMA targeting of castration-resistant prostate cancer: correlation of SUVmax values and absorbed dose estimates. European Journal of Nuclear Medicine. 2017;44:788–800. doi:10.1007/s00259-016-3609-9.

5. **PSMA**

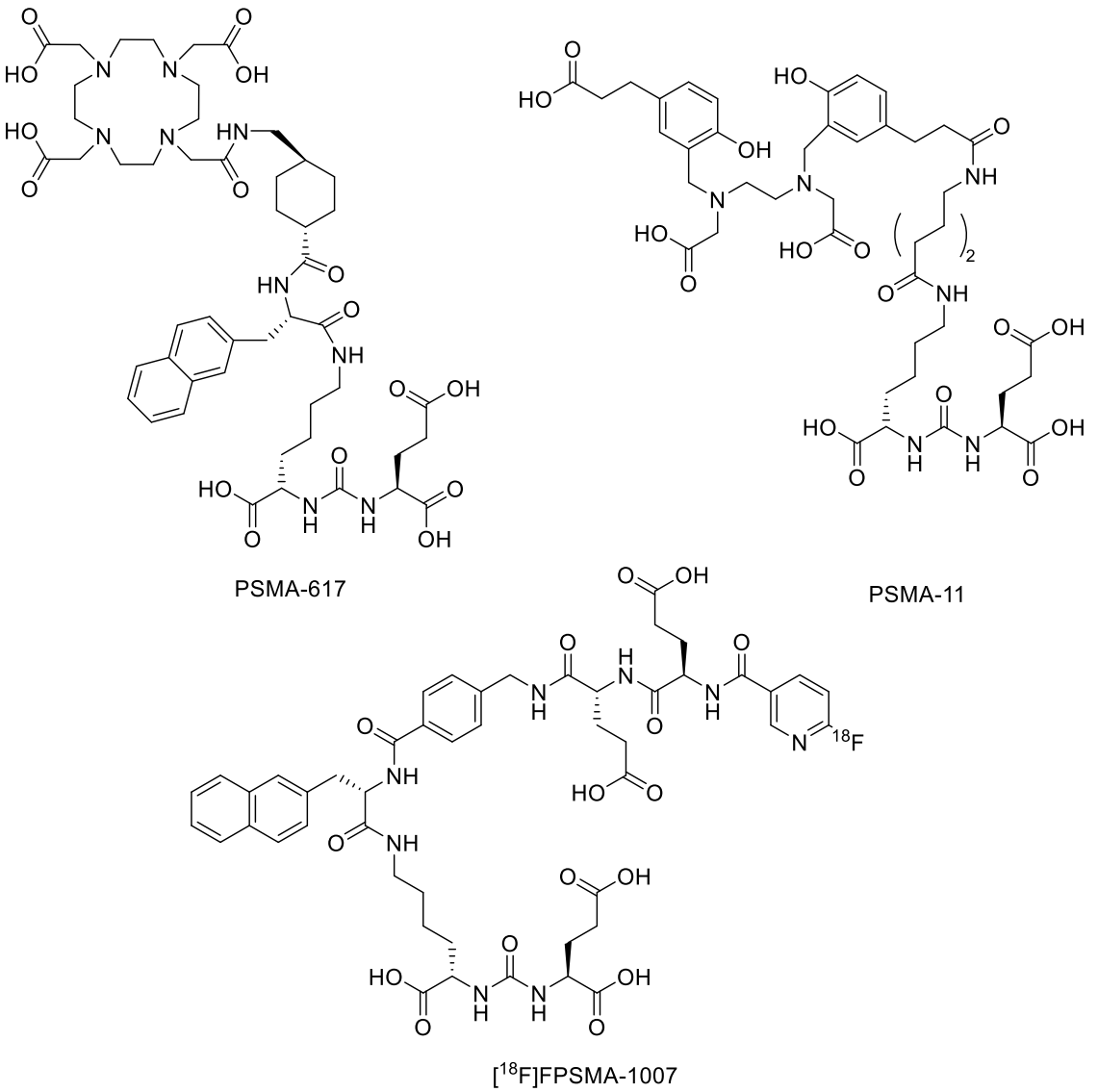

Abbildung 22: Schematische Darstellung verschiedener PSMA-Typen.

Das Prostata-spezifisches Membran-Antigen (PSMA) ist ein Transmembranmolekül im Prostatagewebe und wird bei Prostatakrebs stark überexprimiert. Aufgrund der geringen Expression von PSMA in gesundem Gewebe, mit Ausnahme von Speichel- und Tränendrüsen, ist eine hochdosierte Radioligandentherapie (RLT) möglich. Der aktuell am häufigsten genutzten Tracer ist [^{68}Ga]Ga-PSMA-11. Für die Therapie von kastrationsresistenten Prostatakarzinomen wird [^{177}Lu]Lu-PSMA-617 therapeutisch eingesetzt. Um eine vorab Einschätzung mittels Dosimetrie zu machen, kann [^{44}Sc]Sc-PSMA-617 oder [^{18}F]FPSMA-1007 eingesetzt werden.

5.1 Outcome and safety of re-challenge [^{177}Lu]Lu-PSMA-617 in patients with metastatic prostate cancer

Anna Yordanova[1] Paula Linden[1] Stefan Hauser[2] Michael Meisenheimer[1] Stefan Kürpig[1] Georg Feldmann[3] Florian C Gaertner[1] Markus Essler[1] Hojjat Ahmadzadeh-far[1]

https://doi.org/10.1007/s00259-018-4222-x

[1] Department of Nuclear Medicine, University Hospital Bonn, Germany

[2] Department of Urology, University Hospital Bonn, Germany

[3] Department of Internal Medicine 3, University Hospital Bonn, Germany

Correspondence to:

Hojjat Ahmadzadehfar, MD, MSc

University Hospital Bonn

Department of Nuclear Medicine

Sigmund-Freud-Str. 25, 53127 Bonn

Tel: +49 228 287 19858

Fax: +49 228 287 90 19858

Email: hojjat.ahmadzadehfar@ukbonn.de

Abstract

Background There is a sparse data regarding the feasibility of radioligand therapy (RLT) with [^{177}Lu]Lu-PSMA-617 as a retreatment. We aimed to assess the outcome and safety of re-challenge RLT in patients with progressive prostatic cancer who previously benefited from this therapy.

Materials and methods Assessed were patients who received re-challenge therapy at our department from January 2015 to March 2018. Non-haematological and haematological adverse events were evaluated from laboratory data and clinical reports and were graded according to the Common Terminology Criteria for Adverse Events (CTCAE v. 5.0). Time to prostate-specific-antigen (PSA) progression and overall survival of the study patients were calculated from the date of the first re-challenge cycle. The response data was determined using [^{68}Ga]Ga-PSMA-PET/CT and measurements of the tumor marker PSA.

Results Included in this retrospective study were 30 patients, who were initially treated with a median of 3 cycles (range 1-5) RLT and were eventually retreated after a median of 6 months (range 2 – 26). Each patient received a median of 3 (range 1-6) re-challenge cycles. None of the patients experienced a disabling or life-threatening adverse event (CTC-4). Grade 3 toxicity occurred in 8 patients (27%). Serious adverse events included leucopenia (n=2), neutropenia (n=1), anemia (n=4), thrombopenia (n=4) and elevated renal parameters (n=1). According to PSA-measurements 71% of patients showed a benefit (response / stable) from the first three re-challenge cycles. The median overall survival was 12 months. The survival correlated strongly with the PSA-change after the first cycle re-challenge RLT (p –value was 0.015). Patients with PSA-decrease survived in median 19 months and patients with PSA-increase only 8 months.

Conclusion Re-challenge PSMA therapy is with an acceptable safety profile. The majority of the re-treated patients benefited from the re-challenge therapy. Patients who showed biochemical response could achieve longer survival compared to patients who did not respond.

Keywords: Recurrence; PSMA; ^{177}Lu; prostate cancer, CRPC, radioligand therapy

Background

The prostate-specific membrane antigen (PSMA) is highly expressed especially in androgen independent prostate cancer (PCA), which makes it promising target for the treatment of patients with castrate-resistant PCA [1–6].

The novel ligand PSMA-617 labelled with the beta emitter Lutetium-177 binds specifically PSMA and is being used for the PSMA radioligand therapy (PSMA-RLT). The internalization of the radioligand enables the accumulation of the radioactivity in the tumour tissue and the irradiation from the inside [7–10].

In the last years PSMA-RLT is gaining rapidly interest for the treatment of patients with castration-resistant PCA (CRPC) worldwide [11–13]. Unfortunately, prospective data from randomized phase III prospective trials is lacking, therefore PSMA-RLT remains a last-line option in advanced PCA [14, 15]. This means, that the patients are already castration resistant, metastatic and in most of the cases symptomatic before they start this treatment. But even in this late stage of disease results from several studies implicate that PSMA-RLT is effective and safe in patients with prostate cancer (PCA) [11, 16–24]. Grade 3/4 haematologic toxicities occur in 3 – 11 % of patients. Till now there are no reports of severe non-haematologic toxicities [16, 17, 19–22, 25–27]. The estimated progression-free survival in treated patients ranges in the literature between 4.5 – 13.7 months and the overall survival between 7.5 - 15 months, respectively. This data is very encouraging having in mind the fact that most PCA patients undergo various therapies before they receive the PSMA-radioligand therapy [19–21, 24, 28, 29]. However, in this late stadium of disease, the treatment opportunities for patients, who relapse after RLT are very limited.

Re-administration of RLT in patients who previously benefited from the therapy and experienced no relevant toxicity seems a promising option in these patients. The main focus of this article was to investigate the survival, response and adverse events in patients, who underwent re-challenge radioligand therapy.

Materials and methods

Patients

Included in the analyses were patients with initial disease control after a baseline treatment with PSMA-RLT, who eventually progressed and received, re-challenge PSMA-RLT. The presence of PSMA-positive metastases should have been confirmed in the the [^{68}Ga]Ga-PSMA-11 PET/CT. Patient's data were retrieved from clinical records. Baseline patients´ characteristics such as tumour spread and prior therapies are summarized in

Table 1. The protocol of this retrospective study was in accordance with the requirements of the local ethic committee, the Declaration of Helsinki or comparable ethical standards. All patients agreed with the scientific analysis of their data and gave a written informed consent prior to the therapy.

Treatment

ABX GmbH (Radeberg, Germany) provided the PSMA-617-ligand and IDB (Holland, Bearle-Nassau, Netherlands) the nuclide Lutetium. The radiolabeling proceeded locally. PSMA-RLT was injected intravenously as a slow bolus injection. The administered activity was adapted to the tumour load, renal parameters and bone marrow reserve. The median injected activity was 6.1 GBq per cycle (range 3.8 – 6.7 GBq), followed by 1000 ml infusion of 0.9% NaCl solution. To avoid xerostomia patients had to cool the salivary glands with cool packages, beginning 30 minutes before administration of the radiopharmaceutical. The distribution and tumor-uptake of the radionuclide was recorded using planar whole body scans and SPECT/CT 24 hours after administration.

Toxicity assessment

Clinical data and laboratory profiles incl. renal function parameters and haematological results were recorded for each patient. Blood tests were performed before and after each cycle PSMA-RLT and repeated every 2 weeks for a period of two months after the treatment, and at each follow-up visit. All patients underwent a baseline [^{99m}Tc]Tc-MAG3-renography before starting PSMA-RLT. Additionally, patients with a creatinine-increase or history of renal impairment underwent a [^{99m}Tc]Tc-MAG3-renography before each cycle, including quantitative measurements of the tubular extraction rate. Clinical reports included information about patients' subjective health complains, amount of analgesic drugs administered, weight loss and ECOG status. Adverse events were graded according to the Common Terminology Criteria for Adverse Events (CTCAE v5.0) [30].

Response assessment

Response was demonstrated morphologically by [^{68}Ga]Ga-PSMA-11 PET/CT and biochemically by PSA-measurements. The imaging response has been classified according to adapted PERSIST criteria as complete response (CR), partial response (PR), stable disease (SD) and progressive disease (PD). Additionally, we defined a mixed response (MixR) as partial response of the known metastases and at same time occurrence of new lesions. However, for the MixR the overall tumour load should be stable or less in comparison to the pre-therapeutic imaging. The biochemical response was classified as PR if there was 25% decrease of the PSA-level and as PD if PSA increased more than

25%. PSA.-changes of 25% or less were regarded as SD. Time to prostate-specific-antigen (PSA) progression was calculated from the date of the first re-challenge cycle.

Table 1 Patients characteristics

Characteristic	N (%)
Age	
Mean (range)	71.5 (51 – 88)
ECOG	
0	17 (57)
1	12 (40)
2	2 (3)
Gleason-Score	
Mean (range)	8 (6 – 9)
PSA-level in ng/dl	
Mean (range)	208 (2.6 – 2009)
Extent of the disease	
Bone metastases	29 (97)
< 6 metastases	3 (10)
6-20 metastases	7 (23)
> 20 metastases	15 (50)
diffuse metastases/superscan	4 (13)
Lymph node metastases	26 (87)
Liver metastases	3 (10)
Lung metastases	4 (13)
Prior and ongoing therapies	
Abiraterone	Hx of: 14 (47); ongoing: 7 (23)
Enzalutamide	Hx of: 12 (40); ongoing: 7 (23)
Bisphosphonate or RANKL*- inhibitor	Hx of: 4 (13); ongoing: 10 (33)

Chemotherapy	Hx of: 22 (73)
Ra-223	Hx of: 9 (30)
Prior cycles of RLT	
Median (range)	3 (1 – 5)

***Index:**

- Hx = history

- RANKL = receptor activator of nuclear factor kappa-B ligand

- RLT = radioligand therapy

Statistical analysis

Patient's data were summarized in a database. Frequency analyses, descriptive statistics, and statistical comparison were carried out using SPSS software (IBM SPSS Statistics 24.0, New York). Chi-square test has been performed for comparing responses and the log-rank for comparing survival. Significance level was set at $p < 0.05$. We also used Excel (Microsoft Office 2010) for water-flow analyses of the PSA-changes. Overall survival has been estimated with the Kaplan-Meier method (censored data) and calculated from the date of the initiation of the re-challenge treatment.

Results

Patients and treatment

At our Department of Nuclear Medicine in Bonn we have screened 216 patients, who received PSMA-RLT in the period from November 2014 to March 2018. Of them thirty individuals were included in the analyses. Table 1 represents the patients´ characteristics. In summary, it can be stated that the patient population consisted of mainly elderly males with extensive disease, but in a good general condition. Nearly 73% of the patients underwent prior chemotherapy, about half of the patients had concomitant anti-hormonal therapy such as abiraterone or enzalutamide.

Patients were initially treated with a median of 3 cycles (range 1 to 5 cycles) PSMA-RLT and were eventually retreated with another 3 cycles (range 1 to 6 cycles). The period between last cycle of the baseline therapy and first re-challenge cycle varied between 2 to 26 months, in median 6 months. Overview of the treatment with [^{177}Lu]Lu-PSMA-617 is shown in Figure 1.

The median cumulative administered activity was 17.9 GBq at baseline therapy and 37.4 GBq after the re-challenge treatment. The median activity of the re-challenge treatment was 19.6 GBq and the administered activity pro cycle was 6.1 GBq. If there was response or stable disease after the 1st cycle rechallenge RLT according to PSA-values or Gallium-PSMA-PET/CT, the patients continued the re-treatment (1 to 2 additional cycles) and then were followed up until another progress.

Safety results

The assessed toxicity according to CTC is visualised on Figure 2. Encouragingly, there were no cases of life-threatening (CTC grade 4) adverse events after the re-treatment. However, compared to baseline data of this patients´ cohort (3% CTC grade 3 anemia), there were more grade 3 adverse events. In total 23% of patients experienced serious impairment of the bone marrow function such as thrombopenia (10%), anemia (10%), leucopenia (6%), neutropenia (3%). One patient developed serious renal impairment during the treatment, but it might be disease related because of the rapid progression of the retroperitoneal lymph node metastases.

Seventy percent of patients developed irreversible toxicity (90% low-grade, 10% grade 3). In 13% of cases no irreversible toxicity has been observed, 17% of patients had unknown outcome regarding the course of the laboratory parameters after occurrence of the adverse event.

Table 2 Relevant toxicities after re-treatment with PSMA-RLT according to the CTCAE

Toxicity	Grade 3 (%)	Grade 4 (%)
No toxicity	22 (73.3)	30 (100)
Anemia	3 (9.9)	0 (0.0)
Leucopenia	2 (6.6)	0 (0.0)
Thrombopenia	4 (13.3)	0 (0.0)
Neutropenia	1 (3.3)	0 (0.0)
Elevated renal parameters	1 (3.3)	0 (0.0)
Irreversible toxicitya	2 (6.6)a	0 (0.0)

[a] Irreversible toxicity was observed in 70% of patients (19 patients lowgrade, 2 patients grade 3: irreversible impairment of the renal function and permanent severe anemia)

Table 3 Response rate according to PSA-measurements or [^{68}Ga]Ga-PSMA-PET/CT after the 1st to 4th cycle of re-treatment with PSMA-RLT

Response	**PSA**				**[^{68}Ga]Ga-PSMA-PET/CT**			
No of cycle	1	2	3	4	1	2	3	4
CR in %	0	0	0	0	0	0	0	0
PR in %	53.6	59.1	50.0	55.6	42.9	37.5	-	40
MixR in %	-	-	-	-	28.6	37.5	80	-
SD in %	21.4	22.7	21.4	-	14.3	-	-	-
PD in %	25.0	18.2	28.6	44.4	14.3	25	20	60

***Index:**

The biochemical response was classified as follows:

- complete response: PSA 0.00 ng/dl
- partial response (PR) if PSA decrease > 25%
- progressive disease (PD) if PSA increase > 25%
- stable disease (SD) if PSA-changes ≤ 25%

[^{68}Ga]Ga-PSMA-PET/CT classified according to adapted PERSIST criteria:

- complete response (CR)
- partial response (PR)
- stable disease (SD)
- progressive disease (PD)
- mixed response (MixR) as partial response of the known metastases and at same time occurrence of new lesions; the overall tumour load should be at least stable

Response and survival

The patients were followed up for a median of three months (range 1 – 15 months). Three patients had a follow-up of only one month. Two of these patients came from abroad and

were lost to follow-up after initial email-contact one month after the last treatment. Another patient died one month after the last therapy.

Table 2 shows an overview of the response data after the 1st, 2nd, 3rd and 4th cycle of re-treatment according to PSA-level measurements and [^{68}Ga]Ga-PSMA-PET/CT, respectively. Interestingly, in the PET/CT we had often MixR with new metastases detected although the PSA-level was stable or even decreased. The incidence of MixR was rising after each re-cycle.

The waterfall plots on Figure 3 represent the PSA-change after the 1st to 3rd cycle. Although patients previously benefited from the therapy, we had also patients who were rapidly progressive and did not respond to the re-treatment. Thus, the majority of patients benefited from additional cycles radioligand therapy. PSA-decrease > 25% from 1. to 3. rechallenge cycle was seen in 50-59% of the patients, more than 50% PSA-decline in 40-44%, respectively. Less than one third of patients had a significant PSA-increase (> 25%) after each of the first three re-challenge cycles.

The median time to PSA progression, calculated from the date of the first re-challenge cycle, was 2.8 months (range 1 – 11 months). Most of the patients progressed after the second cycle re-challenge PSMA-RLT (N=9). About one half of these patients showed PSA-increase directly after the treatment and the other half of the patients had initially stable PSA-levels.

The median OS was 25 months after beginning the baseline PSMA-RLT and 12 months after begin of the re-treatment. There was strong correlation between PSA-change after the 1st cycle re-challenge PSMA-RLT and overall survival. Patients with PSA-decrease after the 1st cycle re-challenge RLT survived in median 19 months, which was significantly longer than patients with PSA-increase: only 8 months, respectively. Patients, who had stable PSA-levels (+ /- 25%) had 12 months of median OS. The estimated p–value was 0.015. In contrast, the imaging response in the [^{68}Ga]Ga-PSMA-11 PET/CT did not significantly correlate with the survival.

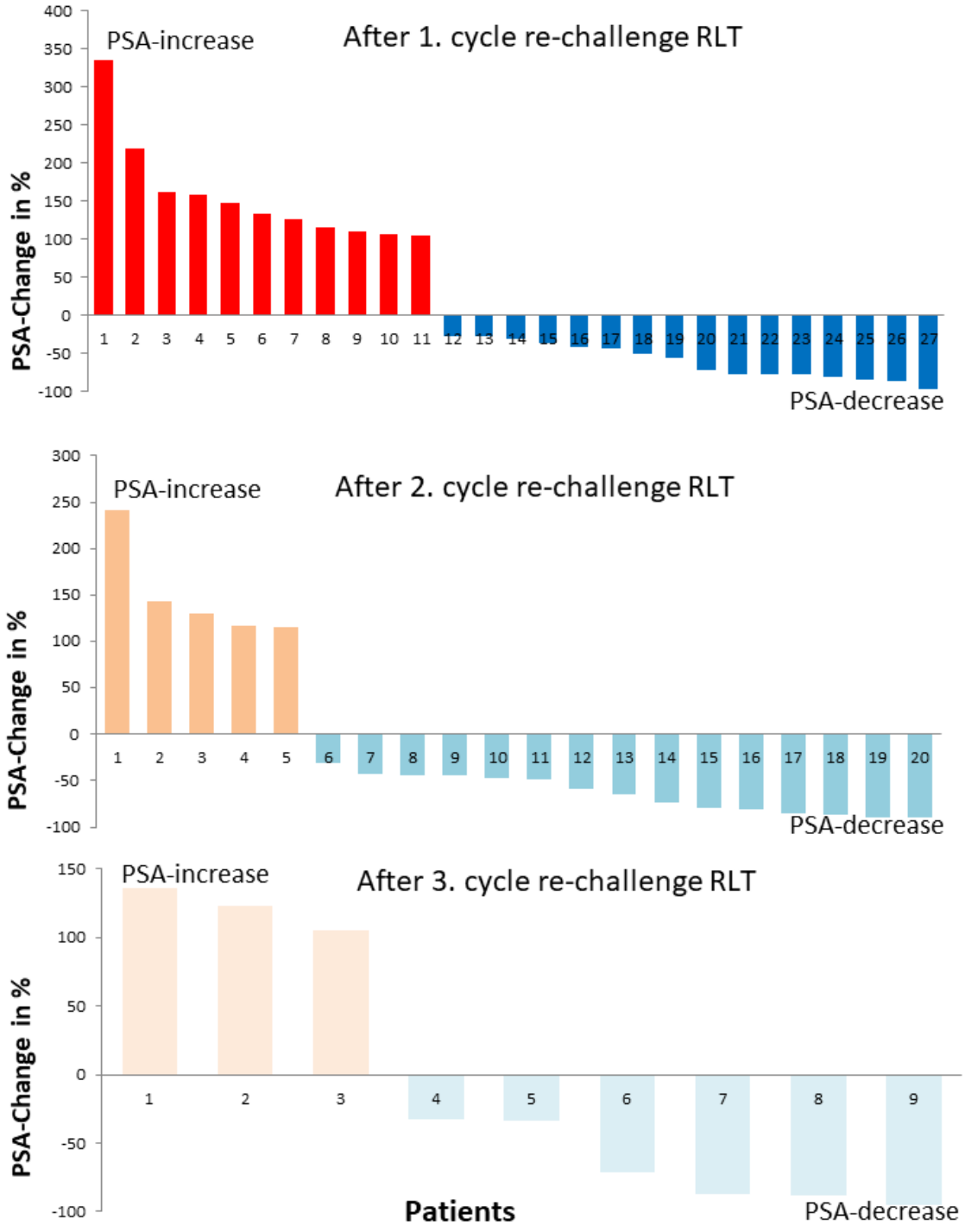

Fig. 1 Waterfall plots. PSA-change after the 1st to 3rd cycle. PSA-decrease > 25% from 1. to 3. PSA-decline of at least 50% was seen in 40-44% of patients. Less than one third of patients had a significant PSA-increase (> 25%) after each of the first three re-challenge cycles.

Figure 2 shows the median survival in the group of patients who received rechallenge PSMA-RLT, compared to the initial screened population. The difference in the overall

survival was significant: 25 months after rechallenge PSMA-RLT vs. 9 months in the patients who received only baseline PSMA-RLT.

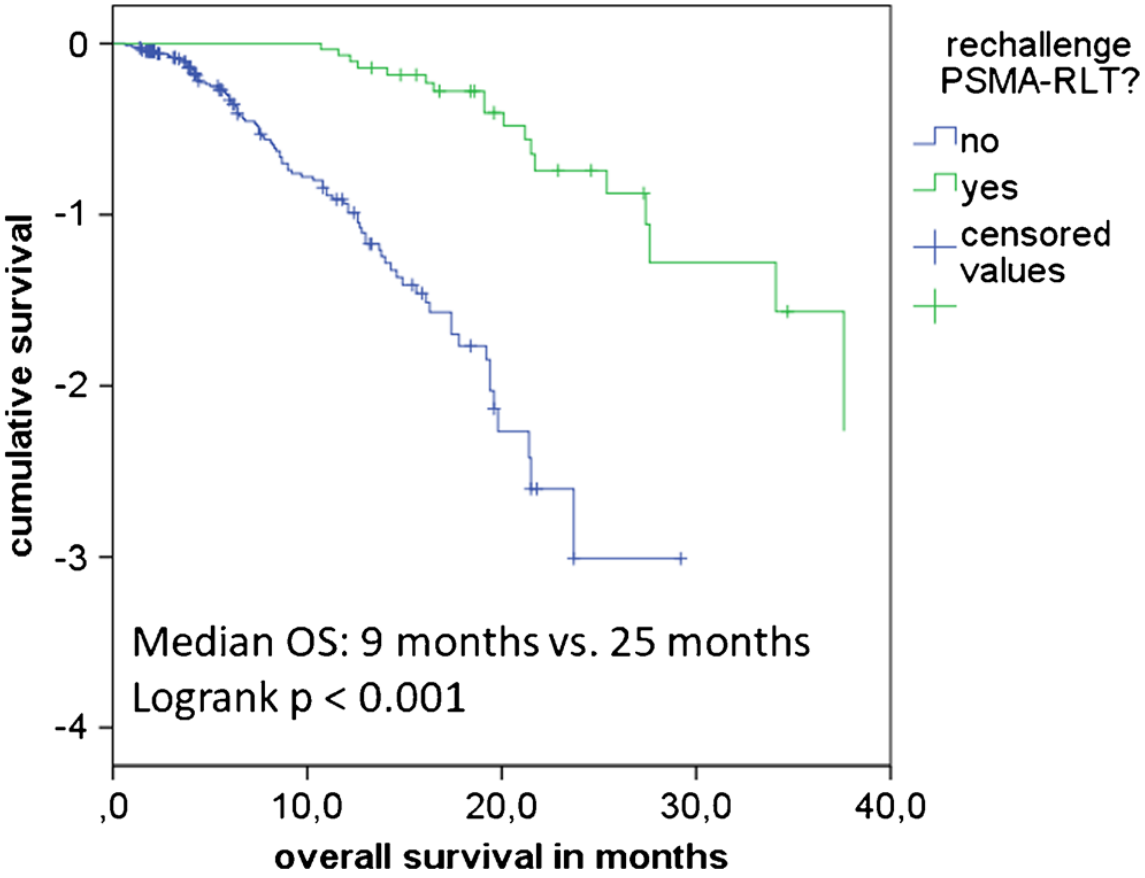

Fig. 2 Survival analysis (Kaplan-Meier Curves) calculated from the 1. cycle PSMA-RLT. From the 216 screened patients, 30 received rechallenge PSMA-RLT. The difference in the median overall survival was significant: 25 months after rechallenge PSMA-RLT vs. 9 months in the remaining patients, who received only a baseline PSMA-RLT (logrank p < 0.001).

Discussion

PSMA-radioligand therapy is a novel therapy-option primarily in patients with CRPC. Currently, a phase III randomised trial is recruiting (VISION-trial) to compare the effect of PSMA-617-RLT with best supportive care in patients with advanced progressive cancer. However, the estimated study completion date is first in May 2021 and till then PSMA-RLT will be expectedly supposed as a last-time treatment option (ClinicalTrials.gov Identifier: NCT03511664).

Several retrospective data implicate that PSMA-RLT is effective and safe in patients with prostate cancer (PCA) [11, 16–24]. This data is very encouraging but also very heterogeneous. For example, progression-free survival in treated patients ranges in the literature between 4.5 – 13.7 months and the overall survival between 7.5 - 15 months, respectively [19–21, 24, 28, 29]. Recently, a phase II study from Melbourne confirmed the favourable safety profile of PSMA-RLT. The estimated PFS was 7 months, the median overall survival was 13.5 months [31].

A current problem is the therapeutic approach when the patients eventually progress after RLT. Most of these patients had prior chemotherapy and novel anti-hormone therapies such as abiterone and enzulatamide and still relapsed. Therefore, in this late stage of disease, it is difficult to find treatment opportunities for patients, who relapse after RLT. Data about retreatments with RLT from a larger group of patients seems to be important in this patients´ population with limited treatment options. In this analyses we focused on the outcome of 30 patients, who underwent re-challenge radioligand therapy.

Similar to other studies about PSMA-RLT we did not observe life-threatening (CTC grade 4) adverse events after the re-treatment. However, compared to the literature (3- 11%) and the baseline data of our patients´ cohort (3% CTC grade 3 anemia), there were more grade 3 heamatotoxicity: 23% of patients [16, 17, 19–22, 25–27]. One patient developed renal impairment during the treatment, but it might be disease related because of the rapid progression of the retroperitoneal lymph node metastases and not necessarily drug related.

[^{68}Ga]Ga-PSMA-PET/CT performed after the first four cycles rechallenge RLT showed increasing incidence of MixR with new metastases detected although the PSA-level was stable or even decreased. According to RECIST criteria, the occurrence of new metastases is regarded as progressive disease [32]. However, because of lacking alternative therapies, we continued the therapy if the PSA-level was at least stable and if the overall tumour mass did not significantly increase under the re-challenge PSMA-RLT. At the end of the analyses we discovered that only PSA-changes after the 1st cycle rechallenge RLT correlated significantly with the overall survival. Thus, the response in the [^{68}Ga]Ga-PSMA-PET/CT was not prognostic for the survival in this patients´cohort. A recent analysis from Cologne demonstrated that therapy effects of PSMA-RLT shown in the [^{68}Ga]Ga-PSMA-PET/CT (SUV, affected bone volume and lymph node diameters), were mostly independent of PSA response [33]. These findings might also explain the discordance between PSA-changes and findings in the [^{68}Ga]Ga-PSMA-PET/CT in our study.

Thus, further studies are needed to evaluate the utility of [^{68}Ga]Ga-PSMA-PET/CT for the treatment management of patients undergoing PSMA-RLT.

The progression-free-survival was defined as the median time to PSA progression and calculated from the date of the first re-challenge cycle. The PFS in our patients was 2.8 months (range 1 – 11 months), which was shorted than PFS-data reported from other studies after primary RLT: 4.5 – 13.7 months [19–21, 28, 29, 31]. The reason might be the increased aggressiveness of disease in these multiple relapsed patients. However, the additional survival estimated with the rechallenge PSMA-RLT was similar to the survival after baseline-treatment: 12 months. This means that the patients achieved much longer median OS than in previous studies reported: 25 months from beginning of the baseline RLT vs. 7.5 – 15 months, respectively [19–21, 28, 29, 31].

Although this is a single centre study, we could include 30 patients who received a total of 181 cycles PSMA-RLT, of these 85 cycles as rechallenge treatment. Possible limitations of the study, is that all the data was collected retrospectively and there might be bias such as a preselection of eminently eligible patients. Moreover, we had two patients lost to follow-up. These patients came from abroad and after initial email-contact one month after the last treatment they were lost to follow-up. Concluding, there is emerging need of prospective studies to confirm the efficacy of PSMA-RLT as a rechallenge treatment.

Conclusion

In summary, the findings of this study suggest that re-challenge [^{177}Lu]Lu-PSMA-617 should be considered as therapeutic option for patients who previously responded to RLT. Thus, there were more serious adverse events as expected, but they might be disease related and not necessarily drug related. Patients who showed biochemical response (PSA-decrease) could achieve longer survival compared to patients who did not respond. The difference between both groups was 11 months and statistically significant.

Re-treatment with RLT appears to be safe and effective, resulting in benefit for most of the patients. Given these encouraging results, further studies of salvage therapies with [^{177}Lu]Lu-PSMA-617 should be designed in the prospective setting.

References

1. Silver DA, Pellicer I, Fair WR, Heston WD, Cordon-Cardo C. Prostate-specific membrane antigen expression in normal and malignant human tissues. Clin Cancer Res. 1997;3:81–5.
2. Santoni M, Scarpelli M, Mazzucchelli R, Lopez-Beltran A, Cheng L, Cascinu S, Montironi R. Targeting prostate-specific membrane antigen for personalized therapies in prostate cancer: morphologic and molecular backgrounds and future promises. J Biol Regul Homeost Agents. 2014;28:555–63.
3. Mhawech-Fauceglia P, Zhang S, Terracciano L, Sauter G, Chadhuri A, Herrmann FR, Penetrante R. Prostate-specific membrane antigen (PSMA) protein expression in normal and neoplastic tissues and its sensitivity and specificity in prostate adenocarcinoma: an immunohistochemical study using mutiple tumour tissue microarray technique. Histopathology. 2007;50:472–83. doi:10.1111/j.1365-2559.2007.02635.x.
4. Ghosh A, Heston WDW. Tumor target prostate specific membrane antigen (PSMA) and its regulation in prostate cancer. J Cell Biochem. 2004;91:528–39. doi:10.1002/jcb.10661.
5. Wang X, Yin L, Rao P, Stein R, Harsch KM, Lee Z, Heston WDW. Targeted treatment of prostate cancer. J Cell Biochem. 2007;102:571–9. doi:10.1002/jcb.21491.
6. Wright GL, Mayer Grob B, Haley C, Grossman K, Newhall K, Petrylak D, et al. Upregulation of prostate-specific membrane antigen after androgen-deprivation therapy. Urology. 1996;48:326–34. doi:10.1016/S0090-4295(96)00184-7.
7. Jamous M, Haberkorn U, Mier W. Synthesis of peptide radiopharmaceuticals for the therapy and diagnosis of tumor diseases. Molecules. 2013;18:3379–409. doi:10.3390/molecules18033379.
8. Benesova M, Schafer M, Bauder-Wust U, Afshar-Oromieh A, Kratochwil C, Mier W, et al. Preclinical Evaluation of a Tailor-Made DOTA-Conjugated PSMA Inhibitor with Optimized Linker Moiety for Imaging and Endoradiotherapy of Prostate Cancer. J. Nucl. Med. 2015;56:914–20. doi:10.2967/jnumed.114.147413.
9. Afshar-Oromieh A, Hetzheim H, Kratochwil C, Benesova M, Eder M, Neels OC, et al. The Theranostic PSMA Ligand PSMA-617 in the Diagnosis of Prostate Cancer by PET/CT: Biodistribution in Humans, Radiation Dosimetry, and First Evaluation of Tumor Lesions. J. Nucl. Med. 2015;56:1697–705. doi:10.2967/jnumed.115.161299.
10. Rajasekaran SA, Anilkumar G, Oshima E, Bowie JU, Liu H, Heston W, et al. A novel cytoplasmic tail MXXXL motif mediates the internalization of prostate-specific

membrane antigen. Mol Biol Cell. 2003;14:4835–45. doi:10.1091/mbc.E02-11-0731.

11. Rahbar K, Afshar-Oromieh A, Jadvar H, Ahmadzadehfar H. PSMA Theranostics: Current Status and Future Directions. Mol Imaging. 2018;17:1536012118776068. doi:10.1177/1536012118776068.

12. Ahmadzadehfar H, Aryana K, Pirayesh E, Farzanehfar S, Assadi M, Fallahi B, et al. The Iranian Society of Nuclear Medicine practical guideline on radioligand therapy in metastatic castration-resistant prostate cancer using 177Lu-PSMA. Iranian Journal of Nuclear Medicine. 2018;26:2–8.

13. Wüstemann T, Haberkorn U, Babich J, Mier W. Targeting prostate cancer: Prostate-specific membrane antigen based diagnosis and therapy. Med Res Rev 2018. doi:10.1002/med.21508.

14. Ahmadzadehfar H, Albers P, Bockisch A, Boegemann M, Böhme C, Burchert W, et al. Lutetium-177-PSMA-Radioligandentherapie: Konsensus im Rahmen der GKV-finanzierten Versorgung zwischen den Hochschulkliniken in Aachen, Bonn, Düsseldorf, Essen und Köln und dem MDK Nordrhein. [Lutetium-177-PSMA radioligand therapy : Consensus within the framework of GKV-funded care between the university hospitals in Aachen, Bonn, Düsseldorf, Essen, and Cologne and the MDK Nordrhein]. Urologe A. 2018;57:709–13. doi:10.1007/s00120-018-0642-2.

15. Fendler WP, Kratochwil C, Ahmadzadehfar H, Rahbar K, Baum RP, Schmidt M, et al. Therapie mit 177Lu-PSMA-617, Dosimetrie und Nachsorge beim metastasierten kastrationsresistenten Prostatakarzinom. [177Lu-PSMA-617 therapy, dosimetry and follow-up in patients with metastatic castration-resistant prostate cancer]. Nuklearmedizin. 2016;55:123–8.

16. Yadav MP, Ballal S, Tripathi M, Damle NA, Sahoo RK, Seth A, Bal C. 177Lu-DKFZ-PSMA-617 therapy in metastatic castration resistant prostate cancer: Safety, efficacy, and quality of life assessment. European Journal of Nuclear Medicine and Molecular Imaging. 2017;44:81–91. doi:10.1007/s00259-016-3481-7.

17. Rahbar K, Schmidt M, Heinzel A, Eppard E, Bode A, Yordanova A, et al. Response and Tolerability of a Single Dose of 177Lu-PSMA-617 in Patients with Metastatic Castration-Resistant Prostate Cancer: A Multicenter Retrospective Analysis. J. Nucl. Med. 2016;57:1334–8. doi:10.2967/jnumed.116.173757.

18. Rahbar K, Bögeman M, Yordanova A, Eveslage M, Schäfers M, Essler M, Ahmadzadehfar H. Delayed response after repeated 177Lu-PSMA-617 radioligand therapy in patients with metastatic castration resistant prostate cancer. European Journal of Nuclear Medicine and Molecular Imaging. 2018;45:243–6. doi:10.1007/s00259-017-3877-z.

19. Rahbar K, Bode A, Weckesser M, Avramovic N, Claesener M, Stegger L, Bögemann M. Radioligand Therapy With 177Lu-PSMA-617 as A Novel Therapeutic Option in Patients With Metastatic Castration Resistant Prostate Cancer. Clin Nucl Med. 2016;41:522–8. doi:10.1097/RLU.0000000000001240.

20. Rahbar K, Ahmadzadehfar H, Kratochwil C, Haberkorn U, Schäfers M, Essler M, et al. German Multicenter Study Investigating 177Lu-PSMA-617 Radioligand Therapy in Advanced Prostate Cancer Patients. J. Nucl. Med. 2017;58:85–90. doi:10.2967/jnumed.116.183194.

21. Kulkarni HR, Singh A, Schuchardt C, Niepsch K, Sayeg M, Leshch Y, et al. PSMA-Based Radioligand Therapy for Metastatic Castration-Resistant Prostate Cancer: The Bad Berka Experience Since 2013. J. Nucl. Med. 2016;57:97S-104S. doi:10.2967/jnumed.115.170167.

22. Kratochwil C, Giesel FL, Stefanova M, Benešová M, Bronzel M, Afshar-Oromieh A, et al. PSMA-Targeted Radionuclide Therapy of Metastatic Castration-Resistant Prostate Cancer with 177Lu-Labeled PSMA-617. J. Nucl. Med. 2016;57:1170–6. doi:10.2967/jnumed.115.171397.

23. Baum RP, Kulkarni HR, Schuchardt C, Singh A, Wirtz M, Wiessalla S, et al. 177Lu-Labeled Prostate-Specific Membrane Antigen Radioligand Therapy of Metastatic Castration-Resistant Prostate Cancer: Safety and Efficacy. J. Nucl. Med. 2016;57:1006–13. doi:10.2967/jnumed.115.168443.

24. Ahmadzadehfar H, Wegen S, Yordanova A, Fimmers R, Kurpig S, Eppard E, et al. Overall survival and response pattern of castration-resistant metastatic prostate cancer to multiple cycles of radioligand therapy using 177LuLu-PSMA-617. European Journal of Nuclear Medicine and Molecular Imaging 2017. doi:10.1007/s00259-017-3716-2.

25. Ahmadzadehfar H, Rahbar K, Kurpig S, Bogemann M, Claesener M, Eppard E, et al. Early side effects and first results of radioligand therapy with (177)Lu-DKFZ-617 PSMA of castrate-resistant metastatic prostate cancer: A two-centre study. EJNMMI Res. 2015;5:114. doi:10.1186/s13550-015-0114-2.

26. Ahmadzadehfar H, Eppard E, Kürpig S, Fimmers R, Yordanova A, Schlenkhoff CD, et al. Therapeutic response and side effects of repeated radioligand therapy with 177Lu-PSMA-DKFZ-617 of castrate-resistant metastatic prostate cancer. Oncotarget. 2016;7:12477–88. doi:10.18632/oncotarget.7245.

27. Yordanova A, Becker A, Eppard E, Kurpig S, Fisang C, Feldmann G, et al. The impact of repeated cycles of radioligand therapy using 177LuLu-PSMA-617 on renal function in patients with hormone refractory metastatic prostate cancer. European Journal of Nuclear Medicine and Molecular Imaging 2017. doi:10.1007/s00259-017-3681-9.

28. Ahmadzadehfar H, Schlolaut S, Fimmers R, Yordanova A, Hirzebruch S, Schlenkhoff C, et al. Predictors of overall survival in metastatic castration-resistant prostate cancer patients receiving 177LuLu-PSMA-617 radioligand therapy. Oncotarget. 2017;8:103108–16. doi:10.18632/oncotarget.21600.

29. Bräuer A, Grubert LS, Roll W, Schrader AJ, Schäfers M, Bögemann M, Rahbar K. 177Lu-PSMA-617 radioligand therapy and outcome in patients with metastasized castration-resistant prostate cancer. European Journal of Nuclear Medicine and Molecular Imaging. 2017;44:1663–70. doi:10.1007/s00259-017-3751-z.

30. references National Cancer Institute Guidelines For Investigators: Adverse event reporting requirements for DCTC DCTD (CTEP and CIP) and DCP INDs and IDEs. 2013. - Google-Suche. https://www.google.de/webhp?sourceid=chrome-instant&ion=1&espv=2&ie=UTF-8#q=references+National+Cancer+Institute+Guidelines+For+Investigators:+Adverse+event+reporting+requirements+for+DCTC+DCTD+(CTEP+and+CIP)+and+DCP+INDs+and+IDEs.+2013. Accessed 17 Dec 2016.

31. Hofman MS, Violet J, Hicks RJ, Ferdinandus J, Thang SP, Akhurst T, et al. [177 Lu]-PSMA-617 radionuclide treatment in patients with metastatic castration-resistant prostate cancer (LuPSMA trial): A single-centre, single-arm, phase 2 study. The Lancet Oncology. 2018;19:825–33. doi:10.1016/S1470-2045(18)30198-0.

32. Eisenhauer EA, Therasse P, Bogaerts J, Schwartz LH, Sargent D, Ford R, et al. New response evaluation criteria in solid tumours: Revised RECIST guideline (version 1.1). European Journal of Cancer. 2009;45:228–47. doi:10.1016/j.ejca.2008.10.026.

33. Taeger P, Hammes J, Hohberg M, Wild M, Schomaecker K, Kobe C, et al. Discrete evaluation of multi-cycle Lu-177-PSMA-617-therapy effects on bone versus lymph node metastases in patients with metastasized castration-resistant prostate cancer (mCRPC). J. Nucl. Med. 2018;59:523.

5.2 Prediction of Normal Organ Absorbed Doses for [^{177}Lu]Lu-PSMA-617 Using [^{44}Sc]Sc-PSMA-617 Pharmacokinetics in Patients With Metastatic Castration Resistant Prostate Carcinoma

Ambreen Khawar, MS,* Elisabeth Eppard, PhD,* Jean Phlippe Sinnes, Dipl. Chem, †
Frank Roesch, PhD, † Hojjat Ahmadzadehfar, MD, MSc,* Stefan Kürpig, PhD,*
Michael Meisenheimer, Dipl. Chem.,* Florian C. Gaertner, MD,*
Markus Essler, MD,* and Ralph A. Bundschuh, MD, PhD*

Received for publication January 29, 2018; revision accepted March 15, 2018.

From the *Department of Nuclear Medicine, University Medical Center Bonn;
and †Institute of Nuclear Chemistry, Johannes Gutenberg University Mainz,
Mainz, Germany.

The manuscript has been seen and approved by all authors.
A.K., F.R., S.K., M.M., and M.E. contributed equally in design and execution of study. E.E., J.P.S., H.A., F.C.G., and R.A.B. contributed in drafting or revising of the manuscript critically for important intellectual content as well as final manuscript approval for submission and publication.
Conflicts of interest and sources of funding: none declared.

Correspondence to: Ambreen Khawar, MS, Nuclear Medicine, Sigmund-Freud-Straße, 25 D-53127, Bonn, Germany. E-mail: ambreen_khawar@hotmail.com.

ISSN: 0363-9762/18/0000–0000
https://doi.org/10.1097/rlu.0000000000002102

ABSTRACT:

Aim: *In vivo* pharmacokinetic analysis of [^{44}Sc]Sc-PSMA-617 was used to determine the normal organ absorbed doses that may result from therapy with [^{177}Lu]Lu-PSMA-617 and to predict the maximum permissible activity of [^{177}Lu]Lu-PSMA-617 for patients with metastatic castration resistant prostate cancer (mCRPC).

Methods: Pharmacokinetics of [^{44}Sc]Sc-PSMA-617 was evaluated in five mCRPC patients using dynamic PET/CT, followed by three static PET/CT acquisitions and blood sample collection over 19.5 h as well as urine sample collection at two time points. Total activity measured in source organs by PET imaging, as well as counts/ml measured in in blood and urine samples were decay corrected back to the time of injection using the half-life of scandium-44. Afterwards, forward decay correction using the half-life of lutetium-177 was performed, extrapolating the pharmacokinetics of [^{44}Sc]Sc-PSMA-617 to that of [^{177}Lu]Lu-PSMA-617. Source organ residence times and organ absorbed doses for [^{177}Lu]Lu-PSMA-617 were calculated using OLINDA/EXM software, bone marrow self-dose was determined using the indirect blood based method and urinary bladder contents residence time was estimated by trapezoidal approximation. The maximum permissible activity of [^{177}Lu]Lu-PSMA-617 was calculated for each patient considering EBRT toxicity limits for radiation absorbed doses to kidneys, bone marrow, salivary glands and whole body.

Results: The predicted mean organ absorbed doses were highest in the kidneys (0.44 mSv/MBq), followed by the salivary glands (0.23 mSv/MBq). The maximum permissible activity was highly variable among patients; limited by whole body absorbed dose (1 patient), bone marrow dose (1 patient) and kidney dose (3 patients).

Conclusions: [^{44}Sc]Sc-PSMA-617 PET/CT imaging is feasible and allows theoretical extrapolation of the pharmacokinetics of [^{44}Sc]Sc-PSMA-617 to that of [^{177}Lu]Lu-PSMA-617, with the intent of predicting normal organ absorbed doses and maximum permissible activity in patients scheduled for therapy with [^{177}Lu]Lu-PSMA-617. Further validation studies are required, correlating the extrapolated organ absorbed doses from [^{44}Sc]Sc-PSMA-617 PET/CT imaging with post-therapeutic dosimetric measurements after [^{177}Lu]Lu-PSMA-617 therapy.

Key words:

[^{177}Lu]Lu-PSMA-617 therapy; [^{44}Sc]Sc-PSMA-617; dosimetric analysis; normal organ absorbed doses; maximum permissible activity.

INTRODUCTION:

Prostate carcinoma is the second most common cancer among men [1, 2]. The prognosis of prostate carcinoma is good at an early stage. With development of refractoriness to hormone replacement therapy in advanced stages, 5-year survival in these patients decreases to 31% [1, 2]. Expression of prostate-specific membrane antigen (PSMA) is up-regulated in metastatic castration-resistant prostate car- cinoma (mCRPC) cells [3, 4]. During the past 2 decades, various studies have evaluated a number of small ligands targeting the extracellular domain of PSMA [4]. With the introduction of the small ligand, PSMA-617 by Benešová et al [5], a highly potent radiopharmaceutical showing a high tumor-to-background ratio has become available for theranostic application. It is now widely used, radiolabeled with ^{68}Ga for PET imaging and with ^{177}Lu for therapy of mCRPC. ^{177}Lu with a half-life of 6.7 days (161.52 hours) and predominant β^- particle emission (mean range, 1 mm) is considered more efficient and safer therapeutic radionuclide compared with ^{90}Y or ^{131}I [4].

Since 2015, several studies have shown a good therapeutic efficacy and a favorable safety profile of [^{177}Lu]Lu-PSMA-617 therapy in mCRPC patients [1, 2, 4–8]. However, physiologic expression of PSMA in the small intestine, proximal renal tubules, and salivary glands was found responsible for toxicity and adverse effects [1, 9, 10]. Occasional cases of reversible or transient xerostomia or grade 2 hematologic toxicity have been reported, yet the incidence of grade 3 or 4 renal, hematologic, and salivary gland toxicity has been found to be low [10, 11].

Kidneys, salivary and lacrimal glands have also been reported to be organs at risk by dosimetric analysis with low pretherapeutic and high posttherapeutic dose of [^{177}Lu]Lu-PSMA-617 using pla- nar ± SPECT imaging [9, 12–16]. [^{68}Ga]Ga-PSMA-617 PET imaging has been evaluated as a basis for dosimetric evaluation, which re- vealed similar kinetics but resulted in lower doses compared with [^{177}Lu]Lu-PSMA-617 [17]. However, both [^{177}Lu]Lu-PSMA-617 and [^{68}Ga]Ga-PSMA-617 PET imaging have drawbacks and inherent limitations for predicting pretherapeutic or intratherapeutic radiation dosimetry.

An overall success of [^{177}Lu]Lu-PSMA-617 therapy with clinically detectable decline in serum prostate-specific antigen has been observed in approximately 70% of mCRPC patients [6, 18]. Evaluation of response patterns after multiple cycles of [^{177}Lu]Lu-PSMA-617 therapy has shown further improvement of response after the first cycle and also induction of response in initial nonresponders at end of the third cycle, hence propagating the use of further therapy cycles in initial nonresponders [6]. It is widely assumed that dose escalation may be used in nonresponders, which is at the moment based only on

individual experiences at the respective centers. Employment of pretherapeutic dosimetric analysis, although highly desirable for dose escalation, has practical limitations. Pretherapeutic dosimetric analysis with [^{68}Ga]Ga-PSMA-617 is of limited use because of its short half-life of only 1.18 hours, compared with the half-life of 6.7 days of its therapeutic counterpart [^{177}Lu]Lu-PSMA-617. Further- more, a recent preclinical comparison of [^{68}Ga]Ga-PSMA-617 with [^{177}Lu]Lu-PSMA-617 has also highlighted that in vivo binding and distribution also differ because of the coordination chemistry of the two radionuclides [19].

In some countries, pretherapeutic dosimetry using low-dose [^{177}Lu]Lu-PSMA-617 planar ± SPECT imaging requires hospitali- zation of the patient because of radiation protection laws. Also, im- aging at multiple time points, as well as blood and urine sampling, leads to increased radiation exposure of the hospital staff. In addition, it is challenging to determine lacrimal gland doses. Last but not least, the results from a low-dose [^{177}Lu]Lu-PSMA-617 study may differ from the biokinetics of higher therapeutic doses of [^{177}Lu]Lu-PSMA-617, owing to the presence of more unlabeled compound in the therapeutic radiopharmaceutical product [8, 12, 13].

Recent studies of PSMA-617 radiolabeled with positron emitter ^{44}Sc (half-life of 3.927 hours) have shown similar in vitro binding characteristics and in vivo biodistribution properties compared with [^{177}Lu]Lu-PSMA-617. It is therefore envisioned as a better pretherapeutic dosimetric evaluation agent [19]. In this study, pretherapeutic [^{44}Sc]Sc-PSMA-617 PET/CT dosimetry has been used to estimate the organ doses of [^{177}Lu]Lu-PSMA-617 therapy by mathematical extrapolation of pharmacokinetics of [^{44}Sc]Sc- PSMA-617 to that of [^{177}Lu]Lu-PSMA-617 in mCRPC patients.

MATERIALS AND METHODS:

All procedures were in accordance with the ethical standards of the institutional review board, and all patients gave written informed consent before PET/CT imaging.

Patient population:

A total of five mCRPC patients with a mean age of 69 years were retrospectively analyzed. 40-62 MBq of [^{44}Sc]Sc-PSMA 617 were injected intravenously (table 1). All patients gave written informed consent before PET/CT imaging. All procedures were in accordance with the ethical standards of the institutional review board.

Preparation of [^{44}Sc]Sc-PSMA-617:

Radiolabeling of GMP-grade PSMA-617 obtained from ABX (Radeberg, Germany) with scandium-44 eluted from a prototype 185 MBq (5 mCi) ^{44}Ti/^{44}Sc-generator (Mainz) was

performed as previously described [20]. Radiolabeling yields of >90% with a radiochemical purity of >99% were achieved.

[^{44}Sc]Sc-PSMA-617 PET/CT imaging protocol:

A Siemens Biograph 2 PET/CT scanner with a 58.5 cm axial and a 16.2 cm longitudinal field of view (FOV) and a spatial resolution of about 6 mm in axial and transversal direction (at a radius of 10 mm) was used for PET/CT imaging. A 30 minute dynamic PET scan (list-mode) of the abdomen (kidneys in FOV) was acquired, followed by a low-dose CT scan. Three whole body (skull to mid-thigh) static scans were acquired at 45 min, 2 h and 19.5 h p.i., each in combination with a preceding low-dose CT for patient positioning and attenuation correction. For qualitative and quantitative analysis, dynamic images were reconstructed from list-mode data (6 frames of 300 s) using an iterative reconstruction algorithm (OSEMwith 8 iterations, 16 subsets) and application of Gaussian filter of 4 mm and were corrected for scatter.

Qualitative analysis

All dynamic and static images were visually analyzed with regard to physiological and pathological tracer distribution as shown in figure 1. Organs with increased tracer uptake were identified as source organs for further dosimetric analysis.

Quantitative dosimetric analysis:

Interview fusion software (MEDISO Medical Imaging Systems, Budapest, Hungary) was used to draw volumes of interest on the CT scan to assess the volume of source organs and to measure the mean activity (kBq/mL) from corresponding coregistered PET images (6 dynamic and 3 static images). Source organs identified for dosi- metric analysis included kidneys, liver, spleen, urinary bladder, small intestine, salivary glands, and whole body. Total source organ activity was calculated by multiplication of the volume of the source organ with corresponding mean activity (kBq/mL) and converted to MBq/mL. Total activity of [^{44}Sc]Sc-PSMA-617 in source organs was extrapolated to a theoretical [^{177}Lu]Lu-PSMA-617 activity at all imaging time points by applying Equation 1.

$$Activity_{Lu\ Corrected} = A(t) \times e^{\frac{0.693 \times t(h)}{3.927\ h}} \times e^{\frac{-0.693 \times t(h)}{161.52\ h}} \quad (25)$$

The physical decay component of scandium-44 was removed by reverse decay correction to the time of injection, leaving only the biological decay component of PSMA-617. By applying forward decay correction with the physical half-life of lutetium-177 (161.52 hours), theoretical [^{177}Lu]Lu-PSMA-617 kinetics were extrapolated for all imaging time points. In case of whole-body activity calculation, above method was applied until the 2-

hour time point. Then physical decay correction for lutetium-177 was carried forward from the 2-hour time point. The reason for this was to remove an error of increment in activity at the last 19.5-hour time point for the whole-body activity calculation.

Percent source organ activity was calculated for all source or- gans by dividing total source organ activity by injected activity and multiplying it with 100. However, for % whole-body activity calcu- lation, instead of whole injected activity, scaled injected activ- ity with respect to proportion of body weight imaged was used as given in equation no 3. As homogenous tracer distribution in remainder of the body (legs and arms not included in the PET/CT FOV) was assumed the % injected dose at time of injection in image was scaled proportional to % weight of the body in image calculated by using equation no 2.

TABLE 1. Characteristics of Study Population

	Age, y	Weight, kg	Hematocrit	Injected Activity, MBq	Injected Activity,MBq/kg
1	70	78	0.33	50.00	0.64
2	72	80	0.30	62.23	0.78
3	67	70	0.39	39.61	0.57
4	70	80	0.30	50.00	0.63
5	67	104	0.29	48.95	0.47
Mean	69	82.4	0.32	50.16	0.62
±SD	2.2	12.76	0.04	8.04	0.11

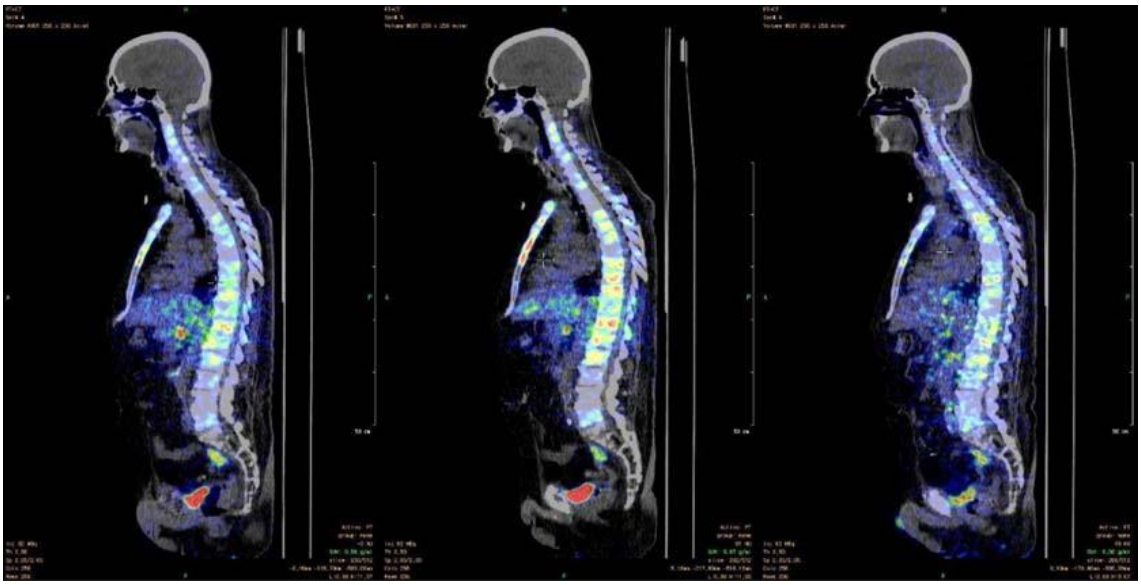

FIGURE 1. Distribution of [^{44}Sc]Sc-PSMA-617 at 45 minutes and 2 and 19.5 hours postinjection (from left to right).

$$\%\ Body\ weight\ (image) = \frac{CT\ volume\ of\ whole\ body\ image \times mean\ CT\ density\ \times 100}{Patient\ weight} \quad (26)$$

$$\%\ Whole\ body\ activity\ (t) = \frac{Activityinstatic\ (skull\text{-}midthigh)image\ (t) \times\ 100}{Scaled\ injected\ activity\ in\ image} \quad (27)$$

Percent source organ activity was used to generate time-activity curves and to calculate residence time using OLINDA/EXM soft- ware (Hermes Medical Solutions, Stockholm, Sweden). Biexponential curve fitting for all source organs and monoexponential curve for the whole body were applied. For determination of residence time of the remainder of the body, the residence times of all source organs except urinary bladder were subtracted from whole-body residence time as explained by Stabin [21].

To determine bone marrow doses, 1-2 ml venous blood samples were collected at nine time points (5, 10, 15, 20, 25, 30, 45 min, 2 and 19.5 h p.i.). Urine samples were collected in pre-weighed containers after 45 min and 2 h static PET/CT imaging. Radioactivity in 1 ml blood and urine samples was measured along with a known standard activity using a 1480 WIZARD^{TM} 3n Gamma counter. Activity data of blood and urine samples were treated in the same way as described for source organs to extrapolate the theoretical activity of [^{177}Lu]Lu-PSMA-617. The indirect blood-based method considering patient hematocrit and patient adjusted bone marrow mass [22–25] was used to calculate the self-dose to the bone marrow. To calculate the residence time of urinary bladder contents, the trapezoidal method was used while taking into account urinary bladder activity in the PET datasets at 45 min, 2 and 19.5 h along with activity in urine samples.

Mean organ absorbed doses were calculated using OLINDA/EXM software. Patient weight was adjusted by multiplying the reference adult male body weight with the fraction determined by dividing the patient weight with the reference adult weight.

Mean residence times, organ absorbed doses (mSv/MBq) and effective doses (mSv/MBq) were calculated. Considering toxicity limits derived from external beam radiotherapy (EBRT) for kidneys, salivary glands, bone marrow, liver, urinary bladder and whole body, the maximum permissible activity and the maximum number of therapy cycles of [^{177}Lu]Lu-PSMA-617 (6 GBq per cycle) that can be administered were determined.

RESULTS:

Extrapolated individual and mean residence times (MBq-h/MBq) of [^{177}Lu]Lu-PSMA-617 are shown in table 2. Highest residence times were observed in the liver, followed by the

kidneys, small intestine, bone marrow, urinary bladder, salivary glands and spleen. Residence times of the remainder of body were highly variable and were highest in a patient with high kidney and bone marrow residence times.

Extrapolated individual and mean organ absorbed doses of [^{177}Lu]Lu-PSMA-617 are given in table 3. The kidneys showed the highest organ absorbed doses (mean 0.44 mSv/MBq), followed by the salivary glands (0.23 mSv/MBq), liver (0.22 mSv/MBq), small intestine (0.14 mSv/MBq) and spleen and urinary bladder wall with 0.12 mSv/MBq each. Mean bone marrow absorbed dose was found to be 0.05 mSv/MBq and mean whole body dose was 0.08 mSv/MBq.

TABLE 2. Individual and Mean Residence Times (MBq-h/MBq)

Organs	PT1	PT2	PT3	PT4	PT5	Mean	±SD
Kidneys	1.07	1.25	1.17	1.96	2.09	1.51	0.48
Liver	3.48	2.85	3.31	6.18	6.46	4.46	1.72
Spleen	0.28	0.19	0.09	0.15	0.20	0.18	0.07
Small intestine	0.83	0.45	0.71	1.05	0.09	0.63	0.37
Bone marrow	0.08	0.66	0.06	0.12	1.67	0.52	0.69
Urinary bladder contents	0.23	0.25	0.18	0.90	0.08	0.33	0.32

Table 3. Individual and Mean Organ Absorbed Doses (mSv/MBq)

Patient (PT)	PT1	PT2	PT3	PT4	PT5	Mean	± SD
Organs							
Adrenals	0.04	0.06	0.04	0.07	0.06	0.05	0.01
Brain	0.08	0.05	0.03	0.05	0.05	0.05	0.02
Esophagus	0.10	0.05	0.03	0.05	0.05	0.06	0.02
Eyes	0.08	0.05	0.03	0.05	0.05	0.05	0.02
Gallbladder wall	0.13	0.06	0.04	0.06	0.06	0.07	0.03
Left colon	0.13	0.05	0.03	0.06	0.06	0.07	0.04
Small intestine	0.20	0.11	0.12	0.19	0.07	0.14	0.06
Stomach wall	0.12	0.05	0.03	0.06	0.05	0.06	0.03
Right colon	0.10	0.05	0.03	0.06	0.06	0.06	0.03
Rectum	0.08	0.05	0.03	0.06	0.05	0.06	0.02
Heart wall	0.09	0.05	0.03	0.06	0.06	0.06	0.02
Kidneys	0.54	0.33	0.34	0.52	0.47	0.44	0.10

Liver	0.24	0.14	0.17	0.29	0.26	0.22	0.06
Lungs	0.09	0.05	0.03	0.05	0.05	0.06	0.02
Pancreas	0.13	0.05	0.03	0.06	0.06	0.07	0.04
Prostate	0.08	0.05	0.03	0.06	0.05	0.06	0.02
Salivary glands	0.11	0.55	0.25	0.18	0.07	0.23	0.19
Red marrow	0.07	0.06	0.03	0.04	0.04	0.05	0.02
Osteogenic cells	0.06	0.04	0.02	0.03	0.03	0.04	0.02
Spleen	0.26	0.11	0.06	0.09	0.10	0.12	0.08
Testes	0.08	0.05	0.03	0.05	0.05	0.05	0.02
Thymus	0.08	0.05	0.03	0.05	0.05	0.05	0.02
Thyroid	0.08	0.05	0.03	0.05	0.05	0.05	0.02
Urinary bladder wall	0.13	0.10	0.07	0.24	0.07	0.12	0.07
Total body	0.17	0.06	0.04	0.06	0.06	0.08	0.05

Absorbed doses (Gy) delivered by one cycle (6 GBq) of [^{177}Lu]Lu-PSMA-617 were estimated, the results are listed in table 4. One cycle of [^{177}Lu]Lu-PSMA-617 resulted in a theoretical mean absorbed dose of 2.65 Gy (range: 2-3.26 Gy) for the kidneys, followed by the salivary glands, liver, small intestine, spleen, urinary bladder, total body and red marrow. The organ receiving the highest dose were the kidneys, with an exception in patient number 2, where the highest absorbed dose was calculated for the salivary glands.

Table 4. Organ Absorbed Doses (in Gy) Received From 1 Cycle of 6 GBq Administration of [^{177}Lu]Lu-PSMA-617

Patient (PT)	PT1	PT2	PT3	PT4	PT5	Mean Organs
Small intestine	1.21	0.65	0.71	1.11	0.39	0.84
Kidneys	3.26	2	2.04	3.13	2.81	2.65
Liver	1.42	0.82	1.02	1.75	1.54	1.31
Salivary glands	0.64	3.3	1.47	1.1	0.39	1.38
Red marrow	0.41	0.37	0.16	0.26	0.21	0.28
Osteogenic cells	0.35	0.24	0.11	0.19	0.17	0.21
Spleen	1.58	0.64	0.36	0.53	0.59	0.74
Urinary bladder wall	0.76	0.62	0.41	1.44	0.42	0.73
Total body	1.02	0.35	0.22	0.38	0.36	0.47

Table 5. Predicted Maximum Permissible Activity (GBq) in Individual Patients Considering Toxicity Limits for Organs With EBRT

Patient (PT)	PT1	PT2	PT3	PT4	PT5	Mean Organs
Small intestine	198.02	366.97	336.13	216.22	611.62	285
Kidneys	42.36	68.86	67.65	44.06	49.15	52.11
Liver	126.58	220.59	176.47	103.09	117.19	137.61
Salivary glands	235.85	45.45	102.04	136.61	379.64	108.71
Red marrow	29.07	32.52	74.07	46.95	56.66	42.52
Urinary bladder wall	472.44	576.92	874.64	250	865.8	492.69
Total body	11.76	34.6	54.2	31.55	33.22	25.75

Maximum permissible activity and maximum number of cycles (6 GBq/cycle) of [^{177}Lu]Lu-PSMA-617 that can be administered in each patient with respect to dose limits derived from EBRT, that is, kidneys (23 Gy), bone marrow (2 Gy), whole body (2 Gy), salivary glands (25 Gy), liver (30 Gy), small intestine (40 Gy), and urinary bladder (60 Gy) are given in Tables 5 and 6, respectively. In patients 1 and 2, maximum permissible activity was determined by the red marrow–absorbed dose, and in patients 3, 4, and 5, the kidney- absorbed dose was the limiting factor. In case of patient 1, also renal dose was high, resulting in a high cumulative dose to the whole body, further limiting the maximum permissible activity. Toxicity limits for the salivary glands, small intestine, and urinary bladder were found to exert no influence in this context.

Comparison of extrapolated organ-absorbed doses (Gy/GBq) from our current study with pretherapeutic low-dose and posttherapeutic high-dose [^{177}Lu]Lu-PSMA-617 therapy radiation dosimetry anal- ysis from the literature (Table 7) showed comparably lower doses to the kidneys and salivary glands but higher doses to the red marrow and total body in our study. The rest of organ-absorbed doses were comparable.

DISCUSION:

Scandium-44 with a half-life of 3.927 hours enables imaging for up to 18 to 20 hours postinjection, which is one of its most important ad vantages over 68Ga-labeled compounds (half-life of 1.18 hours) for dosimetry uses. Therefore, [^{44}Sc]Sc-pSMA-617 is better suited for the evaluation of the biological half-life in vivo, which is an important factor for organ dose calculation, as small errors in the assessment of the biological half-life may result in significant deviations in the result of estimated organ dose. Further knowing that preclinical in vitro and in vivo studies have shown better correlation of [^{44}Sc]Sc-

PSMA-617 with [^{177}Lu]Lu-PSMA-617 as compared with ^{68}Ga-labeled PSMA ligands, we hypothesized that dosimetric analysis from 19.5-hour imaging data of [^{44}Sc]Sc-PSMA-617 could be used to more accurately estimate the potential organ doses delivered by [^{177}Lu]Lu-PSMA-617 in individual patients [19]. Recent dosimetric analysis with [^{44}Sc]Sc-PSMA-617 has further strengthened the fact that it can reliably interpret the pharmacodynamics of PSMA [26]. The mean ± SD of extrapolated residence time for [^{177}Lu] Lu-PSMA-617 for the remainder of the body in our study was 46.58 ± 16.04 hours (range, 22.4–64.12 hours), which is in line with the results of the study of Kabasakal et al [12] (mean ± SD, 37.9 ± 14.6 hours; range, 24.6–62.0 hours). We also observed that patient 1, who had renal insufficiency as well as extensive bone metastasis, exhibited the longest residence time, which is consistent with the observations of Kabasakal et al [12]

References.

Table 6. Predicted Maximum Number of Cycles (6 GBq/Cycle) to Be Administered in Individual Patients Considering Toxicity Limits for Organs With EBRT

Patient (PT)	PT1	PT2	PT3	PT4	PT5	Mean Organs
Small intestine	33	61.16	56.02	36.04	101.94	47.5
Kidneys	7.06	11.48	11.27	7.34	8.19	8.68
Liver	21.1	36.76	29.41	17.18	19.53	22.94
Salivary glands	39.31	7.58	17.01	22.77	63.32	18.12
Red marrow	4.84	5.42	12.35	7.82	9.44	7.09
Urinary bladder wall	78.74	96.15	145.77	41.67	144.3	82.12
Total body	1.96	5.77	9.03	5.26	5.54	4.29

Table 7. Comparison of Organ Absorbed Doses (Gy/GBq) of Current Study With Pre– and Post–[^{177}Lu]Lu-PSMA-617 Therapy Dosimetric Studies[9,12–16]

	Post High-Dose [^{177}Lu]Lu-PSMA-617 Therapy					Pre Low-Dose [^{177}Lu]Lu-PSMA-617 Therapy	From [^{44}Sc]Sc-PSMA-617
Study Name	Delker et al[13]	Kratochwil et al [15]	Fendler et al[9]	Kulkarni et al[14]	Okamoto et al[16]	Kabasakal et al[12]	Current Study
Organs							
Small intestine							0.14
Kidneys	0.6	0.75	0.5/0.6	0.8	0.69	0.88	0.44
Liver	0.11	0.1	0.1		0.11	0.28	0.22

Salivary glands	1.41	1.48	1	1.3	0.58	1.17	0.23
Red marrow	0.012	0.03	0.002	0.03		0.034	0.05
Osteogenic cells							0.04
Spleen	0.1	0.19	0.1				0.12
Urinary bladder wall		0.2					0.12
Total body				0.04	0.05	0.061	0.08
Dose administered, GBq	3.6			5.76	7	0.185	6

The extrapolated mean organ-absorbed doses for [^{177}Lu] Lu-PSMA-617 in our study are comparable with other pretherapeutic and posttherapeutic dosimetry results obtained with [^{177}Lu] Lu-PSMA-617 as shown in Table 7 [9, 12–16]. However, we observed a lower mean absorbed dose in the kidneys, compared with previous studies. This might be explained by the analysis of 3-dimensional (3D) PET/CT activity distribution in the kidneys, as compared with 2D planar gamma camera-based distribution measurement, which has inherent potential of overestimation of kidney dose owing to activity contribution from overlapping organs. On the other hand, we observed higher mean organ-absorbed doses in whole body as com- pared with previous studies. This difference is mainly caused by the high residence time in the remainder of the body in patient 1. The mean organ-absorbed doses in the remaining organs are comparable to the values observed by previous studies.

Pretherapeutic dosimetry aims at improving and tailoring dose delivery to tumor lesions while maintaining safety and avoiding toxicity to normal organs. With previous knowledge from the literature, we mainly considered the kidneys, bone marrow, and salivary gland toxicity as organs at risk of the potential development of adverse effects. Organ-absorbed doses that could result from ad- ministration of6 GBq [^{177}Lu]Lu-PSMA-617 (1 cycle) in all patients were calculated as shown in Table 4. The kidneys received the highest organ dose in most patients except in patient 2, who had the highest dose delivered to the salivary glands.

Calculation of the maximum permissible activity and number of cycles (6 GBq/cycle) with [^{177}Lu]Lu-PSMA-617 to reach EBRT- based organ-absorbed dose limits, as shown in Table 5 and 6, revealed varying results among patients. In patient 1, bone marrow toxicity limits were reached earlier than the kidney toxicity limits; however, the whole-body toxicity limit was reached at even lower activity, which might require strict monitoring and possibly dose reduction in this patient when performing [^{177}Lu]Lu-PSMA-617 therapy.

This finding is consistent with the compromised renal function and high skeletal tumor burden in this patient, which together result in a high dose to the total body.

In patient 2, bone marrow toxicity limits constrained the maximum permissible activity and the maximum number of cycles that can be administered, which is consistent with the observation already discussed in the literature that high skeletal tumor burden can result in high bone marrow–absorbed doses, which might lead to grade 1 to 2 hematologic toxicity from [^{177}Lu]Lu-PSMA-617, especially when bone marrow function is already compromised owing to prior extensive treatment with chemotherapy/radiotherapy [18]. In the remaining 3 patients, kidney toxicity thresholds appeared to be the dose-limiting factor. Overall, except for patient 1, administration of up to 5 cycles of 6 GBq seems to be feasible without reaching toxicity limits.

Although the kidneys were an organ at risk with high organ- absorbed doses, we found that in order to reach EBRT-derived dose limit of 23 Gy a mean cumulative activity of 52 GBq can be administered. It is apparently higher than values found in literature for [^{177}Lu] Lu-PSMA-617, which were calculated to be 30 GBq by Kabasakal et al [12], a difference that can be explained owing to 2D versus 3D dosimetry inherent limitations. Moreover, Delker et al [13] used 3D SPECT of abdomen for dosimetric analysis of [^{177}Lu]Lu-PSMA-617 and reported a mean absorbed dose of 0.6 GY/GBq for kidneys, which may allow up to 38 GBq to be administered safely. Use of monoexponential nonlinear least squares fit to time-activity curve and a linear interpolation from time of injection in contrast to biexponential curve fitting and availability of dynamic data from time of injection in our current study might be the cause of this disparity between Delker et al [13] and our current study. Moreover, it is also believed that toxicity limit for kidneys with [^{177}Lu]Lu-PSMA-617 therapy should be increased [18]. Considering 25 Gy as dose limit for reversible toxicity to salivary glands, it was seen that even in patient 2 with highest salivary glands–absorbed dose it was not a limiting factor for permissible activity calculation in that patient. The finding is supported with evidence of 4% to 25% occurrence of transient reversible xerostomia and dry mouth with [^{177}Lu]Lu-PSMA-617 therapy in various studies [18].

Our current study shows that the conversion from pretherapeutic pharmacokinetic data obtained by [^{44}Sc]Sc-PSMA-617 PET/CT to potential normal organ-absorbed doses for [^{177}Lu]Lu-PSMA- 617 therapy is feasible. However, further studies are warranted to validate extrapolated organ doses from pretherapeutic [^{44}Sc]Sc- PSMA-617 PET/CT with posttherapeutic [^{177}Lu]Lu-PSMA-617 dosimetry data and to correlate dosimetry results

with clinical toxic- ity and adverse effects. Furthermore, the prediction of absorbed doses in tumour lesions by [^{44}Sc]Sc-PSMA-617 PET/CT remains to be investigated.

Conclusion:

Prediction and calculation of organ absorbed doses in patients scheduled for [^{177}Lu]Lu-PSMA-617 therapy seems to be feasible by pre-therapeutic [^{44}Sc]Sc-PSMA-617 PET/CT. It might prove to be helpful in the pre-therapeutic assessment of organs at risk, which seem to be are variable among patients, and eventually aid in tailoring personalized PSMA-targeted radionuclide therapy regimens. However, correlation of clinical toxicity data with pre-therapeutic [^{44}Sc]Sc-PSMA-617 PET/CT based dosimetry results remains to be investigated in larger-scale studies before final conclusions can be drawn.

References

1. Ahmadzadehfar H, Eppard E, Kürpig S, Fimmers R, Yordanova A, Schlenkhoff CD, et al. Therapeutic response and side effects of repeated radioligand therapy with 177Lu-PSMA-DKFZ-617 of castrate-resistant metastatic prostate cancer. Oncotarget. 2016;7:12477–88. doi:10.18632/oncotarget.7245.
2. Rahbar K, Ahmadzadehfar H, Kratochwil C, Haberkorn U, Schäfers M, Essler M, et al. German Multicenter Study Investigating 177Lu-PSMA-617 Radioligand Therapy in Advanced Prostate Cancer Patients. J. Nucl. Med. 2017;58:85–90. doi:10.2967/jnumed.116.183194.
3. Lütje S, Heskamp S, Cornelissen AS, Poeppel TD, van den Broek SAMW, Rosenbaum-Krumme S, et al. PSMA Ligands for Radionuclide Imaging and Therapy of Prostate Cancer: Clinical Status. Theranostics. 2015;5:1388–401. doi:10.7150/thno.13348.
4. Ahmadzadehfar H. Targeted Therapy for Metastatic Prostate Cancer with Radionuclides 2016: InTech. doi:10.5772/64016.
5. Benešová M, Schäfer M, Bauder-Wüst U, Afshar-Oromieh A, Kratochwil C, Mier W, et al. Preclinical Evaluation of a Tailor-Made DOTA-Conjugated PSMA Inhibitor with Optimized Linker Moiety for Imaging and Endoradiotherapy of Prostate Cancer. J. Nucl. Med. 2015;56:914–20. doi:10.2967/jnumed.114.147413.
6. Ahmadzadehfar H, Wegen S, Yordanova A, Fimmers R, Kürpig S, Eppard E, et al. Overall survival and response pattern of castration-resistant metastatic prostate cancer to multiple cycles of radioligand therapy using 177LuLu-PSMA-617. European Journal of Nuclear Medicine. 2017;44:1448–54. doi:10.1007/s00259-017-3716-2.
7. Ahmadzadehfar H, Rahbar K, Kürpig S, Bögemann M, Claesener M, Eppard E, et al. Early side effects and first results of radioligand therapy with (177)Lu-DKFZ-617

PSMA of castrate-resistant metastatic prostate cancer: a two-centre study. EJNMMI Res. 2015;5:114. doi:10.1186/s13550-015-0114-2.

8. Pfestroff A, Luster M, Jilg CA, Olbert PJ, Ohlmann CH, Lassmann M, et al. Current status and future perspectives of PSMA-targeted therapy in Europe: opportunity knocks. European Journal of Nuclear Medicine. 2015;42:1971–5. doi:10.1007/s00259-015-3186-3.
9. FendlerWP, S Reinhardt, IlhanH. Preliminary experiencewith dosimetry, response and patient reported outcome after 177 Lu - PSMA - 617 therapy for metastatic castration - resistant prostate cancer. Eur J Nucl MedMol Imaging. 2015.
10. Yordanova A, Becker A, Eppard E, Kürpig S, Fisang C, Feldmann G, et al. The impact of repeated cycles of radioligand therapy using 177LuLu-PSMA-617 on renal function in patients with hormone refractory metastatic prostate cancer. European Journal of Nuclear Medicine. 2017;44:1473–9. doi:10.1007/s00259-017-3681-9.
11. Baum RP, Kulkarni HR, Schuchardt C, Singh A, Wirtz M, Wiessalla S, et al. 177Lu-Labeled Prostate-Specific Membrane Antigen Radioligand Therapy of Metastatic Castration-Resistant Prostate Cancer: Safety and Efficacy. J. Nucl. Med. 2016;57:1006–13. doi:10.2967/jnumed.115.168443.
12. Kabasakal L, AbuQbeitah M, Aygün A, Yeyin N, Ocak M, Demirci E, Toklu T. Pre-therapeutic dosimetry of normal organs and tissues of (177)Lu-PSMA-617 prostate-specific membrane antigen (PSMA) inhibitor in patients with castration-resistant prostate cancer. European Journal of Nuclear Medicine. 2015;42:1976–83. doi:10.1007/s00259-015-3125-3.
13. Delker A, Fendler WP, Kratochwil C, Brunegraf A, Gosewisch A, Gildehaus FJ, et al. Dosimetry for (177)Lu-DKFZ-PSMA-617: a new radiopharmaceutical for the treatment of metastatic prostate cancer. European Journal of Nuclear Medicine. 2016;43:42–51. doi:10.1007/s00259-015-3174-7.
14. Kulkarni HR, Singh A, Schuchardt C, Niepsch K, Sayeg M, Leshch Y, et al. PSMA-Based Radioligand Therapy for Metastatic Castration-Resistant Prostate Cancer: The Bad Berka Experience Since 2013. J. Nucl. Med. 2016;57:97S-104S. doi:10.2967/jnumed.115.170167.
15. Kratochwil C, Giesel FL, Stefanova M, Benešová M, Bronzel M, Afshar-Oromieh A, et al. PSMA-Targeted Radionuclide Therapy of Metastatic Castration-Resistant Prostate Cancer with 177Lu-Labeled PSMA-617. J. Nucl. Med. 2016;57:1170–6. doi:10.2967/jnumed.115.171397.
16. Okamoto S, Thieme A, Allmann J, D'Alessandria C, Maurer T, Retz M, et al. Radiation Dosimetry for 177Lu-PSMA I&T in Metastatic Castration-Resistant Prostate Cancer: Absorbed Dose in Normal Organs and Tumor Lesions. J. Nucl. Med. 2017;58:445–50. doi:10.2967/jnumed.116.178483.

17. Afshar-Oromieh A, Avtzi E, Giesel FL, Holland-Letz T, Linhart HG, Eder M, et al. The diagnostic value of PET/CT imaging with the (68)Ga-labelled PSMA ligand HBED-CC in the diagnosis of recurrent prostate cancer. European Journal of Nuclear Medicine. 2015;42:197–209. doi:10.1007/s00259-014-2949-6.

18. Emmett L, Willowson K, Violet J, Shin J, Blanksby A, Lee J. Lutetium 177 PSMA radionuclide therapy for men with prostate cancer: a review of the current literature and discussion of practical aspects of therapy. Journal of Medical Radiation Sciences. 2017;64:52–60. doi:10.1002/jmrs.227.

19. Umbricht CA, Benešová M, Schmid RM, Türler A, Schibli R, van der Meulen, Nicholas P., Müller C. 44Sc-PSMA-617 for radiotheragnostics in tandem with 177Lu-PSMA-617-preclinical investigations in comparison with 68Ga-PSMA-11 and 68Ga-PSMA-617. EJNMMI Res. 2017;7:9. doi:10.1186/s13550-017-0257-4.

20. Eppard E, La Fuente A de, Benešová M, Khawar A, Bundschuh RA, Gärtner FC, et al. Clinical Translation and First In-Human Use of 44ScSc-PSMA-617 for PET Imaging of Metastasized Castrate-Resistant Prostate Cancer. Theranostics. 2017;7:4359–69. doi:10.7150/thno.20586.

21. Stabin MG. Fundamentals of Nuclear Medicine Dosimetry. 1st ed. s.l.: Springer-Verlag; 2008.

22. Hindorf C, Lindén O, Tennvall J, Wingårdh K, Strand S-E. Evaluation of methods for red marrow dosimetry based on patients undergoing radioimmunotherapy. Acta Oncol. 2005;44:579–88. doi:10.1080/02841860500244294.

23. S. Shen, G. Denardo, G. Sgouros, R. O'donnell, S. Denardo. Practical determination of patient-specific marrow dose using radioactivity concentration in blood and body. J. Nucl. Med. 1999.

24. Sgouros G, Stabin M, Erdi Y, Akabani G, Kwok C, Brill AB, Wessels B. Red marrow dosimetry for radiolabeled antibodies that bind to marrow, bone, or blood components. Medical Physics. 2000;27:2150–64. doi:10.1118/1.1288393.

25. Siegel JA. Establishing a clinically meaningful predictive model of hematologic toxicity in nonmyeloablative targeted radiotherapy: practical aspects and limitations of red marrow dosimetry. Cancer Biotherapy & Radiopharmaceuticals. 2005;20:126–40. doi:10.1089/CBR.2005.20.126.

26. Khawar A, Eppard E, Sinnes JP, Roesch F, Ahmadzadehfar H, Kürpig S, et al. 44ScSc-PSMA-617 Biodistribution and Dosimetry in Patients With Metastatic Castration-Resistant Prostate Carcinoma. Clin Nucl Med. 2018;43:323–30. doi:10.1097/RLU.0000000000002003.

5.3 [^{44}Sc]Sc-PSMA-617 biodistribution and dosimetry in metastatic castration resistant prostate carcinoma patients (mCRPC)

A. Khawar[1*], E. Eppard[1*], J.P. Sinnes[2*], F. Roesch[2*], H. Ahmadzadehfar[1*], S. Kürpig[1*], M. Meisenheimer[1*], F.C. Gaertner[1*], M. Essler[1*#] R. A. Bundschuh[1*#].

[1] Klinik und Poliklinik für Nuklearmedizin, Universitätsklinikum Bonn

[2] Institut für Kernchemie, Universität Mainz

The manuscript has been seen and approved by all authors

*****these authors contributed equally in design and execution of study

*# senior authorship

Conflict of interest: Nothing to disclose

Corresponding author: Ambreen Khawar, MS Nuclear Medicine

E-mail address: ambreen_khawar@hotmail.com

Telephone number: +49 17623876558

Fax number: +49 (0)228-287 19096

Running title: Radiation dosimetry for [^{44}Sc]Sc-PSMA-617

Keywords:

-mCRPC

-Personalized radiation dosimetry

[^{44}Sc]Sc-PSMA-617

Absorbed organ dose

Critical organ

https://doi.org/10.1097/rlu.0000000000002003

Abstract

Aim: [^{44}Sc]Sc-PSMA-617 with 3.9 h half-life, *in vitro* and *in vivo* characteristics similar to [^{177}Lu]u-PSMA-617 and possibility of delayed imaging after 24 hour or later implies it to be advantageous than [^{68} Ga]Ga-PSMA-617 for pretherapeutic dosimetric assessment

for [^{177}Lu]Lu-PSMA-617 in mCRPC patients. In this study we investigated biodistribution and radiation exposure to normal organs with [^{44}Sc]Sc-PSMA-617 in mCRPC patients.

Methods: Five mCRPC patients (mean age 69 yr) enrolled for [^{177}Lu]Lu-PSMA-617 therapy were injected with 40 - 62 MBq [^{44}Sc]Sc-PSMA-617 i.v., Siemens Biograph 2 PET/CT system was used to acquire dynamic PET data (30 min) in list mode over the abdomen followed by the collection of static PET/CT images (skull to mid-thigh) at 45 min, 2 and about 20 h p.i. Time dependent changes in % activity in source organs (kidneys, bladder, salivary glands, small intestine, liver, spleen and whole body) were determined. Bone marrow and urinary bladder contents residence time were also calculated. Source organs residence time, organ absorbed doses and effective doses were determined using OLINDA/EXM software.

Results: Physiological tracer uptake was seen in kidneys, liver, spleen, small intestine, urinary bladder, salivary glands and in metastases. Kidneys with highest radiation absorbed dose of 3.19E-01 mSv/MBq were the critical organs, followed by urinary bladder wall (2.24E-01 mSv/MBq0, spleen (1.85E-01), salivary glands (1.11E-01) and liver (1.07E-01)mSv/MBq. Red marrow dose was found to be 3.31E-02 mSv/MBq. The mean effective dose of 3.89E-02 mSv/MBq and effective dose of 1.95 mSv was estimated from 50 MBq (treatment planning dose) of [^{44}Sc]Sc-PSMA-617.

Conclusion: [^{44}Sc]Sc-PSMA-617 is found to be safe radiopharmaceutical that can be employed for pre [^{177}Lu]Lu-PSMA-617 therapeutic dosimetric assessment.

INTRODUCTION

Metastatic castration resistant prostate carcinoma (mCRPC) presents a challenging task in treatment of prostatic carcinoma patients [1–4]. Overall survival in mCRPC patients is reported to be less than 19 months [5]. With introduction of prostate specific membrane antigen (PSMA) directed imaging and therapeutic ligands paradigm shift in management of mCRPC has been achieved [6]. Several radionuclide labeled PSMA targeting agents against the external and internal domain of PSMA were developed. Enhanced target binding along with shorter circulation time was achieved using small sized ligands directed against external domain of PSMA [7]. Among the small ligands tested were several urea based compounds, the glutamate phosphoramidates and the 2-(phosphinylmethyl) pentanedioic acids [8, 9]. For diagnostic imaging and treatment follow up of mCRPC patients, these PSMA ligands were labeled with SPECT tracers such as [^{111}In]In-PSMA [10], [^{99m}Tc]Tc-MIP-1404 [11], [^{99m}Tc]Tc-MIP-1405 [11], [^{123}I]I-MIP-1072 [12, 13] and [^{123}I]I-MIP-1095 [6, 12] and PET tracers like [^{68}Ga]Ga-PSMA-HBED-CC/ I&T, 11, 617 [6, 14–19], [^{124}I]I-MIP-1095 [13, 20], [^{18}F]F-DCFBC [4] and [^{18}F]F-DCFPyL [21, 22]. Therapeutic success was achieved with β^- emitting [^{177}Lu]Lu-PSMA-617 [23–25], [^{177}Lu]Lu-PSMA-I&T [26–28], [^{90}Y]Y-PSMA [4] and [^{131}I]I-MIP-1095 [20, 29].

Therapeutic success in terms of objective response with decline in PSA levels to [^{177}Lu]Lu-PSMA-617 therapy in 70% of mCRPC patients has been described [24, 30]. In another review >50% reduction of serum PSA level in 30%-70% of mCRPC patients along with 10%-32% non- responders to [^{177}Lu]Lu-PSMA-617 therapy have been reported [31]. To date no substantial reasoning for lack of response in this fraction of mCRPC patients is provided. However, it is proposed that high dose delivery to tumor lesions while maintaining safety and avoiding toxicity could be a potential solution in enhancing response in resistant population, thus emphasizing role of personalized dosimetry in these patients [31].

At present, for treatment with [^{177}Lu]Lu-PSMA-617 initial administered doses are based on previous experience with PRRT, and escalated according to ongoing individual experience of respective clinicians at various centers.

Emerging concepts of theranostic and personalized medicine in oncology seeks the use of highly sensitive and specific diagnostic PET probes that may later be labeled with therapeutic radionuclide [7]. It is assumed that diagnostic PET agent distribution will predict therapy dose and better therapeutic outcome reliably [7]. Several matching pairs of imaging/therapeutic radionuclides have been proposed that are considered reliable markers of bio kinetics and dose determination. Among them high emphasis is being

placed on generator produced PET radiopharmaceuticals such as gallium-68 and scandium-44 for imaging agents partnered with lutetium-177 based therapies and in future with scandium-47 based therapies [32].

Several urea based compounds using DOTA and DOTAGA as chelators were efficiently labeled with imaging and therapeutic radionuclides and are seen as steps towards personalized therapy planning in mCRPC patients. PSMA-617 is one of the urea based PSMA ligands that has shown high tumor binding, high internalization as well as good labeling with both imaging and therapeutic radionuclides. At the moment PSMA-617 labeled with gallium-68 for imaging and lutetium-177 for therapy is being used in several centers across Germany [15, 33]. Owing to the high advocacy for patient specific dosimetry in improving safety and efficacy of [^{177}Lu]Lu-PSMA-617 therapy, [^{68}Ga]Ga-PSMA-617 PET/CT imaging and low dose [^{177}Lu]Lu-PSMA-617 SPECT and static imaging have been used for dosimetric analysis [31]. For pre therapeutic dosimetry [^{68}Ga]Ga-PSMA-617 ($t_{1/2}$=1.1 h) as imaging counterpart for [^{177}Lu]Lu-PSMA-617 ($t_{1/2}$=6.7days) therapy was found deficient due to its limitation to image beyond 4 h and lower organ absorbed dose calculations. Low dose [^{177}Lu]Lu-PSMA-617 SPECT and planar gamma camera studies has inherent limitations of prolonged hospital stay, multiple time point imaging and data collection which overestimates kidney dose and is deficient to determine lacrimal gland doses. Moreover, it is believed that organ absorbed doses determined by low dose dosimetry are unreliable owing to the fact that high therapeutic doses of [^{177}Lu]Lu-PSMA-617 may follow altered pharmacokinetics resulting in different organ absorbed doses [5]. Hence, longer lived PET labeled PSMA compounds are seen as an alternative for pretherapeutic dosimetry and better dose planning in mCRPC patients.

Recent labeling of DOTATOC with cyclotron produced scandium-44 with half-life of 3.9 h having better energy and sensitivity, provided prolonged imaging up till 23.5 h [33, 34]. [^{44}Sc]Sc-DOTATOC was found to be safe and superior in detection of metastasis which were not apparent in previous [^{68}Ga]Ga-DOTATOC imaging or concurrent ultrasound or magnetic resonance images in patients of neuroendocrine tumors. The same coordination chemistry shared by scandium-44 with lutetium-177 is considered the basis for similar *in vivo*/*in vitro* distribution and characteristics. A recent comparison of [^{44}Sc]Sc-PSMA-617 with [^{68}Ga]Ga-PSMA-617, [^{177}Lu]Lu-PSMA-617 and {^{68}Ga]Ga-PSMA-11 has also revealed that it shares similar *in vivo* kinetics and *in vitro* characteristics as [^{177}Lu]Lu-PSMA-617 while gallium-68 labeled agents did show different kinetics and thus proposes [^{44}Sc]Sc-PSMA-617, a better candidate for pre [^{177}Lu]Lu-PSMA-617 therapy dosimetric assessment in mCRPC patients [35]. In addition to cyclotron production scandium-44

can be produced from a $^{44}Ti/^{44}Sc$ generator, though in lesser activities as compared to cyclotron. Long half-life($t_{1/2}$) of scandium-44 gives added advantages of its possible transport to distant places from site of production [34], feasible delayed imaging with [^{44}Sc]ScPSMA-617 and sentinel node imaging prior to surgery for primary prostate carcinoma . However presence of high energy gamma rays (>909 KeV) is considered a drawback.

Considering all potential benefits specially the pre therapeutic dosimetric analysis for [^{177}Lu]Lu-PSMA-617 this study aims to determine bio distribution and normal organ absorbed doses for [^{44}Sc]Sc-PSMA-617 in mCRPC patients and to explore its use as surrogate marker for pre [^{177}Lu]Lu-PSMA-617 therapy dosimetric evaluation.

Materials and Methods:

All procedures followed were in accordance with the ethical standards of institutional review board and all patients gave written informed consent.

Patient Population:

Between April 2016 to June 2017 five male patients with progressive mCRPC and mean age of 69±2.2 years were enrolled for [^{44}Sc]Sc-PSMA 617 imaging [Table 1]. The injected doses of [^{44}Sc]Sc-PSMA-617 ranged from 40-62 MBq (mean ± SD: 50.16 ± 8.04). All patients except patient no 4, had recieved cycles of [^{177}Lu]Lu-PSMA-617 in addition to conventional therapies.

Preparation of [^{44}Sc]Sc-PSMA-617:

3 ml of scandium-44 obtained after post processing according to literature of eluted ^{44}Sc from prototype 185 MBq (5 mCi) $^{44}Ti/^{44}Sc$ generator (Mainz) was used to label GMP-grade PSMA-617 obtained from ABX (Radeberg, Germany). Quality control for radiochemical yield & purity was checked using TLC with 0.1M sodium citrate; ITLC with1:1 v/v 1 M ammonium acetate/methanol and HPLC with Nucleodur 100-3 C18 ec 125/4; Macherey-Nagel GmbH & Co. KG, Germany. A radiochemical yield of 98% and radiochemical purity of 99% was obtained [36].

[^{44}Sc]Sc-PSMA-617 PET/CT Imaging Protocol:

Siemens Biograph 2 PET/CT scanner with a 58.5 cm axial field of view and a 16.2 cm longitudinal field of view was used for acquiring [^{44}Sc]Sc-PSMA-617 PET/CT imaging over a period of 2 days. The scanner has a spatial resolution of about 6 mm in axial and transversal direction (at a radius of 10 mm). All patients underwent a low dose CT scan of abdomen for attenuation correction and patient positioning with kidneys in field of view,

followed by dynamic imaging of abdomen for 30 minutes in list mode started simultaneously with i.v injection of [^{44}Sc]Sc-PSMA-617. Later static skull to mid-thigh PET/CT images were acquired at 45 min, 2 and 19.5 h post injection (p.i), each preceded by low dose CT examination for patient positioning and attenuation correction. For qualitative and quantitative analysis dynamic images were reconstructed into 6 images of 300s each using iterative reconstruction OSEM.

Qualitative: Analysis

All dynamic and static images were visually analyzed to see physiological and pathological tracer distribution as shown in figure 1 &2. Organs with increased tracer uptake were identified as source organs for further dosimetric analysis.

Table 1: Subject details, injected radioactivity of [^{44}Sc]Sc-PSMA and therapies received

PT No	Age (years)	weight (Kg)	Hct*	Injected Activity(MBq)	Injected Activity MBq/Kg	PSA (ng/ml)	Therapies received
1	70	78	0,33	50,00	0,64	453,00	Lu-177 PSMA (3),	Radio/ chemo and anti Hormone therapy
2	72	80	0,30	62,23	0,78	26,00	Lu-177 PSMA (1),	anti hormone
3	67	70	0,39	39,61	0,57	7,20	Lu-177 PSMA (2),	Radio/ Anti hormonal and bisphosphonate therapy
4	70	80	0,30	50,00	0,63	139,00	----	Radiotherapy

5	67	104	0,29	48,95	0,47	3000,00	Lu-177 PSMA (1)	radio/hormonal/ chemo
Mean	69	82,4	0,32	50,16	0,62			
SD	2,2	12,76	0,04	8,04	0,11			

*Hematocrit

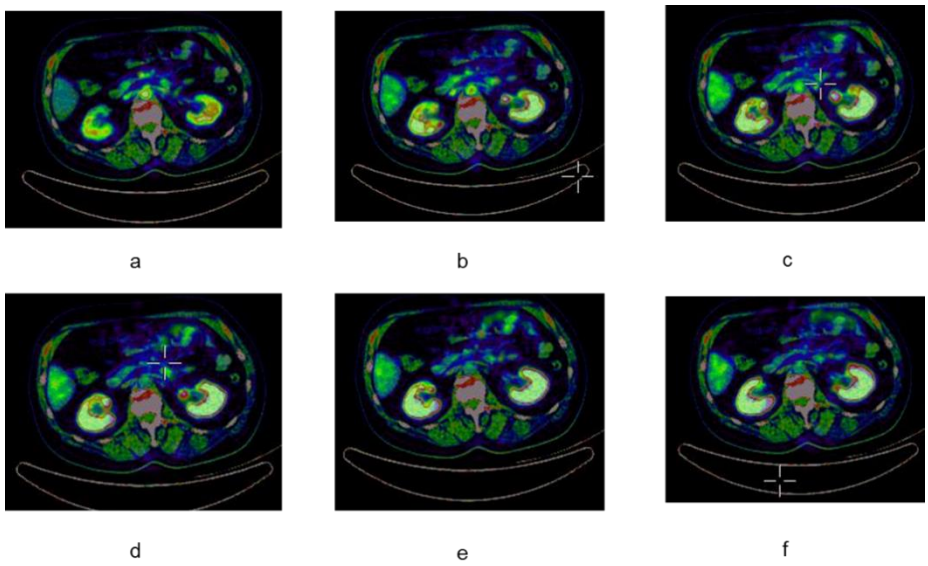

Figure 1: Physiological tracer distribution at (a) 150s, (b) 450s, (c)750s, (d) 1050s, (e) 1350s and (f) 1650s

Quantitative Dosimetric Analysis:

For dosimetric analysis kidneys, liver, spleen, urinary bladder, small intestine, salivary glands and whole body were selected as source organs. MEDISO interview fusion software (MEDISO Medical Imaging Systems, Budapest, Hungary)was used to draw volume of interest (VOI) encompassing each source organ on CT image for calculating source organ volume and to determine mean counts per ml (KBq/ml) from PET image as shown in figure 2. Total source organ activity was calculated by multiplying each source organ volume with corresponding mean counts/ml. Total source organ activity was converted into MBq/ml. OLINDA/EXM software (Hermes, Germany) requires % source organ activities with respect to time for curve fitting and residence time calculation. Hence, % source organ activity for each source organ was calculated by dividing total source organ activity by injected activity and multiplying it with 100.

Assuming homogenous distribution of tracer in remainder of body, % of injected dose in image was scaled proportional to % weight of body in image for % whole body activity calculation.

$$\%\, Body\ weight(image) = \frac{CT\ volume\ of\ whole\ bodyimage \times mean\ CT\ density \times 100}{Patient\ weight}$$

Percent source organ activity were used to generate time activity curves and residence time calculations using OLINDA/EXM software (Hermes, Germany). Mono exponential curve fitting for whole body and bi exponential curve fitting for rest of source organs was applied. For remainder of body residence time, residence time of all source organs except urinary bladder contents was subtracted from whole body residence times [37].

Indirect blood based method with patient based RMBLR and red marrow mass was used to calculate bone marrow self-dose [38–41]. 1-2ml venous blood samples were collected at varying time points i.e., (5, 10. 15, 20, 25, 30, 45) min, 2 and 18 h post injection (Insert references). To calculate residence time for urinary bladder contents, trapezoidal method was used taking into account urinary bladder activity in images at 45 min, 2 and 18 h along with activity in urinary samples. Urine samples were collected in pre weighed containers after 45 min and 2 h static PET/CT imaging. Radioactivity in 1ml blood and urine samples was measured along with known standard activity using 1480 WIZARD^{TM} 3n Gamma counter.

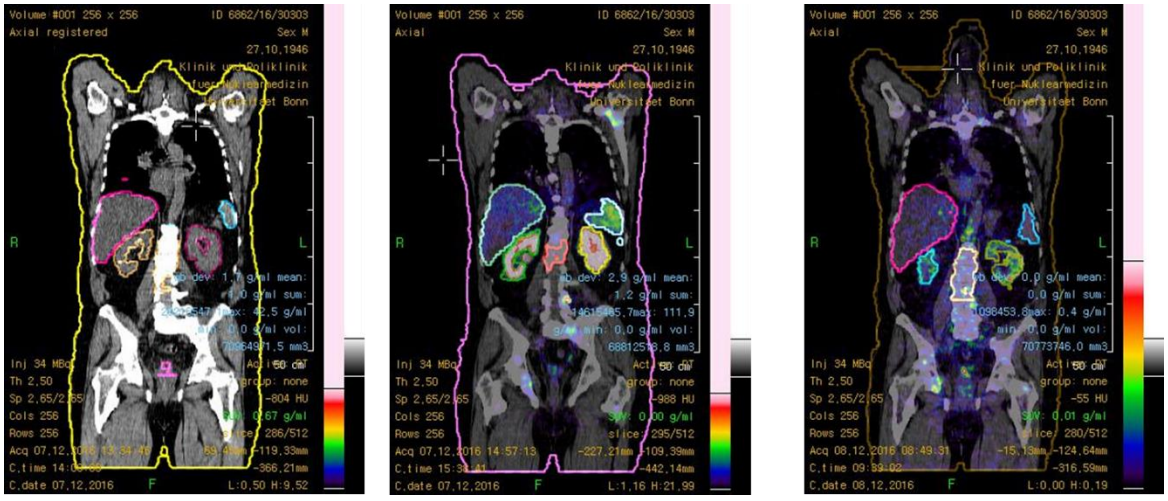

Figure 2: VOI drawn in (a) CT image at 45 min, (b) PET/CT images at 2 h and (c) at 18h.

OLINDA/EXM software (Hermes, Germany) was used to calculate mean organ absorbed doses and effective doses (ICRP103 factors) by adjusting for patient's body weight. It was done by multiplying the reference adult male body weight with fraction determined from dividing the patient weight with reference adult weight. The mean of residence

times, organ absorbed doses (mSv/MBq) and effective doses (mSv/MBq) were calculated. The total effective dose in mSv received after injection of 62 MBq (highest dose injected) and 50 MBq (usual dose injected) of [^{44}Sc] Sc-PSMA-617 was calculated by multiplying the mean effective dose (mSv/MBq) with 62 and 50 MBq respectively.

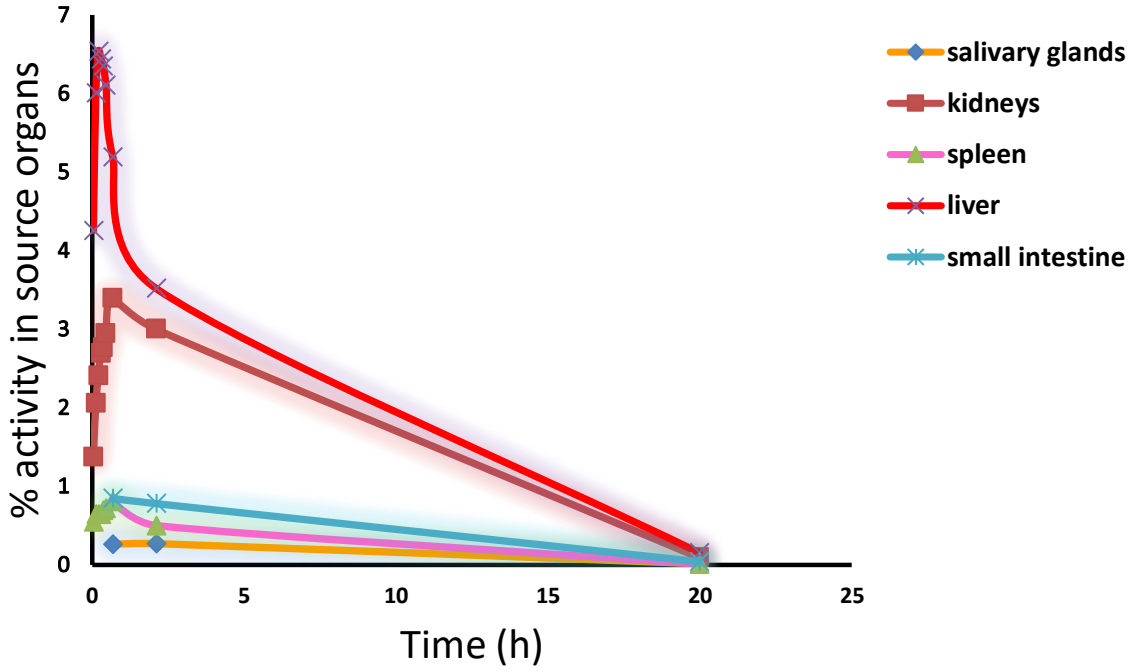

Figure 3: Time dependent changes of % injected activity in source organs.

RESULTS:

Qualitative [^{44}Sc]Sc-PSMA-617 Distribution and Kinetics:

The whole body PET/CT images at 45 m, 2 & 18 h revealed normal physiological uptake of [^{44}Sc]Sc-PSMA-617 in kidneys, liver, spleen, salivary glands, small intestine and urinary bladder. Very faint uptake was also noticed in lacrimal glands with faint to absent uptake in nasal or oral mucosa. Rapid tracer kinetics were seen with peak uptake achieved in organs within an hour as shown in figure 3. Rapid blood clearance and excretion from kidneys created better tumor to soft tissue contrast. Liver exhibited the highest percent activity followed by kidneys, spleen, salivary glands and small intestine. Rapid fall in activity in liver and other source organs was observed. The decrement in kidneys, small intestine and salivary glands was gradual with exception of increase in activity at 2 h in salivary glands and small intestine in only one patient. Pathological uptake was also observed in metastatic bone and soft tissue.

Dosimetry for Normal Organs:

Estimated residence times(MBq-hr/MBq) were found to be prolonged in liver followed by kidneys, urinary bladder, bone marrow and rest of organs as shown in table 2. Table 3 shows the individual patient, mean ± SD organ of absorbed doses and effective doses as calculated by OLINDA/EXM software. The results showed that kidneys received the highest mean absorbed dose of 3.19 E-01 mSv/MBq (range: 1.78 E-01 to 4.88 E-01 mSv/MBq) making it the critical organ followed by urinary bladder wall, spleen, salivary glands, liver and small intestine. Highest dose to kidneys were associated with the fact that they are the main route of excretion for PSMA-617. Bone marrow dose was found to be low and presented as organs with low toxicity risk while considering therapeutic application.

DISCUSSION:

PSMA-617 directed against is a modified version of PSMA-11 directed binding to the external domain of PSMA. Comparative bio distribution studies with PSMA-11 has revealed supremacy of PSMA-617 due to high target binding and subsequent efficient internalization with in prostate carcinoma cells [42]. It has been labeled with gallium-68, lutetium-177, indium-111 and yttrium-90. [^{68}Ga]Ga-PSMA-617 has been in use in many nuclear medicine centres as a counterpart to pre and post [^{177}Lu]Lu-PSMA-617 therapy for disease monitoring [42, 43]. Recently PSMA-617 has been labeled with long lived PET agents like scandium-44 using DOTA as a linking chelator. Preclinical (*in vitro, in vivo)* and clinical studies with scandium-44 labeled peptides and PSMA ligand for neuroendocrine tumors [44] and prostate carcinoma [35] respectively have proposed scandium-44 a better surrogate marker for lutetium-177 based therapies and probable better candidate for pretherapeutic dosimetric analysis.

Table 2: Comparison of Individual and mean residence times (MBq-h/MBq) for [^{44}Sc]Sc &[^{68}Ga]Ga-PSMA-617

			[^{44}Sc]Sc-PSMA-617					[^{68}Ga]Ga-PSMA-617 [42]
PT No	**PT1**	**PT2**	**PT3**	**PT4**	**PT5**	**mean**	**±S.D**	
Organs								
Salivary glands	0.02	0.01	0.01	0.03	0.07	0.03	±0.027	
Kidneys	0.22	0.36	0.12	0.34	0.15	0.24	±0.109	0.132
Liver	0.25	0.78	0.07	0.29	0.37	0.35	±0.263	0.093

Spleen	0.08	0.09	0.02	0.05	0.09	0.07	±0.031	0.009
Small Intestine	0.02	0.04	0.02	0.07	0.08	0.05	±0.029	
Bone marrow	0.06	0.10	0.05	0.09	0.17	0.09	±0.047	
Urinary bladder contents	0.08	0.14	0.12	0.53	0.05	0.18	±0.195	0.07
Remainder of body	2.93	1.11	1.45	1.86	1.76	1.82	±0.684	1.25

Table 3: Individual and mean organ absorbed doses with [^{44}Sc]Sc-PSMA-617 (mSv/MBq)

ORGAN ABSORBED DOSES (mSv/MBq)

	PT 1	PT 2	PT 3	PT4	PT5	Mean	±SD
Organs							
Adrenals	7.91E-02	1.12E-01	4.21E-02	9.19E-02	5.58E-02	7.62E-02	±2.79E-02
Brain	2.67E-02	1.10E-02	1.51E-02	1.80E-02	1.53E-02	1.72E-02	±5.86E-03
Esophagus	3.48E-02	2.67E-02	1.85E-02	2.66E-02	2.17E-02	2.57E-02	±6.17E-03
Eyes	2.65E-02	1.10E-02	1.50E-02	1.78E-02	1.46E-02	1.70E-02	±5.84E-03
Gall bladder wall	5.06E-02	7.29E-02	2.42E-02	4.70E-02	3.97E-02	4.69E-02	±1.77E-02
Left colon	4.16E-02	3.02E-02	2.34E-02	3.74E-02	2.68E-02	3.19E-02	±7.51E-03
Small intestine	5.06E-02	4.69E-02	3.20E-02	7.87E-02	6.69E-02	5.50E-02	±1.81E-02
Stomach wall	4.03E-02	3.09E-02	2.09E-02	3.11E-02	2.53E-02	2.97E-02	±7.29E-03
Right colon	4.05E-02	3.31E-02	2.52E-02	3.56E-02	2.58E-02	3.20E-02	±6.54E-03
Rectum	3.84E-02	2.33E-02	2.55E-02	4.79E-02	2.19E-02	3.14E-02	±1.13E-02
Heart Wall	3.70E-02	2.90E-02	1.96E-02	2.81E-02	2.31E-02	2.74E-02	±6.61E-03
Kidneys	2.93E-01	4.88E-01	1.80E-01	4.56E-01	1.78E-01	3.19E-01	±1.48E-01
Liver	8.52E-02	2.29E-01	2.95E-02	9.67E-02	9.47E-02	1.07E-01	±7.35E-02
Lungs	3.28E-02	2.43E-02	1.76E-02	2.45E-02	2.01E-02	2.39E-02	±5.78E-03
Pancreas	4.31E-02	3.71E-02	2.30E-02	3.68E-02	2.90E-02	3.38E-02	±7.84E-03

Prostate	3.97E-02	2.60E-02	2.77E-02	5.71E-02	2.14E-02	3.44E-02	±1.44E-02
Salivary glands	9.67E-02	3.54E-02	5.23E-02	1.16E-01	2.53E-01	1.11E-01	±8.60E-02
Red Marrow	3.64E-02	3.27E-02	2.47E-02	3.72E-02	3.43E-02	3.31E-02	±5.00E-03
Osteogenic cells	3.04E-02	2.30E-02	1.93E-02	2.78E-02	2.58E-02	2.53E-02	±4.30E-03
Spleen	2.35E-01	2.48E-01	6.38E-02	1.63E-01	2.16E-01	1.85E-01	±7.52E-02
Testes	2.99E-02	1.38E-02	1.82E-02	2.66E-02	1.52E-02	2.07E-02	±7.13E-03
Thymus	3.19E-02	1.79E-02	1.76E-02	2.23E-02	1.79E-02	2.15E-02	±6.12E-03
Thyroid	3.10E-02	1.47E-02	1.73E-02	2.11E-02	1.71E-02	2.02E-02	±6.44E-03
Urinary Bladder wall	1.21E-01	1.72E-01	1.55E-01	6.05E-01	6.84E-02	2.24E-01	±2.16E-01
Total Body	3.36E-02	2.25E-02	1.92E-02	2.84E-01	2.03E-02	7.59E-02	±1.16E-01
Mean effective Dose	0.0389 mSv/MBq						
Effective dose from 50 MBq	1.94 mSv						
Effective dose from 62 MBq	2.41 mSv						

In this study we found the physiological uptake of [^{44}Sc]Sc-PSMA-617 in liver, kidneys, salivary glands, spleen, small intestine, urinary bladder consistent with low level uptake in normal organs of PSMA described in literature [15, 42]. Pathological uptake was seen in both skeletal and soft metastatic tissue. Kidneys were the major route of excretion with rapid peak uptake seen at 45 min and fast clearance showing minimal activity at 18 h concurrent with early uptake and fast clearance characteristic of PSMA-617. Probable toxicity of salivary glands proposed by A Afshar- Oromieh et al due to late trapping of [^{68}Ga]Ga-PSMA-617 in salivary glands [42] was not observed in this study. Increase in activity in 2 h image was observed in only one of the patients which later decreased to minimal activity at 18 h while rest of the patients showed peak uptake at 45 min followed by gradual decrease. The low probability of salivary gland toxicity depicted by kinetics of [^{44}Sc]Sc-PSMA-617 is consistent with dosimetry results of [^{68}Ga]Ga-PSMA-617 [42]. Occurrence of transient xerostomia or mild reversible xerostomia with [^{177}Lu]Lu-PSMA-617 as well as other lutetium-177 labeled PSMA therapies [33, 45–47] also supports that salivary glands toxicity should be of less concern in these patients. Lacrimal glands showed faint uptake with no enhanced accumulation in later images, therefore we considered its activity with in remainder of body activity. Faint to negligible uptake in nasal mucosa was seen with [^{44}Sc]Sc-PSMA-617. The rapid initial uptake in liver and spleen

followed by fast clearance as result of blood pool effect and its clearance from these organs is consistent with literature [42].

Quantitative analysis revealed high total activity and prolonged residence time in liver followed by kidneys, spleen and other organs consistent with results of [^{68}Ga]Ga-PSMA-617. Residence time of source organs with [^{44}Sc]Sc-PSMA-617 were found to be higher than [^{68}Ga]Ga-PSMA-617 [42]. Long half-life of 3.927 h and ability to follow bio kinetics up to 19.5 h or more with [^{44}Sc]Sc-PSMA-617 account for the higher residence times as compared to [^{68}Ga]Ga-PSMA-617. The organ absorbed doses were highest in kidneys followed by urinary bladder wall, spleen, salivary glands, liver and small intestine. Kidneys with mean dose of 3.19E-01 mSv/MBq (range:1.78E-01-4.88E-01 mSv/MBq) were the organs at risk as is with the rest of small ligands based PSMA agents [42, 48]. Urinary bladder wall with mean dose of 2.24E-01 mSv/MBq was the second highest organ to receive dose owing to the kidneys being its physiological route of excretion. Salivary glands received a dose of 1.11E-01mSv/MBq which was higher than [^{68}Ga]Ga-PSMA-I&T but was not reported with [^{68}Ga]Ga-PSMA-617 besides showing a rise in mean SUV at later time points [42]. Bone marrow dose was found to be low consistent with previous dosimetric studies with gallium-68 labeled agents. Mean organ absorbed dose for bone marrow was found to be 3.31 E-02 mSv/MBq and ranged from 2.47 E-02 to 3.72 E-02. Low marrow dose suggests low risk of marrow toxicity with PSMA based therapies. However, the marrow toxicity can vary with burden of bone and marrow metastases in the patient as was found to be highest in patient no 1 with high tumor burden. Further, our results are concurrent with that of [^{68}Ga]Ga-PSMA-617 ,[^{68}Ga]Ga-PSMA-11 and [^{68}Ga]Ga-PSMA-HBED-CC with reference to high to low dose received by organs as shown in figure 4. However absorbed doses were found to be higher for [^{44}Sc]Sc-PSMA-617 than [^{68}Ga]Ga-PSMA-617, [^{68}Ga]Ga-PSMA-11, [^{68}Ga]Ga-PSMA-I&T as shown in figure 4 but less than [^{124}I]I-PSMA [48].

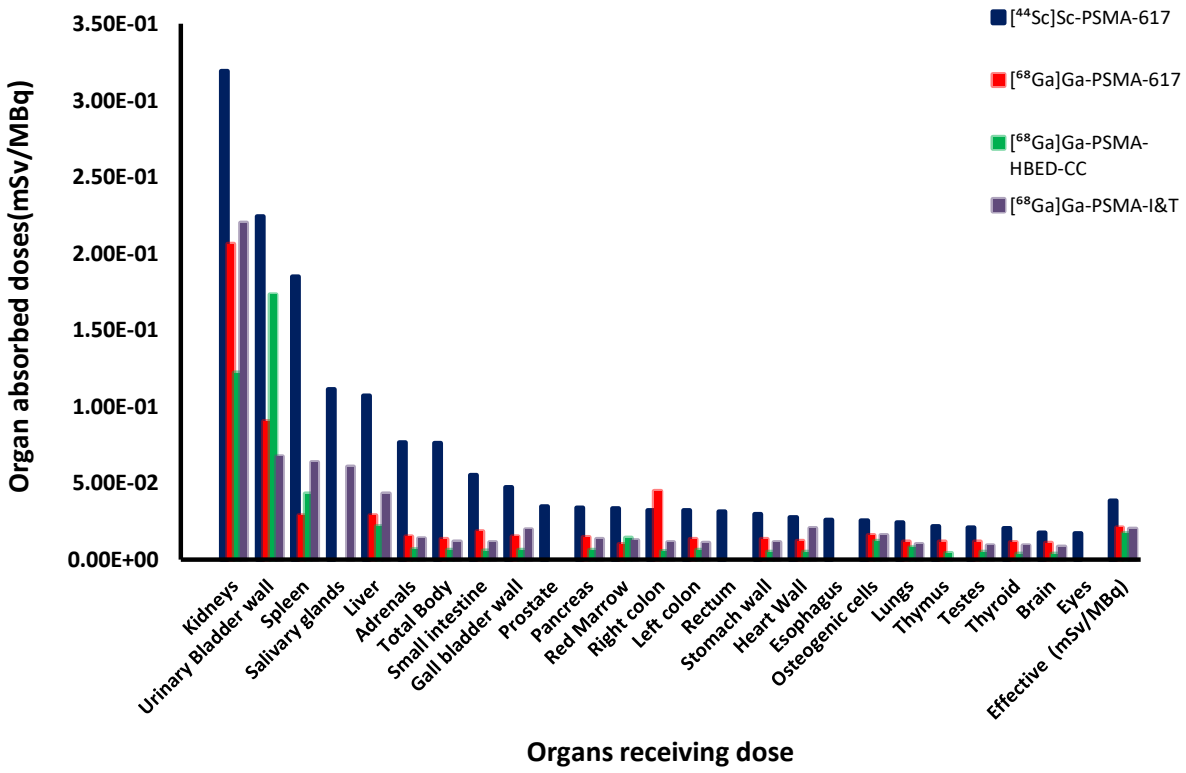

Figure 4: Comparison of Organ Absorbed Doses and effective dose (mSv/MBq) between [^{44}Sc]Sc-PSMA-617 and other [^{68}Ga]Ga-PSMA agents [42, 48].

Comparison of organ absorbed doses of [^{44}Sc]Sc-PSMA-617 with pre and post therapeutic dosimetric results of [^{177}Lu]Lu-PSMA-617 given in table 4 [49–51] and comparison of doses with other gallium labeled PSMA agents also show that it is able to predict doses better than [^{68}Ga]Ga-PSMA-617. However interpatient dosimetric comparison studies of [^{44}Sc]Sc-PSMA-617 with [^{177}Lu]Lu-PSMA-617 are warranted.

The mean effective dose of 3.98E-02 was found to be higher than [^{68}Ga]Ga-PSMA-617, [^{68}Ga]Ga-PSMA-11, [^{68}Ga]Ga-PSMA-I&T but less than [^{124}I]I-PSMA [48]. The total effective dose with usual dose administered (50MBq) of [^{44}Sc]Sc-PSMA-617 was found to be 1.95mSv which was low as compared to rest of gallium-68 labeled PSMA agents as well [^{124}I]I-PSMA. Hence [^{44}Sc]Sc-PSMA-617 having possibility of delayed imaging, higher organ absorbed doses and effective doses less than other PSMA labeled imaging agents and a similar bio distribution to already known ^{68}Ga-PSMA ligands could be a better and safe agent for prediction of therapeutic dosimetry for [^{177}Lu]Lu-PSMA-617. The biodistribution and dosimetric analysis in this study has proved that early uptake kinetics reaching peak followed by clearance of PSMA-617 from source organs up to 19.5 h can easily be interpreted. A comparison of [^{44}Sc]Sc-PSMA-617 kinetics with kinetics of [^{177}Lu]Lu-

PSMA-617 shown by Delker et al [51] as well as *in vivo* kinetics of [^{177}Lu]Lu-PSMA-617 in pre-clinical small animal studies followed for 24 h [52] has shown comparable bio distribution with peak uptake as early as 1 h followed by gradual clearance till 24 h. Hence, suggesting sound reasons for use of this agent in personalized therapy planning. Further studies for interpreting normal organ absorbed doses for [^{177}Lu]Lu-PSMA-617 considering bio kinetic data of [^{44}Sc]Sc-PSMA-617 need to be carried out.

Table 4: Comparison of organ absorbed doses of [^{44}Sc]Sc-PSMA-617 with [^{177}Lu]Lu-PSMA-617in mSv/MBq and [^{68}Ga]Ga-PSMA-617 [42, 49–51]

	[^{44}Sc]Sc-PSMA-617	[^{68}Ga]Ga-PSMA-617	Pre[^{177}Lu]Lu-PSMA-617 therapy	Post[^{177}Lu]Lu-PSMA therapy	
Study name	**Current study**	**Afshar-Oromieh A et. Al [42]**	**Kabasakal L et.al [49]**	**Delker A et.al [51]**	**Okamoto S et.al [50]**
Kidneys	0.32	0.21	0.88	0.6	0.72
Spleen	0.19	0.029		0.1	
Liver	0.11	0.029	0.28	0.1	0.12
Total Body	0.08	.013	0.061		0.06
Red Marrow	0.03	.01	0.034	0.012	
parotid gland			1.17		0.55
submandibular					0.64
lacrimal gland					3.8
Salivary glands	0.11			1.41	

Dosimetric analysis in this study supports that probable organ absorbed doses for therapeutic dose of [^{177}Lu]Lu-PSMA-617 can be determined while using this simple, better and optimized dosimetric study protocol for [^{44}Sc]Sc-PSMA-617. The protocol does not

require hospitalization of the patient, can be completed within 24 hours and most important of all can be incorporated in daily clinical routine. It is important to mention that individual pretherapeutic dosimetric analysis with [^{44}Sc]Sc-PSMA-617 is not necessary for all patients, but for patients not responding to standard doses or having a high cumulative dose or having reduced renal function in the lab.

CONCUSION:

[^{44}Sc]Sc-PSMA-617 with similar *in vivo* and *in vitro* characteristics to [^{177}Lu]Lu-PSMA-617 and low radiation as compared to other known imaging agents for mCRPC seems to be a promising new agent for pre therapeutic dosimetric analysis for [^{177}Lu]Lu-PSMA-617 and therefore for a more individualized tumor therapy. However further studies are warranted, especially to show the benefit for the individual patients.

References

1. Karantanos T, Corn PG, Thompson TC. Prostate cancer progression after androgen deprivation therapy: mechanisms of castrate resistance and novel therapeutic approaches. Oncogene. 2013;32:5501–11. doi:10.1038/onc.2013.206.
2. Hotte SJ, Saad F. Current management of castrate-resistant prostate cancer. Curr Oncol. 2010;17 Suppl 2:S72-9. doi:10.3747/CO.V17I0.718.
3. Maluf FC, Smaletz O, Herchenhorn D. Castration-resistant prostate cancer: systemic therapy in 2012. Clinics. 2012;67:389–94. doi:10.6061/clinics/2012(04)13.
4. Chatalic KLS, Heskamp S, Konijnenberg M, Molkenboer-Kuenen JDM, Franssen GM, Clahsen-van Groningen MC, et al. Towards Personalized Treatment of Prostate Cancer: PSMA I&T, a Promising Prostate-Specific Membrane Antigen-Targeted Theranostic Agent. Theranostics. 2016;6:849–61. doi:10.7150/thno.14744.
5. Pfestroff A, Luster M, Jilg CA, Olbert PJ, Ohlmann CH, Lassmann M, et al. Current status and future perspectives of PSMA-targeted therapy in Europe: opportunity knocks. European Journal of Nuclear Medicine. 2015;42:1971–5. doi:10.1007/s00259-015-3186-3.
6. Afshar-Oromieh A, Babich JW, Kratochwil C, Giesel FL, Eisenhut M, Kopka K, Haberkorn U. The Rise of PSMA Ligands for Diagnosis and Therapy of Prostate Cancer. J. Nucl. Med. 2016;57:79S-89S. doi:10.2967/jnumed.115.170720.
7. Kulkarni HR, Singh A, Schuchardt C, Niepsch K, Sayeg M, Leshch Y, et al. PSMA-Based Radioligand Therapy for Metastatic Castration-Resistant Prostate Cancer: The Bad Berka Experience Since 2013. J. Nucl. Med. 2016;57:97S-104S. doi:10.2967/jnumed.115.170167.

8. Lütje S, Heskamp S, Cornelissen AS, Poeppel TD, van den Broek SAMW, Rosenbaum-Krumme S, et al. PSMA Ligands for Radionuclide Imaging and Therapy of Prostate Cancer: Clinical Status. Theranostics. 2015;5:1388–401. doi:10.7150/thno.13348.

9. Mease RC, Foss CA, Pomper MG. PET imaging in prostate cancer: focus on prostate-specific membrane antigen. Current Topics in Medicinal Chemistry. 2013;13:951–62. doi:10.2174/1568026611313080008.

10. Mottaghy FM, Behrendt FF, Verburg FA. (68)Ga-PSMA-HBED-CC PET/CT: where molecular imaging has an edge over morphological imaging. European Journal of Nuclear Medicine. 2016;43:394–6. doi:10.1007/s00259-015-3212-5.

11. Vallabhajosula S, Nikolopoulou A, Babich JW, Osborne JR, Tagawa ST, Lipai I, et al. 99mTc-labeled small-molecule inhibitors of prostate-specific membrane antigen: pharmacokinetics and biodistribution studies in healthy subjects and patients with metastatic prostate cancer. J. Nucl. Med. 2014;55:1791–8. doi:10.2967/jnumed.114.140426.

12. Kulkarni H, Baum R, Weineisen M, Wester H, Schuchardt C, Wiessalla S, Klette I. Therapy of metastasized castrate-resistant prostate cancer using Lu-177 labeled DOTAGA-PSMA small molecules: first clinical results in a larger patient cohort. J. Nucl. Med. 2015;56:10.

13. C. Zechmann, A. Afshar-Oromieh, Tom Armor, J. Stubbs, W. Mier, B. Hadaschik, et al. I-labeled small molecule (MIP-1095) targeting PSMA for prostate cancer therapy. 2014.

14. Sachpekidis C, Eder M, Kopka K, Mier W, Hadaschik BA, Haberkorn U, Dimitrakopoulou-Strauss A. (68)Ga-PSMA-11 dynamic PET/CT imaging in biochemical relapse of prostate cancer. European Journal of Nuclear Medicine. 2016;43:1288–99. doi:10.1007/s00259-015-3302-4.

15. Afshar-Oromieh A, Malcher A, Eder M, Eisenhut M, Linhart HG, Hadaschik BA, et al. PET imaging with a 68Gagallium-labelled PSMA ligand for the diagnosis of prostate cancer: biodistribution in humans and first evaluation of tumour lesions. European Journal of Nuclear Medicine. 2013;40:486–95. doi:10.1007/s00259-012-2298-2.

16. Weineisen M, Simecek J, Schottelius M, Schwaiger M, Wester H-J. Synthesis and preclinical evaluation of DOTAGA-conjugated PSMA ligands for functional imaging and endoradiotherapy of prostate cancer. EJNMMI Res. 2014;4:63. doi:10.1186/s13550-014-0063-1.

17. Barrio M, Fendler WP, Czernin J, Herrmann K. Prostate specific membrane antigen (PSMA) ligands for diagnosis and therapy of prostate cancer. Expert Rev Mol Diagn. 2016;16:1177–88. doi:10.1080/14737159.2016.1243057.

18. Haberkorn U. PSMA ligands for diagnosis and therapy of prostate cancer. Cancer Imaging 2014. doi:10.1186/1470-7330-14-S1-O10.

19. Afshar-Oromieh A, Hetzheim H, Kübler W, Kratochwil C, Giesel FL, Hope TA, et al. Radiation dosimetry of (68)Ga-PSMA-11 (HBED-CC) and preliminary evaluation of optimal imaging timing. European Journal of Nuclear Medicine. 2016;43:1611–20. doi:10.1007/s00259-016-3419-0.

20. Banerjee SR, Foss CA, Pullambhatla M, Wang Y, Srinivasan S, Hobbs RF, et al. Preclinical evaluation of 86Y-labeled inhibitors of prostate-specific membrane antigen for dosimetry estimates. J. Nucl. Med. 2015;56:628–34. doi:10.2967/jnumed.114.149062.

21. Hsiou-Ting Kuo, J. Pan, K. Lin, H. Merkens, J. Lau, Chengcheng Zhang, et al. Synthesis and Evaluation of 18F-AmBF3-PSMA Derivatives as PET Imaging Agents for Prostate Cancer. 2016.

22. Szabo Z, Mena E, Rowe SP, Plyku D, Nidal R, Eisenberger MA, et al. Initial Evaluation of (18)FDCFPyL for Prostate-Specific Membrane Antigen (PSMA)-Targeted PET Imaging of Prostate Cancer. Molecular Imaging and Biology. 2015;17:565–74. doi:10.1007/s11307-015-0850-8.

23. Ahmadzadehfar H, Wegen S, Yordanova A, Fimmers R, Kürpig S, Eppard E, et al. Overall survival and response pattern of castration-resistant metastatic prostate cancer to multiple cycles of radioligand therapy using 177LuLu-PSMA-617. European Journal of Nuclear Medicine. 2017;44:1448–54. doi:10.1007/s00259-017-3716-2.

24. Ahmadzadehfar H, Rahbar K, Kurpig S, Bogemann M, Claesener M, Eppard E, et al. Early side effects and first results of radioligand therapy with (177)Lu-DKFZ-617 PSMA of castrate-resistant metastatic prostate cancer: A two-centre study. EJNMMI Res. 2015;5:114. doi:10.1186/s13550-015-0114-2.

25. Yordanova A, Becker A, Eppard E, Kürpig S, Fisang C, Feldmann G, et al. The impact of repeated cycles of radioligand therapy using 177LuLu-PSMA-617 on renal function in patients with hormone refractory metastatic prostate cancer. European Journal of Nuclear Medicine. 2017;44:1473–9. doi:10.1007/s00259-017-3681-9.

26. Pillai MRA, Nanabala R, Joy A, Sasikumar A, Russ Knapp FF. Radiolabeled enzyme inhibitors and binding agents targeting PSMA: Effective theranostic tools for imaging and therapy of prostate cancer. Nuclear Medicine and Biology. 2016;43:692–720. doi:10.1016/j.nucmedbio.2016.08.006.

27. Herrmann K, Bluemel C, Weineisen M, Schottelius M, Wester H-J, Czernin J, et al. Biodistribution and radiation dosimetry for a probe targeting prostate-specific membrane antigen for imaging and therapy. J. Nucl. Med. 2015;56:855–61. doi:10.2967/jnumed.115.156133.

28. Das T, Guleria M, Parab A, Kale C, Shah H, Sarma HD, et al. Clinical translation of (177)Lu-labeled PSMA-617: Initial experience in prostate cancer patients. Nuclear Medicine and Biology. 2016;43:296–302. doi:10.1016/j.nucmedbio.2016.02.002.

29. Tesson M, Rae C, Nixon C, Babich JW, Mairs RJ. Preliminary evaluation of prostate-targeted radiotherapy using (131) I-MIP-1095 in combination with radiosensitising chemotherapeutic drugs. J Pharm Pharmacol. 2016;68:912–21. doi:10.1111/jphp.12558.

30. Gaertner FC, Halabi K, Ahmadzadehfar H, Kürpig S, Eppard E, Kotsikopoulos C, et al. Uptake of PSMA-ligands in normal tissues is dependent on tumor load in patients with prostate cancer. Oncotarget. 2017;8:55094–103. doi:10.18632/oncotarget.19049.

31. Emmett L, Willowson K, Violet J, Shin J, Blanksby A, Lee J. Lutetium 177 PSMA radionuclide therapy for men with prostate cancer: a review of the current literature and discussion of practical aspects of therapy. Journal of Medical Radiation Sciences. 2017;64:52–60. doi:10.1002/jmrs.227.

32. Roesch F. Scandium-44: benefits of a long-lived PET radionuclide available from the (44)Ti/(44)Sc generator system. Current Radiopharmaceuticals. 2012;5:187–201. doi:10.2174/1874471011205030187.

33. Rahbar K, Ahmadzadehfar H, Kratochwil C, Haberkorn U, Schäfers M, Essler M, et al. German Multicenter Study Investigating 177Lu-PSMA-617 Radioligand Therapy in Advanced Prostate Cancer Patients. J. Nucl. Med. 2017;58:85–90. doi:10.2967/jnumed.116.183194.

34. Pruszyński M, Majkowska-Pilip A, Loktionova NS, Eppard E, Roesch F. Radiolabeling of DOTATOC with the long-lived positron emitter 44Sc. Appl Radiat Isot. 2012;70:974–9. doi:10.1016/j.apradiso.2012.03.005.

35. Umbricht CA, Benešová M, Schmid RM, Türler A, Schibli R, van der Meulen, Nicholas P., Müller C. 44Sc-PSMA-617 for radiotheragnostics in tandem with 177Lu-PSMA-617-preclinical investigations in comparison with 68Ga-PSMA-11 and 68Ga-PSMA-617. EJNMMI Res. 2017;7:9. doi:10.1186/s13550-017-0257-4.

36. Eppard E, La Fuente A de, Benešová M, Khawar A, Bundschuh RA, Gärtner FC, et al. Clinical Translation and First In-Human Use of 44ScSc-PSMA-617 for PET Imaging of Metastasized Castrate-Resistant Prostate Cancer. Theranostics. 2017;7:4359–69. doi:10.7150/thno.20586.

37. Stabin MG. Fundamentals of Nuclear Medicine Dosimetry 2008. 1st ed. s.l.: Springer-Verlag. doi:10.1007/978-0-387-74579-4_5.

38. Hindorf C, Lindén O, Tennvall J, Wingårdh K, Strand S-E. Evaluation of methods for red marrow dosimetry based on patients undergoing radioimmunotherapy. Acta Oncol. 2005;44:579–88. doi:10.1080/02841860500244294.

39. Sgouros G, Stabin M, Erdi Y, Akabani G, Kwok C, Brill AB, Wessels B. Red marrow dosimetry for radiolabeled antibodies that bind to marrow, bone, or blood components. Medical Physics. 2000;27:2150–64. doi:10.1118/1.1288393.

40. Siegel JA. Establishing a clinically meaningful predictive model of hematologic toxicity in nonmyeloablative targeted radiotherapy: practical aspects and limitations of red marrow dosimetry. Cancer Biotherapy & Radiopharmaceuticals. 2005;20:126–40. doi:10.1089/CBR.2005.20.126.

41. S. Shen, G. Denardo, G. Sgouros, R. O'donnell, S. Denardo. Practical determination of patient-specific marrow dose using radioactivity concentration in blood and body. J. Nucl. Med. 1999.

42. Afshar-Oromieh A, Hetzheim H, Kratochwil C, Benesova M, Eder M, Neels OC, et al. The Theranostic PSMA Ligand PSMA-617 in the Diagnosis of Prostate Cancer by PET/CT: Biodistribution in Humans, Radiation Dosimetry, and First Evaluation of Tumor Lesions. J. Nucl. Med. 2015;56:1697–705. doi:10.2967/jnumed.115.161299.

43. Baum RP, Kulkarni HR. THERANOSTICS: From Molecular Imaging Using Ga-68 Labeled Tracers and PET/CT to Personalized Radionuclide Therapy - The Bad Berka Experience. Theranostics. 2012;2:437–47. doi:10.7150/thno.3645.

44. Singh A, van der Meulen, Nicholas P., Müller C, Klette I, Kulkarni HR, Türler A, et al. First-in-Human PET/CT Imaging of Metastatic Neuroendocrine Neoplasms with Cyclotron-Produced 44Sc-DOTATOC: A Proof-of-Concept Study. Cancer Biotherapy and Radiopharmaceuticals. 2017;32:124–32. doi:10.1089/cbr.2016.2173.

45. Baum RP, Kulkarni HR, Schuchardt C, Singh A, Wirtz M, Wiessalla S, et al. 177Lu-Labeled Prostate-Specific Membrane Antigen Radioligand Therapy of Metastatic Castration-Resistant Prostate Cancer: Safety and Efficacy. J. Nucl. Med. 2016;57:1006–13. doi:10.2967/jnumed.115.168443.

46. Rahbar K, Schmidt M, Heinzel A, Eppard E, Bode A, Yordanova A, et al. Response and Tolerability of a Single Dose of 177Lu-PSMA-617 in Patients with Metastatic Castration-Resistant Prostate Cancer: A Multicenter Retrospective Analysis. J. Nucl. Med. 2016;57:1334–8. doi:10.2967/jnumed.116.173757.

47. Ahmadzadehfar H, Eppard E, Kürpig S, Fimmers R, Yordanova A, Schlenkhoff CD, et al. Therapeutic response and side effects of repeated radioligand therapy with 177Lu-PSMA-DKFZ-617 of castrate-resistant metastatic prostate cancer. Oncotarget. 2016;7:12477–88. doi:10.18632/oncotarget.7245.

48. Pfob CH, Ziegler S, Graner FP, Köhner M, Schachoff S, Blechert B, et al. Biodistribution and radiation dosimetry of (68)Ga-PSMA HBED CC-a PSMA specific probe for PET imaging of prostate cancer. European Journal of Nuclear Medicine. 2016;43:1962–70. doi:10.1007/s00259-016-3424-3.

49. Kabasakal L, AbuQbeitah M, Aygün A, Yeyin N, Ocak M, Demirci E, Toklu T. Pre-therapeutic dosimetry of normal organs and tissues of (177)Lu-PSMA-617 prostate-specific membrane antigen (PSMA) inhibitor in patients with castration-resistant prostate cancer. European Journal of Nuclear Medicine. 2015;42:1976–83. doi:10.1007/s00259-015-3125-3.

50. Okamoto S, Thieme A, Allmann J, D'Alessandria C, Maurer T, Retz M, et al. Radiation Dosimetry for 177Lu-PSMA I&T in Metastatic Castration-Resistant Prostate Cancer: Absorbed Dose in Normal Organs and Tumor Lesions. J. Nucl. Med. 2017;58:445–50. doi:10.2967/jnumed.116.178483.

51. Delker A, Fendler WP, Kratochwil C, Brunegraf A, Gosewisch A, Gildehaus FJ, et al. Dosimetry for (177)Lu-DKFZ-PSMA-617: a new radiopharmaceutical for the treatment of metastatic prostate cancer. European Journal of Nuclear Medicine. 2016;43:42–51. doi:10.1007/s00259-015-3174-7.

52. Benesova M, Schafer M, Bauder-Wust U, Afshar-Oromieh A, Kratochwil C, Mier W, et al. Preclinical Evaluation of a Tailor-Made DOTA-Conjugated PSMA Inhibitor with Optimized Linker Moiety for Imaging and Endoradiotherapy of Prostate Cancer. J. Nucl. Med. 2015;56:914–20. doi:10.2967/jnumed.114.147413.

5.4 Comparison of Tumor Heterogeneity Assessed with Textural Parameters in 68Ga-PSMA PET/CT and 177Lu-PSMA SPECT/CT in Patients with Metastatic Prostate Cancer

Lara Schwarte*1, Lena Thomas1, Elisabeth Eppard1, Michael Meisenheimer1, Christof Weiss-Wichert2, Rolf
Fimmers3, Norbert Zsoter4, Holger Strunk5, Markus Essler1 and Ralph A Bundschuh1
1Department of Nuclear Medicine, Universitaetsklinikum Bonn, Germany
2Mediso GmbH, Germany
[3]Department of Biostatistics, Universitaetsklinikum Bonn, Germany
4Mediso Medical Imaging Systems Ltd, Hungary
5Department of Radiology, Universitaetsklinikum Bonn
Received: November 26, 2018; Published: December 07, 2018
*Corresponding author: Lara Schwarte, Klinik und Poliklinik für Nuklearmedizin, Sigmund-Freud-Str. 25, 53127 Bonn, Germany
http://dx.doi.org/10.26717/BJSTR.2018.11.002161

Abstract

Purpose: Tumor heterogeneity in PET/CT assessed by textural parameters is gaining importance as prospective and predictive feature for multiple clinical applications. Especially in theranostics, PET and SPECT images are often performed in the same patient. Therefore, the aim of this study was to compare, if tumor heterogeneity assessed in PET/CT and SPECT/CT imaging is correlating to each other and results found for tumor heterogeneity assessed in PET may be translated to SPECT imaging. This was evaluated in phantom and patient data.

Subjects and Methods: A self-built heterogeneity phantom as well as 37 patients with metastasized prostate cancer were analyzed. All patients underwent a peptide receptor radionuclide therapy (PRRT, one to four cycles) and received a 68Ga-PSMA PET/CT before and 177Lu-PSMA SPECT/CT directly after each therapy cycle. Both PET/CT and SPECT/CT images were processed with Interview™ Fusion software (Mediso Medical Imaging Systems). The biggest lesions of each patient were selected and manually delineated in both nuclear medicine images. Consequently 36 textural features, including deviation, entropy and different emphases were calculated. In addition, conventional parameters as mean and maximum SUV, and tumor volume were tested as well. Phantom studies were compared directly, and patient data were compared using Bland-Altman Plots.

Results: Overall, 188 metastases in 37 patients were analyzed. In Bland-Altman Plots it was shown that for the majority of the 40 parameters there is no direct comparability between PET/CT and SPECT/CT values. Using the 95% confidence interval, the best parameters could be identified. Long zone low grey level emphasis had a high accordance, 94.7% of the data were contained in 95% confidence interval. For the short zone low grey level emphasis, it was 32.8%, 32.3% for the volume, 34.9% for TLRD, 23.8% for maximum and 21.7% for the mean SUV. Variables such as entropy which are frequently used in tumor heterogeneity have low accordance values. Only 12.2% of the entropy data are contained in the 95% confidence interval. Intensity variation and zone length non-uniformity only have results of 4.2%. Different results were found for the phantom, in which differences in heterogeneity parameters were down to 0.8 % for the best parameter (Zone percentage), also low values were found for Contrast (1.4 %) and Entropy (3.5 %).

Conclusion: This study shows, that in contrast to data obtained by phantom data, in real patients' tumor heterogeneity in PET/CT and SPECT/ CT seems not to be correlating. Therefore, further studies looking in to the clinical value of tumor heterogeneity obtained in SPECT/CT images must be performed in the future to show the values of this modality.
Keywords: Prostate cancer; PSMA-PET/CT; PSMA-SPECT/CT; PRRT; Textural parameters

Introduction

and prognostic information for the individual patient [1]. For different tumor entities it was shown that tumor

Therefore, tumor heterogeneity may be an important step towards heterogeneity is an important factor that can provide predictive

personalized oncologic therapy. As biopsy is not always possible tumor heterogeneity will be evaluated by imaging more often. Even in case a biopsy is performed, one tissue sample can be too less for a complete histopathologic workup, especially assessing heterogeneity [1,2]. Medical imaging methods can be helpful as non-invasive tools to specify tumor heterogeneity. Several texture analyses in computed tomography (CT) have shown good results by quantifying the homogeneity using the structure irregularity: Davnall et al. [3] have published several examples of how medical imaging can be used for tumor heterogeneity. Using CT imaging, Ganehan et al. found patient´s survival can be predicted by tumor heterogeneity in non-small-cell lung cancer [4]. Differentiating between tumor and non-tumor tissue is also possible as Lopes et al. have shown [5]. In their study fractal features in magnet resonance (MR) images of prostate cancer patients

for assessing tissue heterogeneity have been used to distinguish malignant from benign tissue in the prostate [5].

Positron emission tomography (PET) as functional imaging modality seems to have some benefits for assessment of tumor heterogeneity, especially when applied as hybrid technology as PET/CT. Using PET/CT, not only information about morphology can be obtained but also about visualized functionality as metabolism or receptor density for example. By this it is even easier to get information about prognosis and therapy effects. Tixier et al. described that tumor heterogeneity defined by textural analysis can be a predictive parameter for radiation chemotherapy response [6]. They used intra tumoral tracer uptake in [18F]- fluorodeoxyglucose (FDG) PET images of 41 patients with esophageal cancer for their study [6]. In another study tumor heterogeneity assessed in FDG-PET/CT was found to be a strong predictive and prognostic parameter for therapy response and overall survival in patients with colorectal carcinoma [7]. Recently, other radio pharmaceuticals than FDG were found to play an important role in tumor heterogeneity assessed in PET/CT. [18F]-fluoroethyl-L-tyrosine PET to found to differentiate between real progress and pseudo progression in glioblastoma after radio chemotherapy [8]. In a large multicenter evaluation intra tumoral somatostatine receptor heterogeneity was evaluated as prognostic factor for survival after radiopeptid receptor therapy in patients with neuroendocrine tumors [9].

However, to the best of our knowledge, up to now, there is no study investigating the use of single photon emission tomography (SPECT) for assessment of tumor heterogeneity. Especially in patients undergoing radio peptide receptor therapy (PRRT) as in the study by Werner et al. [9] mentioned before patients obtain posttreatment imaging using SPECT technology. As post therapeutic imaging is performed after each cycle of PRRT imaging data would be available faster and at more time points than PET studies in these patients and would therefore be preferable for treatment monitoring if it shows the same predictive and prognostic values. Prostate cancer will strike a large portion of the population as 11.6 % of men will get this diagnose at some point in their life. 9.6% of the newly detected cancers are prostate cancers. The 5-Year relative survival was lifted from 66.0% in 1975 up to 99.3% in 2009 [10]. This big change in survival times can be traced back to the improving screening as well as new treatments options established over the last years. But still there are 26,730 estimated deaths in the US population for 2017 [10]. A recently upcoming treatment in patients with advanced, hormone refractory prostate cancer is radiotherapy with ligands to prostate specific membrane antigen (PSMA) labelled with luthetium-177 [11]. Therefore, the aim of this study was to compare tumor

heterogeneity assessed with textural parameters in PET and SPECT images of patients undergoing treatment and prior PET diagnosis with PSMA ligands.

Materials and Methods

Phantom Study

To simulate a heterogene structure in the phantom, a method first published by Forgacs and colleagues [12] was adapted. Basis for the phantom measurements was a torso phantom according to NEMA NU- 2012 standard with size of 24.1 cm x 30.5 cm x 24.1 cm and a volume of 9.7 liters. Seven 2 ml syringes filled with three different activity concentrations were put together as shown in Figure 1. The syringes were then placed in the torso phantom including background activity (with ratios of 1 to 20, 1 to 15, and 1 to 10 compared to the activity concentration in the syringes). Two settings of these heterogeneity phantoms were used: First it was filled with Gallium-68 in watery solution to simulate the PET/ CT data and the other one was filled with Lutetium-177 in watery solution for the SPECT/CT data. Detailed activity concentrations put in the phantom can be found in Table 1.

Figure 1: Seven 2 ml syringes were put together as shown on the left-hand side to obtain a heterogenic structure as shown on the right-hand side schematically (three different activity concentrations were used to fill the syringes).

Table 1: Activity concentrations that were placed in the syringes and the background for the two different phantom settings. The different activity concentrations have been chosen according to the realistic concentrations to be expected in patient studies.

	^{68}Ga-Phantom	**^{177}Lu-Phantom**
Background	5 kBq/ml	20 kBq/ml
Synringe Group 1	100 kBq/ml	400 kBq/ml
Synringe Group 2	75 kBq/ml	300 kBq/ml

Syringe Groupe 3	50 kBq/ml	200 kBq/ml

Patient Population and Treatment

Thirty-seven patients with metastasized prostate cancer were included in this analysis between February 2015 and April 2016. After the decision of the local tumor conference all patients underwent a [177Lu]-PSMA peptide receptor mediated radionuclide therapy (PRRT). According to consensus recommendation of the Deutsche Gesellschaft für Nuklearmedizin there was a PET/ CT acquired before the first cycle. Every 8 weeks the patients underwent PRRT. Each time a 68Ga-PSMA PET/CT was done before and a 177LU-PSMA SPECT/CT directly after the cycle. Between PET/CT and SPECT/CT was about one week. The patient's median age was 71 years (range 43-82 years), the median Gleason Score was 8 (range 6-10). The number of PRRT cycles differed from one to four (1: n37, 2: n24, 3: n6, 4: n1). This variety in cycles depended on the tolerance and the survival of the patients. During each cycle the median administered activity of 177Lu-PSMA was 6,2 GBq (range 4.1-7.1 GBq). The PSA minimum was 5, the maximum 1030 (median: 178). Due to the retrospective character the ethics statement is waived in our institution by the institutional ethics committee. The patient gave written and informed consents for the treatment and the scientific use of the data.

Gallium-68-DKFZ-PSMA-11 PET/CT Imaging

The PET/CT imaging was-done usinga Biograph 2 PET/CT system (Siemens Medical Solutions, Erlangen, Germany). About 40 to 80 minutes after intravenous injection of in-house produced 68GA-HBED-CC PSMA (105 to 200 MBq, mean 134 MBq) a lowdose CT (16mAs, 130 kV) from the base of skull to mid thighs was acquired. The PET scan was acquired over the same area with 3 or 4 minutes per bed position depending on the body weight of the patient. CT data was reconstructed in 512 to 512 matrices with 5 mm slice thickness. PET data was reconstructed in 128 to 128 matrices with 5mm slices thickness. An attenuation-weighted ordered subsets expectation maximization algorithm was utilized for attenuation and scatter corrections as implemented by the manufacturer using 4 iterations and 16 subsets with a 5 mm post reconstruction Gaussian filter. Same imaging and reconstruction parameters have been used for the acquisition of the phantom data as well.

Lu-177-Imaging

SPECT/CTimaging was performed using a Symbia T2 hybrid SPECT/CT tomograph (Siemens Medical Solutions, Erlangen, Germany). One table position needed 10 minutes using an energy window centered plus/minus 15 % around 208 keV. The window center was acquired as SPECT/CT after a planar whole-body image has been done. CT data was reconstructed in 512 to 512 matrices with 5mm slice thickness. SPECT data was reconstructed in 128 to 128 matrices, also with a slice thickness of 5 mm. For SPECT reconstruction the iterative algorithm implemented by the manufacturer was used including attenuation correction based on the CT data using 4 iterations and 16 subsets and as 5 mm post reconstruction Gaussian filter. Due to staff arrangement the PET/CT and the SPECT/CT have been done from different operators. Same imaging and reconstruction parameters have been used for the acquisition of the phantom data as well.

Data Analysis and Statistical Analysis

Both PET/CT and SPECT/CT images were processed with Interview TM Fusion software (Mediso Medical Imaging Systems Ltd., Hungary). In the phantom data as well as in the patient data lesions were delineated manually, if more than 3 lesions were present, the three biggest lesions were chosen. Delineation was performed on the emission image for both the PET/CT and the SPECT/CT. Consequently, in the delineated volume 36 textural features, including deviation, entropy and different emphases were calculated by the software. The conventional parameters as tumor mean, maximum standardized uptake value (SUV max), tumor volume and total lesion glycolysis (TLG) which is the product of tumor volume and mean uptake, were tested as well. Through this, a comparison between the two imaging methods was made. Chicklore et al. have described the textural parameters in detail [13].

For the phantom data the direct comparison of the values was performed presenting absolute and relative differences. In contrast to this, in patient data Bland-Altman Plots were applied which show the comparison between the same parameters in PET/CT and SPECT/CT. In these Bland- Altman Plots the 95% confidence intervals were calculated. Through this approach it could be determined whether there was a direct comparability between PET/CT and SPECT/CT. All statistical analysis was done using IBM SPSS Statistics 24.

Results:

Phantom

Using the heterogeneity values for PET/CT and SPECT/CT in the different parameters the absolute and relative difference were calculated. Low differences can be shown for

entropy (3.5%), contrast (1.4%) and zone percentage (0.8%). Correlation, size variation and gray level non -uniformity shows values over 18% (18.2%, 18.9% and 18.9%). The most significant results are presented in Table 2. The remaining 20 parameters not mentioned in the table showed differences >20%. A higher heterogeneity was found in PET compared to SPECT.

Patient Population

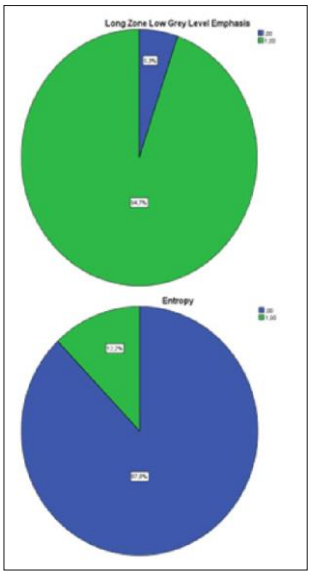

Figure 2: Pie chart of patient data, green marks the 95% confidence interval.

In PET/CT and SPECT/CT images around the first cycle 104 metastases from 37 patients were marked. The mean volume of these metastases was 27.7 ml (range 1.3 to 265.3 ml). In the following cycles the same metastases were identified and delineated if still verifiable. In the second cycle only 65 metastases could be identified, 17 in the third and just 3 in the last one because only one patient of the included patients underwent four treatment cycles. So overall 188 lesions could be detected in four cycles. Using the Bland-Altman Plots and the 95% confidence intervals, it was determined that some parameters had a high consensus (Figures 2 & 3). Long zone low grey level emphasis was the parameter with the highest accordance. 94.7% of the data were contained in the 95% confidence interval. Other parameters with good results were the TLG (34.9%), short zone low grey level emphasis (32.8%) and the volume (32.3%). The conventional parameters as mean and max had lower results. Mean with 21.7% and max with 23.8% in

Table 2: Phantom results.

Parameter	PET	SPECT	Abs. Difference	Rel. Difference
Entropy	6.94	6.70	0.24	3.5%
Homogeneity	0.262	0.225	0.037	14.2%
Correlation	0.773	0.632	0.141	18.2%
Contrast	72.3	73.3	1.0	1.4%
Size Variation	0.0312	0.0371	0.0059	18.9%
Short Zone Emphasis	0.775	0.870	0.095	12.3%
Gray-Level Non-Uniformity	0.0312	0.0371	0.0059	18.9%
Zone Percentage	0.239	0.237	0.002	0.8%
Short Run Emphasis	0.596	0.694	0.098	16.4%

Table 3: Patient results.

Textural feature	% included in the 95% confidence level
Intensity Variation	4.2
Zone Length Non Uniformity	4.2
Short Zone Emphasis	6.9
Complexity	7.4
Long Run High Grey Level Emphasis	8.5
Zone Percentage	9.0
Run Percentage	9.5
Long Zone Emphasis	10.6
Long Run Emphasis	10.6
Homogeneity	11.1
Contrast	11.1
Short Run Emphasis	11.1
Long Zone High Grey Level Emphasis	11.6

Minimum	12.2
Entropy	12.2
Correlation	12.2
Short Zone High Grey Level Emphasis	13.2
Run Length Non Uniformity	13.2
Gray Level Non Uniformity	13.8
Sum	14.3

the 95% confidence level. The entropy frequently used in tumor heterogeneity only achieved a low level (12.2%). The lowest results in this study have the zone length non-uniformity and the intensity variation both with only 4.2%. The results of these measurements are presented in Figure 2 and Tables 2 & 3.

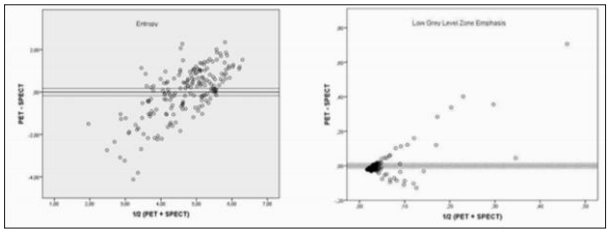

Figure 3: Bland-Altman Plots of patient data for Entropy (top) and Low Gray Level Zone Emphasis (bottom).

High Grey Level Run Emphasis	14.3
Size Variation	14.8
Busyness	14.8
Gray Level Non Uniformity	14.8
Short Run High Grey Level Emphasis	14.8
High Grey Level Zone Emphasis	15.3
Maximal Diameter	17.5
Coarseness	18.0
Kurtosis	19.0

Short Run Low Grey Level Emphasis	19.6
Mean SUV	21.7
Deviation	22.2
Low Grey Level Run Emphasis	22.8
Maximum	23.8
Long Run Low Grey Level Emphasis	25.9
Low Grey Level Zone Emphasis	28.0
Volume	32.3
Short Zone Low Grey Level Emphasis	32.8
TLG	34.9
Long Zone Low Grey Level Emphasis	94.7

Discussion

In this study, we analyzed whether tumor heterogeneity in PET/CT and SPECT/CT imaging using PSMA-ligands is comparable. The data obtained by phantom studies showed a high correlation ($p<0.01$) in some parameters like entropy and contrast. As these parameters have shown prognostic and predictive value in previous studies [3-8], this could be an advantage for individual treatment decisions in the course of therapy after each treatment cycle as SPECT images can be done using the therapeutic activity without additional absorbed dose and cost for the patient. Therefore, this could be used as a prognostic factor equivalent to heterogeneity assessed in PET images. Several other studies (1;4-9) proved that benefit. However, the results of our study with a cohort consisting of 37 patients were different. Big discrepancies between the individual parameters have been found. Even within one category of parameters a large discrepancy was detected in 95% confidence intervals. The long zone low grey level emphasis had 94.7% of the data in contained in the 95% confidence interval, while the short zone low grey level emphasis contained only 32.8%.

This study has some limitations which the reason for may be this discrepancies in the patient cohort. The metastases were delineated manually. It is not clear how big the influence of the interobserver variability to the heterogeneity is. But with this high ranges in 95% confidence levels we assume that little mistakes in marking the lesions would not

have changed the results perceptible. Furthermore, the discrepancy between two parameters from the same imaging modality can also not be clarified by mistakes in manually marking the lesions because each parameter is the result of the same measurement. Delineating the lesions both on PET/CT and SPECT/CT images separately, small deviations in the parameters can be produced but these small deviations can not be responsible for non-correlation tumor heterogeneity in our patients. PET/CT images were acquired approximately one week before SPECT/CT images. In the week between the patients received their PRRT. Potential changes in the tumor due to the additional week time and the treatment itself may be the reason for these differences and should be investigated further. The operators for the PET/CT and the SPECT/CT were not the same. Both operators are well instructed with the equipment, so we think this point does not have a big influence on the quality of the pictures.

Our study was performed with a limited number of 37 patients. The significance of the results of such a small group of patients must be considered. Tixier et al. conducted a study [14] with only 16 patients and their results were that textural parameters are reproducible. That should be an incentive to perform other studies with higher patient number to verify how significant the results are. Before our analyses with real patient data we received data obtained by phantoms which had great results with small relative differences as 0.8 % for zone percentage, 1.4 % for contrast and 3.5 % for entropy. It is striking, that parameters such as entropy which have been shown in other studies as the most important textural parameters [6] have such low 95% confidence intervals in our study as entropy with just 12.2%. Variables like this are frequently used in tumor heterogeneity and now have low accordance values in PET/CT and SPECT/CT. Normally they are used in only one imaging method. For the PET/CT we used 68Ga-PSMA and for the SPECT/ CT 177Lu-PSMA. Both are ligands to prostate specific membrane antigen, but both have different pharmacological properties [15]. So, we can assume that one of the two methods is more accurate than the other in marking every tumor cell of the prostate cancer.

Also, it must be mentioned, that PET data is normally acquired between 40 to 80 minutes after injection of the tracer while SPECT data was acquired about 24 hours after the treatment was performed. Not only the PSMA differs in PET/CT and SPECT/CT but also the spatial resolution. The volume of the tumor metastases that were marked and analyzed in this study may vary because of these two differences in PET/CT and SPECT/CT.

Conclusion

Tumor heterogeneity in PET/CT and SPECT/CT in patients is not correlating in contrast to the data obtained by phantoms. While some parameters, such as the long zone low grey level emphasis have high correlations (94.7%) other parameters as intensity variation have very low results (4.2%). The gap between short zone low grey level emphasis with 32.8% and the long zone low grey level emphasis with 94.7% is remarkable.Therefore, results obtained for textural as prognostic and predictive markers in PET/CT can not be simply transferred to SPECT/CT data. The importance and necessity of studies correlating heterogeneity assessed in SPECT/ CT data with clinical findings is still given.

Declarations

Ethics Approval and Consent to Participate

Due to the retrospective character the ethics statement is waived in our institution by the institutional ethics committee. The patient gave written and informed consents for the treatment and the scientific use of the data.

Consent for Publication

Not applicable

Availability of Data and Material

The data sets generated during and/or analyzed during the current study are not publicly available due to data privacy protection laws but are available from the corresponding author on reasonable request and within the boundaries of German privacy protection law.

Funding

No third party funding was available for this work.

Authors Contributions

LS carried out the patient data analysis and wrote the manuscript, LT performed the phantom studies and the data evaluation of the phantom studies, EE and MM provided radioactivity used for the phantom studies and helped filling the phantom, CWW was involved in the conception of the study, RF did perform statistical analysis, NZ coded the software for analysis of textural parameters, HS and ME corrected the manuscript, RB made the concept for the study and wrote parts of the manuscript.

Competing Interests

RB is Consultant for Bayer Healthcare (Leverkusen, Germany) and Eisai GmbH (Frankfurt, Germany). RB has a non-commercial research agreement and is on the speakers list with Mediso Medical Imaging (Budapest, Hungary). CWW and NZ are employed by Mediso Medical Imaging (Budapest, Hungary). All other authors had no conflicts of interest to disclose.

References

1. Gerlinger M, Rowan AJ, Howrswell S, M Math, James Larkin, et al. (2012) Intratumor heterogeneity and branched evolution revealed by multiregion sequencing. N Engl J Med 366: 883-892.
2. Yang Z, Tang LH, Klimstra DS (2011) Effect of tumor heterogeneity on the assessment of Ki67 labeling index in well-differentiated neuroendocrine tumors metastatic to the liver: implications for prognostic stratification. Am J S rg Pathol 35(6): 853-860.
3. Davnall F, Yip CD, Ljungqvist G, Selmi M, Ng F, et al. (2012) Assessment of tumor heterogeneity: an emerging imaging tool for clinical practise? Insights Imaging 3(6): 573-589.
4. Ganeshan B, Panayiotou E, Burnand K, Dizdarevic S, Miles K (2012) Tumour heterogeneity in non -small cell lung carcinoma assessed by CT texture analysis: a potential marker of survival. Eur Radiol 22: 796-802.
5. Lopes R, Ayache A, Makni N, Puech P, Villers A, et al. (2011) Prostate cancer characterization on MR images using fractal features. Med Phys 38(1): 83-95.
6. Tixier F, Le Rest CC, Hatt M, Albarghach N, Pradier O, et al. (2011) Intratumor heterogeneity characterized by textural features on baseline 18F-FDG PET images predicts response to concomitant radiochemotherapy in esophageal cancer. J Nucl Med 52(3): 369-378.
7. Bundschuh RA, Dinges J, Neumann L, Seyfried M, Zsótér N, et al. (2014) Textural Parameters of tumor heterogeneity in 18F-FDG PET/CT for therapy response assessment and prognosis in patients with loally advanced rectal cancer. J Nucl Med 55(6): 891-897.
8. Kebir S, Khurshid Z, Gaertner FC, Essler M, Hattingen E, et al. (2017) Unsupervised consensus cluster analysis of [18F]-fluoroethyl-Ltyrosine positron emission tomography identified textural features for the diagnosis of pseudoprogression in high-grade glioma. Oncota get 8(5): 8294-8304.
9. Werner RA, Lapa C, Ilhan H, Higuchi T, Buck AK, et al. (2017) Surviaval prediction in patients undergoing radionuclide therapy based on intratumoral somatostatin-receptor heterogeneity. Oncotarget 8(4): 7039-7049.
10. National Cancer Institute, Surveillance, Epidemiology, and End Results Program, Cancer Stat Facts: Prostate Cancer.
11. Virgolini, Kiljunen T, Joensuu T, Kairemo K, Uprimny C, et al. (2017) 177Lu-PSMA-617 radioligand therapy for patient with lymph node metastatic prostate cancer. Oncotarget 8(39): 66112-66116.

12. Forgacs, Hermann Pall Jonsson, Magnus Dahlbom, Freddie Daver, Matthew D DiFranco, et al. (2016) A study on the Basic Criteria for Selecting Heterogeneity Parameters of F18-FDG PET images. PloS One 11(10): e0164113.
13. Chicklore S, Goh V, Siddique M, Roy A, Marsden PK, et al. (2013) Quantifying tumor heterogeneity in 18F-FDG PET/CT imaging by texture analysis. Eur J Nucl Med Mol Imaging 40(1): 133-140.
14. Tixier, Hatt M, Le Rest CC, Le Pogam A, Corcos L, et al. (2012) Reprodicibility of tumor uptake heterogeneity characterization through textural feature analysis in 18F-FDG PET. J Nucl Med 53(5): 693-700.
15. Umbricht CA, Martina Benešová, Raffaella M Schmid, Andreas Türler, Roger Schibli, et al. (2017) 44Sc-PSMA-617 for radiotheragnostics in tandem with 177Lu-PSMA-617 - preclinical investigations in comparison with 68Ga-PSMA-11 and 68Ga-PSMA-617. EJNMMI Res 7: 9.

6. **Weitere Projekte**

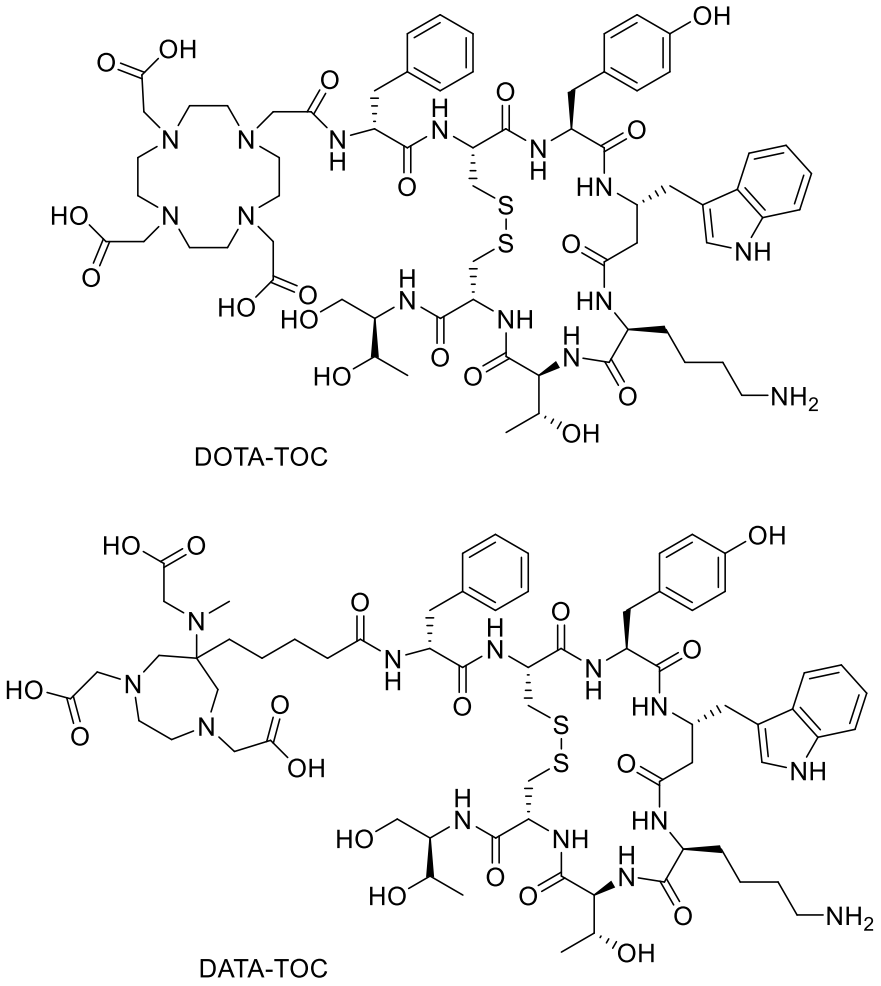

Abbildung 23: Schematische Darstellung der Tracer DATA-TOC und DOTA-TOC.

Somatostatin-Rezeptoren (SSTR) gehören zur Gruppe von G-Protein-gekoppelten Rezeptoren, die in Neuronen und endokrinen Zellen vorkommen und eine hohe Dichte im Gehirn, in peripheren Neuronen, in der endokrinen Pankreas und im Gastrointestinaltrakt aufweisen. Die meisten Neuroendokrinen Tumore (NET) überexprimieren SSTRs, die als Targets für die Bildgebung und Radionuklidbehandlung verwendet werden können. NET sind eine heterogene Gruppe verschiedener Neoplasmen, die in den Zellen neuroendokrinen Ursprungs in vielen verschiedenen Organen entstehen, am häufigsten jedoch im Gastrointestinaltrakt und in der Lunge. Da die metabolische Stabilität von natürlichem Somatostatin sehr gering ist, wurden synthetische Analoga mit wesentlich höherer Stabilität entwickelt wozu unter anderem DOTA-TOC und DATA-TOC zählen.

6.1 Manual vs. automated 68Ga-radiolabeling - a comparison of optimized processes

Michael Meisenheimer[1,2], Stefan Kürpig[1], Markus Essler[1], Elisabeth Eppard[2]

[1]Department of Nuclear Medicine, University Hospital Bonn, D-53127 Bonn, Germany

[2]PositronPharma, Providencia, Santiago de Chile, Chile

https://doi.org/10.1002/jlcr.3821

* Correspondence: michael.meisenheimer@ukbonn.de; Tel.: +49-228-287-16897

Abstract

A critical factor for clinical practice is the production of ^{68}Ga-radiopharmaceuticals manufactured manually or through an automated procedure. ^{68}Ga-radiopharmaceuticals are often prepared manually, although this method can lead to an increased operator´s radiation dose and potential variability within production.

The present work compares ^{68}Ga-radiolabeling (PSMA-11; DOTA-TOC) utilizing a cassette module (GAIA; Elysia-Raytest; Germany) with a manual setup for routine clinical production with regard to process reliability and reproducibility.

A total 837 routine production batches from 2015-2017 were retrospectively analysed. PSMA-11 and DOTA-TOC were radiolabeled with gallium-68 manually as well as on a cassette module system. Quality control, as well as statistical analysis were performed.

There were significant differences between these production processes in terms of radioactivity yield (AY) and radiochemical yield (RCY), as well as process duration. For, e.g., [^{68}Ga]Ga-PSMA-11 the average difference between manual and automated process is 6.7 min (process duration), 17.5 % (AY) and 10.2 % (RCY).

The automated process is superior to manual method in all categories and presents significant improvements of ^{68}Ga-radiolabeling for routine clinical production in terms of reliability and reproducibility with the additional advantage of reduced operator's radiation exposure.

Keywords: Gallium-68; Clinical routine; DOTA-TOC; PSMA-11; Automation; Cassette module

Introduction

In recent years, the application of ^{68}Ga-radiopharmaceuticals has increased for positron emission tomography (PET) imaging in research as well as in clinical practice. Gallium-68 is available from a ^{68}Ge/^{68}Ga-generator due to its convenient nuclear properties. Its radiolabeling potential with cyclic conjugates and its short half-life ($T_{1/2}$ = 67.71 min) qualifies it for PET imaging with probes of short biological half-life [1].

The rise of gallium-68 started with the development of somatostatin analogue edotreotide (DOTA-TOC), which targets tumours overexpressing somatostatin receptors [2]. Rapid accumulation in neoplastic tissue and fast clearance from healthy organs enables the delivery of a high dose of radiation on the target site and thus preserves the surrounding healthy tissue [3]. DOTA as chelator makes it possible to apply the same molecule for diagnosis and therapy simply by the choice of radionuclide. This so-called theranostic approach, nowadays well established with gallium-68/lutetium-177 as diagnostic/therapeutic pair, initiated the growing interest in radiometals for clinical application beyond technetium-99m.

With the introduction of PSMA-11 and PSMA-617 for prostate cancer theranostics [4, 5], a second boom of the still exotic PET radionuclide gallium-68 started. Prostate cancer (PC) is one of the most common causes of cancer-related mortality in western societies [6]. Prostate specific membrane antigen (PSMA) is a transmembrane molecule in prostate tissue and highly overexpressed in prostate cancer [7, 8]. Its extracellular N-terminal part, containing the catalytic domain, is suitable for selective tumour targeting [9]. Due to the low expression of PSMA in healthy tissue, with the exception of salivary and lacrimal glands, high-dose radioligand therapy (RLT) is possible. As low-molecular weight compounds presented very promising properties as prostate cancer imaging agents [10–13] urea-based peptidomimetic inhibitors with a high affinity to PSMA were developed. From those potent agents the DOTA derivative PSMA-617 emerged as a powerful theranostic tool for prostate cancer. Both compounds, PSMA-11 and PSMA-617 are now well established in clinical practice.

One of the critical factors in clinical practice is the production of a radiopharmaceutical. In many cases, preparation of ^{68}Ga-radiopharmaceuticals is still manual (Figure 12), although this method would not be adequate for routine clinical applications. The two main problems are the radiation dose to the operator to and potential variability within production.

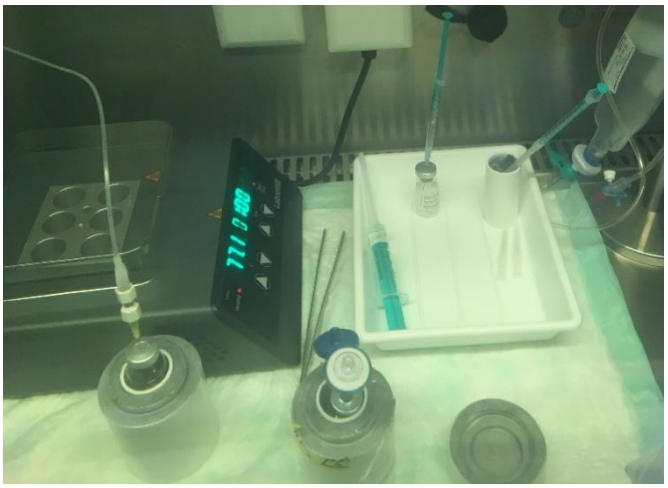

Figure 12: Example setup of a manual ^{68}Ga-radiolabeling for clinical practice.

To avoid these problems in clinical routine two general concepts were established. Using: (1) synthesis modules and most recently (2) radiolabeling single vial cold kits. Both concepts should guarantee an easy, safe and reliable production of ^{68}Ga-radiopharmaceuticals with stable high yields and pharmacopoeia compliant product quality.

The radiolabeling kits should make the production of ^{68}Ga-radiopharmaceuticals as easy as the production of ^{99m}Tc-radiopharmaceuticals. As stated by the European Pharmacopoeia (Ph. Eur.) in general chapter “Extemporaneous Preparation of Radiopharmaceuticals” is the marketing authorisation holder of a licensed kit responsible to ensure that the kit complies with the requirements of its marketing authorisation, while the radiopharmacy using that licensed kit carries the responsibility for the quality of the preparation and the handling. If the instructions for use are not strictly followed or if one or more components used for the preparation do not have marketing authorisation it is the responsibility of the radiopharmacy to demonstrate that the quality of the final preparation is suitable for the intended use [14].

Consequently, preparation as well as quality control of a licensed kit require at least the equipment according to the instructions provided by the manufacturer. In addition, minimum contaminated waste materials remain. It has to be noted that this is only true for licensed kits in combination with a licensed generator. In contrast, unlicensed kits or a licensed kit used with an unlicensed generator also requires quality control according to the monograph and additionally, local authorities may require more detailed quality control even for licensed kits.

Admittedly, those kits contain relatively high amounts of precursor and additional filler materials, still require manual handling and are not available for most precursors and applications. Up to now, only cold kits for radiolabeling PSMA-11 (e.g. illumet™) and DOTA-TOC (e.g. NETSPOT®; TOCScan) are commercially available. In addition, the use of unpurified generator eluates require very strict specifications for the generators in terms of ^{68}Ge-breakthrough to avoid radionuclidic impurities in the final product. Nevertheless, they are a possibility for small sites to offer ^{68}Ga-radiopharmaceuticals to their patients without great expense.

Compared to kit preparations, the synthesis module-based production (Figure 13) requires a fully equipped laboratory and quality control. Starting with the increased use of gallium-68 in nuclear medicine automation of the traditional manual synthesis was promoted. Today those systems are designed with respect to Good Manufacturing Practice Guidelines provided for example by the FDA, EU/EMA, ICH, WHO or others [15]. They use software and methods designed to minimize user interventions and utilize single-use consumables produced under GMP standard.

Accordingly, the amount of contaminated waste materials is higher due to the procedure as well the complete quality control. Nevertheless, these systems are suitable for a variety of tracers and in most cases for several radionuclides (e.g. Scintomics GRP series; Eckert & Ziegler Modular-Lab PharmTracer; Trasis AllInOne). Additionally, the module system enhances the production process in terms of higher reliability and reduced variability [3, 16, 17].

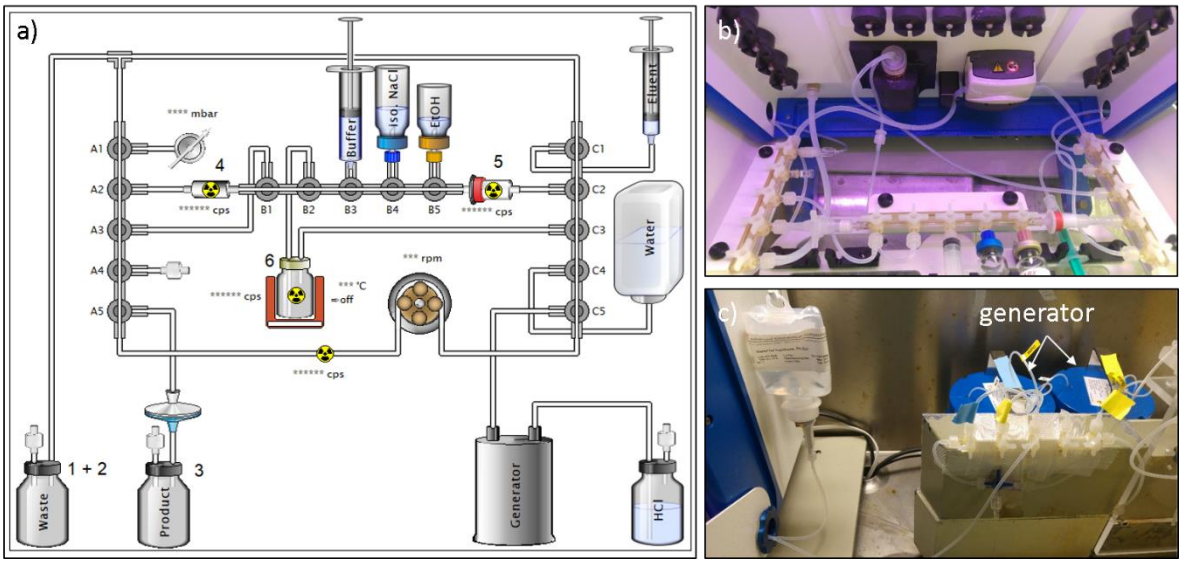

Figure 13: Example for an automated module system used in clinical routine (GAIA, Elysia-Raytest). (a) Screenshot of the graphical user interface of module showing the method used. (b) Cassette mounted in the open module. (c) Module-generator setup in the hot cell.

The present work focuses on the advantages of a commercial automated cassette module for the radiolabeling of bioconjugates with gallium-68 in clinical practice compared to the manual radiolabeling. Both compounds applied (DOTA-TOC; PSMA-11) were produced in our nuclear medicine frequently using a manual method which was optimized for our site-specific needs. The replacement by a module was indispensable to satisfy the authorities and improve staff radiation safety. This retrospective study compares the site-specific optimized standard manual procedure with the standard process given by the manufacturer and a site-specific adjusted.

Performance evaluation of the module used was in terms of AY and RCY. The yields AY and RCY were measured for reliability and reproducibility of the process.

Materials and Methods

Automated Synthesis

Gallium-68 was obtained from a 1.85 GBq $^{68}Ge/^{68}Ga$-generator (iThemba Labs, South-Africa). Synthesis was performed on the automated cassette module GAIA from Elysia-Raytest (Straubenhardt, Germany), utilizing the standard radiolabeling methods. The detectors of the synthesis module were calibrated with a dose calibrator (ISOMED 2010, MED Nuklear-Medizintechnik Dresden GmbH, Dresden, Germany) as reference. DOTA-

TOC, PSMA-11, standard fluidic and reagent kit (contains all consumables necessary except peptide) for gallium-68 radiolabeling of peptides, all GMP-grade, were purchased from ABX advanced biochemical compounds (Radeberg, Germany). The SCX included in the reagent kit was replaced by 200 mg Strata SCX (Phenomenex, USA). Optimization of the constitution of the reaction mixture occurred with regard to the different SCX and optimum pH for the respective precursor. Automated synthesis includes subsequent C18 purification as well as sterile filtration. Ethanol Ph. Eur. was purchased from Merck (Darmstadt, Germany).

44.88±5.54 µL DOTA-TOC (1 mg/mL) were radiolabeled in 3.35±0.19 mL ammonium acetate buffer (0.08 M; reagent kit), 473.13±24.46 µL eluent (reagent kit) and 200 µL ethanol with 1.292±0.385 GBq gallium-68. After radiolabeling (94±2 °C; 479.1±12.2 s), the reaction mixture (total volume of 4.07±0.22 mL) was diluted with 5 mL water (ethanol concentration ~2 %). The diluted reaction mixture subsequently passed over a C_{18} cartridge and washed with water. The purified product eluted with 1.5 mL 60 vol% ethanol followed by 8.5 mL saline and sterile filtered to obtain the final formulation.

25.79±4.27 µL PSMA-11 (0.1 mg/mL) were radiolabeled in 3.65±0.16 mL ammonium acetate buffer (0.08 M; reagent kit), 460.19±19.03 µL eluent (reagent kit), and 201.69±22.93 µL ethanol with 1.289±0.233 GBq gallium-68. After radiolabeling (85±2 °C; 310±9 s), the reaction mixture (total volume of 4.44±0.21 mL) was diluted with 5 mL water (ethanol concentration ~2 %). The diluted reaction mixture subsequently passed over a C_{18} cartridge and washed with water. The purified product eluted with 1.5 mL 60 vol% ethanol followed by 8.5 mL saline and sterile filtrated to obtain the final formulation.

Manual Synthesis

Gallium-68 was obtained from a 1.85 GBq $^{68}Ge/^{68}Ga$-generator (iThemba Labs, South-Africa). The eluate was post-processed using ethanol based post-processing as previously described [18]. The manual synthesis was carried out in a MHR 13 thermo shaker (Hettich-Benelux, Geldermalsen, Netherlands) at a temperature of 95°C. After addition of the ^{68}Ga-eluate (composition 90 vol% ethanol/10 vol% 0.9 N HCl) to the reaction mixture pH was measured and adjusted if needed. 3 M ammonium acetate solution as well as solutions for ^{68}Ga-post-processing were produced in house.

55.89±7.81 µL DOTA-TOC (1 mg/mL) were radiolabeled in 0.93±0.17 mL ammonium acetate solution and 1.02±0.14 mL eluate containing 1.294±0.455 GBq gallium-68 at a pH of 3.6-3.8. The reaction mixture was diluted with water a.i. and passed over a C18

cartridge. The final product was eluted with 1.5 mL 60 vol% ethanol followed by 8.5 mL saline solution and sterile filtrated into the product vial.

43.70±19.30 µL PSMA-11 (0.1 mg/mL) were radiolabeled in 1.00±0.08 mL ammonium acetate solution and 1 mL eluate containing 1.368±0.353 GBq gallium-68 at a pH of 4-4.2. The reaction mixture was diluted with 8 mL saline and sterile filtrated into the final product vial.

Quality Control

For quality control, an aliquot of 50 µL was retained from the final product before measurement of radioactivity. All chemicals were pure or analytical grade and used as received, unless otherwise specified. Radioactivity of the final product was measured with a dose calibrator (ISOMED 2010, MED Nuklear-Medizintechnik Dresden GmbH, Dresden, Germany). RCP was determined using silica-gel coated aluminium TLC-plates (silica 60 F254.5X4.5 cm Merck, Darmstadt, Germany), as well as glass microfiber chromatography paper impregnated with silica-gel (iTLC-SG, Agilent Technologies, Santa Clara, California) and analysed using a single trace radioTLC-scanner (PET-miniGita, Elysia-Raytest, Straubenhardt, Germany) and evaluation software (Gina Star TLC, Elysia-Raytest, Straubenhardt, Germany). For DOTA-TOC, iTLC-strips were developed in 0.1 M citric buffer (pH 4, Merck, Darmstadt, Germany) as well as in 1 M ammonium acetate/methanol (1:1), for PSMA-11 a TLC-strip was developed in 0.1 M citric buffer (pH 4, Merck, Darmstadt, Germany) and an iTLC-strip in 1 M ammonium acetate/methanol (1:1). Additionally, radioHPLC was used to determine the radiochemical purity (RCP) and identification of the product species. RadioHPLC was performed utilizing Agilent 1260 Infinity II reverse phase HPLC system (Agilent Technologies, Santa Clara, California) equipped with Gabi γ-HPLC flow detector (Elysia-Raytest, Straubenhardt, Germany) and a PC interface running Gina Star (Elysia-Raytest, Straubenhardt, Germany). A Nucleodur 100-3 C18 ec 125/4 column (Macherey-Nagel GmbH & Co. KG, Düren, Germany) was used. The gradient utilized mobile phase A (deionized water + 0.01 % TFA) and mobile phase B (acetonitrile + 0.01 % TFA). Flow rate was 0.7 mL/min starting with 100 % A /0 % B to 0 % A/100 % B within 20 min. Afterwards, gradient parameters change to 50 % A/50 % B within 5 min. pH was measured using pH-indicator strips MColorpHast 2.0-9.0 (Merck, Darmstadt, Germany). The approximate half-life of gallium-68 was determined using the dose calibrator (ISOMED 2010, MED Nuklear-Medizintechnik Dresden GmbH, Dresden, Germany). The energy of gallium-68 and germanium-68 content were measured using a multi-channel-analyser for γ-spectroscopy (MUCHA, Elysia-

Raytest. Straubenhardt, Germany). Appearance was checked visually. Filter integrity was tested with GAIA (Elysia-Raytest, Straubenhardt, Germany).

Calculations

Radiochemical purity (RCP) was determined by radioTLC and radioHPLC unless otherwise stated.

AY as well as RCY were calculated in two different ways. First, based on the activity trapped on the SCX, activity trapped on C18 and remaining activity on C_{18} after final formulation, all measured during the process with the detector included in the module. Second based on the activity of the final product vial, measured using a dose calibrator, and the activity trapped on SCX as determined by the detector included in the module. Unless otherwise stated AY and RCY presented were calculated with method one.

$t_{process}$ was calculated based on the time points obtained when measuring the final product activity and the activity trapped on the SCX (module) or measured in the eluate (manual method). $t_{process}$ depends on the setup of the module and the time needed transferring the final product to the dose calibrator and is therefore site-specific.

Volume activity (A_v) and apparent molar activity were calculated based on activity of the final product measured with the dose calibrator.

Statistics were calculated with PRISM Version 8.0.2. All data (based on the revised data set) are expressed as mean ± SD. Groups were compared using the t-test. All statistical tests are two tailed, with a p-value of 0.05 representative for significance.

Results

In the present study reliability and reproducibility of automated radiolabeling were compared to manual radiolabeling. All data obtained from routine clinical production were retrospectively analysed with regard to these questions. Automated radiolabeling was performed using a cassette module system (GAIA, Elysia-Raytest. As the present study focuses on the module performance, module independent parameters were not discussed in detail.

[^{68}Ga]Ga-DOTA-TOC

A data set of 306 batch records consisting of 47 manual and 259 automated synthesis were analysed (Table).

Table 1: Comparison of GAIA and manual synthesis data for [^{68}Ga]Ga-DOTA-TOC including and excluding non-process related production failures.

		Complete data set				**Revised data set**			
		GAIA		**Manual**		**GAIA**		**Manual**	
		M	***SD***	***M***	***SD***	***M***	***SD***	***M***	***SD***
Process	***n***	*259*		*47*		*229*		*34*	
	A_{Start} [GBq]	*1.292*	*0.385*	*1.294*	*0.455*	*1.304*	*0.388*	*1.300*	*0.257*
	$A_{Product}$ [GBq]	*0.915*	*0.276*	*0.655*	*0.277*	*0.963*	*0.236*	*0.714*	*0.257*
	$t_{Process}$ [mm:ss]	*18:35*	*5:53*	*22:52*	*3:47*	*18:19*	*5:41*	*22:21*	*2:50*
	***AY [%]*[1]**	*78.4*	*15.2*	*55.2*	*20.2*	*81.0*	*11.1*	*62.3*	*13.1*
	***RCY [%]*[2]**	*89.1*	*17.4*	*69.5*	*19.7*	*92.2*	*12.7*	*74.4*	*16.3*

[1]non decay corrected; [2]decay corrected

The mean (M) starting activities and corresponding standard deviations (SD) are in the same range for both automated and manual synthesis.

There are significant differences between both methods for process duration. Conducting the manual method leads to the final product within an average of 22:52±3:47 min compared to 18:35±5:53 min with the automated method (Table)

The significantly lower yield of 55.2±20.2 % (AY) for the manual method vs to 78.4±15.2 % (AY) for the automated process reflects the prolonged synthesis duration and process variabilities. Similar results were found for the process duration independent decay corrected yields (RCY), 69.5±19.7 % for the manual method vs to 89.1±17.4 % for the automated process.

Admittedly, the data set includes data from all batches produced independently from the cause of failed synthesis. This affects the standard deviation, the measures of reliability and reproducibility, as well as the AY, the measure for suitability and RCY and the measure for performance of the entire process. As the goal was to compare two processes, the data set was analysed again to determine the causes of the particular failed synthesis. A failure is a synthesis producing a final product not fulfilling the product specification (based on the monograph for [^{68}Ga]Ga-DOTA-TOC of the European Pharmacopoeia [14]). It did not matter whether further purification was possible or not. Causes of failed synthesis where identified and classified in process related (e.g. malfunctioning solution

transfer) and non-process related (e.g. low peptide quality). Exclusion of data of non-process related failed synthesis leads to the revised data set.

Overall data of 43 synthesis (13 manual; 30 GAIA) where excluded. This means removal of 14.1 % (27.7 % manual, 11.6 % GAIA) failed syntheses induced by non-process related causes. Non-process related causes observed were low peptide quality, incorrect or poor preparation of the synthesis by the operator, a damaged generator and a power failure in the building. There are 0 failed synthesis in the revised data set for both methods.

As shown in Table , both processes starting activities and process duration are nearly unaffected (22:21±2:50 min manual; 18:19±5:41 min GAIA). The mean values for AY and RCY increase whereas the standard deviation drops, from 55.2±20.2 % to 62.3±13.1 % (AY) and 69.5±19.7 % to 74.4±16.3 % (RCY) for the manual and 78.4±15.2 % to 81.0±11.1 % (AY) and 89.1±17.4 % to 92.2±12.7 % (RCY) for the automated procedure, while synthesis duration remains nearly unaffected.

Within the evaluation period, the automated process was customized with two adjustments to improve radiolabeling. The manual method remained unchanged for all batches performed.

First, substitution of the Agilent SCX cartridge, provided with the kit, by Phenomenex SCX cartridge. Second, additional 5 vol% ethanol in the reaction mixture.

Therefore, the effect of the particular adjustments on the automated process was analyzed by pooling and processing the corresponding batch records. Overall, three subgroups were created. First, synthesis utilizing the original Agilent SCX provided with the radiolabeling kit, without additional ethanol (20 batches). Second, synthesis with the substitute Phenomenex SCX without additional ethanol (28 batches). Third, synthesis with the substitute Phenomenex SCX with 5 vol% ethanol in the reaction mixture (181 batches). All data, depicted Figure 14, was obtained from the revised data set.

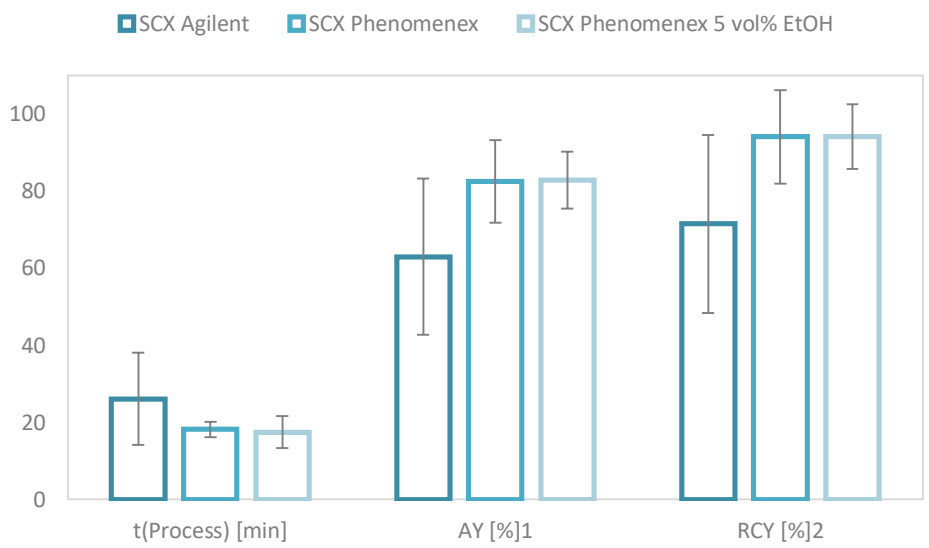

Figure 14: GAIA synthesis utilizing the original method compared to the two implemented adjustments [^{68}Ga]Ga-DOTA-TOC taking the revised data set as a basis. [1]non-decay corrected; [2]decay corrected

As shown in Figure 14, the effect of the two adjustments on yields as well as reproducibility is significant. The process duration drops from 26:04±11:59 min to 17:29±4:07 min, which means a reduction of 33 %. Simultaneously, AY increases from 63.0±20.3 % to 82.8±7.4 % and RCY from 71.5±23.1 % to 94.2±8.4 %.

Table 2: Comparison of final method of GAIA synthesis of [^{68}Ga]Ga-DOTA-TOC utilizing Phenomenex SCX and 5 vol% ethanol compared to manual. The revised data set was used as basis for this comparison. Data of the complete revised data set is included too.

		Revised data set		**Additional 5 vol% EtOH SCX Phenomenex**		**Manual synthesis**	
		M	**SD**	***M***	***SD***	***M***	***SD***
Process	***n***	*229*		*181*		*34*	
	A_{Start} [GBq]	*1.304*	*0.388*	*1.318*	*0.219*	*1.300*	*0.257*
	$A_{Product}$ [GBq]	*0.963*	*0.236*	*1.024*	*0.191*	*0.714*	*0.257*

$t_{Process}$ *[mm:ss]*	*18:19*	*5:41*	*17:29*	*4:07*	*22:21*	*2:50*
***AY [%]*[1]**	*81.0*	*11.1*	*82.8*	*7.4*	*62.3*	*13.1*
***RCY [%]*[2]**	*92.2*	*12.7*	*94.2*	*8.4*	*74.4*	*16.3*

[1]non decay corrected; [2]decay corrected

Table compares the final method utilized with GAIA, including the substitute SCX cartridge and 5 vol% ethanol in the reaction mixture (181 batch records), with manual synthesis (34 batch records). The mean starting activities and corresponding standard deviations are in the same range for both automated and manual synthesis.

There were significant differences between both methods for process duration. The manual method leads to the final product within an average of 22:21±2:50 min compared to 17:29±4:07 min with the optimized automated method (Table).

The significantly lower yield of 62.3±13.1 % (AY) for the manual method opposite to 82.8±.7.4 % (AY) for the automated process reflects the prolonged synthesis duration and process variabilities of the manual method. Decay corrected yields (RCY) are similar, 74.4±16.3 % for the manual method vs to 94.2±8.4 % for the automated process.

[^{68}Ga]Ga-PSMA-11

A data set of 531 batch records consisting of 190 manual and 341 automated synthesis were analysed (Table). For the automation of the PSMA-11 radiolabeling, the experiences obtained from the [^{68}Ga]Ga-DOTA-TOC-synthesis were directly implemented. Therefore, only a comparison of the optimized manual and automated procedures is possible.

Table 3: Comparison of GAIA and manual synthesis data for [^{68}Ga]Ga-PSMA-11 including and excluding non-process related failed productions.

		Complete data set				**Revised data set**			
		GAIA		**Manual**		**GAIA**		**Manual**	
		M	**SD**	**M**	**SD**	**M**	**SD**	**M**	**SD**
Process	**n**	341		190		296		165	
	A_{Start} [GBq]	1.289	0.233	1.368	0.353	1.302	0.215	1.387	0.334

$A_{Product}$ [GBq]	1.039	0.265	0.914	0.284	1.097	0.199	0.970	0.230
$t_{Process}$ [mm:ss]	15:07	4:12	21:50	6:22	14:49	2.41	20:48	5:19
AY [%][1]	83.3	16.0	66.8	14.5	88.0	7.3	70.5	8.6
RCY [%][2]	92.1	18.6	83.0	16.4	97.3	9.8	87.1	9.4

[1]non decay corrected; [2]decay corrected

Like for [^{68}Ga]Ga-DOTA-TOC the starting activities are in the same range for both automated and manual synthesis.

Both methods show significant differences. Conducting the manual method leads to the final product within an average of 21:50 ±6:22 min compared to 15:07±4:12 min with the automated method (Table).

Comparing the activity yields, significantly lower yields of 66.8±14.5 % (AY) for the manual method opposite to 83.3±16.0 % (AY) for the automated process reflected this prolonged synthesis duration. The RCY show similar results 83.0±16.4 % for the manual method opposite to 92.1±18.6 % for the automated process. Admittedly, the data set includes data from all batches produced independently from the cause of failure rate. Again, revision of the data set leads to the exclusion of overall 70 failed syntheses (25 manual; 45 GAIA), which means an exclusion of 13.2 % (13.2 % manual, 13.2 % GAIA) failed synthesis induced by non-process related causes. None of these batches failed because of the process used. Non-process related causes observed were low peptide quality, incorrect or poor preparation of the synthesis by the operator, aborted connection pc-device and a damaged generator. There are 0 failed synthesis in the revised data set for both methods.

As shown in Table for both processes, the mean values increase while the standard deviation drops significantly after revision, from 66.8±14.5 % to 70.5±8.6 % (AY) and 83.0±16.4 % to 87.1±9.4 % (RCY) for the manual and 83.3±16.0 % to 88.0±7.3 % (AY) and 92.1±18.6 % to 97.3±9.8 % (RCY) for the automated synthesis.

For the automated synthesis of [^{68}Ga]Ga-PSMA-11, the product was obtained within 14:49 ± 2:41 min on average, which decreases the time needed by ~ 30 %. After validation of the process, it usually runs without further disturbances, so stable time values are as expected. The radiochemical yield is 97.3 ± 9.8 % on average, which is an increase of ~ 11 %.

Quality Control

Quality control was performed according to the specifications given by the European Pharmacopoeia (Ph. Eur.) in the monograph for [^{68}Ga]Ga-DOTA-TOC [14]. For both production methods as well as for both tracers the specifications were always met. Radiochemical purity of the final products was determined with >99 % on average independent from the production route.

Statistical analysis

The comparison of automated syntheses [^{68}Ga]Ga-PSMA-11 with manual syntheses [^{68}Ga]Ga-PSMA-11 showed a p-value of $p < 0.001$. For the comparison of automated syntheses [^{68}Ga]Ga-DOTA-TOC with manual syntheses [^{68}Ga]Ga-DOTA-TOC showed a p-value of $p < 0.001$. Both showed, by conventional criteria, a difference, which is considered statistically significant.

Discussion

In the present study, synthesis data from the 2015-2017 period of clinical routine were analysed and compared. 837 batch records were considered in the complete data set. In order only to compare the performance of both processes the complete data set was revised as described in the results

During this period a total of ten ^{68}Ge/^{68}Ga-generators, with nominal ^{68}Ga-activity of 1.85 GBq at calibration time, were used. The generators were replaced every 4 months to ensure batch activities higher than 750 MBq per batch, which adds up to three to four patients per batch. Accordingly, the average starting activities are in the same range independently from tracer or synthesis method but with high standard deviations.

Considering generator physics, the validity of activity related data (e.g. product activity, molar activity) and corresponding standard deviations have to be handled with care. It explains the high standard deviation of the starting activities and partially the high standard deviation of the product activities. For this reason, the yields are of greater significance, both AY and RCY. These values and corresponding standard deviations describe the suitability of a process for a particular radiolabeling reaction.

The average difference in process duration between both methods is 4.3 min ([^{68}Ga]Ga-DOTA-TOC) and 6.7 min ([^{68}Ga]Ga-PSMA-11) considering the respective complete data set as well as 4.0 min ([^{68}Ga]Ga-DOTA-TOC) and 6.0 min ([^{68}Ga]Ga-PSMA-11) for the revised data set. This is equivalent to a loss of ~ 4.0 % of ^{68}Ga-activity of [^{68}Ga]Ga-

DOTA-TOC respectively ~ 6.0 % [^{68}Ga]Ga-PSMA-11 due to the longer process duration of the manual method. AY reflects this result, which is significantly lower for the manual method compared to the automated process. This difference would increase even if the start of synthesis (SoS) for both methods would be the same, which was not possible due to the setup of the manual radiolabeling. For the automated process, SoS the time point of activity measurement of ^{68}Ga-activity trapped on the SCX (before post-processing) was used. As starting activity and SoS, the time point of activity measurement of ^{68}Ga-activity, eluted from the SCX cartridge (after post-processing), was used. One reason for this is radiation protection for the operator. To measure the activity trapped on the SCX, as the module automatically does, manual removal of the SCX would be necessary. This manual intervention would increase the radiation dose of the operator. The time point of activity measurement at SoS was used for decay correction. Therefore, the process duration excludes the ^{68}Ga-eluate post-processing for the manual method while it is included for the automated synthesis. The calculated average time difference and loss of ^{68}Ga-activity is accordingly underestimated. For both methods, the loss of gallium-68 due to retention on the SCX cartridge is less than 1 % of the starting activity.

Additionally, since PSMA-11 has to be taken into account, the automated synthesis includes a subsequent C_{18} purification step, while the manual process works without C_{18} purification.

Nevertheless, synthesis time observed for the manual method is longer than for the automated process. The synthesis set up of the manual method explains this curious result. While the module system measures radioactivity online, these measurements require manual intervention operation.

Additionally, the manual method established at the institution contains a pH measurement to ensure radiolabeling with optimum results after the addition of the eluate to the reaction mixture, followed by manual closing and crimping of the reaction vial. Although this step is not necessary, it is included and executed as described in the documented procedure. The manual pH adjustment in the case of too high aberrations leads to prolonged mean synthesis duration compared to the automated method where an intervention for pH measurement is not possible. While the automated process has defined periods for the entire process steps, the synthesis duration of the manual method is depending on the operator´s skills and device set-up. For example, factors are speed and routine of the operator, or distance and reachability of the dose calibrator in relation to the working area. Accordingly, for the manual method a higher standard deviation is anticipated.

As end of synthesis (EoS) the time point of measuring the product activity in the final formulation was defined. For both processes, measurement of product activity is performed manually after withdrawal of the quality control sample. As the module cannot measure the final product activity automatically and to eliminate deviations due to the withdrawal of the quality control sample the product activity was not used to determine AY and RCY. Calculation of AY and RCY are based on the activity measured after trapping and elution on the C_{18} cartridge in relation to the starting activity. The manual synthesis of PSMA-11 is an exception. Here the calculation is based on the activity values for product and start activity. This proceeding reduces the influence of the manual withdrawal of the quality control sample. For e.g. the automated process stops after final formulation and the operator has to disconnect the product vial, retrieve the product sample and transfer the vial to the measurement chamber manually. For [^{68}Ga]Ga-DOTA-TOC (revised data set) the process duration from SoS until end of final formulation was found to be 16.17±0.42 min while the average duration of removal and measurement of the product vial needs 2.40±5.63 min.

The prolonged synthesis duration found for the manual process is also reflected by the AY, which is defined as the non-decay corrected amount of radioactive product (expressed in Bq) obtained from a starting amount of radioactivity. AY is significantly dependent on process duration, losses of radioactivity in the system (e.g. tubing, needles, syringes, vials) and the radiolabeling yield of the reaction. The average difference found between both methods was 23.2 % ([^{68}Ga]Ga-DOTA-TOC) and 16.5 % ([^{68}Ga]Ga-PSMA-11) considering the respective complete data set as well as 18.7 % ([^{68}Ga]Ga-DOTA-TOC) and 17.5 % ([^{68}Ga]Ga-PSMA-11) for the revised data set. For both radiopharmaceuticals, the automated process is significantly better than the manual method, although the automated process produces more contaminated waste material than the manual synthesis.

Within the evaluation period, two adjustments of the automated [^{68}Ga]Ga-DOTA-TOC process were implemented in clinical routine production. As these changes should improve the process, the revised data set was analysed with regard to these adjustments.

First, Phenomenex SCX was exchanged with the original provided SCX cartridge (Agilent SCX). This adjustment was necessary due to the use of iThemba ^{68}Ge/^{68}Ga-generators in clinical routine. In a detailed screening with different generators and cartridges, this cartridge showed a better performance in combination with the iThemba generator. As the iThemba ^{68}Ge/^{68}Ga-generator is eluted with 0.6 N HCl the capacity of the original Agilent SCX cartridge was exhausted. This results in an unwanted premature wash-off

of gallium-68 from the SCX during generator elution, leading to reduced starting activity as shown in Figure.

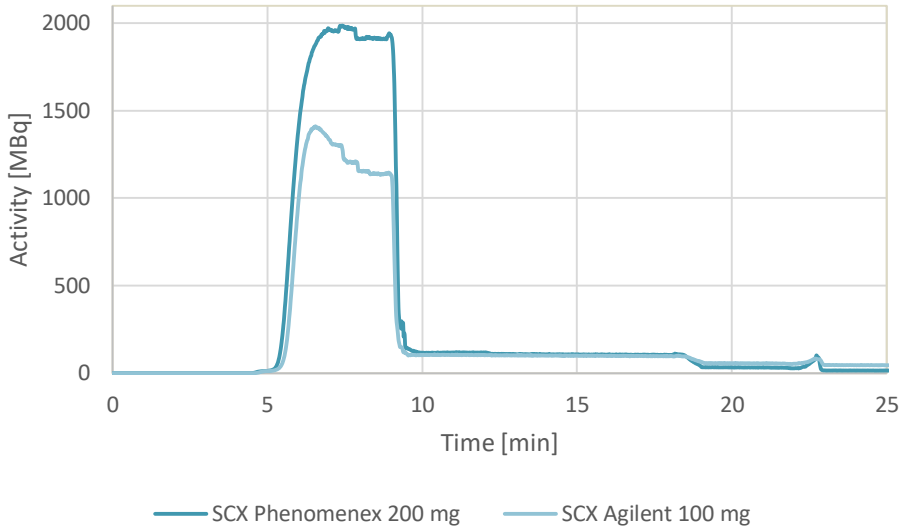

Figure 4: Trapping of gallium-68 during elution of an iThemba ^{68}Ge/^{68}Ga-generator using 0.6 N HCl on the Phenomenex SCX and the original Agilent SCX during the automated process. The generator was used under the same conditions (first elution of the day, last elution longer than 12 h ago).

Exchange of the SCX resulted in a significant increase of AY (average difference of 16.5 %) and RCY (average difference 22.6 %) due to distinct reduced process duration (average difference 7.87 min). Additionally, the reliability and reproducibility of the process increased as shown by the almost halved standard deviations for AY and RCY. Incomplete trapping of the SCX cartridge also influenced the eluted activities, leading to reduced yields.

Second, additional 5 vol% ethanol was added to the reaction mixture mainly to inhibit radiolysis [19–21], the effect of improving radiolabeling efficacy as described in literature [18, 22, 23] was just secondary as the process was not changed in terms of temperature, or heating time. As expected, there are no significant differences in process duration (0.72 min) and RCY (0.10 %). In addition, the standard deviations decrease again. Nevertheless, inhibition of radiolysis is effective as determined by HPLC Figure 4.

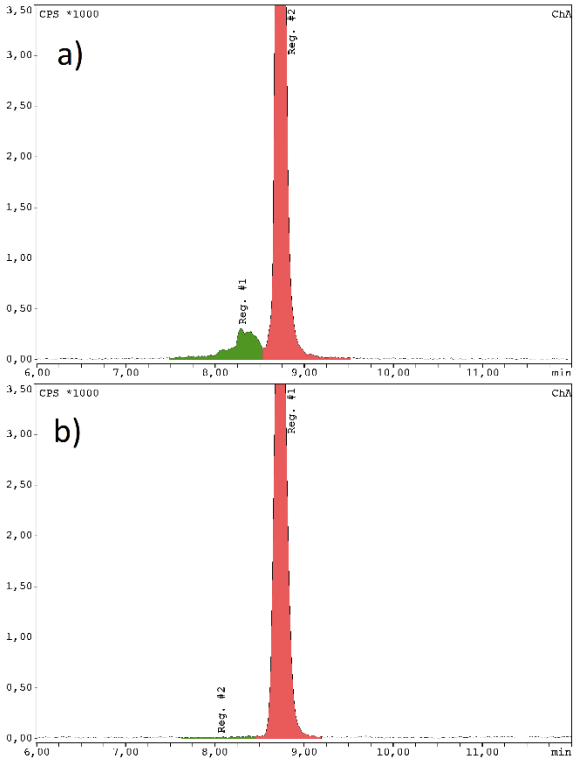

Figure 5: RadioHPLC chromatograms of [^{68}Ga]Ga-DOTA-TOC representing a synthesis without (a) and with additional ethanol (b) in the reaction mixture. Sample collection took place directly after final formulation. In region 1 (8.12±0.13 min) radiolysis by-products can be found. The signal at 8.66±0.08 min in region 2 indicates the product [^{68}Ga]Ga-DOTA-TOC.

As the two adjustments were directly adopted to the PSMA-11 process, no data exists for the use of the original SCX or without additional ethanol.

Both automated methods are able to provide the entire radiopharmaceutical with a high reproducibility and AY, as well as RCY and are significantly superior to the manual methods. With average AY higher than 75 % and average RCY higher than 90 %, the automated methods are very well designed for the synthesis of ^{68}Ga-radiopharmaceuticals. When compared to the manual procedure, the automated process provides higher yields, higher reliability and lower radiation doses to the operator, although it also leads to more contaminated waste material. The international Commission on Radiological Protection (ICRP) proposed principles of radiological protection [24]:

1. The Principle of Justification: Any decision that alters the radiation exposure situation should do more good than harm.

2. The Principle of Optimization of Protection: The likelihood of incurring exposure, the number of people exposed, and the magnitude of their individual doses should all be kept as low as reasonably achievable (ALARA), taking into account economic and societal factors.
3. The Principle of Application of Dose Limits: The total dose to any individual from regulated sources in planned exposure situations other than medical exposure of patients should not exceed the appropriate limits specified by the Commission.

Assuming that the principles one and three will be observed, it would be logically consistent to switch from the manual method to the much more stable automated procedure with regards to radiation protection of the operator. As example, for PSMA-11, based on 1000 MBq starting activity the automated synthesis would yield 880 MBq final product, while the manual method only yields 705 MBq (difference of 175 MBq). An amount, which could be required for an additional 70 kg patient administering 2.0 MBq/kg bodyweight.

Table 4: Consequences of GAIA and manual yields using the example of [^{68}Ga]Ga-PSMA-11 for comparison assuming 70 kg heavy patients, administering 2 MBq/kg bodyweight and 30 min between final release of the product as well as every injection.

Patient No.	**Injection time [min]**	**Activity required [MBq]**	**Activity provided [MBq]**	
			GAIA	**Manual**
			1000	
	0		880	705
1	30	190	690	515
2	60	259	431	256
3	90	352	79	--

As shown in Table for the manual method, one less patient dose would be available resulting in a need for another synthesis including all consequences (e.g. radiation exposure for operator; costs for material, contaminated waste materials).

Conclusions

The evaluation of these 837´s clinical routine batch records (a set of 723 revised data) revealed that the automated procedure established utilizing a cassette module is superior to the traditional established manual method for routine production. This is true for a complete labeling process duration, AY as well as RCY.

Although these systems and their accessories are relatively expensive in acquisition, they have several advantages over the manual mode as well the kit-type radiolabeling method:

- Suitability for a wide range of tracers and radionuclides
- Improves practicality of harmonized and standardized multicentre clinical trials [21]
- Reduced amounts of precursor possible (e.g. 2.58±0.42 µg PSMA-11 for automated process compared to 25 µg PSMA-11 in the cold kit (e.g. ANMI SA, Belgium)
- Radiation protection
- Reduced risk of cross contamination and viable/non-viable particles due to the use of disposable, sterile reagent KITs and manifolds

Besides that, main advantages of automation are its higher reliability, better reproducibility and time saving. This is also supported by the findings of other studies investigating automated radiolabeling [17, 25, 26].

The t-tests showed a significant difference between manual and automated synthesis. For both [^{68}Ga]Ga-PSMA-11 and [^{68}Ga]Ga-DOTA-TOC, the automated synthesis mode is superior to the manual synthesis.

Author Contributions: Conceptualization E.E.; Data Curation, E.E. and M.M.; Formal Analysis, E.E. and M.M.; Investigation, E.E. and M.M.; Methodology, E.E.; Project Administration, E.E.; Writing – Original Draft Preparation, M.M.; Writing – Review & Editing, E.E.; Supervision, E.E.

Funding: This research was funded by BONFOR, grant number O-140.0008

Acknowledgments:

Conflicts of Interest: The authors declare no conflict of interest.

References

1. Breeman WAP, Jong M, Blois E, Bernard BF, Konijnenberg M, Krenning EP. Radiolabelling DOTA-peptides with ^{68}Ga. Eur. J. Nucl. Med. Mol. Imaging. 2005;32:478–85. doi:10.1007/s00259-004-1702-y.
2. Breeman WAP, Blois Ed, Sze Chan H, Konijnenberg M, Kwekkeboom DJ, Krenning EP. ^{68}Ga-labeled DOTA-Peptides and ^{68}Ga-labeled Radiopharmaceuticals for Positron Emission Tomography: Current Status of Research, Clinical Applications, and Future Perspectives. Sem. Nucl. Med. 2011;41:314–21.

3. Iori M, Capponi PC, Rubagotti S, Esposizione LR, Seemann J, Pitzschler R, et al. Labelling of 90 Y- and 177 Lu-DOTA-Bioconjugates for Targeted Radionuclide Therapy: A Comparison among Manual, Semiautomated, and Fully Automated Synthesis. Contrast Media Mol Imaging. 2017:1–12. doi:10.1155/2017/8160134.

4. Eder M, Schäfer M, Bauder-Wüst U, Hull W-E, Wängler C, Mier W, et al. 68 Ga-Complex Lipophilicity and the Targeting Property of a Urea-Based PSMA Inhibitor for PET Imaging. Bioconjugate Chem. 2012;23:688–97. doi:10.1021/bc200279b.

5. Benesova M, Schafer M, Bauder-Wust U, Afshar-Oromieh A, Kratochwil C, Mier W, et al. Preclinical Evaluation of a Tailor-Made DOTA-Conjugated PSMA Inhibitor with Optimized Linker Moiety for Imaging and Endoradiotherapy of Prostate Cancer. J. Nucl. Med. 2015;56:914–20. doi:10.2967/jnumed.114.147413.

6. Ferlay J, Steliarova-Foucher E, Lortet-Tieulent J, Rosso S, Coebergh JWW, Comber H, et al. Cancer incidence and mortality patterns in Europe: Estimates for 40 countries in 2012. Eur J Cancer. 2013;49:1374–403. doi:10.1016/j.ejca.2012.12.027.

7. Israeli RS, Powell CT, Corr JG, Fair WG, Heston WD. Expression of the prostate-specific membrane antigen. Cancer Research. 1994;54:1807–11.

8. Israeli RS, Powell CT, Fair WG, Heston WD. Molecular cloning of a complementary DNA encoding a prostate-specific membrane antigen. Cancer Research. 1993;53:227–30.

9. Davis MI, Bennett MJ, Thomas LM, Bjorkman PJ. Crystal structure of prostate-specific membrane antigen, a tumor marker and peptidase. Proc Natl Acad Sci U S A. 2005;102:5981–6. doi:10.1073/pnas.0502101102.

10. Afshar-Oromieh A, Zechmann CM, Malcher A, Eder M, Eisenhut M, Linhart HG, et al. Comparison of PET imaging with a (68)Ga-labelled PSMA ligand and (18)F-choline-based PET/CT for the diagnosis of recurrent prostate cancer. European Journal of Nuclear Medicine and Molecular Imaging. 2014;41:11–20. doi:10.1007/s00259-013-2525-5.

11. Lutje S, Heskamp S, Cornelissen AS, Poeppel TD, van den Broek SAMW, Rosenbaum-Krumme S, et al. PSMA Ligands for Radionuclide Imaging and Therapy of Prostate Cancer: Clinical Status. Theranostics. 2015;5:1388–401. doi:10.7150/thno.13348.

12. Rinnab L, Simon J, Hautmann RE, Cronauer MV, Hohl K, Buck AK, et al. (11)Ccholine PET/CT in prostate cancer patients with biochemical recurrence after radical prostatectomy. World J Urol. 2009;27:619–25. doi:10.1007/s00345-009-0371-7.

13. Small EJ. Monoclonal antibody therapy for prostate cancer: finally a reality? J Clin Oncol. 2004;22:2515–6. doi:10.1200/JCO.2004.04.901.

14. European pharmacopoeia: 8.6 to 8.8. Strasbourg: Council Of Europe; 2015.

15. https://www.gmp-compliance.org/guidelines/gmp-guidelines.

16. Martin R, Jüttler S, Müller M, Wester H-J. Cationic eluate pretreatment for automated synthesis of [^{68}Ga]CPCR4.2. Nucl. Med. Biol. 2014;41:84–9. doi:10.1016/j.nucmedbio.2013.09.002.

17. Aslani A, Snowdon GM, Bailey DL, Schembri GP, Bailey EA, Roach PJ. Gallium-68 DOTATATE Production with Automated PET Radiopharmaceutical Synthesis System: A Three Year Experience. Asia Ocean J Nucl Med Biol. 2014;2:75–86.

18. Eppard E, Wuttke M, Nicodemus PL, Rösch F. Ethanol-based post-processing of generator derived ^{68}Ga towards kit-type preparation of ^{68}Ga-radiopharmaceuticals. Journal of Nuclear Medicine. 2014;55:1023–8.

19. Mu L, Hesselmann R, Oezdemir U, Bertschi L, Blanc A, Dragic M, et al. Identification, characterization and suppression of side-products formed during the synthesis of high dose ^{68}Ga-DOTA-TATE. Appl Radiat Isot. 2013;76:63–9. doi:10.1016/j.apradiso.2012.07.022.

20. Jensen SB, Käkelä M, Jødal L, Moisio O, Alstrup AKO, Jalkanen S, Roivainen A. Exploring the radiosynthesis and in vitro characteristics of 68 GaGa-DOTA-Siglec-9. J Labelled Comp Radiopharm. 2017;60:439–49. doi:10.1002/jlcr.3525.

21. Velikyan I. 68Ga-Based radiopharmaceuticals: production and application relationship. Molecules. 2015;20:12913–43. doi:10.3390/molecules200712913.

22. Pérez-Malo M, Szabó G, Eppard E, Vagner A, Brücher E, Tóth I, et al. Improved Efficacy of Synthesizing *MIII-Labeled DOTA Complexes in Binary Mixtures of Water and Organic Solvents. A Combined Radio- and Physicochemical Study. Inorganic Chemistry. 2018;57:6107–17. doi:10.1021/acs.inorgchem.8b00669.

23. Eppard E, Pèrez-Malo M, Rösch F. Improved radiolabeling of DOTATOC with trivalent radiometals for clinical application by addition of ethanol. EJNMMI radiopharm. chem. 2017;1:314. doi:10.1186/s41181-016-0010-8.

24. The 2007 Recommendations of the International Commission on Radiological Protection. ICRP publication 103. Ann ICRP. 2007;37:1–332. doi:10.1016/j.icrp.2007.10.003.

25. Boschi S, Lodi F, Malizia C, Cicoria G, Marengo M. Automation synthesis modules review. Appl Radiat Isot. 2013;76:38–45. doi:10.1016/j.apradiso.2012.09.010.

26. Ben Azzouna R, Alshoukr F, Leygnac S, Guez A, Gonzalez W, Rousseaux O, et al. A new (68)Ga anionic concentration and purification method for automated synthesis of (68)Ga-DOTA or NODAGA conjugated peptides in high radiochemical purity. J Labelled Comp Radiopharm. 2015;58:403–10. doi:10.1002/jlcr.3316.

6.2 Ethanol effects on ^{68}Ga-radiolabelling efficacy and radiolysis in automated synthesis utilizing NaCl post-processing

Michael Meisenheimer, Stefan Kürpig, Markus Essler, Elisabeth Eppard[*#]

Department of Nuclear Medicine, University Hospital Bonn, D-53127 Bonn, Germany

[*]actual adress: PositronPharma S.A, Rancagua 878, 7500921 Providencia, Chile

*Corresponding author: eeppard@positronpharma.cl; PositronPharma S.A, Rancagua 878, 7500921 Providencia, Chile

https://doi.org/10.1186/s41181-019-0076-1

Abstract

Recent studies showed that ethanol in the reaction mixture improves radiolabelling with trivalent radiometals in terms of precursor amount, reaction time, reaction temperature and radiolysis. With regard to clinical application, this effect is of practical interest in radiopharmacy. The aim of this study was to evaluate whether the positive effect of ethanol can be exploited in automated systems utilizing NaCl-post processing.

Gallium-68 was obtained from a 1.85 GBq ^{68}Ge/^{68}Ga-generator. Radiolabelling was performed on an automated ^{68}Ga-labelling cassette module. The standard labelling protocol was used without modifications. 0 – 40 vol% ethanol were added to the reaction mixture. Quality control was performed using radioHPLC and radioTLC.

Utilization of additional ethanol on an automated cassette module can be achieved by adding ethanol directly to the buffer solution without further modifications of the standard procedure. Radiolysis was decreased significantly as analysed by radioHPLC. It was possible to combine the positive effects of ethanol on radiolabelling efficacy and radiolysis with the standard labelling procedure of an automated cassette module system. The whole process guarantees safe preparation of highly pure ^{68}Ga-peptide for clinical application.

Keywords: Gallium-68; Radiolysis; Radiolabelling yield; Quality control; Ethanol; Module system

Introduction

One of the most versatile chelators available is the macrocycle 1,4,7,10-tetraazacyclotetradecane 1,4,7,10 tetra acetic acid (DOTA). It is known since 1976 [1] and was initially used as complexing agent for lanthanides, as it forms stable complexes with most bivalent and trivalent metals [2]. In addition, the synthesis of DOTA is very simple and fast, which facilitates the development of many derivatives equipped with various functional groups, which also enable a medical application. The first, and until today used, medical application of DOTA is as the contrast agent gadoteric acid were unfunctionalized DOTA is complexing Gd^{3+} [3].

In nuclear medicine one of the first DOTA derivatives utilized was DOTA-(0)-Phe(1)-Tyr(3))octreotide (DOTA-TOC). It can be applied for both diagnosis, radiolabelled e.g. with gallium-68, or therapy, with e.g. lutetium 177 [4]. The biological active site in DOTA-TOC, TOC, is a somatostatin analogous that binds to somatostatin receptors.

Somatostatin receptors (SSTR) belong to the group of G-protein-coupled receptors. Five subtypes are known (SSTR1-SSTR5), whereby alternative splicing of the SSTR2-mRNA lead to two subtypes, namely SSTR2A and SSTR2B [5]. These receptors are overexpressed in a number of neuroendocrine tumours (NET) [6] why they are well suited as targets for tumour targeting of NETs (Figure 15).

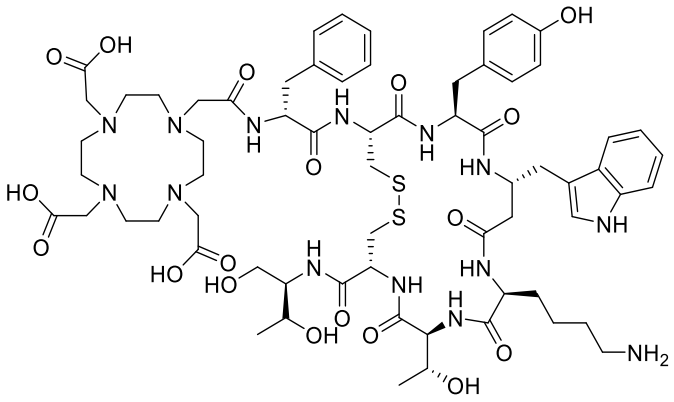

Figure 15: DOTA-conjugated octreotide (DOTA-TOC).

Radiolabelling of DOTA-TOC can be performed manually or automatically, utilizing a labelling module. Due to the increased radiation exposure for the operator, manual labelling should be avoided in the context of clinical routine where high levels of activity are used. To meet the requirements of radiation protection, radiation exposure should be minimized as far as possible. Correspondingly, automated radiolabelling is preferable to manual synthesis. Besides radiation protection, automation also offers the advantages

of a more reliable and repeatable process. Reliability is one of the most important factors in routine production, as quantity and quality of the product must always be guaranteed, which can be ensured by utilizing a module system.

When high-energy particles or ionizing radiation passes through matter, ions and excited molecules are formed (radiolysis products). A number of secondary processes occur following ionization and excitation. Radiolysis cannot be excluded in radiolabelling when high levels of activity are applied. Unfortunately, on the one hand, removal of those radiolysis products is time-consuming and complicated, as well as the verification that they are no longer present in the final product. On the other hand, they can cause undesired and serious side effects when they remain in the final product. Therefore, it is essential to reduce radiolysis by utilizing compounds insensitive to radiation or additives (e.g. radical scavengers) extenuating radiolysis. In clinical context, the applied scavenger should be suitable for human use. Scavengers suitable for human use are ascorbic acid or ethanol. In the proposed labelling process, ethanol is used during the post-processing step. Consequently, it is obvious, to use ethanol as a scavenger. Ethanol is a class 3 solvent that is commonly used as solvent or additive, increasing the solubility of pharmaceuticals or acting as a preservative. Ethanol biocompatible, not showing toxicity or immunoreactivity issues, GMP compatible and has no biological target binding capability [7]. Class 3 solvents may remain indeterminate and unmentioned up to a proportion of 0.5%, but if there is more in a pharmaceutical this must be stated in terms of quantity and identity [8]. Previous studies demonstrated the positive influence of ethanol on radiolabelling behaviour and yield as well as the reduction of radiolysis of the product in manual syntheses [9–12]. Building upon these results, the combination of a more reliable and repeatable method (automation) with a scavenger further improving radiolabelling, should lead to an automated process with a) less peptide needed b) reduced radiolysis by-products c) minimized radiation exposure d) maximized reliability and repeatability. Moreover, all these factors together lead to a cost optimized radiopharmaceutical production.

This work deals with the transfer of ethanol improved radiolabelling to an automated cassette module with prefabricated cassettes and chemical kits with the least possible changes. Therefore, the given process with sodium chlorine post-processing [13] was changed in terms of ethanol content. During the preparation of the cassette, 0-30 vol% ethanol was added to the buffer and synthesis performed without any further changes. Due to reaction volume issues, also buffer modifications were necessary. To obtain comparable results for an ethanol range of 0-40 vol% all experiments were repeated with the new buffer.

Materials and Methods

Gallium-68 was obtained from a ^{68}Ge/^{68}Ga-generator (iThemba Labs, South-Africa). Synthesis was performed utilizing an automated cassette module (GAIA, Elysia-Raytest, Straubenhardt, Germany). Standard fluidic kit and reagent kit for ^{68}Ga-radiolabelling of peptides (ABX advanced biochemical compounds GmbH, Radeberg, Germany) were used. As SCX (strong cation exchanger) 200 mg STRATA SCX (Phenomenex, USA) was used instead of standard SCX included in the reagent kit. TraceSelect water as well as ethanol Ph. Eur. was purchased from Merck (Darmstadt, Germany).

DOTA-TOC was obtained from ABX (ABX advanced biochemical compounds GmbH, Radeberg, Germany), and diluted with TraceSelect water to achieve a final concentration of 1 mg/ml.

DOTA-TATE, obtained from ANASPEC (Fremont, California, USA), was diluted with TraceSelect water to achieve a final concentration of 1 mg/ml.

The standard labelling method provided by the manufacturer: 50 µg DOTA-TOC were labelled with 500 µl post-processed ^{68}Ga-eluate in 3.6 ml buffer (0.08 M ammonium acetate buffer, pH 4.5), 8 min, 95 °C. After dilution with ~5 ml water subsequent C18 purification of the crude product followed. The product was eluted with 1.5 ml 60 vol% ethanol from the cartridge and finally formulated with 8.5 ml saline and sterile filtered.

The standard labelling method was used with following modifications. 10 µg DOTA-TOC were labelled with 500 µl post-processed ^{68}Ga-eluate in 520 µl buffer (0.5 M ammonium acetate buffer, pH 4.5) containing 0-40 vol% ethanol. 8 min, 95 °C. After dilution with ~5 ml water subsequent C18 purification of the crude product followed. The product was eluted with 1.5 ml 60 vol% ethanol from the cartridge and finally formulated with 8.5 ml saline and sterile filtered.

For all tests the standard radiolabelling procedure (software method) provided by the manufacturer was used.

All chemicals were of pure or analytical grade and used as received, unless otherwise specified.

For quality control, an aliquot was retained from the final formulation. Quality control was performed with silica-gel coated aluminium TLC-plates (silica 60 F254.5x4.5 cm, Merck, Darmstadt, Germany) as well as glass microfiber chromatography paper impregnated with silica-gel (iTLC-SG, Agilent Technologies, Santa Clara, California). Analysis was performed with a single trace radioTLC-scanner (PET-miniGITA, Elysia-Raytest,

Straubenhardt, Germany) and evaluation software (GinaStar TLC, Elysia-Raytest, Straubenhardt, Germany). Development of silica TLC-plates was conducted in 0.1 M citrate buffer (pH 4) and 1 M ammonium acetate/methanol (1:1) for iTLC-plates. Radio-HPLC was used to determine the radiochemical purity and content of radiolysis products. RadioHPLC was performed using Agilent 1260 Infinity II reverse phase HPLC system (Agilent Technologies, Santa Clara, California) equipped with Gabi γ-HPLC flow detector (Elysia-raytest, Straubenhardt, Germany) and a PC interface running Gina Star software (Elysia-raytest, Straubenhardt, Germany). A Nucleodur 100-3 C18 ec 125/4 column (Macherey-Nagel GmbH & Co. KG, Düren, Germany) was used. The gradient elution system utilized mobile phase A (deionized H_2O + 0.01 % TFA) and mobile phase B (100 % acetonitrile + 0.01 % TFA) at a flow rate of 0.7 mL/min, starting with 100 % A/0 % B changing within 20 min to 0 % A/100 % B, after which gradient parameters are returning to 50 % A/50 % B during the next 5 min. Radioactivity was measured with a dose calibrator (ISOMED 2010, MED Nuklear-Medizintechnik Dresden GmbH, Dresden, Germany).

The radiochemical yield was determined based on the decay corrected values of six measuring points (Figure): 1. Waste after generator elution. 2. Waste. 3. Final product. 4. Residual SCX activity. 5. Residual activity of the C18. 6. The reactor. Measuring points 2-6 where measured at the end of the syntheses.

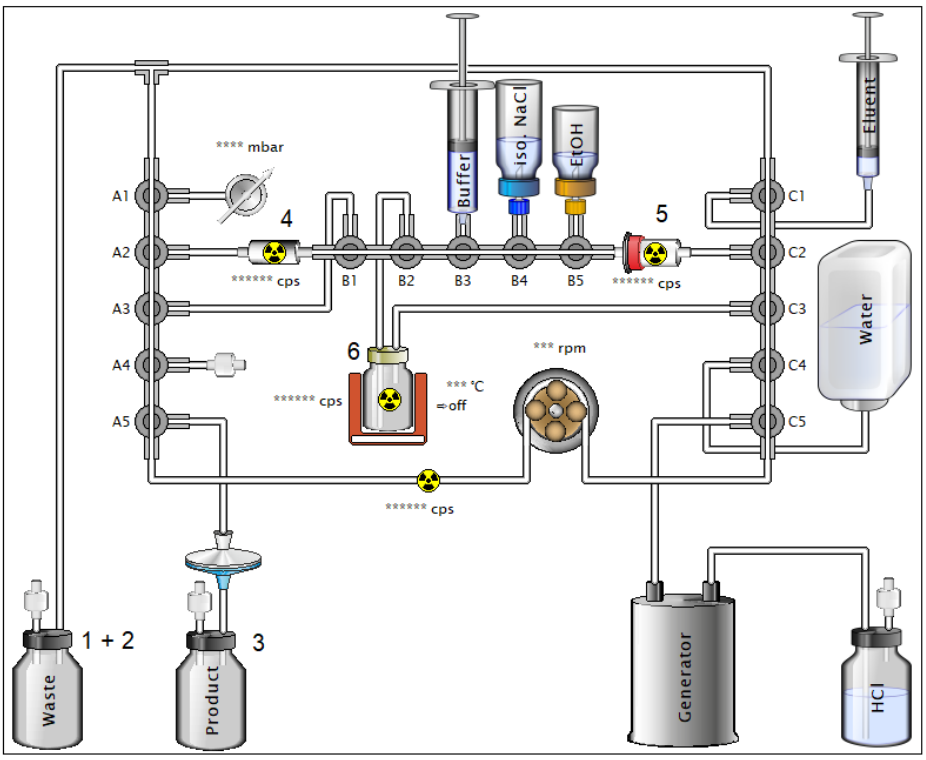

Figure 2: Schematic illustration of the built-in cassette. Visible is the tubing system connecting all three manifolds which has five three-way valves that are operated automatically. Numbers 1-6 indicate radioactivity measurement points.

Unless otherwise stated each experiment was performed at least four times to determine the standard deviation.

Statistics were calculated with PRISM Version 8.0.2. All data are expressed as mean ± SD. Groups were compared using the t-test. All statistical tests are two tailed, with a p-value of 0.05 representative for significance.

Results

The manufacturer of the cassette module recommends the use of 50 µg (35.17 nmol) DOTA-TOC for repeatable and reliable results with guaranteed activity yields > 70 %. To be able to determine any effect of ethanol on radiolabelling yields, it was necessary to determine an initial state without ethanol addition, were radiolabelling yields are low enough to measure any effect of ethanol. Systematic reduction of the recommended amount of peptide, confirmed a minimum of 10 µg (7.03 nmol) necessary for reliable automated radiolabelling which was used as initial state.

Starting from this initial state, the content of ethanol in the reaction mixture was increased until 40 vol% were achieved. Due to limited volume of the reactor, it was necessary to

modify the buffer with regard of total reaction volume. 3.6 ml buffer with additional 40 vol% ethanol resulted in to an overfull reactor and thus to severe synthesis errors. For this reason, the buffer concentration was increased from 0.08 M (original buffer included in the kit) to 0.5 M. All experiments described used the higher concentrated buffer. Statistical comparison between the results obtained for each buffer showed no statistical significance (Table 5).

Table 5: Radiochemical yield compared from DOTA-TOC with 0.08 M buffer and 0.5 M buffer.

Vol% ethanol	RCY with 0.08 M buffer [%]	RCY with 0.5 M buffer [%]	P-value
0	21.73±7.79	24.38±14.64	0.7601
10	40.09±11.70	42.11±6.99	0.2809
20	75.26±4.59	75.52±2.56	0.0752
30	95.27±3.46	96.25±2.71	0.1284

Since a C18 purification step is included in the synthesis process, radiochemical purity was always ≥ 98% confirmed by radioTLC and radioHPLC.

Purification via C18 is problematic with organic solvent concentrations higher than 10 vol%. Above this limit, complete trapping of the analyte is not secured. Therefore, manufacturers recommend dilution of the analyte to below 10 vol%. The standard radiolabelling procedure (software method) provided by the manufacturer of the module includes a dilution step before C18 purification. During this step, the reaction mixture is diluted with a total of 5 ml water and cooled down to 40 °C. This reduces the ethanol concentration from 0-40 vol% during reaction to 0-5.7 vol%. This concentration is uncritical with regard to C18 purification (Table).

Table 2: Ethanol content after dilution of the reaction mixture and corresponding activity found in the waste fraction after C18 trapping as well as on C18 after elution of the product.

Vol% ethanol	Ethanol content after dilution [%]	Activity in waste [%]	Activity remaining on C18 [%]
0	0	55.71±7.73	7.45±6.44
10	0.99	27.51±12.02	15.87±9.88
20	2.21	9.18±1.20	10.18±2.47
30	3.86	0.32±0.08	1.74±0.28

40	5.66	4.27±1.28	3.31±1.58

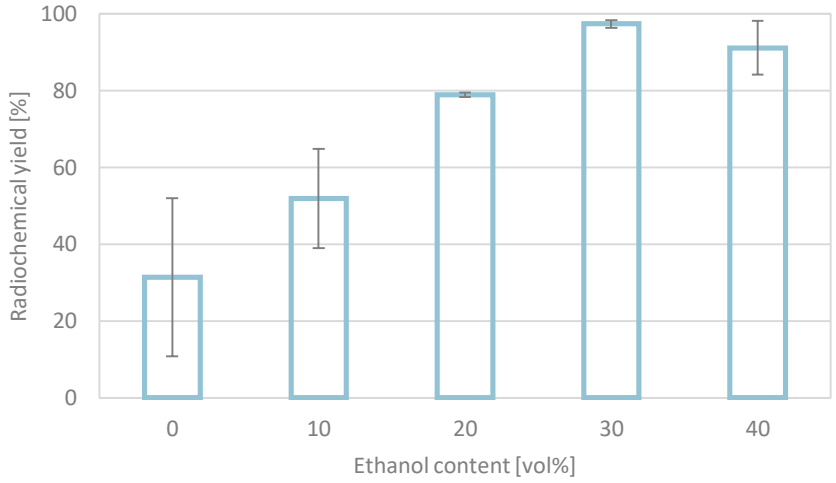

Figure 3: Radiochemical yield depending on ethanol content (vol%) in the reaction mixture. 10 µg (7.03 nmol) DOTA-TOC, T=95 °C, t=420 s, 500 µl eluent solution, 0.52 ml 0.5 M ammonium acetate buffer (pH 4.5) for 0-40 vol% ethanol, overall pH 3.6-3.8. All experiments were performed minimum 4 times.

Figure shows influence of ethanol on radiochemical yield and reliability of the process at low precursor amounts. Five different concentrations of ethanol were tested with regard to their influence on yield during radiolabelling process. To ensure that the data can be evaluated statistically, all experiments were repeated at least 4 times. As expected, the yield increased from 0 to 30 vol% [9, 12]. The low yield at 0 vol% and 10 vol% is accompanied by a low repeatability expressed in a high standard deviation. One possible factor, which influence the repeatability of the reaction, is the transfer of the peptide in the buffer. Due to the very small amount of peptide already, lowest losses within the syringe and tubing system have a significant effect on radiochemical yields. As the repeatability is decreasing with increasing ethanol content, it can be assumed that the peptide transfer from syringe to reactor via tubing is improved. Actually, ethanol has an influence on solubility of the peptide, thus less peptide adheres to the tubing's. Accordingly, the losses of peptide during transfer in the tubing system are reduced to a minimum. As a result, even at very low precursor concentrations, the repeatability of the synthesis increases. The radiochemical yield (≥ 97%) can be compared to a production with 50 µg (35.15 nmol) of DOTA-TOC which is recommended according to supplier's report.

Figure also shows decreased radiolabelling yield and repeatability for 40 vol% ethanol compared to 30 vol%. This could be explained by the influence of ethanol on the pH

value of the reaction (measured) which was not in the optimum range of 3.6-3.8 and by the different behaviour of the ethanol mixtures compared to a pure aqueous solution in the tubing's. The different behaviour could be explained by the differences in density and viscosity of the two substances and their mixtures. Pure ethanol has a 20 % higher viscosity and a density 21 % lower than water [14]. Compared to these results, up to 40 vol% stable and high yields were described in literature [9, 15]. However, these results were obtained in an open vial under constant reaction conditions and without long transfer ways via tubing. Despite of everything no statistical significance was found comparing 30 vol% and 40 vol% ethanol ($p = 0.0954$).

Nevertheless, the effect of ethanol on radiolabelling is significant. Statistical comparison of the different ethanol concentration among each other showed no statistical significance for the increase from 0 vol% to 10 vol% and 30 vol% to 40 vol%. For all other combinations statistical significance is given. Easy adaption to automated synthesis and the considerable increase in radiolabelling yields with only one fifth of precursor amount are two arguments for the use of ethanol in daily routine.

A second beneficial effect of ethanol is its ability to inhibit radiolysis [7, 11, 16]. Radiolysis of the precursor occurs as soon as precursor and activity meet each other. The effect of radiolysis inhibition can be shown using radioHPLC.

According to pharmacopoeia, above a value of 0.5 vol% ethanol [8] in the product must be indicated, therefore the maximum possibly quantity present in the final product was calculated. Within this risk assessment, maximum retention of ethanol on the C18 cartridge was supposed.

Before purification, 5 ml water is added to the reactor and then the entire mixture is passed over the C18 cartridge. Afterwards, the reactor is flushed with air until the remaining solution from the C18 has been removed from the reactor. The volume of the remaining solution was determined with a maximum value below 250 µl ($n \geq 10$).

If this remainder on the C18 cartridge is assumed to be pure ethanol, which would be added to the amount of ethanol used for the purification process, the maximum ethanol content in the final product would be 10.85 vol%.

Figure 4 shows two radioHPLC chromatograms of [^{68}Ga]Ga-DOTA-TOC synthesized with (a) and without (b) 5 vol% ethanol in the reaction mixture. To achieve comparable results, in both cases, the quality control sample collection took place directly after final formulation and termination of synthesis. Radiolysis by-products are highlighted in green

in the range of 6.7-7.2 min. For simplification it is assumed that by-products detected are formed primarily during the reaction and almost not after the C18 purification step which includes ethanol as eluent.

The amount of radiolysis by-products formed without ethanol as additive in the reaction mixture was 5.87 ± 1.08% (n = 150) in comparison to 1.03 ± 0.47 % (n = 200) utilizing 5 vol% ethanol as radiolysis inhibitor in the reaction mixture. This was found to be statistically significant ($p<0.0001$).

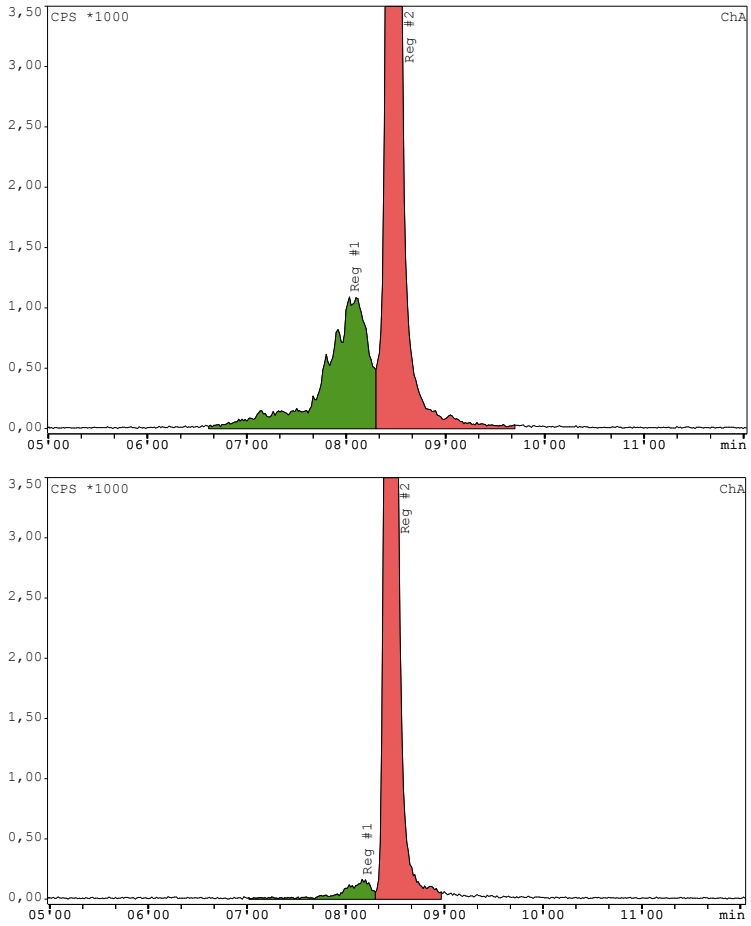

Figure 4: RadioHPLC chromatograms representing a synthesis without (a) and with additional ethanol (b) in the reaction mixture. Sample collection took place directly after final formulation. In region 1 (8.12 ± 0.13 min) radiolysis by-products can be found. The signal at 8.66 ± 0.08 min in region 2 indicates the product.

As the results for the combination of ethanol with an automated process utilizing NaCl post-processing [13] were so clear for DOTA-TOC it was checked, if results can be transferred to another DOTA-conjugated peptide (e.g. DOTA-TATE). Therefore, optimized conditions with 30 vol% ethanol were used for radiolabelling 10 µg (6.96 nmol) DOTA-TATE. In these experiments (n = 4) radiochemical yields of 97.00 ± 0.93 % and radiochemical purity of ≥ 98 % was obtained. Compared to 10 µg (7.03 nmol) DOTA-TOC with 99.10 ± 0.79 % and a radiochemical purity of ≥ 98 %, the results where similar, as expected. Statistical comparison of the results of DOTA-TOC with DOTA-TATE showed no significance Figure .

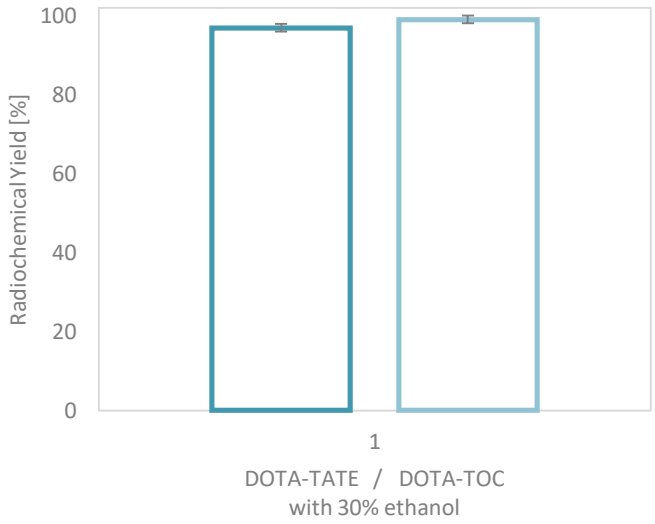

Figure 5: Comparison of the mean radiochemical yield values of DOTA-TATE and DOTA-TOC with 30 vol% ethanol. 10 µg (6.96 nmol) DOTA-TATE or 10 µg (7.03 nmol) DOTA-TOC, T=95 °C, t=420 s, 500 µl eluent solution, 0.52 ml 0.5 M ammonium acetate buffer (pH 4), overall pH 3.6-3.8. All experiments were performed minimum 4 times.

Conclusions

Ethanol can improve an automated cassette-based synthesis utilizing NaCl post-processing in terms of precursor amount, repeatability and radiolysis. This can be easily achieved by adding 10 vol% ethanol to the reaction mixture already and leads to optimal results utilizing an ethanol content of 30 vol%.

It is an effective way to decrease the amount of peptide. Reliable and repeatable synthesis can already be achieved with 10 µg (7.03 nmol) of DOTA-TOC utilizing 30 vol%

ethanol. This is only one fifth of the precursor amount recommended by the manufacturer of the module system.

Furthermore, it has been shown that radiolysis is already significantly reduced even with only 5 vol% ethanol in the reactor. This is of practical interest especially in clinical daily practise.

Author Contributions

Conceptualization E.E.; Data Curation, S.K., E.E. and M.M.; Formal Analysis, E.E. and M.M.; Investigation, S.K., E.E. and M.M.; Methodology, E.E.; Project Administration, S.K., M.E. and E.E.; Writing – Original Draft Preparation, M.M.; Writing – Review & Editing, E.E.; Supervision, E.E.

.

Funding

This study was funded by BONFOR (grant number O-140.0008).

Conflicts of Interest

The authors declare that they have no conflict of interest.

Ethics approval and consent to participate

The authors declare that they have no conflict of interest.

Consent for publication

Not applicable.

Acknowledgements

Not applicable.

References

1. Stetter H, Frank W. Complex Formation with Tetraazacycloalkane-N,N?,N?,N?-tetraacetic Acids as a Function of Ring Size. Angewandte Chemie International Edition in English. 1976;15:686. doi:10.1002/anie.197606861.

2. Alexander V. Design and Synthesis of Macrocyclic Ligands and Their Complexes of Lanthanides and Actinides. Chem. Rev. 1995;95:273–342. doi:10.1021/cr00034a002.

3. Caravan P, Ellison JJ, McMurry TJ, Lauffer RB. Gadolinium(III) Chelates as MRI Contrast Agents: Structure, Dynamics, and Applications. Chemical Reviews. 1999;99:2293–352. doi:10.1021/cr980440x.

4. Lamberts SW, Reubi JC, Bakker WH, Krenning EP. Somatostatin receptor imaging with 123I-Tyr3-Octreotide. Z Gastroenterol. 1990;28 Suppl 2:20–1.

5. Prasad V, Fetscher S, Baum RP. Changing role of somatostatin receptor targeted drugs in NET: Nuclear Medicine's view. J Pharm Pharm Sci. 2007;10:321s-337s.

6. S. Petersenn. Neuroendokrine Tumoren: Seltene medizinische Phänomene. In: Essener Unikate.

7. Velikyan I. 68Ga-Based radiopharmaceuticals: production and application relationship. Molecules. 2015;20:12913–43. doi:10.3390/molecules200712913.

8. European Pharmacopoeia, 9th edition 2019, English: Subscription to Supplement 6 + Supplement 7 + Supplement 8. 1st ed. Stuttgart: Deutscher Apotheker Verlag; 2018.

9. Eppard E, Pèrez-Malo M, Rösch F. Improved radiolabeling of DOTATOC with trivalent radiometals for clinical application by addition of ethanol. EJNMMI radiopharm. chem. 2017;1:314. doi:10.1186/s41181-016-0010-8.

10. Helm L, Merbach AE. Inorganic and Bioinorganic Solvent Exchange Mechanisms. Chem. Rev. 2005;105:1923–60. doi:10.1021/cr030726o.

11. Mu L, Hesselmann R, Oezdemir U, Bertschi L, Blanc A, Dragic M, et al. Identification, characterization and suppression of side-products formed during the synthesis of high dose ^{68}Ga-DOTA-TATE. Appl Radiat Isot. 2013;76:63–9. doi:10.1016/j.apradiso.2012.07.022.

12. Pérez-Malo M, Szabó G, Eppard E, Vagner A, Brücher E, Tóth I, et al. Improved Efficacy of Synthesizing *MIII-Labeled DOTA Complexes in Binary Mixtures of Water and Organic Solvents. A Combined Radio- and Physicochemical Study. Inorganic Chemistry. 2018;57:6107–17. doi:10.1021/acs.inorgchem.8b00669.

13. Mueller D, Klette I, Baum RP, Gottschaldt M, Schultz MK, Breeman WAP. Simplified NaCl Based ^{68}Ga Concentration and Labeling Procedure for Rapid Synthesis of ^{68}Ga Radiopharmaceuticals in High Radiochemical Purity. Bioconjugate Chem. 2012;23:1712–7. doi:10.1021/bc300103t.

14. Weber W. Über die Druckabhängigkeit der Viskosität von Alkohol-Wasser-Gemischen. Rheol Acta. 1975;14:1012–25. doi:10.1007/BF01516304.

15. Eppard E, Wuttke M, Nicodemus PL, Rösch F. Ethanol-based post-processing of generator derived ^{68}Ga towards kit-type preparation of ^{68}Ga-radiopharmaceuticals. Journal of Nuclear Medicine. 2014;55:1023–8.

16. Scott PJH, Hockley BG, Kung HF, Manchanda R, Zhang W, Kilbourn MR. Studies into radiolytic decomposition of fluorine-18 labeled radiopharmaceuticals for positron emission tomography. Appl Radiat Isot. 2009;67:88–94. doi:10.1016/j.apradiso.2008.08.015.

6.3 Clinical evaluation of [^{68}Ga]Ga-DATA-TOC in comparison to [^{68}Ga]Ga-DOTA-TOC in patients with neuroendocrine tumours

Gaertner FC[1*+], Plum T[1+], Kreppel B[1], Eppard E[1], Meisenheimer M[1], Strunk H[2], Bundschuh RA[1], Sinnes JP[3], Rösch F[3], Essler M[1]

[1]Department of Nuclear Medicine, University Hospital Bonn, D-53127 Bonn, Germany

[2]Department of Radiology, University Hospital Bonn, Germany

[3]Institute of Nuclear Chemistry, Johannes Gutenberg-University Mainz, Germany

*Corresponding author: florian.gaertner@ukbonn.de, Tel. +49-(0)228-287-15181. Fax +49-(0)228-287-19096.

[+]equal contribution

https://doi.org/10.1016/j.nucmedbio.2019.08.006

Abstract

[^{68}Ga]Ga-DATA-TOC is a new radiolabelled somatostatin-analogue for positron emission tomography (PET) imaging of neuroendocrine tumours. Its advantage over DOTA-conjugated compounds is the possibility for high-efficiency labelling with gallium-68 quickly at room temperature without the need for product purification, which enables the development of an instant kit-type labelling method. We evaluated its imaging characteristics in patients with neuroendocrine tumours in comparison to [^{68}Ga]Ga-DOTA-TOC.

19 patients imaged with [^{68}Ga]Ga-DATA-TOC were retrospectively analysed and uptake in normal tissues was compared with a group of 19 patients imaged with [^{68}Ga]Ga-DOTA-TOC. 10 patients imaged with [^{68}Ga]Ga-DATA-TOC had a history of [^{68}Ga]Ga-DOTA-TOC imaging before and were additionally analysed to obtain biodistribution data of both tracers in the same patients. In 5 patients showing stable disease between both examinations, tumour uptake, lesion detectability and lesion conspicuity of both tracers were evaluated.

Uptake of [^{68}Ga]Ga-DATA-TOC in normal organs with expression of the somatostatin receptor was 25-47% lower compared to [^{68}Ga]Ga-DOTA-TOC. Background of [^{68}Ga]Ga-DATA-TOC was 40-41% lower in the liver. A higher retention of [^{68}Ga]Ga-DATA-TOC was observed in the blood (up to 67%) and in the lungs (up to 44%). Tumour uptake (SUV) was 22-31% lower for [^{68}Ga]Ga-DATA-TOC. However, no significant differences were observed for tumour-to-background ratios and lesion detectability. Regarding liver metastases, [^{68}Ga]Ga-DATA-TOC uptake (SUV) reached 69-73% of [^{68}Ga]Ga-DOTA-TOC uptake, but tumour-to-background ratios of [^{68}Ga]Ga-DATA-TOC were 105-110% of [^{68}Ga]Ga-DOTA-TOC ratios.

We demonstrated the feasibility of the new PET tracer [^{68}Ga]Ga-DATA-TOC for imaging of patients with neuroendocrine tumours, showing a comparable performance to [^{68}Ga]Ga-DOTA-TOC. [^{68}Ga]Ga-DATA-TOC has the potential for development of an instant kit-type labelling method at room temperature similar to ^{99m}Tc-labelled radiopharmaceuticals, which might help to increase the availability of ^{68}Ga-labelled somatostatin analogues for clinical routine use.

Keywords: Gallium-68; DATA-TOC; DOTA-TOC; instant kit-type labelling; PET/CT; somatostatin receptor (SSTR); neuroendocrine tumours (NET)

Background

Functional imaging of the somatostatin receptor (SSTR) plays a central role in the management of patients with neuroendocrine tumours. It is recommended for staging and follow-up of well-differentiated neuroendocrine tumours [1–5]. PET imaging using ^{68}Ga-labelled somatostatin analogues such as [^{68}Ga]Ga-DOTA-TOC is widely employed in the clinical routine, next to ^{111}In- and ^{99m}Tc-labelled somatostatin analogues used for planar scintigraphy and SPECT [6, 7].

While ^{111}In- and ^{99m}Tc-based tracers are widely available and easy to access, planar scintigraphy and even SPECT techniques have limitations in terms of spatial resolution, sensitivity and the imaging protocols are significantly elongated compared to PET examinations [8]. SSTR-scintigraphy is usually performed at 4 h, 24 h and up to 48 h post injection in the case of ^{111}In-labelled octreotide, whereas a complete SSTR PET/CT procedure can usually be completed within 2 h. Furthermore, ^{68}Ga-labelled SSTR PET tracers result in a lower effective radiation dose to the patients compared to ^{111}In-labelled compounds. Most importantly, the PET/CT technique delivers high-resolution cross-sectional images of the whole body, whereas SSTR scintigraphy only delivers planar images of the whole body and SPECT techniques are usually limited to imaging of single bed positions in the clinical practice. Accordingly, various studies report a superior image quality and improved performance of SSTR PET using ^{68}Ga-labelled somatostatin analogues with a high clinical impact compared with SSTR scintigraphy and SPECT, especially due to detection of additional tumour foci (including metastases and occult primary tumours) and an overall higher accuracy [9, 10]. However, radiochemical production of these compounds requires specialized facilities and trained personnel, limiting their availability.

Next to DOTA, other chelators have been developed which show excellent stability when bound to gallium-68, such as DATA. The major advantages in labelling DATA-conjugates with gallium-68 in comparison to DOTA-conjugates are that no heating is required during the process, and a high labelling efficiency eliminating the need for product purification after radiochemical synthesis. Especially the elimination of a purification step after synthesis, which is usually performed by solid phase extraction (SPE), paves the way for the development of an instant kit-type labelling method for ^{68}Ga-PET tracers [11–14].

An instant kit-type preparation method of ^{68}Ga-labelled PET tracers would help to decrease preparation time, reduce personnel involvement and preparation costs and overall increase availability of PET imaging employing ^{68}Ga-labelled conjugates. In this context, [^{68}Ga]Ga-DATA-TOC is extremely easy to synthesize within a few minutes at room

temperature in nearly quantitative yields [11–13]. It's *in vitro* binding affinities to SSTR expressing tumour cell lines as well as its pharmacodynamics in tumour-bearing mice revealed a close similarity to [^{68}Ga]Ga-DOTA-TOC [14].

Accordingly, the aim of the current study was to translate those findings into the clinics. Imaging properties of the newly developed DATA-coupled somatostatin analogue [^{68}Ga]Ga-DATA-TOC were evaluated in comparison to the established compound [^{68}Ga]Ga-DOTA-TOC in patients with neuroendocrine tumours.

Patients and Methods

Radiochemical synthesis of [^{68}Ga]Ga-DATA-TOC and [^{68}Ga]Ga-DOTA-TOC

Gallium-68 was obtained from a half year old ^{68}Ge/^{68}Ga-generator (iThemba Labs, South-Africa). Synthesis was performed utilizing an automated cassette module (GAIA, Elysia-Raytest, Straubenhardt, Germany). Standard fluidic kit and reagent kit for gallium-68 radiolabelling of peptides (ABX advanced biochemical compounds GmbH, Radeberg, Germany) were used. 200 mg STRATA SCX (Phenomenex, USA) was used instead of standard SCX included in the reagent kit. TraceSelect water as well as ethanol Ph. Eur. was purchased from Merck (Darmstadt, Germany).

DOTA-TOC was obtained from ABX and diluted with TraceSelect water to achieve a final concentration of 1 mg/ml. Radiolabelling was performed using 41.2±3.0 µg DOTA-TOC. Subsequent C-18 purification was performed. The final product was obtained in isotonic sodium chlorine solution.

DATA-TOC was synthesized as described earlier [11–13] and diluted with TraceSelect water to achieve a final concentration of 1 mg/ml. Radiolabelling of DATA-TOC was performed using 45.8±4.9 µg DATA-TOC, providing nearly identical apparent molar activities for both tracers. Subsequent C-18 purification was performed and the final product was obtained in isotonic sodium chlorine solution.

For quality control, an aliquot of 50 µl was retained from the final product before measurement of radioactivity. All chemicals were pure or analytical grade and used as received unless otherwise specified. Radioactivity of the final product was measured with a dose calibrator (ISOMED 2010, MED Nuklear-Medizintechnik Dresden GmbH, Dresden, Germany). Radiochemical purity was determined using silica-gel coated aluminium TLC-plates (silica 60 F254.5X4.5 cm Merck, Darmstadt, Germany) as well as glass microfiber chromatography paper impregnated with silica-gel (iTLC-SG, Agilent Technologies, Santa Clara, California) and analysed using a single trace radioTLC-scanner (PET-

miniGita, Elysia-Raytest, Straubenhardt, Germany) and evaluation software (Gina Star TLC, Elysia-Raytest, Straubenhardt, Germany). TLC/iTLC-strips were developed in 0.1 M citric buffer (pH 4, Merck, Darmstadt, Germany) and 1 M ammonium acetate/methanol (1:1). Additionally, radioHPLC was used to determine the radiochemical purity and identification of the product species. RadioHPLC was performed utilizing Agilent 1260 Infinity II reverse phase HPLC system (Agilent Technologies, Santa Clara, California) equipped with Gabi γ-HPLC flow detector (Elysia-Raytest, Straubenhardt, Germany) and a PC interface running Gina Star (Elysia-Raytest, Straubenhardt, Germany). A Nucleodur 100-3 C18 ec 125/4 column (Macherey-Nagel GmbH & Co. KG, Düren, Germany) was used. The gradient utilized mobile phase A (deionized water + 0.01% TFA) and mobile phase B (acetonitrile + 0.01% TFA) at a flow rate of 0.7 ml/min starting with 100% A / 0% B to 0% A / 100% B within 20 min after which gradient parameters change to 50% A / 50% B within 5 min. pH was measured using pH-indicator strips MColorpHast 2.0-9.0 (Merck, Darmstadt, Germany). The approximate half-life of gallium-68 was determined using a dose calibrator (ISOMED 2010, MED Nuklear-Medizintechnik Dresden GmbH, Dresden, Germany). The energy of gallium-68 as well as germanium-68 breakthrough were measured using a multi-channel-analyzer for γ-spectroscopy (MUCHA, Elysia-Raytest, Straubenhardt, Germany). Appearance was checked visually. Filter integrity was tested with GAIA (Elysia-Raytest, Straubenhardt, Germany).

Non-decay corrected (AY) as well as decay corrected radiochemical yield (RCY) were calculated based on the activity trapped on the SCX, activity trapped on C-18 and remaining activity on C-18 after final formulation as measured by the module. Volume activity (A_v) and apparent molar activity were calculated based on activity of the final product.

PET acquisition

Long-acting somatostatin analogues were discontinued 3-8 weeks before PET/CT. After obtaining informed consent for PET/CT imaging, 20 mg furosemide were injected intravenously, followed by [^{68}Ga]Ga-DATA-TOC or [^{68}Ga]Ga-DOTA-TOC, respectively (2 MBq/kg body weight). PET/CT was performed on a Biograph 2 PET/CT scanner (Siemens Medical Solutions, Erlangen, Germany). PET emission data was acquired from pelvis to head using 6 to 8 bed positions (3D mode), emission time was 4 minutes per bed position. PET images were reconstructed iteratively (attenuation weighted OSEM, 4 iterations, 8 subsets), including scatter, random and decay correction and images were smoothed by a 5 mm Gaussian filter. Attenuation correction was performed using low-dose CT data (16 mAs, 130 kV, without i.v. contrast).

Image analysis

Circular volumes of interest (VOI) were drawn on fused PET/CT images using Interview Fusion software (Version 3.00.060.0000, Mediso Ltd., Budapest, Hungary) for calculation of standardized uptake values (SUV). Spherical VOIs were used for the following organs: 50 mm diameter for brain, lungs and mediastinum; 30 mm diameter for liver and muscle; 20 mm diameter for spleen, bone and kidney cortex; 15 mm diameter for the pituitary gland and the adrenal glands. 15 mm spherical VOIs were used to measure uptake in tumour lesions. In each organ system, a maximum of three metastases (with the highest intensity) were analysed.

Tumour to background ratios were calculated by dividing tumour uptake (SUV_{max} and SUV_{mean}) by SUV_{mean} of the corresponding normal background tissues (normal liver for liver metastases, normal bone for bone metastases and muscle tissue for lymph node metastases and primary tumours).

Tumour burden was assessed by segmenting all tumour lesions with an isocontour technique. The volume (ml) and activity (Bq) of all VOIs in a patient was added together to yield the total tumour volume and to calculate the fraction of activity taken up by the tumour.

Visual analysis was performed independently by two experienced nuclear medicine physicians. [^{68}Ga]Ga-DATA-TOC and [^{68}Ga]Ga-DOTA-TOC PET/CT images were reviewed separately from each other two weeks apart. All lesions deemed malignant by the reviewing physician were counted by organ system and visual conspicuity of each lesion was rated by a scoring system (1: faint uptake, 2: moderate uptake, 3: intense uptake). After completing the initial evaluation, [^{68}Ga]Ga-DATA-TOC and [^{68}Ga]Ga-DOTA-TOC PET/CT images were reviewed side-by-side to match lesions with each other. Lesions that could not be matched (i.e. lesions that were only identified in one of the two examinations) were assigned a conspicuity score of 0 (no uptake) and were added to the list of non-detected lesions for the corresponding tracer.

Comparison of [^{68}Ga]Ga-DATA-TOC and [^{68}Ga]Ga-DOTA-TOC uptake in normal organs was performed in two groups of different patients who underwent either [^{68}Ga]Ga-DATA-TOC or [^{68}Ga]Ga-DOTA-TOC PET/CT (main collective). Furthermore, a sub-collective of patients who underwent [^{68}Ga]Ga-DATA-TOC PET/CT was identified who had undergone [^{68}Ga]Ga-DOTA-TOC PET/CT during the course of their disease before. Additional analysis of this sub-collective was performed in order to allow an intra-individual comparison of [^{68}Ga]Ga-DATA-TOC and [^{68}Ga]Ga-DOTA-TOC uptake in the same patients.

In the sub-collective, patients with clinical stable disease between the [^{68}Ga]Ga-DOTA-TOC and [^{68}Ga]Ga-DATA-TOC PET/CT examinations (no change of clinical symptoms; no CT-morphologic or other signs of progression; change of serum chromogranin A levels < 10% or serum chromogranin A in normal range) who did not undergo specific anti-tumour therapy except for biotherapy with non-radioactively labelled somatostatin analogues and in whom the biotherapy regimen was not changed between [^{68}Ga]Ga-DOTA-TOC and [^{68}Ga]Ga-DATA-TOC PET/CT were selected for analysis.

Statistical analysis

Statistical analysis was performed using IBM SPSS Statistics (Version 23, International Business Machines Corporation, Armonk, NY, USA). The Mann-Whitney-U test for two independent samples was used to test for differences of mean values between the [^{68}Ga]Ga-DATA-TOC and [^{68}Ga]Ga-DOTA-TOC groups in the main collective and the Wilcoxon test for two related samples was used to compare [^{68}Ga]Ga-DATA-TOC and [^{68}Ga]Ga-DOTA-TOC uptake (SUV_{max} and SUV_{mean}) in the same patients in the sub-collective. Visual lesion conspicuity using ordinal data (scores 0-3) was evaluated using the sign test for two related samples. The ratio of male and female patients between two groups and differences in lesion detection rates were tested for significant differences using the χ^2 test. A p-value < 0.05 was regarded as statistically significant.

Results

Synthesis and purity of [^{68}Ga]Ga-DATA-TOC

Radiolabelling of DATA-TOC with 1.09±0.13 GBq gallium-68 was performed on an automated cassette module system with 89.93±16.9% radiochemical yield (77.43±15.04% AY). A volume activity of 78.00±21.61 MBq/ml and apparent molar activity of 24.70±5.95 MBq/nmol was obtained. Radiochemical purity was higher than > 95%. In terms of quality control the final product fulfilled all requirements requested by the European Pharmacopoeia for [^{68}Ga]Ga-DOTA-TOC. Stability of the final preparation in saline, ethanol and plasma was tested over a period of two half-lives of the isotope and confirmed with TLC as well as HPLC, the results obtained were according to literature [11].

Main collective

Patient characteristics

19 patients who underwent [^{68}Ga]Ga-DATA-TOC PET/CT were retrospectively analysed and compared to a group of 19 patients who underwent [^{68}Ga]Ga-DOTA-TOC PET/CT. The two groups showed no significant differences in age ([^{68}Ga]Ga-DATA-TOC: 62.0±15.5 years, [^{68}Ga]Ga-DOTA-TOC: 63.5±13.1 years, $p > 0.05$), weight ([^{68}Ga]Ga-DATA-TOC: 82.5±29.6 kg, [^{68}Ga]Ga-DOTA-TOC: 75.4±14.2 kg, $p > 0.05$), mean injected activity ([^{68}Ga]Ga-DATA-TOC: 1.84±0.53 MBq/kg, [^{68}Ga]Ga-DOTA-TOC: 1.63±0.44 MBq/kg, $p > 0.05$), time of imaging ([^{68}Ga]Ga-DATA-TOC: 52.5±18.6 min, [^{68}Ga]Ga-DOTA-TOC: 65.1±27.1 min, $p > 0.05$), gender ([^{68}Ga]Ga-DATA-TOC: 47% male, [^{68}Ga]Ga-DOTA-TOC: 53% male, $p > 0.05$), fraction of patients undergoing biotherapy ([^{68}Ga]Ga-DATA-TOC: 63%, [^{68}Ga]Ga-DOTA-TOC: 53%, $p > 0.05$), kidney function ([^{68}Ga]Ga-DATA-TOC: serum creatinine 0.86±0.10 mg/dl (n=15), [^{68}Ga]Ga-DOTA-TOC: serum creatinine 0.97±0.30 mg/dl (n=14), $p > 0.05$), total tumour volume ([^{68}Ga]Ga-DATA-TOC: 44±50 ml, [^{68}Ga]Ga-DOTA-TOC: 160±405 ml, $p > 0.05$) and total tumour uptake ([^{68}Ga]Ga-DATA-TOC: 0.57±0.85%, [^{68}Ga]Ga-DOTA-TOC: 2.80±7.61%, $p > 0.05$).

A neuroendocrine tumour was histologically proven in 37/38 patients (97%), while one patient underwent [^{68}Ga]DOTA-TOC PET/CT due to clinical suspicion of a NET (diarrhoea, elevated chromogranin A), however without pathological imaging findings. One of the patients suffered from two NETs (duodenal NET and ileum NET). Overall, localizations of NETs were (in descending order of frequency) pancreas 10 (26%), ileum 7 (18%), lung 4 (11%), unknown primary 4 (11%), rectum 3 (8%), colon 2 (5%), duodenum 2 (5%), medullary thyroid cancer 2 (5%), appendix 2 (5%), jejunum 1 (3%) and stomach 1 (3%). Ki-67 index was available for 31 patients (mean 8.9±9.1%, range 1%-35%). Grade was G1 in 9 patients (23.7%), G2 in 19 patients (50.0%), G3 in 3 patients (7.9%) and unknown in 7 patients (18.4%). The primary tumour was present in 9 patients (23.7%) at the time of PET/CT imaging. Liver metastases were present in 21 patients (55.3%), lymph node metastases in 14 patients (36.8%) and bone metastases also in 14 patients (36.8%).

Biodistribution in normal organs

Uptake of [^{68}Ga]Ga-DATA-TOC in organs with physiologic SSTR-expression (adrenal glands, pituitary gland and spleen) was significantly lower compared to [^{68}Ga]Ga-DOTA-

TOC. Details are listed in Table 6 and a graphical representation is shown in Figure 16a and b.

Table 6: Uptake of [^{68}Ga]Ga-DATA-TOC and [^{68}Ga]Ga-DOTA-TOC in organs with physiologic expression of the SSTR in the main collective

Organ		**Spleen**		**Adrenals**		**Pituitary**	
Parameter		**SUV_{max}**	**SUV_{mean}**	**SUV_{max}**	**SUV_{mean}**	**SUV_{max}**	**SUV_{mean}**
DATA-TOC	**Mean**	15.37	12.72	6.93	4.03	3.17	1.71
	SD	6.32	5.33	1.89	1.06	1.23	0.55
	N	16		37		19	
DOTA-TOC	**Mean**	26.48	23.21	13.15	7.66	4.63	2.28
	SD	11.46	10.50	5.29	3.04	1.67	0.74
	N	15		36		19	
Ratio DATA-TOC / DOTA-TOC		58.0%	54.8%	52.7%	52.7%	68.5%	75.0%
***p*[a]**		**<0.05**	**<0.05**	**<0.05**	**<0.05**	**<0.05**	**<0.05**

[a]: Mann-Whitney-U test for two independent samples

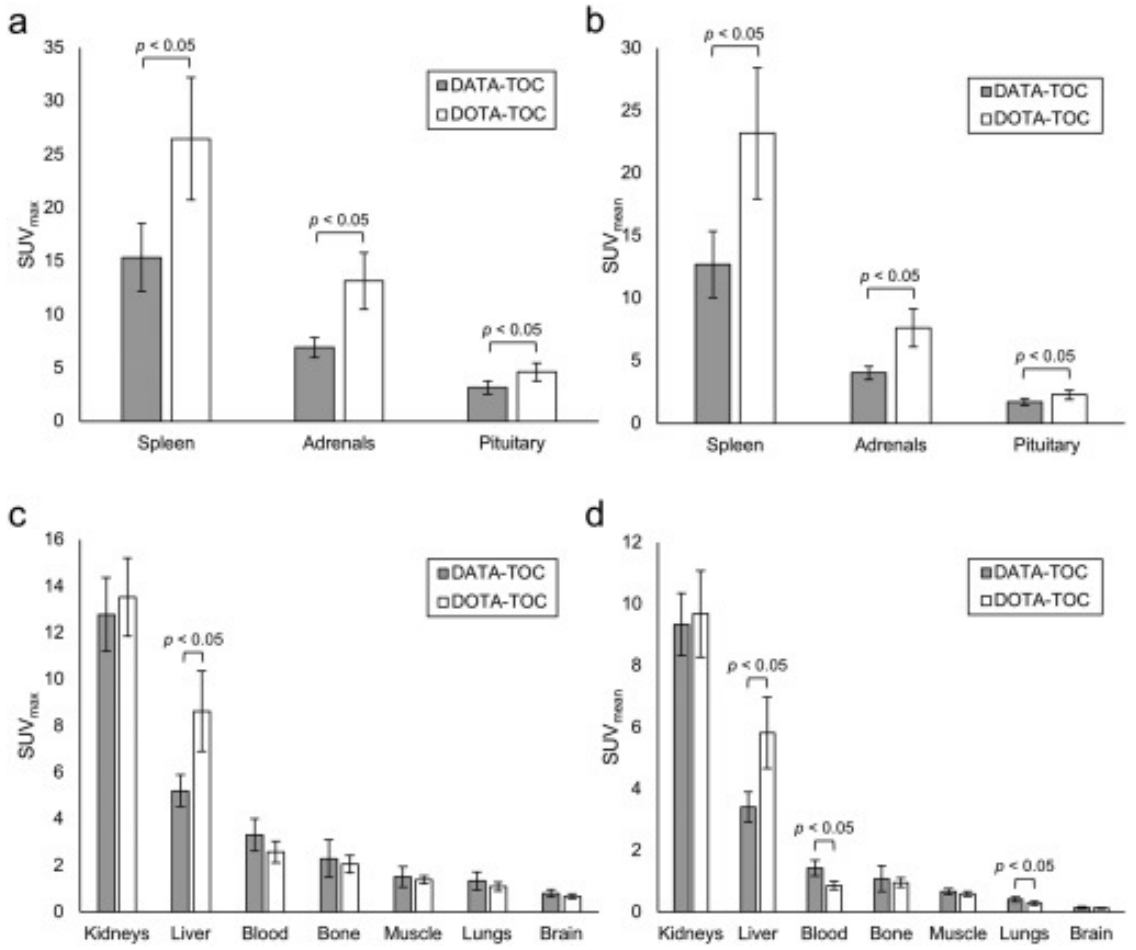

Figure 16: Uptake of [^{68}Ga]Ga-DATA-TOC and [^{68}Ga]Ga-DOTA-TOC in normal tissues in two groups of different patients (each group: n=19). Error bars represent one standard deviation. Significant differences are indicated by brackets. a, b: [^{68}Ga]Ga-DATA-TOC shows lower SUV_{max} and SUV_{mean} compared to [^{68}Ga]Ga-DOTA-TOC in normal tissues with physiologic expression of the SSTR. c, d: [^{68}Ga]Ga-DATA-TOC shows lower background uptake in the liver in comparison to [^{68}Ga]Ga-DOTA-TOC, while a higher background activity of [^{68}Ga]Ga-DATA-TOC was observed in the mediastinal blood pool and in lung tissue (regarding SUV_{mean})

Uptake of [^{68}Ga]Ga-DATA-TOC in the liver was significantly lower compared to [^{68}Ga]Ga-DOTA-TOC, while uptake of [^{68}Ga]Ga-DATA-TOC was higher in the blood pool and in the lungs. There were no significant differences between [^{68}Ga]Ga-DATA-TOC and [^{68}Ga]Ga-DOTA-TOC uptake in other organs. Details are listed in Table 7 and a graphical representation is shown in Figure 16c and 1d.

Table 7: Uptake of [^{68}Ga]Ga-DATA-TOC and [^{68}Ga]Ga-DOTA-TOC in background organs in the main collective

Organ	Parameter	DOTA-TOC N	DOTA-TOC SD	DOTA-TOC Mean	DATA-TOC N	DATA-TOC SD	DATA-TOC Mean	Ratio DATA-[illegible]	p^a
Kidneys	SUV_{max}	38	3.36	13.52	35	3.17	12.78	94.5%	>0.05
	SUV_{mean}		2.81	9.69		2.02	9.34	96.4%	>0.05
Liver	SUV_{max}	19	3.45	8.63	19	1.35	5.21	60.4%	**<0.05**
	SUV_{mean}		2.32	5.83		0.99	3.41	58.6%	**<0.05**
Blood	SUV_{max}	19	0.92	2.59	19	1.39	3.32	128.2%	>0.05
	SUV_{mean}		0.27	0.86		0.51	1.44	167.1%	**<0.05**
Bone	SUV_{max}	19	0.75	2.06	19	1.62	2.30	111.5%	>0.05
	SUV_{mean}		0.31	0.96		0.83	1.09	113.2%	>0.05
Muscle	SUV_{max}	19	0.35	1.39	19	0.88	1.51	108.8%	>0.05
	SUV_{mean}		0.16	0.59		0.20	0.67	112.9%	>0.05
Lungs	SUV_{max}	19	0.40	1.09	19	0.78	1.34	122.1%	>0.05
	SUV_{mean}		0.13	0.29		0.16	0.42	143.7%	**<0.05**
Brain	SUV_{max}	19	0.22	0.68	19	0.31	0.81	119.4%	>0.05
	SUV_{mean}		0.04	0.12		0.05	0.14	116.4%	>0.05

[a]: Mann-Whitney-U test for two independent samples

Tumour lesions

SUV_{max} for all tumour lesions was in the range of 3.0–54.9 for [^{68}Ga]Ga-DATA-TOC and in the range of 1.5–48.6 for [^{68}Ga]Ga-DOTA-TOC, SUV_{mean} was in the ranges of 1.7-42.9 and 0.8–33.0, respectively.

Tumour to background ratios of all tumour lesions were 1.8–45.9 for [^{68}Ga]Ga-DATA-TOC and 1.4–134.9 for [^{68}Ga]Ga-DOTA-TOC regarding SUV_{max} and 1.3–32.0 and 0.8-114.0, regarding SUV_{mean}.

Sub-collective

Patient characteristics

The sub-collective consists of 10 of the 19 patients (5 male, 5 female) who underwent [^{68}Ga]Ga-DATA-TOC PET/CT and had undergone [^{68}Ga]Ga-DOTA-TOC PET/CT during the course of their disease previously.

Mean age was 69.1±11.1 years at the time of [^{68}Ga]Ga-DATA-TOC PET/CT and 68.5±11.0 years at the time of [^{68}Ga]Ga-DOTA-TOC PET/CT. The time interval between [^{68}Ga]Ga-DATA-TOC and [^{68}Ga]Ga-DOTA-TOC PET/CT was 7.1±2.3 months (range 5.1–12.6 months). The mean weight was 75.2±17.4 kg. There were no significant differences regarding mean injected activity ([^{68}Ga]Ga-DATA-TOC: 1.93±0.53 MBq/kg, [^{68}Ga]Ga-DOTA-TOC: 1.71±0.48 MBq/kg, $p > 0.05$), imaging time ([^{68}Ga]Ga-DATA-TOC: 49.5±16.1 min, [^{68}Ga]Ga-DOTA-TOC: 52.7±23.9 min, $p > 0.05$) and kidney function ([^{68}Ga]Ga-DATA-TOC: serum creatinine 0.91±0.08 mg/dl (n=8), [^{68}Ga]Ga-DOTA-TOC: 0.91±0.12 mg/dl (n=9), $p > 0.05$).

Biodistribution in normal organs

Similar to the results of the main collective, uptake of [^{68}Ga]Ga-DATA-TOC in organs with physiologic expression of the SSTR (adrenal glands, pituitary gland, spleen) was also lower compared to [^{68}Ga]Ga-DOTA-TOC in the sub-collective. Details are listed in Table 8 and a graphical representation is shown in Figure 17a and 2b.

Table 8: Uptake of [^{68}Ga]Ga-DATA-TOC and [^{68}Ga]Ga-DOTA-TOC in organs with physiologic expression of the SSTR in the sub-collective

Organ	**Spleen**	**Adrenals**	**Pituitary**

N		7		19		10	
Parameter		**SUV_{max}**	**SUV_{mean}**	**SUV_{max}**	**SUV_{mean}**	**SUV_{max}**	**SUV_{mean}**
DATA-TOC	**Mean**	11.33	9.58	6.79	4.08	2.86	1.63
	SD	3.97	3.65	1.97	0.96	0.74	0.32
DOTA-TOC	**Mean**	21.05	18.56	11.21	6.72	4.15	2.06
	SD	9.42	8.49	4.70	2.58	1.15	0.54
Ratio DATA-TOC / DOTA-TOC		53.8%	51.6%	60.6%	60.7%	68.9%	79.2%
***p*[a]**		>0.05	**<0.05**	**<0.05**	**<0.05**	**<0.05**	**<0.05**

[a]: Wilcoxon test for two related samples

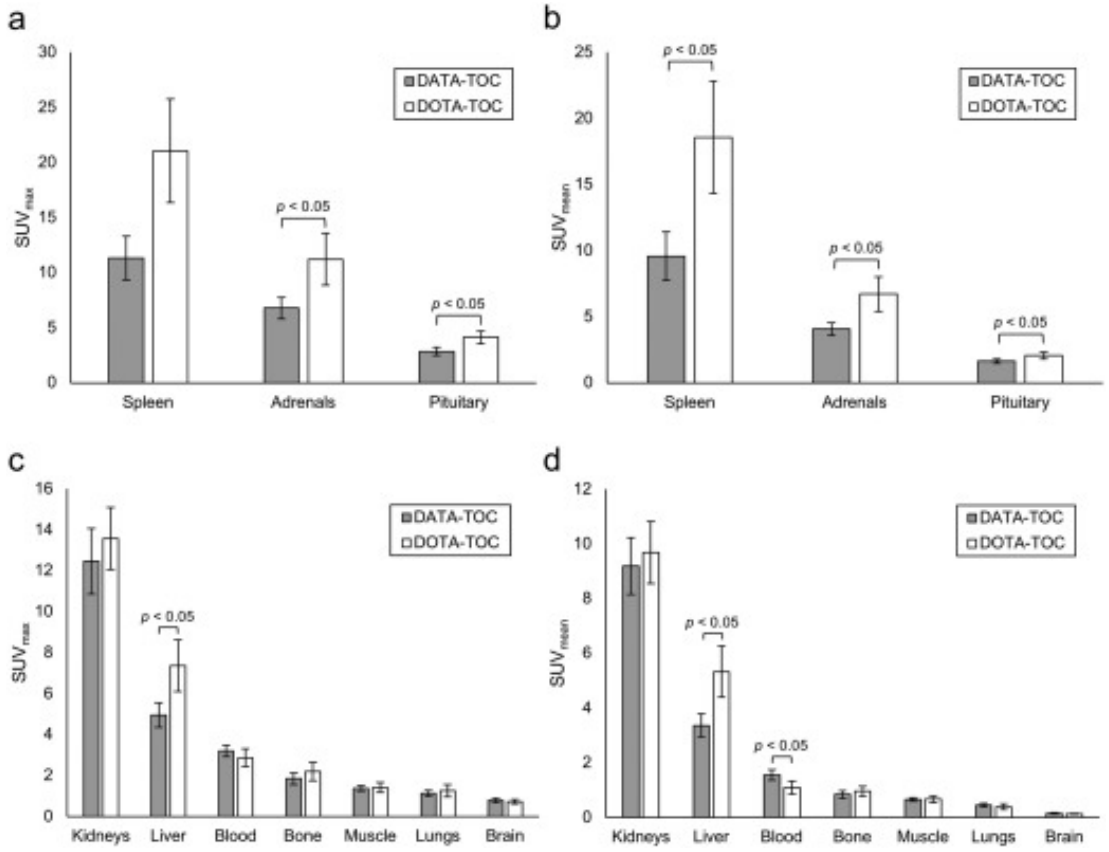

Figure 17: Uptake of [^{68}Ga]Ga-DATA-TOC and [^{68}Ga]Ga-DOTA-TOC in the sub-collective of n=10 patients who underwent [^{68}Ga]Ga-DOTA-TOC PET/CT about 7 months before [^{68}Ga]Ga-DATA-TOC PET/CT. Error bars represent one standard deviation. Signifi-

cant differences are indicated by brackets. a, b: [^{68}Ga]Ga-DATA-TOC shows lower SUV_{max} and SUV_{mean} compared to [^{68}Ga]Ga-DOTA-TOC in normal tissues with physiologic expression of the SSTR. c, d: [^{68}Ga]Ga-DATA-TOC shows lower background uptake in the liver in comparison to [^{68}Ga]Ga-DOTA-TOC, while a higher background activity of [^{68}Ga]Ga-DATA-TOC was observed in the mediastinal blood pool (regarding SUV_{mean})

Comparable to the main collective, uptake of [^{68}Ga]Ga-DATA-TOC in the liver was significantly lower and tracer retention of [^{68}Ga]Ga-DATA-TOC was significantly higher in the mediastinal blood pool. No significant differences were observed in other organs. Details are listed in Table 9 and a graphical representation is shown in Figure 17c and 2d.

Table 9: Uptake of [^{68}Ga]Ga-DATA-TOC and [^{68}Ga]Ga-DOTA-TOC in background organs in the sub-collective

Organ	N	Parameter	DATA-TOC		DOTA-TOC		Ratio	p^a
Kidneys	**18**	**SUV_{max}**	**Mean**	**SD**	**Mean**	**SD**	91.7%	>0.05
Liver	**10**	**SUV_{mean}**	12.45	3.20	13.57	3.05	94.9%	>0.05
Blood	**10**	**SUV_{max}**	9.19	2.08	9.68	2.28	67.2%	**<0.05**
Bone	**10**	**SUV_{mean}**	4.95	1.19	7.36	2.50	63.1%	**<0.05**
Muscle	**10**	**SUV_{max}**	3.36	0.84	5.33	1.86	112.0%	>0.05
Lungs	**10**	**SUV_{mean}**	3.21	0.56	2.86	0.88	142.3%	**<0.05**
Brain	**10**	**SUV_{max}**	1.55	0.38	1.09	0.47	84.1%	>0.05
		SUV_{mean}	1.85	0.58	2.20	0.90	88.4%	>0.05
		SUV_{max}	0.84	0.27	0.95	0.35	97.0%	>0.05
		SUV_{mean}	1.37	0.29	1.41	0.49	97.9%	>0.05
		SUV_{max}	0.65	0.13	0.67	0.23	90.0%	>0.05
		SUV_{mean}	1.12	0.29	1.25	0.60	113.9%	>0.05
		SUV_{max}	0.45	0.13	0.39	0.20	108.8%	>0.05
		SUV_{mean}	0.79	0.22	0.72	0.23	117.2%	>0.05
			0.15	0.05	0.13	0.03		

[a]: Wilcoxon test for two related samples

Tumour lesions

Two of the 10 patients in the sub-collective were excluded from analysis due to therapy with [^{177}Lu]Lu-DOTA-TATE and radiotherapy of bone metastases, two patients were excluded due to changes of chromogranin A of more than 10% and one patient was excluded due to initiation of biotherapy between [^{68}Ga]Ga-DOTA-TOC and [^{68}Ga]Ga-DATA-TOC PET/CT. The remaining 5 patients were eligible for intra-individual comparison of tracer uptake in tumour lesions, the time interval between the two examinations was 7.5±3.0 months (range 5.1–12.6 months).

Both tracers delivered good image quality with high image contrast, allowing the detection of SSTR-positive tumour lesions (see Figure 18).

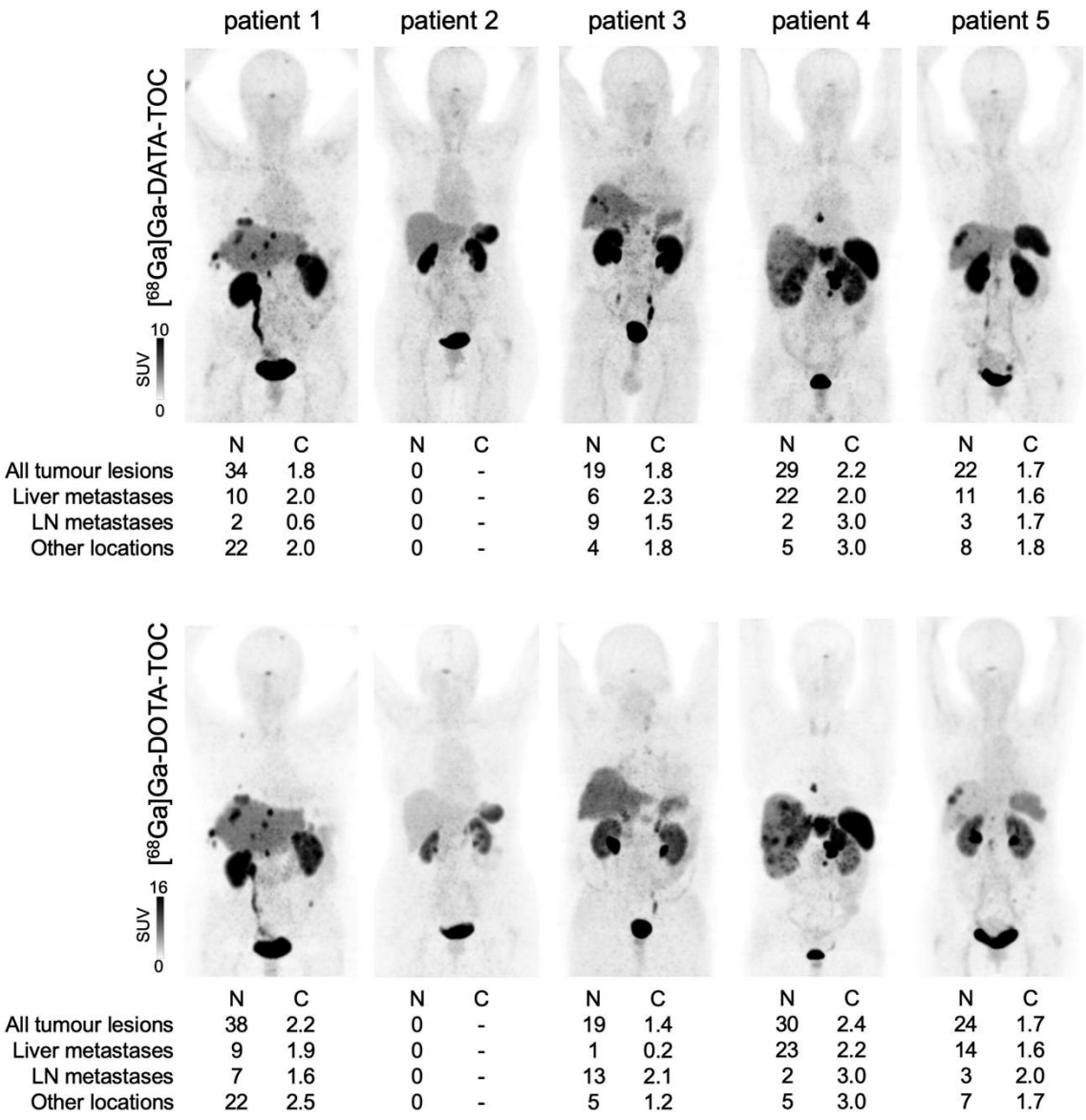

	patient 1		patient 2		patient 3		patient 4		patient 5	
	N	C	N	C	N	C	N	C	N	C
All tumour lesions	34	1.8	0	-	19	1.8	29	2.2	22	1.7
Liver metastases	10	2.0	0	-	6	2.3	22	2.0	11	1.6
LN metastases	2	0.6	0	-	9	1.5	2	3.0	3	1.7
Other locations	22	2.0	0	-	4	1.8	5	3.0	8	1.8

	patient 1		patient 2		patient 3		patient 4		patient 5	
	N	C	N	C	N	C	N	C	N	C
All tumour lesions	38	2.2	0	-	19	1.4	30	2.4	24	1.7
Liver metastases	9	1.9	0	-	1	0.2	23	2.2	14	1.6
LN metastases	7	1.6	0	-	13	2.1	2	3.0	3	2.0
Other locations	22	2.5	0	-	5	1.2	5	3.0	7	1.7

Figure 18: Sample images (maximum intensity projection, MIP) of [^{68}Ga]Ga-DATA-TOC PET (top row, SUV 0-10) and [^{68}Ga]Ga-DOTA-TOC PET (bottom row, SUV 0-16) in the five patients of the sub collective eligible for intra-individual biodistribution comparison. Both tracers show a similar biodistribution with specific accumulation in organs with physiologic SSTR expression (i.e. the pituitary gland) and in tumour lesions.

Uptake of [^{68}Ga]Ga-DATA-TOC (SUV) was significantly lower in tumour lesions compared to [^{68}Ga]Ga-DOTA-TOC, however, tumour to background ratios were not significantly different between the two tracers, regarding all tumour lesions, as well as analysis of subgroups of liver metastases and lymph node metastases. Details are listed in Table 10 and Table 11 and a graphical representation is shown in figure 4.

Table 10: Uptake of [^{68}Ga]Ga-DATA-TOC and [^{68}Ga]Ga-DOTA-TOC in tumour lesions in the sub-collective

Organ		**All tumour lesions**		**Liver metastases**		**Lymph node metastases**	
N		**20**		**11**		**7**	
Parameter		**SUV_{max}**	**SUV_{mean}**	**SUV_{max}**	**SUV_{mean}**	**SUV_{max}**	**SUV_{mean}**
DATA-TOC	**Mean**	9.31	6.33	10.03	7.21	6.27	3.71
	SD	3.81	2.91	1.91	1.67	3.46	1.95
DOTA-TOC	**Mean**	12.94	9.08	13.69	10.49	8.68	4.77
	SD	7.49	6.35	5.85	5.19	4.90	2.30
Ratio DATA-TOC / DOTA-TOC		71.9%	69.7%	73.2%	68.7%	72.2%	77.8%
***p*[a]**		**<0.05**	**<0.05**	**<0.05**	**<0.05**	**<0.05**	**<0.05**

[a]: Wilcoxon test for two related samples

Table 11: Tumour-to-background ratios of [^{68}Ga]Ga-DATA-TOC and [^{68}Ga]Ga-DOTA-TOC in the sub-collective

Organ		**All tumour lesions**		**Liver metastases**		**Lymph node metastases**	
N		**20**		**11**		**7**	
Parameter		**SUV_{max}: BKG**	**SUV_{mean}: BKG**	**SUV_{max}: BKG**	**SUV_{mean}: BKG**	**SUV_{max}: BKG**	**SUV_{mean}: BKG**
DATA-TOC	**Mean**	7.48	4.78	2.93	2.12	11.48	6.67
	SD	6.96	4.48	0.64	0.62	6.33	3.26
DOTA-TOC	**Mean**	9.84	6.31	2.65	2.02	14.05	7.71
	SD	13.42	9.71	1.31	1.10	8.91	4.36
Ratio DATA-TOC / DOTA-TOC		76.0%	75.7%	110.4%	104.7%	81.7%	86.5%

***p*[a]**	>0.05	>0.05	>0.05	>0.05	>0.05	>0.05

[a]: Wilcoxon test for two related samples

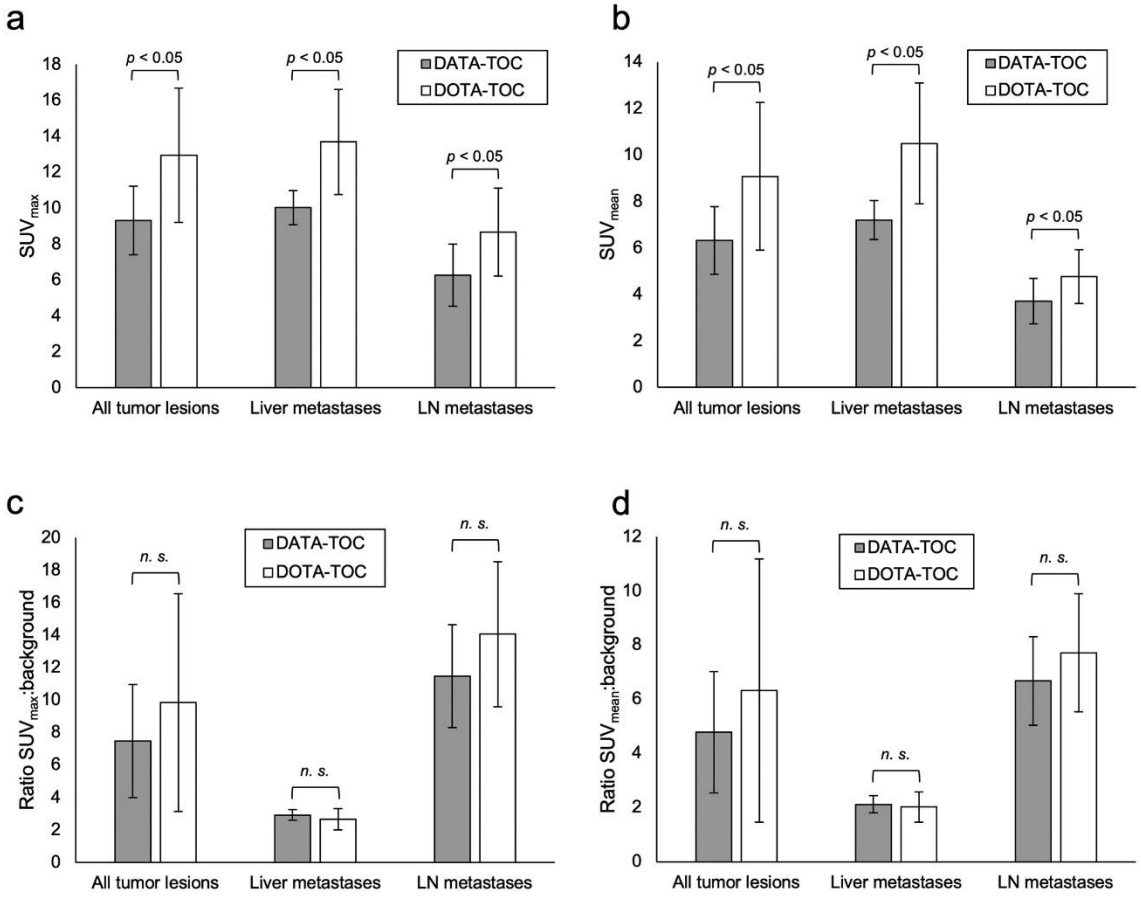

Figure 19: Uptake of [^{68}Ga]Ga-DATA-TOC and [^{68}Ga]Ga-DOTA-TOC in the sub-collective of n=5 patients with clinical stable disease who underwent [^{68}Ga]Ga-DOTA-TOC PET/CT about 7 months before [^{68}Ga]Ga-DATA-TOC PET/CT. Error bars represent one standard deviation. a, b: [^{68}Ga]Ga-DATA-TOC shows lower SUV_{max} and SUV_{mean} compared to [^{68}Ga]Ga-DOTA-TOC in tumour lesions, which was significant for all tumour lesions and in the subgroup of liver metastases. c, d: Uptake ratios (tumour to background ratios) of [^{68}Ga]Ga-DATA-TOC showed no significant differences in comparison to [^{68}Ga]Ga-DOTA-TOC uptake ratios.

On visual analysis, both reviewers detected 104 tumour lesions by [^{68}Ga]Ga-DATA-TOC and 111 lesions by [^{68}Ga]Ga-DOTA-TOC, with no significant differences in lesion detectability and lesion conspicuity. No significant differences were observed in detectability and conspicuity of liver metastases. Regarding lymph node metastases, lesion conspicuity was significantly lower in the [^{68}Ga]Ga-DATA-TOC images and 9 lesions were missed

by [^{68}Ga]Ga-DATA-TOC (16 lesions vs 25 lesions), which however did not reach the level of significance ($p > 0.05$). In the remaining organ systems, no differences were observed lesion detectability and conspicuity. Details are listed in Table 12

Table 12: Lesion detectability and conspicuity of [^{68}Ga]Ga-DATA-TOC and [^{68}Ga]Ga-DOTA-TOC in the sub-collective.

		Lesion detection			Lesion conspicuity	
		detected (n)	missed (n)	p^a	mean con-spicuity	p^b
All tumour lesions	DATA-TOC	104	18	>0.05	1.86	>0.05
Liver metastases	DOTA-TOC					
Lymph node metastases	DATA-TOC	111	11	>0.05	1.97	>0.05
Other lesions	DOTA-TOC	49	6	>0.05	1.93	**<0.05**
	DATA-TOC	47	8	>0.05	1.76	>0.05
	DOTA-TOC	16	9		1.36	
	DATA-TOC	25	0		2.00	
	DOTA-TOC	39	3		2.07	
		39	3		2.21	

[a]: χ^2 test

[b]: Sign test for two related samples

Discussion

Both [^{68}Ga]Ga-DATA-TOC and [^{68}Ga]Ga-DOTA-TOC showed pronounced accumulation in organs with physiologic expression of the SSTR and in neuroendocrine tumour lesions.

Uptake (SUV) of [^{68}Ga]Ga-DATA-TOC in organs with physiologic SSTR-expression (pituitary gland, adrenal glands, spleen) was lower compared to [^{68}Ga]Ga-DOTA-TOC, which points to a lower specific uptake of [^{68}Ga]Ga-DATA-TOC. Also, tumour lesions showed significantly lower [^{68}Ga]Ga-DATA-TOC uptake compared to [^{68}Ga]Ga-DOTA-TOC, which was true for all tumour lesions, as well as for the subgroups of liver metastases and lymph node metastases.

On the other hand, tumour to background ratios did not differ significantly between [^{68}Ga]Ga-DATA-TOC and [^{68}Ga]Ga-DOTA-TOC. Regarding liver metastases, tumour to background ratios of [^{68}Ga]Ga-DATA-TOC were even slightly higher compared to [^{68}Ga]Ga-DOTA-TOC, which was caused by a significantly lower background uptake of [^{68}Ga]Ga-DATA-TOC in normal liver tissue.

Regarding lesion detectability and lesion conspicuity, overall a slightly higher number of lesions was detected by [^{68}Ga]Ga-DOTA-TOC, with a higher mean lesion conspicuity, which however did not reach the level of significance. Subgroup analysis showed a tendency for a lower detectability of lymph node metastasis for [^{68}Ga]Ga-DATA-TOC, which however did not reach the level of significance, while conspicuity of lymph node metastases was significantly lower for [^{68}Ga]Ga-DATA-TOC. On the other hand, we observed a trend for a higher detectability and conspicuity of liver metastases for [^{68}Ga]Ga-DATA-TOC, which can be attributed to the lower physiological background uptake of [^{68}Ga]Ga-DATA-TOC in liver tissue. There were no noticeable differences in detectability and conspicuity of tumour lesions in other organs.

The results of visual analysis are in line with semi-quantitative SUV analysis, showing a significantly lower background uptake of [^{68}Ga]Ga-DATA-TOC in liver tissue, which might be advantageous for detection of liver metastases. On the other hand, the lower detectability and conspicuity of lymph node metastases might be explained by a lower specific accumulation of [^{68}Ga]Ga-DATA-TOC in SSTR-positive tissues. [^{68}Ga]Ga-DATA-TOC showed a higher retention in the blood pool compared to [^{68}Ga]Ga-DOTA-TOC, which might lead to a higher unspecific background activity in normal tissues, however no significant differences were observed for uptake in muscle or bone tissues, which served as reference organs for calculation of tumour-to-background ratios in our study.

As impairments of kidney function might alter tracer distribution, we retrospectively assessed serum creatinine at the time of the PET/CT examinations in patients where data on blood tests were available. No significant differences in serum creatinine levels were observed between the [^{68}Ga]Ga-DATA-TOC and [^{68}Ga]Ga-DOTA-TOC groups, thus an interference of kidney function with biodistribution data seems unlikely in our collective.

It is well known that biotherapy with long-acting somatostatin analogs can impact normal organ uptake of [^{68}Ga]Ga-DOTA-TATE, as published by Haug et al. in 2011 and more recently by Ayati et al. in 2018 [15, 16]. In our collective, there was no significant difference in the fraction of patients receiving biotherapy in the groups undergoing either [^{68}Ga]Ga-DATA-TOC PET/CT or [^{68}Ga]Ga-DOTA-TOC PET/CT, therefore an interference of biotherapy effects with the results of our study regarding the differences in biodistribution between the two tracers seems unlikely.

To exclude a potential effect of tumour burden on tracer biodistribution in normal organs in terms of a “tumour sink effect”, we quantified tumour burden (tumor volume and fraction of activity taken up by the tumour) in the main collective. Both parameters did not differ significantly between the two groups, thus our results are unlikely to be affected by a potential tumour sink effect.

There are limitations to our study. In the sub-collective, the [^{68}Ga]Ga-DOTA-TOC PET/CT examination was performed about 7 months before [^{68}Ga]Ga-DATA-TOC PET/CT. Therefore, even though only patients with clinical stable disease were assessed, a systematic interference of tumour dynamics with uptake evaluation cannot be excluded. Though no significant differences were observed between [^{68}Ga]Ga-DATA-TOC and [^{68}Ga]Ga-DOTA-TOC regarding lesion detectability in our current evaluation, the small number of patients eligible for tumour uptake evaluation (n=5) does not allow to draw a definite conclusion. Further analysis of the clinical performance of [^{68}Ga]Ga-DATA-TOC PET/CT in a larger patient collective is warranted.

Conclusions

[^{68}Ga]Ga-DATA-TOC is a promising new PET radiotracer for the detection of neuroendocrine tumour lesions. The most important aspect is its ability for radiolabelling with gallium-68 at room temperature with a high efficacy, eliminating the need for a final purification step and thus paving the way for the development of an instant kit-type radiolabelling method [11–14].

In our study, a particular focus was on the subgroup of patients diagnosed by both the tracers and to study the potential of [^{68}Ga]Ga-DATA-TOC in the detection of liver metastases. A significantly lower physiologic background uptake in the liver of [^{68}Ga]Ga-DATA-TOC compared to [^{68}Ga]Ga-DOTA-TOC resulted in slightly higher (though not statistically significant) tumour-to-background ratios for liver metastases. Visual analysis showed a trend for a higher detectability and conspicuity of liver metastases for [^{68}Ga]Ga-DATA-TOC.

The new ^{68}Ga-DATA-octreotide tracer has substantial advantages over similar DOTA-conjugated analogues as it allows an instant kit-type preparation at room temperature as established in the radiolabelling of ^{99m}Tc-radiopharmaceuticals. Our current study, showing the clinical feasibility of [^{68}Ga]Ga-DATA-TOC PET/CT for imaging of patients with neuroendocrine tumours, provides first clinical evidence that the chemistry and pharmacology of [^{68}Ga]Ga-DATA-TOC successfully translates into patient studies.

Acknowledgements: We thank the technicians at the PET facility for performing the patient scans. We thank Dr. Stefan Kürpig for synthesis of [^{68}Ga]Ga-DATA-TOC and [^{68}Ga]Ga-DOTA-TOC.

Conflicts of interest: RB: consultant for Bayer Healthcare and Eisai; non-commercial research agreement with and speaker for Mediso Medical Imaging. ME: consultant for Bayer, Novartis, Eisai and Ipsen.

Funding: EE: research grant from the University Hospital Bonn, Germany (BONFOR O-140.0008).

Ethical approval: All procedures performed in studies involving human participants were in accordance with the ethical standards of the institutional and/or national research committee and with the principles of the 1964 Declaration of Helsinki and its later amendments or comparable ethical standards. [^{68}Ga]Ga-DATA-TOC and [^{68}Ga]Ga-DOTA-TOC were administered in compliance with The German Medicinal Products Act, AMG §13 2b, and in accordance with the responsible regulatory body. Informed consent was obtained from all patients before undergoing PET/CT imaging. For this type of study (retrospective study), additional formal consent from the patients to participate in the retrospective analysis was not required.

References

1. Niederle B, Pape U-F, Costa F, Gross D, Kelestimur F, Knigge U, et al. ENETS Consensus Guidelines Update for Neuroendocrine Neoplasms of the Jejunum and Ileum. Neuroendocrinology. 2016;103:125–38. doi:10.1159/000443170.

2. Falconi M, Eriksson B, Kaltsas G, Bartsch DK, Capdevila J, Caplin M, et al. ENETS Consensus Guidelines Update for the Management of Patients with Functional Pancreatic Neuroendocrine Tumors and Non-Functional Pancreatic Neuroendocrine Tumors. Neuroendocrinology. 2016;103:153–71. doi:10.1159/000443171.

3. Öberg K, Hellman P, Ferolla P, Papotti M. Neuroendocrine bronchial and thymic tumors: ESMO Clinical Practice Guidelines for diagnosis, treatment and follow-up. Ann Oncol. 2012;23 Suppl 7:vii120-3. doi:10.1093/annonc/mds267.

4. Öberg K, Knigge U, Kwekkeboom D, Perren A. Neuroendocrine gastro-entero-pancreatic tumors: ESMO Clinical Practice Guidelines for diagnosis, treatment and follow-up. Ann Oncol. 2012;23 Suppl 7:vii124-30. doi:10.1093/annonc/mds295.

5. Strosberg JR, Halfdanarson TR, Bellizzi AM, Chan JA, Dillon JS, Heaney AP, et al. The North American Neuroendocrine Tumor Society Consensus Guidelines for Surveillance and Medical Management of Midgut Neuroendocrine Tumors. Pancreas. 2017;46:707–14. doi:10.1097/MPA.0000000000000850.

6. Geijer H, Breimer LH. Somatostatin receptor PET/CT in neuroendocrine tumours: update on systematic review and meta-analysis. European Journal of Nuclear Medicine and Molecular Imaging. 2013;40:1770–80. doi:10.1007/s00259-013-2482-z.

7. Barrio M, Czernin J, Fanti S, Ambrosini V, Binse I, Du L, et al. The Impact of Somatostatin Receptor-Directed PET/CT on the Management of Patients with Neuroendocrine Tumor: A Systematic Review and Meta-Analysis. J. Nucl. Med. 2017;58:756–61. doi:10.2967/jnumed.116.185587.

8. Maxwell JE, Sherman SK, Menda Y, Wang D, O'Dorisio TM, Howe JR. Limitations of somatostatin scintigraphy in primary small bowel neuroendocrine tumors. J Surg Res. 2014;190:548–53. doi:10.1016/j.jss.2014.05.031.

9. Gabriel M, Decristoforo C, Kendler D, Dobrozemsky G, Heute D, Uprimny C, et al. 68Ga-DOTA-Tyr3-octreotide PET in neuroendocrine tumors: comparison with somatostatin receptor scintigraphy and CT. J. Nucl. Med. 2007;48:508–18. doi:10.2967/jnumed.106.035667.

10. Deppen SA, Blume J, Bobbey AJ, Shah C, Graham MM, Lee P, et al. 68Ga-DOTA-TATE Compared with 111In-DTPA-Octreotide and Conventional Imaging for Pulmonary and Gastroenteropancreatic Neuroendocrine Tumors: A Systematic Review and Meta-Analysis. J. Nucl. Med. 2016;57:872–8. doi:10.2967/jnumed.115.165803.

11. Seemann J, Waldron B, Parker D, Roesch F. DATATOC: a novel conjugate for kit-type 68Ga labelling of TOC at ambient temperature. EJNMMI radiopharm. chem. 2017;1:4. doi:10.1186/s41181-016-0007-3.

12. Seemann J, Waldron BP, Roesch F, Parker D. Approaching 'Kit-Type' Labelling with (68)Ga: The DATA Chelators. ChemMedChem. 2015;10:1019–26. doi:10.1002/cmdc.201500092.

13. Spang P, Herrmann C, Roesch F. Bifunctional Gallium-68 Chelators: Past, Present, and Future. Semin Nucl Med. 2016;46:373–94. doi:10.1053/j.semnuclmed.2016.04.003.

14. Nock BA, Kaloudi A, Nagel J, Sinnes J-P, Roesch F, Maina T. Novel bifunctional DATA chelator for quick access to site-directed PET 68Ga-radiotracers: preclinical proof-of-principle with Tyr3octreotide. Dalton Trans. 2017;46:14584–90. doi:10.1039/c7dt01684k.

15. Haug AR, Rominger A, Mustafa M, Auernhammer C, Göke B, Schmidt GP, et al. Treatment with octreotide does not reduce tumor uptake of (68)Ga-DOTATATE as measured by PET/CT in patients with neuroendocrine tumors. J. Nucl. Med. 2011;52:1679–83. doi:10.2967/jnumed.111.089276.

16. Ayati N, Lee ST, Zakavi R, Pathmaraj K, Al-Qatawna L, Poon A, Scott AM. Long-Acting Somatostatin Analog Therapy Differentially Alters 68Ga-DOTATATE Uptake in Normal Tissues Compared with Primary Tumors and Metastatic Lesions. J. Nucl. Med. 2018;59:223–7. doi:10.2967/jnumed.117.192203.

6.4 [^{68}Ga]Ga-DATA5m.SA.FAPi PET/CT: Specific Tracer-uptake in Focal Nodular Hyperplasia and potential Role in Liver Tumor Imaging

Kreppel B[1], Gaertner FC[1], Marinova M[2], Attenberger[2], U, Meisenheimer M[1], Toma M[3], Kristiansen G[3], Feldmann G[4], van der Veken, P[6], Moon, Euy Sung, Rösch[5] F, Essler M[1]

[1]Department of Nuclear Medicine, University Medical Center Bonn, Bonn, Germany

[2]Department of Radiology, University Medical Center Bonn, Bonn, Germany

[3]Department of Pathology, University Medical Center Bonn, Bonn, Germany

[4]Department of Internal Medicine III, University Medical Center Bonn, Bonn, Germany

[5]Department of Nuclear Chemistry, Johannes Gutenberg University, Mainz, Germany

[6]Department of Pharmaceutical Sciences, Laboratory of Medical Biochemistry, University of Antwerp, 2610 Wilrijk, Belgium

Corresponding author:

Dr. Barbara Kreppel

Department of Nuclear Medicine

University Medical Center Bonn,

Venusberg-Campus 1

53127 Bonn

Germany

Email: barbara.kreppel@ukbonn.de

Phone: 0228 287 19858

https://doi.org/10.1055/a-1164-5667

Abstract

Fibroblast activating protein (FAP) is a membrane bound serine protease increased in activated fibroblasts occurring during tissue remodeling in benign and malignant diseases. Carcinoma-associated fibroblasts (CAF) contribute to the formation of tumor stroma promoting tumor growth, angiogenesis as well as immune-escape. Quinoline-based FAP-specific enzyme inhibitors (FAPis) labeled with ^{68}Ga were recently introduced as novel, highly effective PET-tracers for tumor imaging. Here we report about a thyroid carcinoma patient with increased Tg level without ^{131}I-positive lesions. A [^{68}Ga]Ga-DATA 5m.SA.FAPi-PET/CT was performed to detect resectable metastases. We found no metastases but a focal traceraccumulation in the liver. Histology revealed that the tracer-accumulation corresponded to focal nodular hyperplasia expressing FAPi in fibrous septa. The case presented indicated that FAPi-PET helps to detect fibrous remodeling in benign and malignant tumors. This may be helpful especially in differential diagnosis of liver tumors.

Keywords: FAPi, PET/CT, fibroblast activating protein (FAP), focal nodular hyperplasia (FNH), metastasized thyroid carcinoma

Background

Fibroblast activating protein (FAP) is a membrane bound serine protease up-regulated in activated fibroblasts. These are essential for tissue remodeling in wound healing, chronic inflammation as well as in carcinoma associated fibroblasts (CAF) in several types of cancer [1–6]. Subject of recent developments are new ^{68}Ga-labelled PET tracers that operate as FAP-specific enzyme inhibitors (FAPi). The inhibitor is a small molecule based on a 4,4-difluoroproline-quinoline motif with a carbonitrile warhead that binds to FAP and blocks its chemical reaction. This highly potent inhibitor, referred to as UAMC 1110, combines high affinity respectively high inhibition ability to FAP and in opposite towards DPPs and PREP [7]. Various tumors and proliferating tissue show an uptake of this tracer. FAPi shows rapid washout from normal tissue facilitating high-contrast images. This is particularly advantageous as the sensitivity of FDG-PET is low in regions with high or inhomogenous glucose metabolism such as brain, heart or the liver [8]. Therefore, FAPi-PET may be superior to FDG-PET in these regions. The new class of FAPi-radiopharmaceuticals utilizes a squaric acid (SA) motif as part of the structure connecting the inhibitor moiety UAMC 1110 with various chelators such as DOTA and DATA, yielding precursors of type DOTA.SA.FAPi or DATA^{5m}.SA.FAPi. All compounds are of low nanomolar binding affinity to FAP and excellent selectivity towards other proteases [9].

Focal nodular hyperplasia (FNH) is the second most common benign liver tumor. The development is based on non-specific hyperplasia in response to a vascular transformation. In addition, an association with the intake of contraceptives containing estrogen is suspected. Diagnosis is usually based on sonography, contrast-enhanced CT or MRI. FNH is frequently an accidental finding. Therapy is usually not necessary. In difficult cases, however, a biopsy may also be necessary to rule out hepatocellular adenoma or carcinoma as well as metastases from extrahepatic tumors [10, 11].

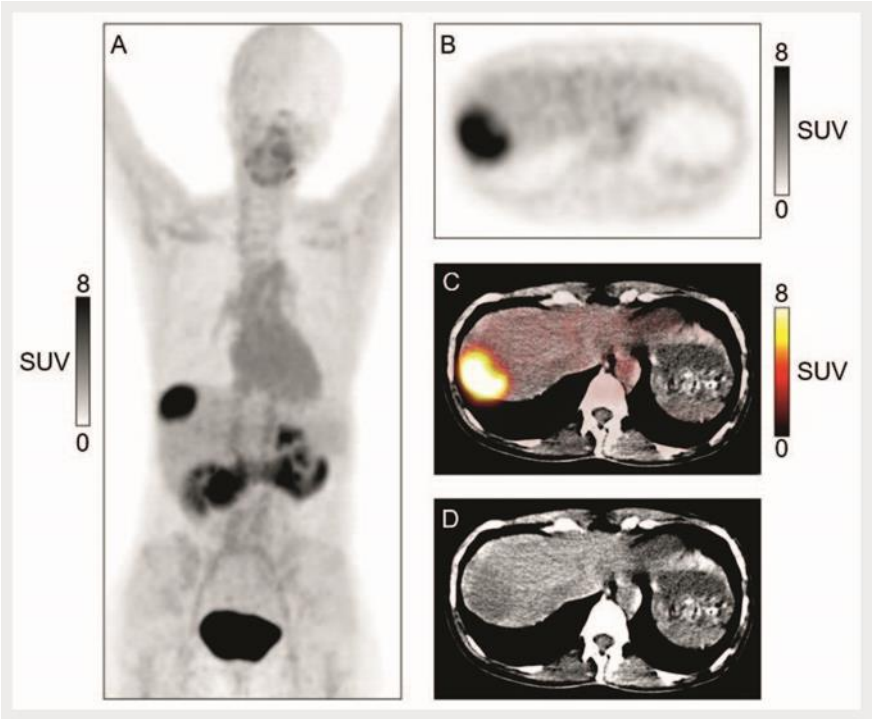

Fig. 6 FAPi-PET/CT. Intensive tracer uptake in liver segment 8. In low-dose CT-technique without contrast medium there is only a faint hypodense lesion.

Case presentation

We report about a 44-year old female with thyroid carcinoma initially metastasized to the lung. The primary tumor was first diagnosed in 1998 and treated with surgery and 8 cycles of ^{131}I radiotherapy. As the tumormarker Tg was rising and ^{131}I whole body scans were negative, we decided to perform a [^{68}Ga]Ga-DATA 5m.SA.FAPi PET/CT for restaging to potentially find tumor manifestations accessible to resection.

In the present study we used the DATA^{5m}.SA.FAPi option because of its slightly better IC_{50} values (0.7 nM for Ga-DATA^{5m}.SA.FAPi vs. 1.4 for Ga-DOTA.SA.FAPi) and because of its ease of preparation in an instant kit-type protocol. Radiolabeling of [^{68}Ga]Ga-DATA^{5m}.SA.FAPi (obtained from the Department of Chemistry, JGU Mainz, Germany) was carried out in 3.34 ± 0.04 mL 0.08 M ammonium acetate buffer (ABX advanced biochemical compounds GmbH, Radeberg, Germany) pH= 3.6,with ^{68}Ga obtained from a 1.85 GBq ^{68}Ge/^{68}Ga-generator. Manual synthesis was carried out in a thermo shaker at a temperature of 50 °C for 8 min.

Radiochemical yield was ≥92 %, radiochemical purity ≥97 %.

The patient was intravenously administered with 210 MBq [^{68}Ga]Ga-FAPi. Whole body static imaging was performed 82 minutes p. i. with an acquisition time of 4 min per bed position using a Siemens Biograph 2 PET/CT machine.

PET/CT images did not show increased tracer-uptake in the neck region or in pulmonary lesions, but a focal tracer-enrichment in liver segment 8 corresponding to a faint hypodense lesion in native low-dose computed tomography (CT) (Figure 1). For further work-up, a MRI scan was performed and a CT-guided biopsy was taken. MRI shows a typical pattern of FNH (Figure 2). Histopathological examination using microscopy and immunohistochemistry (FAP, glutamin synthetase and cytokeratin 7) showed evidence of FNH. The sections stained positive for FAP in immunohistochemistry (Figure 3).

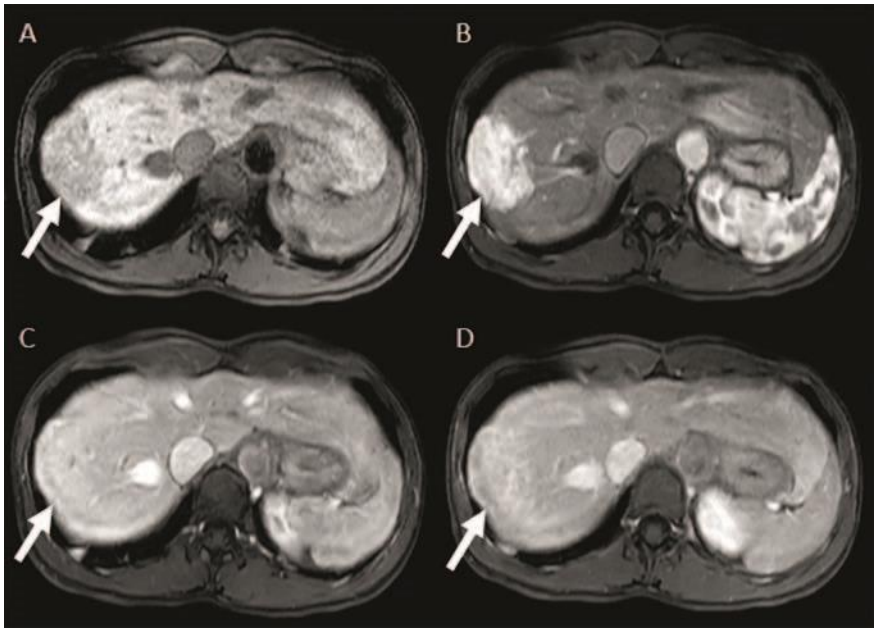

Fig. 7 MRI of the liver. MR-images demonstrate T1-weighted native A and contrast-enhanced (B–D postcontrast dynamic) sequences in a transversal plane of 44-year old female patient with an incidental finding of a big unclear focal liver lesion at the right liver lobe. A On the native T1-weighted image the liver mass (white arrow) at the right liver lobe appears hypointense compared to the surrounding normal liver. B The liver lesion shows an intense early homogeneous contrast enhancement on the arterial phase and is more hyperintense than the liver parenchyma. C, D The liver lesion is almost isointense to the surrounding liver parenchyma on portal venous C and venous D phase with no central fibrotic scar seen. The mass cannot be clearly distinguished from the liver parenchyma.

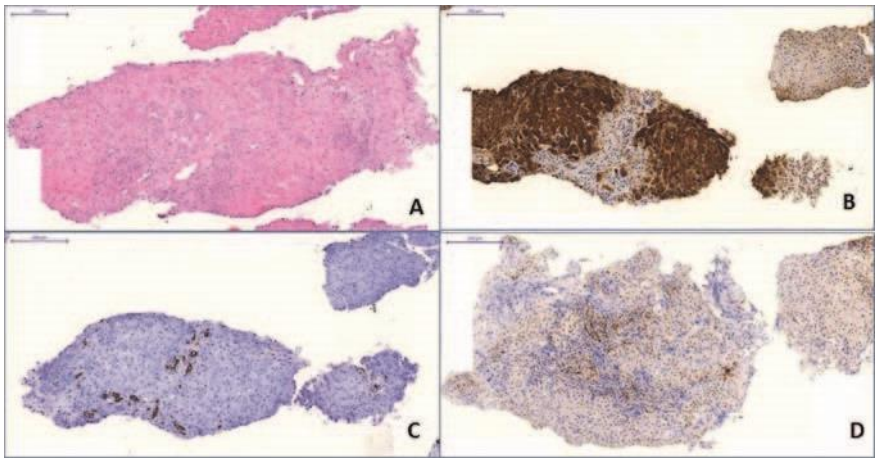

Fig. 8 3 Histopathology of the FAPi-positive lesion. A HE-staining. Liver tissue with nodular structured benign hepatocytes, separated by fibrous septa. Large dystrophic vessels appear in the fibrous septa. B FAP-immunohistochemistry. FAP-positive fibroblasts are present in the fibrous septa. C Glutaminsynthetase-immunohistochemistry. Large areas of hepatocytes expressing Glutaminsynthetase. D Cytokeratin 7-immuohistochemistry. Proliferating neoductuli in the fibrous septa.

Discussion and conclusions

The case presented here demonstrates that FAPi-PET/CT may be helpful to characterize a variety of malignant and benign tumors. In addition, the present case also provides indications of possible pitfalls, which should be taken into account when interpreting FAPi-PET. It seems surprising to us that activated fibroblasts are present in FNH suggesting a functional role for growth of this tumor type. It will be important to see whether other benign liver tumors such as adenomas or hemangiomas also harbor activated fibroblasts detectable by PET-imaging. In our opinion it is very likely that most malignant liver tumors show high FAPi-accumulation. Possibly, also tissue remodeling in cirrhosis leads to activation of fibroblasts resulting in FAPIuptake. In this case, FAPi-PET may be useful to detect active progression of cirrhosis. Finally, FAPi-PET may be helpful for radiation therapy planning in liver tumors as FDG-PET has a high background in the liver hampering target volume definition. FAPi-PET may also play a role in planning of checkpoint-inhibitor treatment of hepatocellular carcinoma in the future, as activated fibroblasts modulate immune cell functions in tumor stroma. We propose that FAPiPET will play a vital role in diagnosis and molecular characterization of liver tumors in the future.

References

1. P S Acharya. Fibroblast activation protein: a serine protease expressed at the remodeling interface in idiopathic pulmonary fibrosis. Hum Pathol. 2006;37:352.
2. C Egger. Effects of the fibroblast activation protein inhibitor, PT100, in a murine model of pulmonary fibrosis. Eur J Pharmacol. 2017;809:64.
3. P Giuffrida. Biomarkers of intestinal fibrosis – one step towards clinical trials for stricturing inflammatory bowel disease. United European Gastroenterol J. 2016;4:523.
4. M T Levy. Fibroblast activation protein: a cell surface dipeptidyl peptidase and gelatinase expressed by stellate cells at the tissue remodelling interface in human cirrhosis. Hepatology. 1999;29:1768.
5. J I López. Fibroblast activation protein predicts prognosis in clear cell renal cell carcinoma. Hum Pathol. 2016;54:100.
6. L Rovedatti. Fibroblast activation protein expression in Crohn's disease strictures. Inflamm Bowel Dis. 2011;17:1251.
7. K Jansen. Extended structure-activity relationship and pharmacokinetic investigation of (4-quinolinoyl)glycyl-2-cyanopyrrolidine inhibitors of fibroblast activation protein (FAP). J Med Chem. 2014;57:3053.
8. F L Giesel. 68Ga-FAPI PET/CT: Biodistribution and Preliminary Dosimetry Estimate of 2 DOTA-Containing FAP-Targeting Agents in Patients with Various Cancers. J Nucl Med. 2019;60:386.
9. Moon ES, Elvas F, Vliegen G, Lombaerde S de, Vangestel C, Bruycker S de, et al. Targeting fibroblast activation protein (FAP): next generation PET radiotracers using squaramide coupled bifunctional DOTA and DATA5m chelators. EJNMMI radiopharm. chem. 2020;5:19. doi:10.1186/s41181-020-00102-z.
10. A K Koehne de Gonzalez. Current concepts in the immunohistochemical evaluation of liver tumors. World J Hepatol. 2015;7:1403.
11. S Rebouissou. Molecular pathogenesis of focal nodular hyperplasia and hepatocellular adenoma. J Hepatol. 2008;48:163.

6.5 Targeting Targeting glucose transport and the NAD pathway in tumor cells with STF-31 - a reevaluation

Dominik Kraus[1], Jan Reckenbeil[1], Nadine Veit[2], Stefan Kuerpig[3], Michael Meisenheimer[3], Imke Beier[1], Helmut Stark[1], Jochen Winter[4#] and Rainer Probstmeier[2,#]

[1] Department of Prosthodontics, Preclinical Education, and Material Sciences, University of Bonn, Bonn, Germany

[2] Neuro- and Tumor Cell Biology Group, Department of Nuclear Medicine, University of Bonn, Bonn, Germany

[3] Department of Nuclear Medicine, University of Bonn, Bonn, Germany

[4] Oral Cell Biology Group, Department of Periodontology, Operative and Preventive Dentistry, University of Bonn, Bonn, Germany

[#]both authors have contributed equal amount of work

*Corresponding author: Rainer Probstmeier, Neuro- and Tumor Cell Biology Group, Department of Nuclear Medicine, University Hospital of Bonn, Sigmund-Freud-Str. 25, D-53127 Bonn, Germany; Tel: +49-228-287-19162; Fax: +49-228-287-11016; E-mail: r.probstmeier@uni-bonn.de

https://doi.org/10.1007/s13402-018-0385-5

Abstract

Targeting glucose metabolism is a promising way to interfere with tumor cell proliferation and survival. However, controversy exists about the specificity of some anticancer drugs. Especially the potency of STF-31 has been inconsistently discussed in this context. In this respect, we have analysed the impact of glucose transporter (GLUT) inhibitors fasentin and WZB117, nicotinamide phosphoribosyltransferase (NAMPT) inhibitor GMX1778 and STF-31 on tumor cell proliferation and survival as well as on glucose uptake efficiency.

When tumor cell lines A172 (glioblastoma), BHY (oral squamous cell carcinoma), HeLa (cervix adenocarcinoma), HN (head neck cancer), HT-29 (colon carcinoma) and MG-63 (osteosarcoma) were treated with these compounds, a complex reaction pattern emerged, whereby tumor cell proliferation and survival threatening concentrations varied by more than one order of magnitude amongst the cell lines. Threatening effects of GMX1778- and STF-31-treatment could be partially abolished by (i) nicotinic acid (NA), but only in nicotinic acid phosphoribosyltransferase (NAPRT) expressing cells lines and (ii) nicotinamide mononucleotide (NMN) in all cell lines, supporting the classification of STF-31 as a NAMPT inhibitor.

In short-time [^{18}F]-fluoro-deoxyglucose uptake experiments GLUT inhibitor WZB-117 application led to an almost complete inhibition in all cell lines, whereas fasentin-provoked inhibition was more cell-line dependent with a maximal value of about 35% in A172, BHY, HeLa and HT-29 cells. STF-31 inhibited glucose uptake in all cell lines in the range of 25 to about 50%. These data support the classification of STF-31 as a GLUT inhibitor. All together our data demonstrate a dual action of STF-131, serving as a NAMPT as well as a GLUT inhibitor, whereby the latter one seems to become only pronounced at higher STF-31 concentrations. The molecular basis of such a dual reaction pattern and its appearance in small compounds previously designated as specific NAMPT inhibitors needs further investigation.

Keywords: fasentin, glucose transporter, GMX1778, NAMPT, STF-31, WZB117

Background

It is well established that tumor cells exhibit special metabolic requirements in comparison to normal non-proliferating cells [1, 2]. During the last years considerable efforts have been made to target tumor-specific metabolic alterations in the context of therapeutic regimen [1–3]. Based on historical reasons, such efforts first concentrated on the so-called Warburg effect, a metabolic phenotype, in which metabolic energy is preferentially conserved by inefficient glucose fermentation to lactate rather than through the mitochondrial oxidative tricarboxylic acid cycle or oxidative phosphorylation [1, 4]. Whereas normal non-proliferating cells produce large amounts of lactate only under anaerobic conditions, most cancer cells do so regardless of the availability of oxygen and the presence of fully functional mitochondria [5]. The advantage of anaerobic glucose fermentation is still a matter of discussion, although it probably serves as an adaption of proliferating cells to facilitate the consumption of nutrients needed to produce new cells [1]. In this context, metabolites of the tricarboxylic acid cycle are subjected to anabolic pathways in particular generating amino acids instead of serving as electron donors for driving the mitochondrial electron transport chain for ATP synthesis [6].

At present, targeting glucose transport and its metabolism during glycolysis is thought to represent a promising strategy for tumor therapy [7]. The cellular uptake of glucose is realized by two subgroups of specific transporter molecules: facilitative glucose transporters (GLUT) that mediate an energy-independent bidirectional transport and Na+/glucose co-transporters (SGLT) that translocate glucose in an active manner [8]. In human, the GLUT family consists out of thirteen structurally related members, whereby GLUT1 is the most ubiquitously expressed molecule in tissues and cultured cells [8]. In cancer, GLUT1 is the predominant overexpressed isoform of glucose transporters [5]. Following uptake, glucose is metabolized in the glycolytic pathway into triose-phosphates, which are then further oxidized. In this process NAD+ is required as an electron acceptor molecule in the glycolytic pathway by glyceraldehyde 3-phosphate dehydrogenase for triose-phosphate oxidation, whereby it is reduced into NADH. Glycolysis cannot sustain unless NAD+ is regenerated. This is enabled by the reduction of pyruvate into lactate and, thereby, the oxidation of NADH into NAD^+, which is then available as electron acceptor molecule. In general, cells use four biosynthetic pathways to generate NAD+: (i) a complex de novo pathway using the catabolism of tryptophan, (ii) the Preiss-Handler salvage pathway that utilizes nicotinic acid (NA, also known as niacin or vitamin B3) in a three step process for NAD+ generation, (iii) a second salvage pathway that uses nicotinamide

(NAM; i.e. the main NAD+ precursor in mammals [9], which is first converted to nicotinamide mononucleotide (NMN) via nicotinamide phosphoribosyltransferase (NAMPT). The second step involves three NMN adenyltransferases and leads to the formation of NAD+ [10, 11]) and finally (iv) a third salvage pathway that uses nicotinamide riboside (NR) as a precursor and is connected to the NAM salvage pathway [9]. A schematic presentation of these metabolic reactions is given in Figure 20.

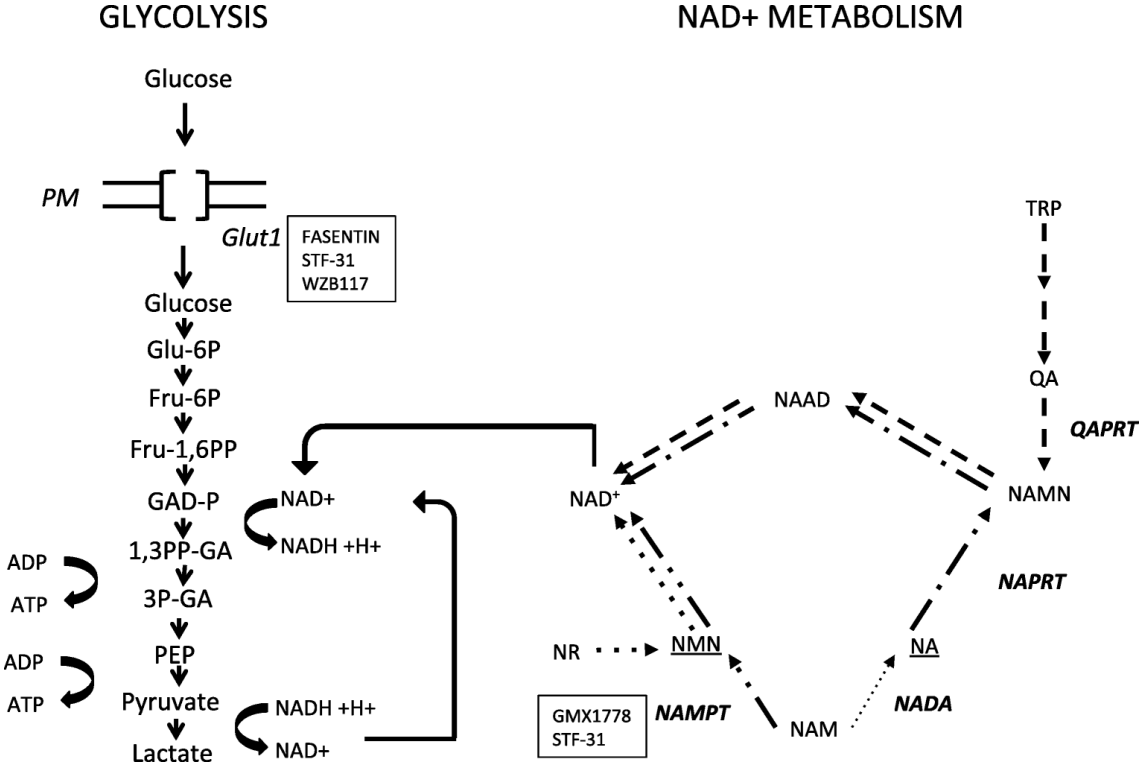

Figure 20: Glycolysis and mammalian NAD+ metabolic pathways. *Glycolysis*: Glu-6P, glucose-6-phosphate; Fru-6P, fructose-6-phosphate; Fru-1,6PP, fructose 1,6-bisphosphate; GAD-P, glyceraldehyde-3-phosphate; 1,3PP-GA, 1,3-biphosphoglycerate; 3P-GA, 3-phosphoglycerate; PEP, phosphoenolpyruvate. The isomerization of 3-phosphoglycerate to 2-phosphoglycerate is not shown. PM, plasma membrane. *NAD+ metabolism*: The de novo and the three salvage pathways are shown. De novo pathway, dashed arrows; Preiss-Handler salvage pathway, dashed and once dotted arrows; NAMPT salvage pathway, dashed and twice dotted arrows; nicotinamide riboside salvage pathway, dotted arrows. Thin dotted arrow indicates the absence of NADA in mammals. Enzymes are indicated with a bold and italic diction. NA, nicotinic acid; NAAD, nicotinic acid adenine dinucleotide; NAD+, Nicotinamide adenine dinucleotide (oxidized); NADA, nicotinamide deaminase; NAM, nicotinamide; NAMN, nicotinic acid mononucleotide; NMN, nicotinamide mononucleotide; NR, nicotinamide riboside; QA, quinolinic acid; TRP, trypto-

phan; NAMPT, nicotinamide phosphoribosyltransferase; NAPRT, nicotinic acid phosphoribosyltransferase; QAPRT, quinolinic acid phosphoribosyltransferase. Some intermediates between tryptophan and QA are not given. Inhibitors are framed and placed next to the affected molecule (GLUT1 or NAMPT). Compounds used to rescue inhibitor treatment are underlined.

The number of GLUT inhibitors available is presently restricted. Whereas for most of them their specificity toward GLUTs is established, STF-31 has remained a controversial candidate: This compound was initially described by Chan et al. [12] as a specific GLUT1 inhibitor in Hippel-Lindau (VHL) tumor suppressor gene (VHL)-deficient renal carcinoma cells that inhibits glucose uptake and interacts with GLUT1 in cellular extracts. This selective sensitivity has been attributed to an increased protein half-life of hypoxia–inducible factor (HIF) expression provoked by VHL deficiency that leads to alterations in gene expression [12]. Recently, however, STF-31 has been reported to target NAMPT and, thereby, attacking cancer cell viability [13]. Also the selective toxicity of STF-31 toward human pluripotent stem cells has been attributed to its inhibition of a NAD^+ salvage pathway [14]. Mainly based on the observation that a STF 31-raised decrease in glucose uptake becomes detectable only after 18h, it has been argued that this effect is due to an inhibition of glycolysis raised by NAD+ depletion [14, 15]. In myeloma cells the action of STF-31 has been ascribed to the inhibition of GLUT1 [16]. However, in this study only incubation times longer than 12 hours were analysed. Comparable data were presented for breast and ovarian cancer cells [17].

In the present study, we have investigated the effect of STF-31 on glucose transport and NAD+ metabolism in comparison to the two GLUT inhibitors fasentin and WZB117 as well as the NAMPT inhibitor GMX1778. We provide evidence, that STF-31 has a dual function and serves as a NAMPT as well as a GLUT-inhibitor in a concentration-dependent manner.

Materials and Methods

Materials

Fasentin, WZB117, STF-31 were from Merck Millipore. GMX1778, nicotinic acid (NA) and nicotinamide mononucleotide (NMN) were from Sigma. [^{18}F]-fluoro-deoxyglucose ([^{18}F]FDG; in 0,9% sodium chloride) was kindly supplied by Advanced Accelerator Applications (Bonn, Germany). The following antibodies were used for Western blots:

αGLUT1 (dilution 1:500; Merck Millipore), αNAPRT (dilution 1:1000; Thermo Fischer Scientific), αβ-actin and αGAPDH (for both dilution 1:1000; Cell Signalling Technology).

Cell lines and culture conditions

For routine cultivation, human cell lines A172 (glioblastoma), BHY (oral squamous cell carcinoma), HeLa (cervix adenocarcinoma), HN (head neck cancer), HT-29 (colon carcinoma) and MG-63 cells (osteosarcoma) were maintained in DMEM, 10% fetal calf serum (FCS). Under experimental conditions, serum concentration was reduced to 1% or 0% (glucose uptake experiments only).

Total RNA isolation, cDNA synthesis and quantitative RT-PCR analysis

Total RNA isolation and cDNA synthesis were performed as described [18]. Real-time PCR was processed with 50 ng cDNA using the iQ™ SYBR® Green Supermix (Bio-Rad Laboratories) in an iCycler Thermal Cycler (Bio-Rad). Gene and sequence specificities of the relevant primers (Metabion) as well as PCR efficiencies are given in Table 1. For quantification, cDNA was first denatured for 10 min at 95 °C. Then 40 cycles consisting with intervals of 15 sec at 95 °C (denaturing step), 30 sec at primer-specific temperature (annealing step) and 30 sec at 72°C (elongation step) were performed. The expression level of the β actin and GAPDH genes were used as internal reference standards.

Table 13: Genes, primer sequences and PCR amplification characteristics.

Gene	***Primer sequences (sense/antisense)***	***Efficiency***	***Annealing temperature (°C)***
β-actin	5´-CATGGATGATGATATCGCCGCG-3′ 5´-ACATGATCTGGGTCATCTTCTCG-3′	1.84	69
GAPDH	5´-TGGTATCGTGGAAGGACTCA-3′ 5´-CCAGTAGAGGCAGGGATGAT-3′	1.93	67
GLUT1	5´-GCATCCTCATCGCCCAGGTG-3′ 5´-CGCAGCTTCTTTAGCACAC-TCTTGG-3′	1.94	69
NAPRT	5´-CAGGTGGAGCCACTACTGC-3′ 5´-CGTGTTGTTTCCAGTCAGCC-3′	2.06	69

Western blot analysis

Western blot analyses were carried out as already described in detail [18]. Total protein was isolated in the presence of protease inhibitors (0.5 mM PMSF; Roche complete Mini ULTRA mix). Protein concentrations were determined with the Pierce™ BCA Protein Assay Kit. Proteins were separated by SDS-PAGE and electrophoretically transferred onto a PVDF membrane (0.45 µm) (Millipore, Darmstadt, Germany).

Cell proliferation and viability assay

To determine cell viability and proliferation, crystal violet, LDH, and XTT assays were performed: (1) For the crystal violet assay, 1000 to 5000 cells were seeded per well in 96 well plates, incubated overnight in normal culture medium and then cultured in DMEM containing 1% FCS for up to four days in the absence or presence of experimental compounds. Cells were then fixed in 5% formaldehyde in phosphate-buffered saline (PBS) for 15 min and stained for 1h with 0.05% crystal violet in Aqua dest. Cells were washed twice with Aqua dest. and air-dried. 150 µl of methanol were added per well and the optical density at 540 nm was measured. (2) The assay was carried out as described previously with the "LDH Cytotoxicity Assay Kit" from Roche [19]. (3) For the XTT assay (from Promokine), cells were seeded in 96-well-plates (10.000 cells per well in 100 µl of complete culture medium) and cultivated for 24h. Complete culture medium was then replaced by 100 µl of serum-free medium with or without experimental compounds and cells were cultivated for further 24h. After the addition of XTT reaction solution for 4h, absorbance was determined at 490 nm with a correction wavelength of 670 nm. The XTT assay reflects the general metabolic activity or the rate of glycolytic NADH production [20].

Glucose uptake assay

Cells were seeded in 24 well plates ($1.5x10^5$ cells per well) in complete culture medium and incubated overnight. Medium was then replaced by glucose-free DMEM and experimental compounds were added in a final volume of 400 µl for 30 min. Then 370 kBq, corresponding to 10 µCi (equal to 150 to 300 pmol) of [^{18}F]FDG (specific activity of 2.5 to 5.0 GBq/µmol) were added in 100 µl per well for further 30 min. Cells were then washed twice with PBS and solubilized in PBS containing 3% Triton X-100. Radioactivity was measured in a gamma-counter (Type) and values adjusted according to the decay of fluorine-18.

Statistics

For statistical analysis a specific software program was used (GraphPad Software Version 5, San Diego CA, USA). Mean ± standard error mean (SEM) were calculated and one-way analysis of variance (ANOVA) and the post-hoc Tukey`s multiple comparison tests were applied to determine statistical differences between control and treated groups. P-values less than 0.05 were considered to be statistically significant. In some experiments for data analysis an unpaired Student's t-test was used.

Results

STF-31 and GLUT-inhibitors fasentin and WZB-117 interfere with tumor cell in a distinct manner

Based on the fact that STF-31 was first described as a specific GLUT1 inhibitor that specifically kills renal carcinoma cells [12], we first analysed its impact on the metabolism of tumor cells that represent a comprehensive spectrum of selected cancer entities and compared the drugs' impact with the one of the two established GLUT1 inhibitors fasentin and WZB117. For that purpose A172 glioblastoma, BHY oral squamous cell carcinoma, HeLa cervix adenocarcinoma, HN head neck cancer, HT-29 colon carcinoma and MG63 osteosarcoma cells were cultivated in the absence or presence of the three compounds at concentrations of 0.1 to 100 μM for one day and the XTT assay was used to monitor metabolic activity. The XTT assay reflects the general metabolic activity or the rate of glycolytic NADH production [20].

After a culture period of 1 day, tumor cells tolerated fasentin and WZB117 up to a concentration of 10 μM (Figure 21). At higher concentrations, considerable metabolic perturbations became visible in a cell line-specific manner, whereby at a concentration of 50 μM the highest toxicity rates were observed in HeLa (about 75%) and MG-63 cells (about 55%) for fasentin and in HeLa (about 70%) and A172 cells (about 60%) for WZB117. At a concentration of 100 μM, fasentin exhibited its highest perturbation rate in MG-63 cells (about 90%) whereas the highest rate for WZB117 was observed in A172 (about 80%) and HeLa cells (about 77%). In general, the two GLUT inhibitors were well tolerated up to a "threshold concentration" of about 10 μM by all tumor cells. Then, a further increase in concentration led to a sharp decline in the survival rate. STF-31, in contrast, showed a considerable cytotoxic effect already at a concentration of 1 μM that was in the range of 40 to 50% for HeLa, HN and MG-63 cells and of 30% for HT-29 and BHY cells. A172 cells were almost resistant to STF-31 treatment even at the highest

concentration of 100 μM. In general, the perturbing metabolic impact of STF-31 treatment showed a slow but continuous increase when drug concentrations were raised without the appearance of an obvious “threshold concentration”. These data demonstrate that STF-31, when compared to fasentin and WZB117, perturbs cell metabolism already at lower concentrations indicating either a higher target affinity or the interaction with different target molecules.

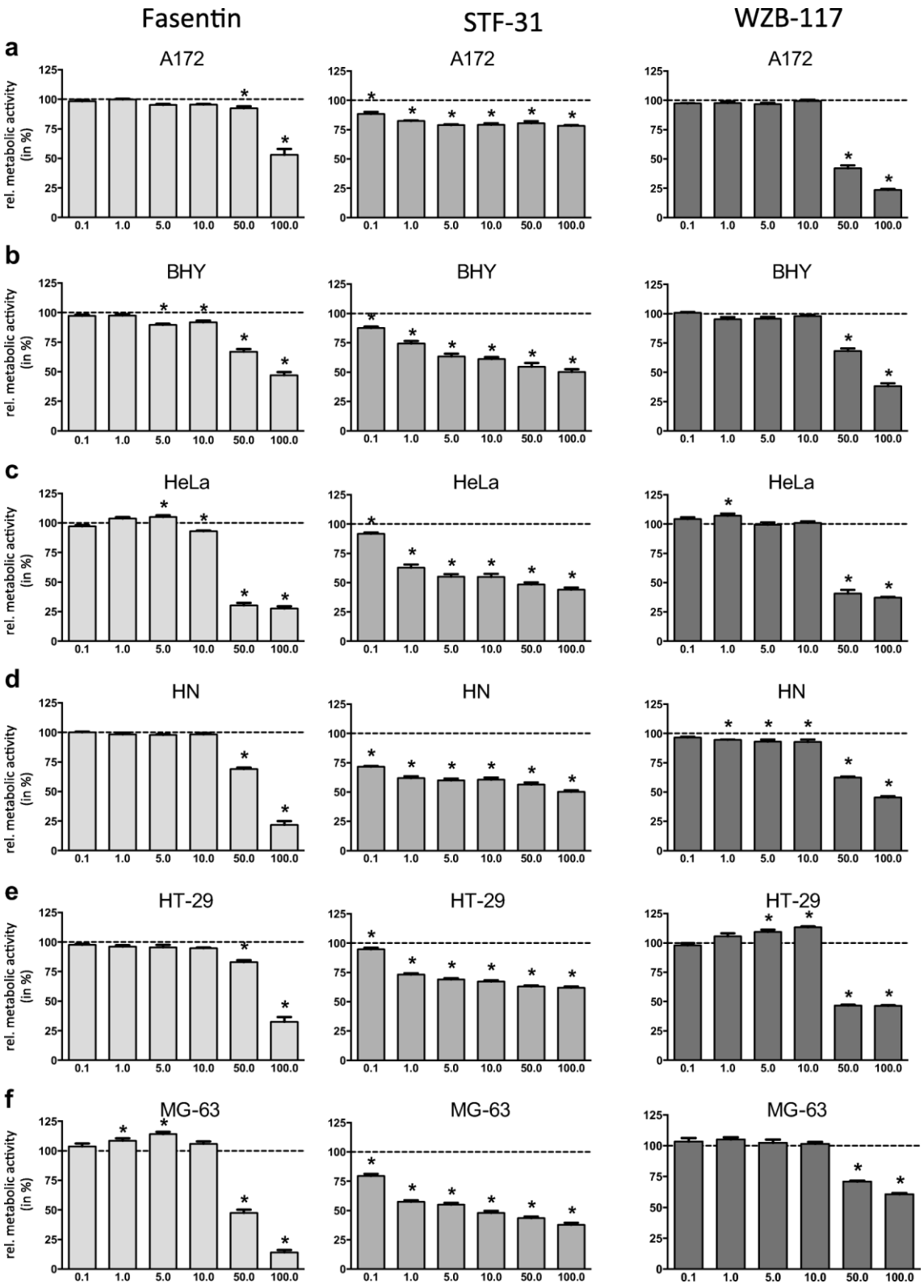

Figure 21: Metabolic perturbation by GLUT inhibitors in tumor cells after short-time culture. Human tumor cells (a: A712, b: BHY, c: HeLa, d: HN, e: HT-29, f: MG-63) were cultivated in 96-well plates for one day in the absence or presence of fasentin (FAS),

WZB117 (WZB) or STF-31 (STF) at the indicated concentrations (in µM). Metabolic activity was determined by XTT assay and relative values are given in respect to the one of untreated cells (set as 100%). Data are means + SEM from at least three independent experiments. Statistically significant differences versus control ($p < 0.05$) are marked with asterisks (*).

STF-31 and NAMPT inhibitor GMX1778 interfere with tumor cell proliferation in a comparable manner

More recently, however, STF-31 has been demonstrated to function as a NAMPT inhibitor [13]. Thus, we next compared the drugs' impact on cell proliferation and survival with the one of the well-established NAMPT inhibitor GMX1778 [21] in the absence or presence of NMN or NA. As outlined above (see Figure 20), NMN is the reaction product of NAMPT that can be converted to NAD^+ in a single step. Supplementation with NA allows NAD^+ generation only when the Preiss-Handler salvage pathway is intact and, in particular, needs the expression of functional NAPRT [22]. A four-day treatment with STF-31 (50 µM) or GMX1778 (5 µM) led to a comparable inhibition of proliferation, whereby inhibitory effects were most pronounced in A172, BHY, HeLa and MG-63 cells and occurred at intermediate levels in HN and HT-29 cells (Figure 22a). NA (10 µM) provoked a strong rescue effect in HeLa, HN and HT-29 and a moderate one in GMX1778-, but not in STF-31-treated BHY cells. A172 or MG-63 cells could not be rescued by NA supplementation. At STF-31 concentrations in the range of 0.1 to 1.0 µM the inhibition of proliferation was less pronounced or almost absent and, thus, a rescue effect becomes irrelevant (Figure 22b). The inability of NA to restore proliferation in A172 and MG63 cells after STF-31 or GMX1778 treatment is most likely due to NAPRT-deficiency, as verified by RT-PCR (Figure 22d; for A172 cells see also [23]) and Western blot analysis (Figure 22e). Such a relationship has recently been described for other tumors and tumor cell lines [22, 24]. The behaviour of STF-31-treated BHY cells can not be satisfactorily explained, but may be due to lowered NAPRT protein expression, that is surprisingly also present in HN cells (Figure 22e). In the presence of NMN (100 µM) a pronounced rescue effect was evident in all STF-31- or GMX1778-treated cell lines (Figure 22c). The extent of the NMN-dependent rescue effect did not correlate with NAMPT transcript expression level (not shown). As for NA, also exclusive NMN treatment led to a small but significant increase in cell proliferation (Figure 22c). In sum, our data underline that NAMPT is a cellular target of STF-31.

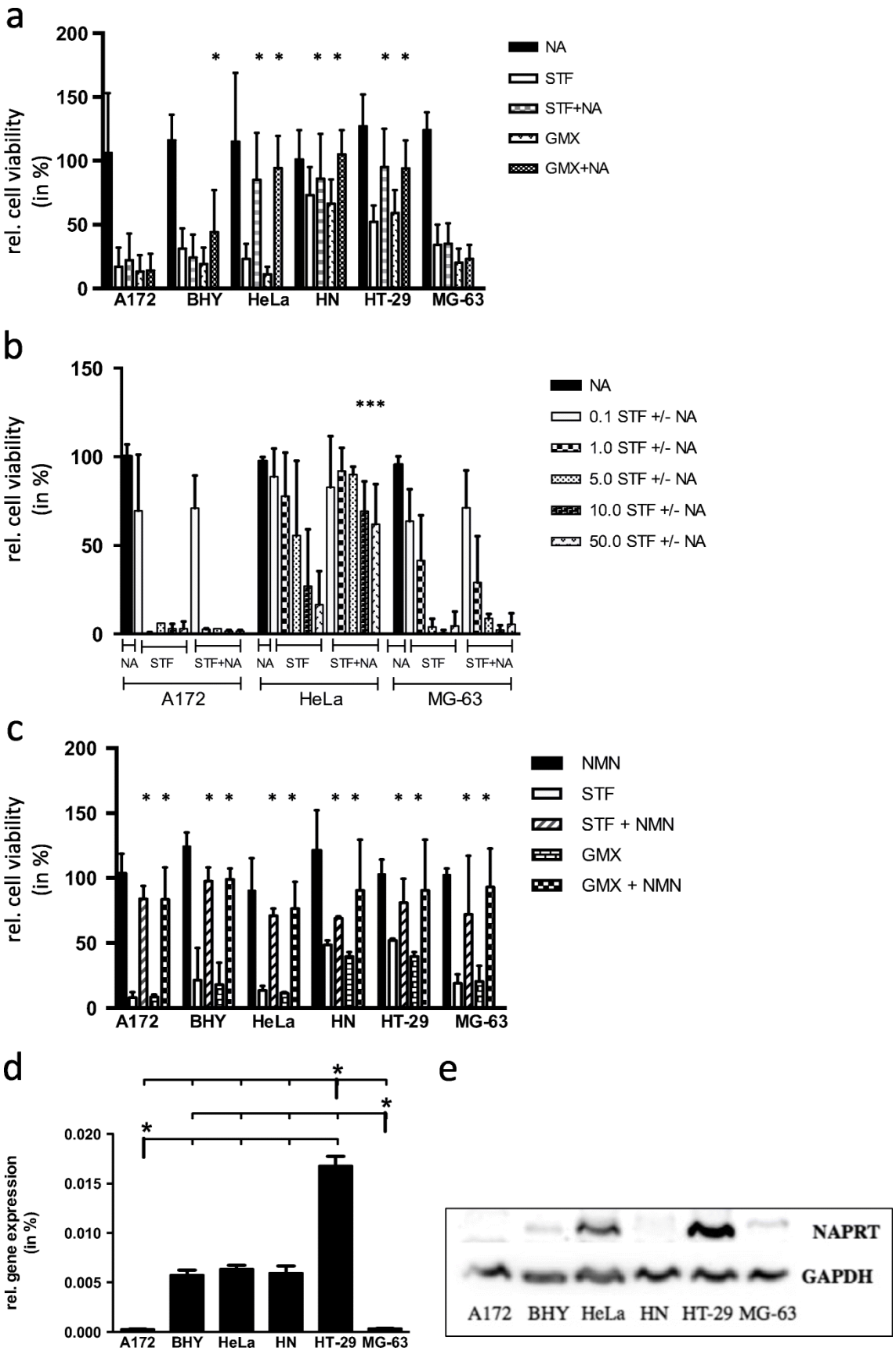

Figure 22: Rescue effects in NAMPT- or GLUT-inhibitor-treated tumor cells after long-time culture in the absence or presence of NA or NMN. a-c: Human tumor cells were

cultivated in 96-well plates (1000 to 5000 cells per well) for four days in 50 (a,b), 0.1, 1, 5, 10 μM STF-31- (b) or 5 μM GMX1778- (a,c) containing medium supplemented with 10 μM NA (a,b) or 100 μM NMN (c). Asterisks (*) in a to c mark statistical differences ($p < 0.05$) of STF-31- or GMX1778-treated cells, rescued with either NA (a,b) or NMN (c). In control experiments, cells were cultured in the presence of NA or NMN only. Cell viability was determined by crystal violet assay. Data are means + SEM from at least three independent experiments. d-e: NAPRT-specific mRNA (d) or protein (e) expression in tumor cells as determined by qPCR (d) or Western blot (e) analysis. Data in (d) are normalized to mRNA expression of internal standard genes and given as means + SEM from two independent experiments. Statistically significant differences versus control ($p < 0.05$) are marked with asterisks (*).

STF-31 as well as GLUT inhibitors fasentin and WZB177 inhibit glucose uptake in tumor cells

To analyse the direct impact of STF-31 in GLUT-inhibition we finally performed glucose uptake assays. To rule out indirect effects raised by STF-31-mediated inhibition of glycolysis and mitochondrial oxidation after longer time periods [14], a total assay time of 1 h was chosen. The absolute uptake values varied in the range of 5 to 10% of the input [^{18}F]FDG radioactivity. Thus, for a direct comparison of the uptake rate all six lines had to be treated in parallel in each experiment. After an incubation time of 30 min with [^{18}F]FDG in serum- and glucose-free medium, the uptake rate varied by a maximum of about factor two between the cell lines, but depicted no significant statistical difference (Figure 23a). These variations seen for the uptake efficiency were only partially reflected in the expression level of GLU1 protein (Figure 23b), suggesting a substantial contribution of other GLUT isoforms in glucose uptake.

We next examined if the four compounds interfered with cellular uptake of glucose (Figure 23c). 50 μM STF-31 significantly inhibited glucose uptake in all cell lines in the range of 25 up to about 50% (Figure 23c). As comparable rates of inhibition (with a maximal variation of ± 5%) were obtained in the presence of 100 μM NMN, a contribution of NAMPT inactivation in glucose uptake inhibition is rather unlikely. At STF-31 concentrations of 1 or 10 μM no significant uptake inhibition took place (Figure 23c). In none of the cell lines glucose uptake was inhibited by 5 μM GMX1778 (Figure 23c). WZB-117 (50 μM) provoked a strong inhibition in the range of more than 90% in all cell lines. Cells treated with 100 μM of fasentin were either inhibited in the range of 35% (A1723, BHY, HeLa and HT-29 cells) or 20 to 10% (HN and MG-63 cells; although not significant).

Within the frame of the assay, cytotoxic effects could be ruled out for all compounds as revealed by extracellular LDH analysis (Figure 23d).

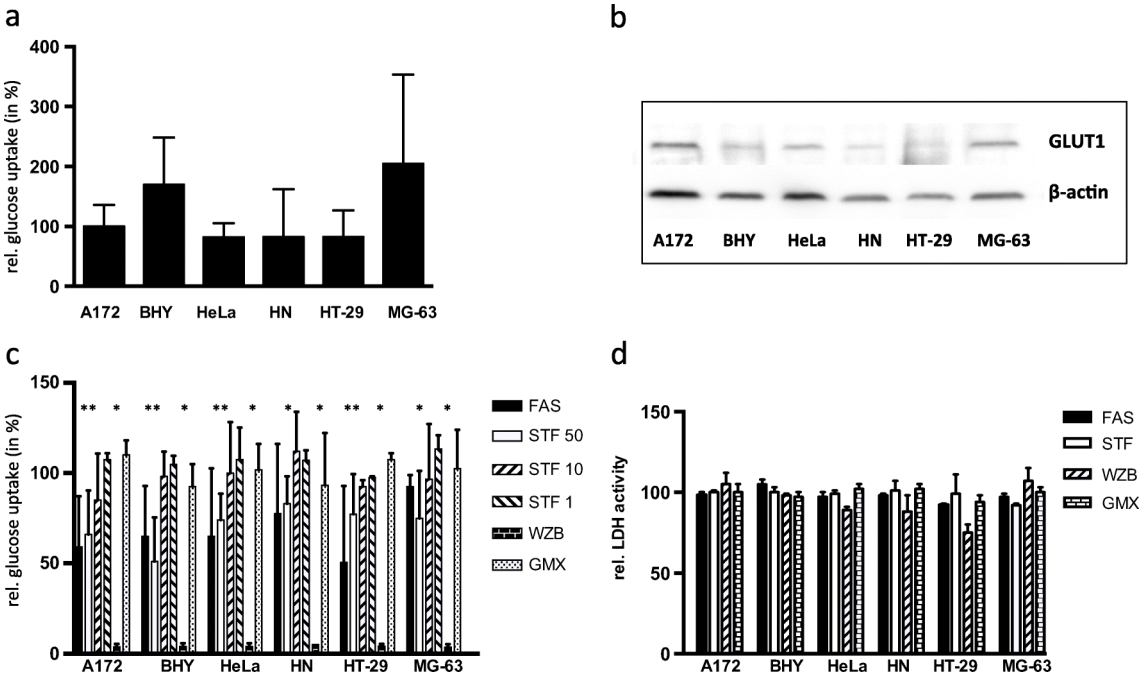

Figure 23: Glucose uptake inhibition in NAMPT- or GLUT-inhibitor-treated tumor cells. **a**: Human tumor cells were cultivated in 24 well plates (1.5 x 10^5 cells per well) for 30 min in the presence of 370 kBq [^{18}F]FDG (equal to 150 to 300 pmol) in 500 µl serum-free medium. Data were normalized relative to the uptake of A172 cells that was set as 100%. The average + SEM of at least four independent experiments is shown. **b:** Western blot analysis of GLUT1-specific protein expression in tumor cells. **c:** Tumor cells were incubated for 30 min in serum and glucose-free medium with [^{18}F]FDG as specified in (**a**) either in the absence or presence of 100 µM fasentin (FAS), 50, 10 or 1 µM STF-31 (STF), 50 µM WZB117 (WZB) or 5 µM GMX1778 (GMX). The uptake of [^{18}F]FDG in the absence of further compounds was set at 100% for each cell line and the corresponding values in the presence of compounds are given. Asterisks (*) indicate statistically differences ($p < 0.05$) between STF-31 and GMX1778-treated cells. **d**: Evaluation of cytotoxic activity by LDH assay after 1h-incubation of tumor cells in the presence or absence of compounds. Relative LDH activity present in the culture supernatant without compounds is calculated as "*optical density supernatant* : *optical density lysate* x 100" and was set as 100% for each cell line. Thus, values considerably higher than 100 indicate cytotoxic effects. Data are means + SD from three independent experiments.

Discussion

As the question if NAPMT or GLUT1 is the principal cellular target of STF-31 is still debatable, we have re-examined the drugs' specificity. Mainly based on short-time uptake experiments with [^{18}F]FDG we demonstrated that at concentrations in the range of 50 μM STF-31 considerably inhibits glucose uptake. As the total assay time did not exceed 60 min, it is unlikely that this effect is indirect and raised by a preceding inhibition of glycolysis and mitochondrial oxidation as suggested for the cytotoxic impact of STF-31 on human pluripotent stem cells [14]. These authors provided convincing evidence that in such cells STF-31 started to inhibit glucose uptake only 18 hours after drug addition, corresponding to three hours after a decline in the extracellular acidification rate. In these studies, STF-31 was used at concentrations in the lower micromolar range, because of the high sensitivity of those cells towards this drug. According to our experience, such low concentrations did not interfere with short-time glucose uptake. An additional aspect that strongly supports the potency of STF-31 as a GLUT inhibitor is the inability of 5 μM GMX1778 to interfere with glucose uptake in our assay system (Figure 23c). Hereby, we used GMX1778 at least at a 50-fold higher concentration than needed to almost totally abolish NAMPT activity or to induce complete cell death after longer time periods [21].

Another aspect that needed to be mentioned in this context is that in some STF-31-treated cell lines (i.e. A172, HN, HT-29) no further pronounced decrease in cell proliferation is detectable in the presence of higher drug concentrations, although a response at low initial concentrations can be observed (see Figure 21). Such a phenomenon might be explained by the saturation in components involved in cellular uptake mechanisms, or the exhaustion of essential cofactors necessary for the drugs' mode of action [25].

In their initial work, Chan and coauthors [12] demonstrated that the action of STF-31 involves the inhibition of metabolic pathways, inter alia of glucose uptake. However, uptake analysis was performed earliest 24 h after drug application at a low concentration of 5 μM and, thus, does not rule out indirect effects as argued by Kropp et al. [14]. Also our data (see Figure 23c) suggest that a long-lasting inhibitory action is mainly due to an interference with NAMPT activity. Beside these data, Chan and colleagues [12] provided additional experimental evidence that strongly supports a direct participation of STF-31 in glucose uptake such as the affinity-purification of GLUT1 in a STF-31-dependent manner. Moreover, molecular modelling predicted docking of the drug within the central channel of GLUT1.

The classification of STF-31 as NAMPT inhibitor by Adams et al. [13] is based on data that inter alia (i) demonstrated a high correlation of low NAMPT transcript levels and high sensitivity towards STF-31 as well as established NAMPT inhibitors in cytotoxicity assays performed with a panel of about 700 cancer cell lines, and (ii) verified a NAMPT H191R mutation confers resistance to STF-31 and other NAMPT inhibitors as well. Although these data strongly suggest NAMPT as a principal target of STF-31, they can not rule out an additional interference with GLUT1. This type of interaction becomes relevant only at higher drug concentrations or within special cellular and molecular requirements.

We have also performed glucose uptake experiments with GMX1778 concentrations of 10 to 50 µM and observed inhibition rates that were in the range or even higher than the ones observed with 50 µM STF-31. In LDH assays we detected no cytotoxic effects after a 1h treatment and even after a 24h treatment only a partial cytotoxicity was observed that was less pronounced than the complete cell death described by Watson et al [21] for HeLa cells at a GMX1778 concentration as low as 3 nM. Kropp and coworkers [14] have described for human pluripotent stem cells in inhibition of glucose uptake earliest 18 h after application of low, i.e. 2.5 µM, STF-31 concentrations. As the temporal appearance of glucose uptake inhibition roughly paralleled the temporal inhibition of glycolysis and mitochondrial oxidative metabolism these authors argued that the former one is a consequence of the latter. In our hands, STF-31 and also GMX1778 significantly inhibit glucose uptake in a concentration-dependent manner already after a 1h-treatment and, thus, point to a broadened range of activities of these drugs. The observed temporal delay of drug effects may be due to drug metabolism raised by phase I enzymes (cytochrome P450; Flavin-containing monooxygenases), which are known to play a crucial role in xenobiotic degradation [26, 27]. Such new functional drug-specific metabolites could possess unknown mode of actions.

All together we suppose that STF-31 can function as a NAMPT as well as a GLUT1 inhibitor, whereby its action as NAMPT inhibitor in respect to confer cytotoxicity seems to be more pronounced in most cancer cells. The particular efficacy of each inhibitory activity may depend on the specific cellular context. High expression levels of GLUT1 in conjunction with low expression levels of other GLUTs could increase the cells' sensitivity towards the GLUT1-specific inhibitory action of STF-31, whereas low expression levels of NAMPT could favor the NAMPT-specific inhibitory action of the drug.

Conflicts of interest: None declared.

References

1. Vander Heiden MG, Cantley LC, Thompson CB. Understanding the Warburg effect: the metabolic requirements of cell proliferation. Science. 2009;324:1029–33. doi:10.1126/science.1160809.
2. El Mjiyad N, Caro-Maldonado A, Ramírez-Peinado S, Muñoz-Pinedo C. Sugar-free approaches to cancer cell killing. Oncogene. 2011;30:253–64. doi:10.1038/onc.2010.466.
3. Granchi C, Fancelli D, Minutolo F. An update on therapeutic opportunities offered by cancer glycolytic metabolism. Bioorganic & Medicinal Chemistry Letters. 2014;24:4915–25. doi:10.1016/j.bmcl.2014.09.041.
4. WARBURG O. On the origin of cancer cells. Science. 1956;123:309–14. doi:10.1126/science.123.3191.309.
5. Moreno-Sánchez R, Rodríguez-Enríquez S, Marín-Hernández A, Saavedra E. Energy metabolism in tumor cells. FEBS J. 2007;274:1393–418. doi:10.1111/j.1742-4658.2007.05686.x.
6. Danhier P, Bański P, Payen VL, Grasso D, Ippolito L, Sonveaux P, Porporato PE. Cancer metabolism in space and time: Beyond the Warburg effect. Biochim Biophys Acta Bioenerg. 2017;1858:556–72. doi:10.1016/j.bbabio.2017.02.001.
7. Porporato PE, Dhup S, Dadhich RK, Copetti T, Sonveaux P. Anticancer targets in the glycolytic metabolism of tumors: a comprehensive review. Front Pharmacol. 2011;2:49. doi:10.3389/fphar.2011.00049.
8. Zhao F-Q, Keating AF. Functional properties and genomics of glucose transporters. Curr Genomics. 2007;8:113–28. doi:10.2174/138920207780368187.
9. Hassa PO, Haenni SS, Elser M, Hottiger MO. Nuclear ADP-ribosylation reactions in mammalian cells: where are we today and where are we going? Microbiol Mol Biol Rev. 2006;70:789–829. doi:10.1128/MMBR.00040-05.
10. Magni G, Amici A, Emanuelli M, Raffaelli N, Ruggieri S. Enzymology of NAD+ synthesis. Adv Enzymol Relat Areas Mol Biol. 1999;73:135-82, xi. doi:10.1002/9780470123195.ch5.
11. Roulston A, Shore GC. New strategies to maximize therapeutic opportunities for NAMPT inhibitors in oncology. Mol Cell Oncol. 2016;3:e1052180. doi:10.1080/23723556.2015.1052180.
12. Chan DA, Sutphin PD, Nguyen P, Turcotte S, Lai EW, Banh A, et al. Targeting GLUT1 and the Warburg effect in renal cell carcinoma by chemical synthetic lethality. Sci Transl Med. 2011;3:94ra70. doi:10.1126/scitranslmed.3002394.

13. Adams DJ, Ito D, Rees MG, Seashore-Ludlow B, Puyang X, Ramos AH, et al. NAMPT is the cellular target of STF-31-like small-molecule probes. ACS Chem Biol. 2014;9:2247–54. doi:10.1021/cb500347p.

14. Kropp EM, Oleson BJ, Broniowska KA, Bhattacharya S, Chadwick AC, Diers AR, et al. Inhibition of an NAD^+ salvage pathway provides efficient and selective toxicity to human pluripotent stem cells. Stem Cells Transl Med. 2015;4:483–93. doi:10.5966/sctm.2014-0163.

15. Boheler KR, Bhattacharya S, Kropp EM, Chuppa S, Riordon DR, Bausch-Fluck D, et al. A human pluripotent stem cell surface N-glycoproteome resource reveals markers, extracellular epitopes, and drug targets. Stem Cell Reports. 2014;3:185–203. doi:10.1016/j.stemcr.2014.05.002.

16. Matsumoto T, Jimi S, Migita K, Takamatsu Y, Hara S. Inhibition of glucose transporter 1 induces apoptosis and sensitizes multiple myeloma cells to conventional chemotherapeutic agents. Leuk Res. 2016;41:103–10. doi:10.1016/j.leukres.2015.12.008.

17. Xintaropoulou C, Ward C, Wise A, Marston H, Turnbull A, Langdon SP. A comparative analysis of inhibitors of the glycolysis pathway in breast and ovarian cancer cell line models. Oncotarget. 2015;6:25677–95. doi:10.18632/oncotarget.4499.

18. Kraus D, Reckenbeil J, Wenghoefer M, Stark H, Frentzen M, Allam J-P, et al. Ghrelin promotes oral tumor cell proliferation by modifying GLUT1 expression. Cell Mol Life Sci. 2016;73:1287–99. doi:10.1007/s00018-015-2048-2.

19. Murmann T, Carrillo-García C, Veit N, Courts C, Glassmann A, Janzen V, et al. Staurosporine and extracellular matrix proteins mediate the conversion of small cell lung carcinoma cells into a neuron-like phenotype. PLoS ONE. 2014;9:e86910. doi:10.1371/journal.pone.0086910.

20. Berridge MV, Herst PM, Tan AS. Tetrazolium dyes as tools in cell biology: New insights into their cellular reduction. In: : Elsevier; 2005. p. 127–152. doi:10.1016/S1387-2656(05)11004-7.

21. Watson M, Roulston A, Bélec L, Billot X, Marcellus R, Bédard D, et al. The small molecule GMX1778 is a potent inhibitor of NAD+ biosynthesis: strategy for enhanced therapy in nicotinic acid phosphoribosyltransferase 1-deficient tumors. Mol Cell Biol. 2009;29:5872–88. doi:10.1128/MCB.00112-09.

22. Xiao Y, Elkins K, Durieux JK, Lee L, Oeh J, Yang LX, et al. Dependence of tumor cell lines and patient-derived tumors on the NAD salvage pathway renders them sensitive to NAMPT inhibition with GNE-618. Neoplasia. 2013;15:1151–60. doi:10.1593/neo.131304.

23. Sahm F, Oezen I, Opitz CA, Radlwimmer B, Deimling A von, Ahrendt T, et al. The endogenous tryptophan metabolite and NAD+ precursor quinolinic acid confers resistance of gliomas to oxidative stress. Cancer Research. 2013;73:3225–34. doi:10.1158/0008-5472.CAN-12-3831.

24. O'Brien T, Oeh J, Xiao Y, Liang X, Vanderbilt A, Qin A, et al. Supplementation of nicotinic acid with NAMPT inhibitors results in loss of in vivo efficacy in NAPRT1-deficient tumor models. Neoplasia. 2013;15:1314–29. doi:10.1593/neo.131718.

25. Stewart DJ, Raaphorst GP, Yau J, Beaubien AR. Active vs. passive resistance, dose-response relationships, high dose chemotherapy, and resistance modulation: a hypothesis. Invest New Drugs. 1996;14:115–30. doi:10.1007/BF00210782.

26. Guengerich FP, Munro AW. Unusual cytochrome p450 enzymes and reactions. J Biol Chem. 2013;288:17065–73. doi:10.1074/jbc.R113.462275.

27. Cashman JR, Zhang J. Human flavin-containing monooxygenases. Annu. Rev. Pharmacol. Toxicol. 2006;46:65–100. doi:10.1146/annurev.pharmtox.46.120604.141043.

7. Zusammenfassung und Ausblick

Teilprojekt DOTA-ZOL

Die Ursachen für die Probleme, die im Rahmen der Implementierung von DOTA-ZOL auftraten, konnten gefunden und größtenteils erfolgreich adressiert werden.

Basierend auf den dabei gewonnen Erfahrungen, konnte erfolgreich eine manuelle Markierungsmethode mit Gallium-68 entwickelt und validiert werden. Es konnte erfolgreich nachgewiesen werden, dass neben dem richtigen pH-Wert der Reaktionslösung, ein wesentlicher Einflussfaktor für die Radiomarkierung das Reaktionsgefäß ist (Abbildung 24). Dieses kann, bei ansonsten gleichen Reaktionsbedingungen, einen Unterschied von bis zu 60 % in der Reaktionsausbeute der Komplexierung bedingen. Das wiederum hat direkte Konsequenzen für die Automatisierung, da hier das optimale Reaktionsgefäß nicht verfügbar ist. Durch die Anpassung des Reaktorgefäßes konnte die Ausbeute der manuellen Markierung soweit stabilisiert und erhöht werden das eine Aufreinigung des Endproduktes nicht mehr notwendig ist.

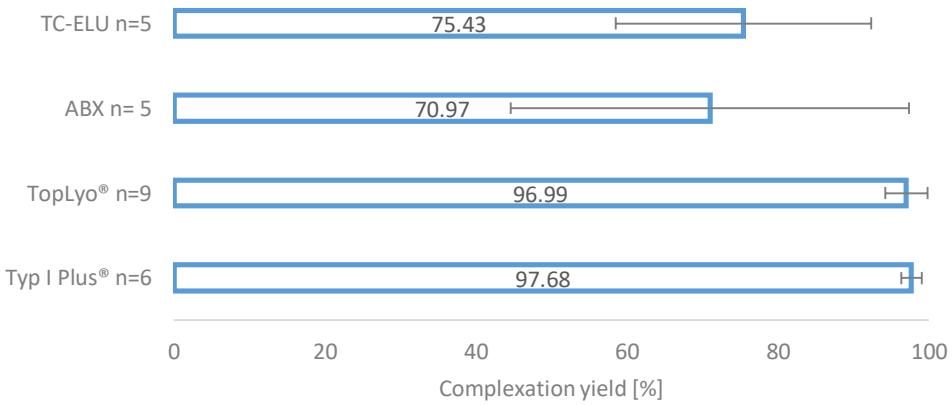

Abbildung 24: Vergleich der vier verschiedenen Reaktorgefäße für die Radiomarkierung. Zwei normale Glasreaktoren, sowie zwei silikonbeschichtete Glasreaktoren (siehe auch S. 73).

Ein weiteres Problem, die Aufreinigung des Produktes konnte trotz intensiver Bearbeitung nicht abschließend gelöst werden. Da für die Modulsynthese das optimale Reaktionsgefäß noch nicht verfügbar ist, wäre hier eine SPE-Aufreinigung dringend notwendig. Da trotz intensivem Screening bisher keine praktikable Lösung gefunden werden konnte ist eine Anpassung der Kassetten und des Moduls wahrscheinlich die einfachere und schnellere Variante. Nichtsdestotrotz sollten weitere Anstrengungen hinsichtlich der

SPE-Aufreinigung unternommen werden um in Zukunft für diesen Tracer eine verlässliche, automatisierte Synthese nutzen zu können.

Während der Arbeit musste auch die Qualitätskontroll-Methode genauer untersucht werden. Es stellte sich dabei heraus, dass diese nicht zuverlässig alle Komponenten auflösen konnte und zusätzlich zum Teil falsch negative Ergebnisse lieferte. Dadurch wurden vermehrt Synthesen mit gutem Produkt verworfen. Darüber hinaus war es nicht möglich die bereitgestellten HPLC-Methoden zu reproduzieren. Dadurch wurde es notwendig sowohl eine passende DC- als auch HPLC-Methode zu finden. Die neue entwickelte DC-Methode basiert zum Teil aus der bereitgestellten. Diese schafft es eindeutige und zuverlässige Aussagen über die Reinheit des Produktes zu machen. Die neue HPLC-Methode löst alle Komponenten des Produktes und der Vorstufen auf, jedoch kann die sehr kurze Retentionszeit zwischen den einzelnen Peaks zu Überlagerungen und Fehlern führen. Die aktuelle HPLC-Methode bietet daher noch Potential für weitere Verbesserungen insbesondere hinsichtlich der Auftrennung der Substanzen.

Teilprojekt: PSMA

Die optimierte Methode zur Markierung von PSMA-11 mit Ethanolzusatz konnte erfolgreich in den klinischen Alltag implementiert und etabliert werden.

Die erste automatisierte Modulsynthese für [^{177}Lu]Lu-PSMA-617, die für die Routineproduktion von Patientendosen geeignet ist, wurde etabliert. Darauf aufbauend wurde eine Patientenstudie realisiert. Hier wurde die Überebensrate von Patienten mit Radioligandtherapie (RLT) gegen eine Gruppe ohne RLT untersucht. Es konnte ein signifikanter Unterschied zu gunsten der RLT-Gruppe nachgewiesen werden. Die wiederholte RLT Behandlung scheint sicher und wirksam zu sein und für die meisten Patienten einen Nutzen zu bringen. Zukünftig kann es ein Ansatz sein die RLT schon früher, vor der terminalen Phase der Erkrankung, einzusetzen wie es aktuell der Stand ist, und dadurch die Prognose der Patienten weiter zu verbessern.

Die Markierung von PSMA-617 mit dem neuen PET-Isotop Scandium-44 wurde ebenfalls erfolgreich und nach den Vorgaben der Pharmakopoeia entwickelt. In den damit durchgeführten Machbarkeitsstudien zeigte sich, dass [^{44}Sc]Sc-PSMA-617 eine höhere Ähnlichkeit zum Therapeutikum [^{177}Lu]Lu-PSMA-617 aufweist als das etablierte [^{68}Ga]Ga-PSMA-11. Durch die höhere Halbwertszeit des Scandium-44 ($t_{1/2}$ = 4,042 h) ist die Biokinetik im Patienten bis 19,5 h nachverfolgbar. Das führt dazu, dass die Dosimetrie vor und nach der Therapie besser bestimmt werden kann. Hiermit ist dann eine bessere Individualtherapie erreichbar.

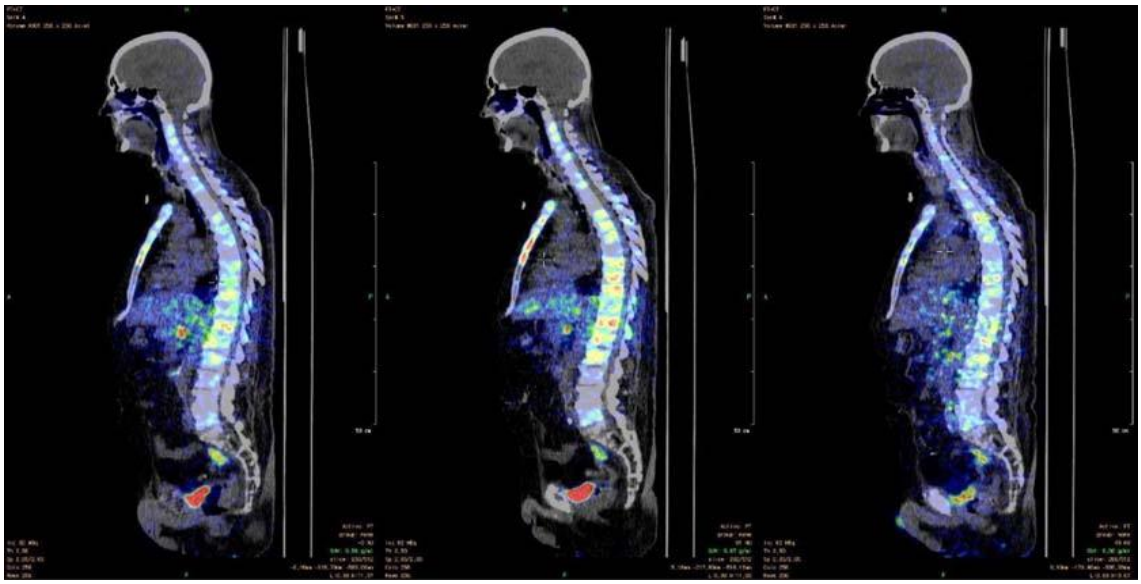

Abbildung 25: Verteilung von [^{44}Sc]Sc-PSMA-617 nach 45 Minuten sowie 2 und 19,5 Stunden nach der Injektion (von links nach rechts) (siehe auch S. 160).

Die Vorhersage und Berechnung der absorbierten Organdosen bei Patienten, für die eine [^{177}Lu]Lu-PSMA-617-Therapie vorgesehen ist, kann durch prätherapeutisches PET/CT mit [^{44}Sc]Sc-PSMA-617 verwirklicht werden. Diese Methode ist hilfreich bei der Beurteilung der Risikoorgane, die bei den einzelnen Patienten zum Teil sehr variabel sind. So ist eine Personalisierung der PSMA-gerichteten Radionuklid-Therapie umsetzbar. Sollte eine breitere Anwendung mit ^{44}Sc-markierten Radiotracern realisiert werden, können diese Vorteile einer verbesserten Therapieplanung, aber auch einem einfacheren Patientenmanagement, einem breiteren Patientenspektrum zur Verfügung gestellt werden. Die ^{44}Sc-Markierung kann dabei an Einrichtungen erfolgen, die ein Zyklotron zur Verfügung haben. Die Anwendung selbst muss dabei jedoch nicht zwingend vor Ort erfolgen. Durch die längere Halbwertszeit des Isotops ist auch ein Transport über weitere Strecken realisierbar. Aufgrund dieser Eigenschaften ist Scandium-44 besonders für Regionen mit geringer Zyklotron-Abdeckung und/oder großen Distanzen zwischen Zyklotron und PET-Zentrum interessant.

Teilprojekt: Prozessoptimierung

Es war möglich, statistisch signifikante Unterschiede zwischen der automatisierten und der manuellen Markierung nachzuweisen, wobei die Modulsynthese für beide untersuchten Tracer die bessere Leistung zeigte. Des Weiteren konnte eine signifikante Ausbeutensteigerung der Synthesen mit Ethanol-Zusatz nachgewiesen werden. Gestützt durch die statistische Analyse konnten die Methoden aller vorhandenen Tracer hinsichtlich Markierungseffizienz und Radiolyseanteil optimiert werden.

Diese Optimierungen sind geeignet für eine breite Palette von Tracern und Radionukliden. Daneben konnte gezeigt werden, dass geringere Mengen an Precursor notwendig sind (z. B. 2,58±0,42 µg PSMA-11 für das automatisierte Verfahren im Vergleich zu 25 µg PSMA-11 im Cold Kit z. B. ANMI SA, Belgium).

Der Schutz vor Strahlung für den Operator kann durch eine automatisierte Synthese verbessert werden. Das Risiko von Kreuzkontaminationen durch Partikeln wird verringert mit der Verwendung von sterilen Einweg-Reagenzien-KITs und Kassetten.

Daneben sind die Hauptvorteile der Automatisierung die höhere Zuverlässigkeit, bessere Reproduzierbarkeit und Zeitersparnis. Dies wird auch durch die Ergebnisse anderer Studien unterstützt, die sich mit der automatisierten Radiomarkierung beschäftigen.

Teilprojekt: Kontrolle zellulärer Transportmechanismen

Insgesamt kann, gestützt auf die [^{18}F]FDG-Experimente, vermutet werden, dass STF-31 sowohl als NAMPT- als auch als GLUT1-Inhibitor fungieren kann. Die Wirkung als NAMPT-Inhibitor scheint dabei, in Bezug auf die meisten Krebszellen, ausgeprägter zu sein. Die besondere Wirksamkeit der einzelnen inhibitorischen Aktivitäten hängt vom spezifischen zellulären Kontext ab. Hohe Expressionsniveaus von GLUT1 in Verbindung mit niedrigen anderer GLUTs könnten die Empfindlichkeit der Zellen gegenüber der GLUT1-spezifischen hemmenden Wirkung von STF-31 erhöhen, während niedrige Expressionsniveaus von NAMPT die NAMPT-spezifische inhibitorische Wirkung des Medikaments begünstigen könnten.

Teilprojekt: Implementierung neuer Tracer für klinische Studien

In dieser Arbeit konnte eine standardisierte Modulsynthesekasette etabliert werden. Durch die individuelle Voruntersuchung jedes neuen Tracers waren dann nur geringe Anpassungen an diese Grundkasette notwendig, um den Tracer aus der Forschung in die klinische Routine zu etablieren und validieren. Diese Grundlage ermöglichte den Einsatz verschiedener Tracer wie unter anderem DATA-TOC. Da mit DOTA-TOC ein etablierter Tracer für neuroendokrine Tumore vorhanden ist, war wichtig zu zeigen welche Unterschiede sich zwischen DATA-TOC und DOTA-TOC ausmachen lassen.

Eine signifikant niedrigere physiologische Hintergrundaufnahme in der Leber von [^{68}Ga]Ga-DATA-TOC im Vergleich zu [^{68}Ga]Ga-DOTA-TOC führte zu leicht höheren (wenn auch nicht statistisch signifikanten) Tumor-zu-Hintergrund-Verhältnissen für Lebermetastasen. Die Studie, welche das klinische Potential von [^{68}Ga]Ga-DATA-TOC PET/CT für die Bildgebung von Patienten mit neuroendokrinen Tumoren demonstriert,

liefert den ersten Beweis, dass [^{68}Ga]Ga-DATA-TOC als Alternative zum etablierten Diagnostikum [^{68}Ga]Ga-DOTA-TOC angewendet werden kann.

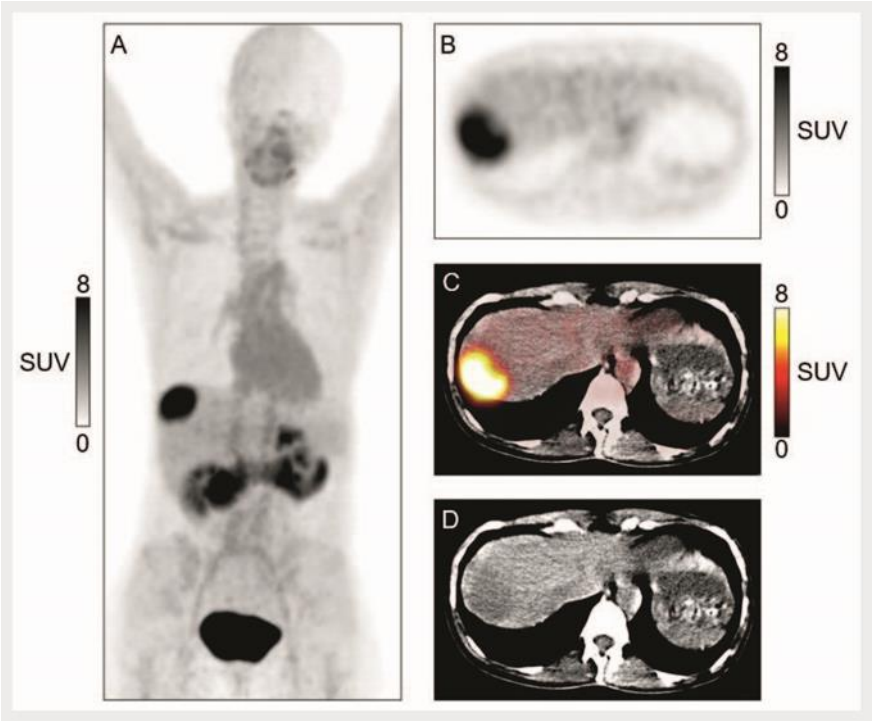

Abbildung 26: Erste [^{68}Ga]Ga-DATA-FAPi-PET/CT Bilder aus dem Uniklinikum Bonn. Intensive Tracer-Aufnahme im Lebersegment 8 (siehe auch S.278).

Ein weiterer DATA-basierter Radiotracer, der in die klinische Routine aufgenommen werden konnte, war [^{68}Ga]Ga-DATA-FAPI. Es konnte eine automatisierte Synthese, sowie eine adäquate Qualitätskontroll-Methode entwickelt werden. Das so zur Verfügung gestellte [^{68}Ga]Ga-DATA-FAPI konnte in einer ersten Patientenstudie, Fibroblasten und Lebertumore im PET/CT sichtbar machen. Vor allem im bereich aktiver Fibroblasten, die bei unterschiedlichen Tumorarten während des Wachstums der versorgenden Blutgefäße aktiv sind, könnte [^{68}Ga]Ga-DATA-FAPI für die Diagnostik eine wirksame Unterstützung liefern.

Abkürzungsverzeichnis

#

$\bar{\nu}_e$ *Antineutrino*
ν_e *Neutrino*

€

€ *Euro*

°

°C *Grad Celsius*

A

a *Jahr*
A *Massenzahl*, *Aktivität*
AAZTA *1,4-Bis(carboxymethyl)-6-[bis(carboxymethyl)]amino-6-methylperhydro-1,4-diazepin*

B

B-Feld *Magnetfeld*

C

c *Lichtgeschwindigkeit*
CT *Computertomographie*

D

d *Tage*
D *Deutschland*, *Dosis*
DATA *(6-pentansäure)-6-(amino)methy-1,4-diazepinetriacetat*
DC *Dünnschichtchromatographie*
DNA *Desoxyribunukleinsäure*
DOTA *1,4,7,10-Tetraazacyclododecan 1,4,7,10-Tetraessigsäure*
D_R *Energiedosis*
DTPA *Diethylentriaminpentaessigsäure*

E

e^- *Elektron*
E *Energie*
e^+ *Positron*
EC *electron capture*
EDTA *Ethylendiamintetraessigsäure*

EDTMP *Ethylendiamintetramethylen Phosphorsäure*
E-Feld *elektrisches Feld*
EM *Elektromagnetisch*
eV *Elektronenvolt*
Eγ *Photonenenergie*

F

F *Targetfläche*
FAPi *Fibroblasten-Aktivierungs-Protein-Inhibitoren*
FCH *Fluormethyl-Cholin*
FDG *2-Fluor-2-Desoxy-D-Glucose*
FEC *Fluorethyl-Cholin*

G

Glut *Glucosetransporter*
GMP *Gute Herstellungspraxis*

H

h *Stunden, Planck'sche Wirkungsquantum*
HDP *Hydroxymethylenbisphosphonat*
HPLC *Hochleistungsflüssigchromatographie*
H_R *Äquivalentsdosis*
Hz *Hertz*

I

IUPAC *International Union of Pure and Applied Chemistry*

J

J *Joule*

K

K *Komplexbildungskonstante, Kern*
KZ *Koordinationszahl*

M

m *Meter*
m_0 *Ruhemasse*
MDP *Methylendiphosphonat*
m_e *Elektronenmasse*
MeV *Megaelektronenvolt*
min *Minuten*
Mio *Millionen*
mRNA *Boten-Ribonukleinsäure*

MRT *Magnetresonanztomographie*
mSv *milliSievert*
^{m}X *metastabile Form des Nuklids*

N

n *Neutron*
N *Kernzahl*
NAPMT *Nicotinamide Phosphoribosyltransferase*
NET *neuroendokrinen Tumore*
nm *Nanometer*
NOTA *1,4,7 Triazacyclononane-triessigsäure*
N_T *Teilchenzahl im Target*

P

PET *Positronen-Emissions-Tomographie*
PSA *Prostataspezifisches Antigen*
PSMA Prostataspezifisches Mebranantigen

Q

q *Bewertungsfaktor*, *Ladung*
Q_R *Qualitätsfaktor*

R

r *Radius*
RLT *Radioligandtherapie*, *Radioligandentherapie*
RT *Raumtemperatur*

S

s *Sekunde*
SGLT *Natrium/Glucosetransporter*
SPE *Festphasenextraktion*
SPECT *Einzelphotonen-Emissionscomputertomographie*
SSTR *Somatostatin-Rezeptoren*
STF-31 *$C_{23}H_{25}N_3O_3S$, GLUT1 Inhibitor*
Sv *Sievert*

T

t *Zeit*
$t_{1/2}$ *Halbwertszeit*
TATE *(Tyr3)-Octreotat*
THP *Tris(hydroxypyridinon)*
THz *Terrahertz*
TOC *D-Phe-cyclo[Cys-Tyr-D-Trp-Lys-Thr-Cys]-Thr(ol)*
TRAP *Methyl (hydroxymethyl)phosphinsäure*

V

V *Volumen*

W

W_0 *Austrittsarbeit*

X

X *Mutternuklid*

X^* *Nuklid im angeregten Zustand*

Y

Y *Tochternuklid*

Z

Z *Protonenzahl*

ZOL *Zoledronsäure*

A

α *Alphazerfall*

B

β *Betazerfall*

β^- *Beta-Minus-Zerfall*

β^+ *Beta-Plus-Zerfall*

Γ

γ *Gamma*

Λ

λ *Zerfallskonstante, Wellenlänge*

N

ν *Frequenz*

P

ρ *Dichte*

Σ

σ *Wirkungsquerschnitt*

Ω

ω *Wechselwirkungswahrscheinlichkeit*

Abbildungsverzeichnis

Tabellenverzeichnis

Danksagung

An dieser Stelle möchte ich einen Dank aussprechen an alle Personen, die mich bei der Anfertigung meiner Dissertation unterstützt haben.

Besonders danken möchte ich Prof. Markus Essler für die hervorragende Unterstützung bei der Durchführung und der Umsetzung der gesamten Arbeit.

Außerdem möchte ich mich bei Dr. Elisabeth Eppard und Dr. Stefan Kürpig bedanken, die mich im auf meinem Weg geführt und unterstütz haben und ohne deren lieben Worten diese Arbeit nicht möglich gewesen wäre.

Nicht zuletzt muss ich zudem dem Team der Nuklearmedizin in Bonn meinen Dank äußern, die meine Arbeit durch ihre Unterstützung beeinflusst haben.

Meiner Frau und Familie danke ich für ihre Geduld, die Ermutigungen und Zusprüche während der Arbeit an dieser Dissertation.

Eidestatliche Erklärung

„Hiermit versichere ich, Michael Meisenheimer, eidesstatlich, dass ich die vorliegende Arbeit – abgesehen von den ausdrücklich bezeichneten Hilfsmitteln – persönlich, selbständig und ohne Benutzung anderer als der angegebenen Hilfsmittel angefertigt wurde, sowie die aus anderen Quellen direkt oder indirekt übernommenen Daten und Konzepte unter Angabe der Quelle kenntlich gemacht sind. Die vorgelegte Arbeit ist nicht bereits anderweitig als Dissertation eingereicht worden, desweiteren ist kein früherer Promotionsversuch unternommen worden. Für die Erstellung der vorgelegten Arbeit ist keine fremde Hilfe, insbesondere keine entgeltliche Hilfe von Vermittlungs- bzw. Beratungsdiensten, in Anspruch genommen worden.

Köln, 17. April 2022, Michael Meisenheimer

Publikationen:

2020 **Meisenheimer, M.**, Kürpig, S., Essler, M., Eppard, E. Maunual vs automated ^{68}Ga-radiolabelling – A comparison of optimized processes. J Labelled Comp Radiopharm. 2020; 63:162-72. Doi 10.1002/jlcr.3821.

2020 **Michael Meisenheimer**, Stefan Kürpig, Markus Essler and Elisabeth Eppard DOTA-ZOL: A Promising Tool in Diagnosis and Palliative Therapy of Bone Metastasis—Challenges and Critical Points in Implementation into Clinical Routine; *Molecules* 2020, 25(13), 2988

2019 Khawar, A., Eppard, E., Roesch, F., Ahmadzadehfar, H., Kürpig, S., **Meisenheimer, M.**, Gaertner, F., Essler, M., Bundschuh R., Biodistribution and post-therapy dosimetric analysis of [^{177}Lu]Lu-DOTA-^{ZOL} in patients with osteoblastic metastases: first results; *EJNMMI Res* **9,** 102 (2019)

2019 **Meisenheimer, M.**, Kürpig, S., Essler, M., Eppard, E., Ethanol effects on ^{68}Ga-radiolabelling efficacy and radiolysis in automated synthesis utilizing NaCl post-processing; *EJNMMI radiopharm. chem.* **4,** 26 (2019)

2019 F.C. Gärtner, T. Plum B. Kreppel E. Eppard **M. Meisenheimer** H. Strunk R.A. Bundschuh J.P. Sinnes F. Rösch M. Essler; Clinical evaluation of [^{68}Ga]Ga-DATA-TOC in comparison to [^{68}Ga]Ga-DOTA-TOC in patients with neuroendocrine tumours; *Nuclear Medicine and Biology* Volumes 76–77, September–October 2019, Pages 1-9

2019 Khawar, A., Eppard, E., Roesch, F., Ahmadzadehfar, H., Kürpig, S., **Meisenheimer, M.**, Gaertner, F., Essler, M., Bundschuh, R., Preliminary results of biodistribution and dosimetric analysis of [^{68}Ga]Ga-DOTAZOL: a new zoledronate-based bisphosphonate for PET/CT diagnosis of bone diseases; *Ann Nucl Med* 33, 404–413 (2019)

2019 Yordanova, A., Linden, P., Hauser, S. **Meisenheimer, M.**, Kürpig, S., Feldmann, G., Gaertner, F., Essler, M., Ahmadzadehfar, H. Outcome and safety of rechallenge [177Lu]Lu-PSMA-617 in patients with metastatic prostate cancer; *Eur J Nucl Med Mol Imaging* 46, 1073–1080 (2019)

2018 Lara Schwarte, Lena Thomas, Elisabeth Eppard, **Michael Meisenheimer**, Christof Weiss-Wichert, Rolf Fimmers, et al. Comparison of Tumor Heterogeneity Assessed with Textural Parameters in ^{68}Ga-PSMA PET/CT and 177Lu-PSMA SPECT/CT in Patients with MetastaticProstate Cancer; *Biomed J Sci & Tech* Res 11(5)-2018. BJSTR. MS.ID.002161. DOI: 10.26717/ BJSTR.2018.11.002161. Volume 11- Issue 5: 2018

2018 Kraus, D., Reckenbeil, J., Veit, N. Kürpig, S., **Meisenheimer, M.**, Beier, I., Stark, H., Winter, J., Probstmeier, R. Targeting glucose transport and the NAD pathway in tumor cells with STF-31: a re-evaluation; *Cell Oncol*. 41, 485–494 (2018)

2018 Ambreen Khawar; Elisabeth Eppard; Jean Sinnes; Frank Roesch; Hojjat Ahmadzadehfar; Stefan Kürpig; **Michael Meisenheimer**; Florian Gaertner; Markus Essler; Ralph Bundschuh; Prediction of Normal Organ Absorbed Doses for [177Lu]Lu-PSMA-617 Using [^{44}Sc]Sc-PSMA-617 Pharmacokinetics in Patients With Metastatic Castration Resistant Prostate Carcinoma; *Clinical Nuclear Medicine*. 43(7):486–491, JULY 2018

2018 Ambreen Khawar; Elisabeth Eppard; Jean Sinnes; Frank Roesch; Hojjat Ahmadzadehfar; Stefan Kürpig; **Michael Meisenheimer**; Florian Gaertner; Markus Essler; Ralph Bundschuh; [^{44}Sc]Sc-PSMA-617 Biodistribution and Dosimetry in Patients With Metastatic Castration-Resistant Prostate Carcinoma; *Clinical Nuclear Medicine*. 43(5):323–330, MAY 2018

Konferenzbeiträge:

2019 M Haendeler, A Khawar, S Kuerpig, **M Meisenheimer**, M Essler, R Bundschuh Biodistribution and radiation dosimetry of [^{68}Ga]Ga-RM2 Poster PET und SPECT: Prostata-Karzinom; 57. Jahrestagung der Deutschen Gesellschaft für Nuklearmedizin

2017 **M. Meisenheimer**, S. Kürpig, E. Eppard; Radiolabelling of DOTAMZOL on automated module system using NaCl post-processing; 22.Symposium on Radiopharmaceutical Sciences; International Symposium on Radiopharmaceutical Sciences

2017 **M. Meisenheimer**, S. Kürpig, E. Eppard; Radiolabelling of DOTAMZOL on automated module system using NaCl post-processing; Arbeitsgemeinschaft Radiochemie und Radiopharmazie der Deutschen Gesellschaft für Nuklearmedizin

2016 Elisabeth Eppard, **Michael Meisenheimer**, Ana de la Fuente, Stefan Kürpig, Markus Essler, Frank Roesch, Radiolabelling of DOTAMZOL with ^{68}Ga and ^{44}Sc for clinical application Endocrine Abstracts (2016) 47 OC34

2016 **M. Meisenheimer**, E. Eppard, A. de La Fuente, S. Kürpig, F. Rösch, M. Essler; „Automatisierte Radiomarkierung von DOTAMZOL mit NaCl-Post Prozessing“; Arbeitsgemeinschaft Radiochemie und Radiopharmazie der Deutschen Gesellschaft für Nuklearmedizin